Sheffield Hallam University

A Sheffield Hallam University thesis

DEVELOPMENT AND EVALUATION OF FIRE RETARDENT UNSATURED POLYESTER CLAY NANOCOMPOSITES

Katie Charlesworth

A thesis submitted in partial fulfilment of the

requirements of

Sheffield Hallam University

for the degree of Doctor of Philosophy

2007

The work described in this thesis was carried out by the author in the Materials and Engineering Research Institute, Sheffield Hallam University, between September 2003 and September 2006. The author declares that this work has not been submitted for any other degree. The work is original except where acknowledged by reference.

Author:

(Katie Charlesworth)

Director of Studies:

(Professor Christopher Breen)

There are lots of people I would like to thank for a huge variety of reasons.

Firstly, I would like to thank my Supervisor, Professor Chris Breen. I could not have imagined having a better advisor and mentor for my PhD, with his enthusiasm, and great efforts to explain things clearly and simply, especially throughout my thesis writing period. His little anecdotes and alternate ways of explaining things still make me smile.

I am also very grateful to Francis who helped me a tremendous amount throughout my PhD and made a great second supervisor. I would like to say a big thank you to all of the guys in the student office who were always willing to provide a welcome distraction when things were not going to plan. I could not have got through without the support of my friends in Sheffield and I would especially like to thank Jill who endured the PhD experience with me and could always understand exactly what I was going through.

I would like to say a huge thank you to my fiancé Eric for putting up with a very difficult and unpredictable me for the last year, without his love and support I believe I may have finally cracked during the endless re-writes of my thesis.

Most of all, I would like to thank my family, and especially my parents, for their understanding, endless patience and encouragement when it was most required. To them I dedicate this thesis.

Abstract

The research in this PhD thesis is an important part of a larger study aimed at developing the next generation of fire-resistant, lightweight, structural materials (Surefire). The Surefire project aimed to develop a new class of materials that exhibited properties such as strength, stiffness, hardness and fire performance to compete with conventional materials. The aim was to achieve this through the synergistic integration of both nano size (particulate) and micro size (fibrous) reinforcements within an unsaturated polyester matrix. A new fire retardant unsaturated polyester resin system capable of UL94 classification V0 was developed. The novel approach used to achieve this innovative class of material did not include halogenated compounds, but instead combined state of the art nano-scale particles with existing but un-revealed know-how to achieve a new class of material.

Initial studies concentrated on the characterisation of a range of alkylammonium and alkylphosphonium organoclays. This was followed by in-depth studies of the polymer layered silicate nanocomposite (PLSN) materials. A range of commercial nanoclays were sourced, and characterised. In addition a range of modified clays were developed to improve fire performance and compatibility. Intercalated nanoclays in polyester resin formed an integral, dense char and therefore provided good fire protection. Phosphonium-modified clays exhibited greater thermal stability and provided enhanced fire performance but were more expensive and batch quality was variable. The addition of nanoclays and the fire retardant dimethyl methyl phosphonate (DMMP) to the resin caused a synergistic improvement in fire performance in one particular type of resin, possibly due to the particular type of modification used, but not revealed. The addition of 5-10wt% clay can interfere with crosslink density of the composite resin so this issue was addressed by producing surfactants which offered a cross-linking group, vinyl and methacrylate groups in particular on the end of the alkyl tail. The best formulations incorporated tributylhexadecylphosphonium clay (Bu16-MMT) which achieved a UL94 V0 classification making them competitive with the fully halogenated resins investigated in the benchmarking stage.

A novel 'one-pot' synthesis method for the production of PLSN, by the in-situ polymerisation of UP in the presence of a tributylhexadecylphosphonium surfactant and Na^+ Cloisite, was shown to be successful. Whereas, other novel PLSN formulations incorporating a range of triphenylphosphonium cations were encouraging but have, so far, only provided limited success.

The Surefire resin system was estimated to be between 19 and 24% cheaper than brominated and chlorinated resins, while offering similar fire performance, together with the added benefit of eliminating toxic halogenated species. Surefire resins offer significant potential as non-halogenated, fire retardant resins, although additional work would be necessary to exploit these results commercially. The key areas of future focus should include (i) identifying why the most successful, non-halogenated resin exhibits better fire performance than the other resins, (ii) understanding the origins of the synergy between the resin and additives particularly the clay, (iii) developing a better appreciation of suitable applications and (iv) confirming suitability for purpose through further testing.

Table of Contents

Chapter 1

VI

Chapter 6

List of Abbreviations

AFM	- Atomic Force Microscopy
APP	- Ammonium Polyphosphate
ATR	- Attenuated Total Reflectance Spectroscopy
Bu16-MMT	- tributylhexadecylphosphonium clay
CEC	- Cation Exchange Capacity
Crystic 189LV	- Low Viscosity Orthophthalic Unsaturated Polyester Resin
Crystic 272	- Isophthalic Unsaturated Polyester Resin
Crystic D3644LV	- Chlorinated Unsaturated Polyester Resin
Crystic PD7343	- Brominated Unsaturated Polyester Resin
Crystic R935	- Isophthalic Unsaturated Polyester Resin
DTA-MMT	- decyltrimethylammonium Clay
ω-DTA-MMT	- ω-decyltrimethylammonium Clay
DMMP	- Dimethyl methyl phosphonate
DMTA	- Dynamic Mechanical Thermal Analysis
DSC	- Differential Scanning Calorimetry
DTA	- Differential Thermal Analysis
EGA	- Evolved Gas Analysis
FT-IR	- Fourier Transform Infrared Spectroscopy
GC-MS	- Gas Chromatography Coupled with Mass Spectrometry
HDT	- Heat Distortion Temperature
HRR	- Heat Release Rate
LOI	- Limiting Oxygen Index
MCT	- Mercury Cadmium Telluride
MEKP	- Methyl ethyl ketone peroxide (Catalyst M)
MLR	- Mass Loss Rate
MMT	- Montmorillonite
Na-MMT	- Sodium Montmorillonite
NMR	- Nuclear Magnetic Resonance Imaging
OLS	- Organically Layered Silicate
PHRR	- Peak Heat Release Rate
PLSN	- Polymer Layered Silicate Nanocomposite
PMMA	- Polymethylmethacrylate
PS	- Polystyrene
SEM	- Scanning Electron Microscopy
TA3-MMT	- [3(methacryloylamino)propyl] trimethylammonium Clay
TEM	- Transmission Electron Microscopy
TGA	- Thermogravimetric Analysis
TG-MS	- Thermogravimetric Analysis Coupled with Mass Spectrometry
TMA	- Thermo-mechanical Analysis
TP8-MMT	- (1-octyl) triphenylphosphonium Clay
TP10-MMT	- decyltriphenylphosphonium Clay
ω-TP10-MMT	- ω- decyltriphenylphosphonium Clay
TP12-MMT	- n-dodecyl triphenylphosphonium Clay
TP14-MMT	- (1-tetradecyl) triphenylphosphonium Clay
TP16-MMT	- n-hexadecyltriphenylphosphonium Clay
TP3MM-MMT	- [3(methacryloyl)propyl] triphenylphosphonium Clay
TP6MM-MMT	- [6(methacryloyl)propyl] triphenylphosphonium Clay
TP8MM-MMT	- [8(methacryloyl)propyl] triphenylphosphonium Clay
TP10MM-MMT	- [10(methacryloyl)propyl] triphenylphosphonium Clay
UL94	- Underwriters Laboratory Test for Flammability
UP	- Unsaturated Polyester
XRD	- X-ray Diffraction
XRF	- X-ray Fluorescence

1. Introduction

The research in this PhD thesis is an important part of a larger study aimed at developing the next generation of fire-resistant, lightweight, structural materials (Surefire [1-1]). Surefire was a DTI funded project under the LINK Basic Technologies for Industrial Application programme. The project aimed to develop a brand new class of materials that exhibited properties such as strength, stiffness, hardness and fire performance to compete with conventional materials. The consortium consisted of 2 RTD organisations Sheffield Hallam University and NetComposites together with 7 specialist SME – Scott Bader, Jones Stroud insulations, Fibre technology, Plastech TT, E & F Composites, Rapra Technology and Fairline Boats, all based in the UK. The aim was to achieve this through the synergistic integration of both nano size (particulate) and micro size (fibrous) reinforcements within an unsaturated polyester matrix. The main target outputs were low weight structural parts with high fire and temperature performance, solvent resistance and corrosion performance, and coating systems exhibiting scratch resistance and fire performance.

A new fire retardant unsaturated polyester resin system capable of UL94 classification V0 was developed. The novel approach used to achieve this innovative class of material did not include halogenated compounds, but instead combined state of the art nano-scale particles with existing but un-revealed know-how to achieve a new class of material. This new material was specifically developed through a collaborative project for use in industrial applications where fire retardancy is paramount, such as the mass transport, off-shore and infrastructure sectors.

The thesis in itself was split into five different parts:
1) Selection of organoclays and resins for further study
2) Exploration of commercially available organophosphonium ions as clay modifiers
3) Preparation of novel surfactants and their use as clay modifiers
4) Evaluation of fire resistant properties
5) Study of Organoclay decomposition using TG-MS

Initial studies concentrated on the characterisation of a range of alkylammonium and alkylphosphonium organoclays. This was followed by in-depth studies of the polymer layered silicate nanocomposite (PLSN) materials. A range of commercial nanoclays were sourced, characterised and the modified clays were developed to improve fire performance and compatibility. Intercalated nanoclays in polyester resin formed an integral, dense char and therefore provided good fire protection. Phosphonium-modified clays exhibited greater thermal stability and provided enhanced fire performance but were more expensive and batch quality was variable. The addition of nanoclays and the fire retardant dimethyl methyl phosphonate (DMMP) to the resin caused a synergistic improvement in fire performance in one particular type of resin (Crystic 189LV), possibly due to the particular type of molecular end caps used, but not revealed. The addition of 5-10wt% clay can interfere with crosslink density of the composite resin so this issue was addressed by producing surfactants which offered a cross-linking group on the end of the alkyl tail, vinyl and methacrylate groups in particular. The best formulations incorporated tributylhexadecylphosphonium clay (Bu16-MMT) which achieved a UL94 V0 classification making them competitive with the fully halogenated resins investigated in the benchmarking stage.

These new materials have the potential to open up a significant range of applications in areas such as construction, offshore and mass transit where fire performance and lightweight have always been critical issues. An end-user interest group was formed from UK companies who were interested in using non-halogenated fire retardant resin systems. The membership included companies from a wide range of industries. The opinions of the end-user interest group helped steer the developments within the project. A number of key applications were determined by the end-user interest group:

- Aerospace components (replacement of phenolic prepreg with a cheaper system)
- Underground rail infrastructure (replacement of epoxy strengthening/repair patches with a cheaper, less toxic system)
- Construction panels and modules (replacement of halogenated resins with a less toxic system)
- Construction and transportation profiles (replacement of halogenated pultrusion resins with a less toxic system)

A number of products were selected for trial and these included an under bonnet duct for Caterpillar trucks and a bar top lid for a Phantom 46 luxury performance motor yacht. Both products required high temperature operating performance with the bar top lid, which encloses a cooking griddle reaching temperatures up to 300 °C. The under bonnet duct was produced using standard and nano-materials and slight differences in the gel times were recorded (30 minutes for standard and 90 minutes for nano-material) however, no comparable difference could be detected between both moulded parts after 24 hours in terms of shape/stiffness. Further work is still undergoing on the Phantom 46 bar top in order to apply nanotechnology to resist temperature on this component.

The total cost of the Surefire resin system was compared to halogenated resin systems. The Surefire resin system was estimated to be cheaper than brominated and chlorinated resins, and was estimated to be between 19 and 24% cheaper than halogenated systems with similar fire performance, plus the added benefit of eliminating toxic halogenated species. The work in this thesis is entirely my own, the role of the project partners is detailed below in Table 1–1.

Table 1–1 SUREFIRE project partners

Organisation	Description	Project Role
NetComposites	Technology developer and licensor	Project manager, process development
Plastech Thermoset Tectonics Ltd	Designer and manufacturer of tooling systems	Development of tool coatings, manufacture of case study tooling
E&F Composites Ltd	Moulder of composite components	Process development, design and manufacture of case study component
Jones Stroud Insulations Ltd	Manufacturer of fibre-reinforced intermediate products	Development, manufacture and testing of prepregs
Scott Bader Ltd	Manufacturer of resin systems and coatings	Development and supply of resins
Fibre Technology Ltd	Manufacturer and suppliers of steel fibres	Development and supply of steel fibres
Rapra Technology Ltd	Technology developer and licensor	Development and characterisation of resin and coating systems
Fairline Boats Ltd	Manufacturer of luxury boats	Design and manufacture of case study component

1.1 Clays, Organoclays and Nanocomposite Materials

One of the most promising directions for technological development in the 21st century is nanotechnology. Nanocomposite materials are of great interest within the plastics industry. These materials incorporate organically modified layered silicates, often referred to as organoclays, within a host matrix as low quantity (i.e. ≤ 5 wt%) fillers dispersed at the nanometre-level. This dispersion of clay platelets has led to the general description of this class of materials as PLSNs [1-2].

Substantial property improvements have been demonstrated with nanocomposites when compared to virgin polymers. Properties that have revealed improvements include:

- Mechanical properties e.g. strength, modulus and dimensional stability [1-3,1-4, 1-5, 1-6]

- Decreased permeability to gases, water and hydrocarbons [1-7, 1-8, 1-9, 1-10, 1-11]

- Flame retardancy and reduced smoke emissions [1-12, 1-13, 1-14]

- Thermal stability and heat distortion temperature (HDT) [1-11, 1-15, 1-16, 1-17]

- Ionic conductivity [1-18, 1-19]

- Optical clarity in comparison to conventionally filled polymers [1-20]

- Increased biodegradability of biodegradable polymers [1-21]

Often this enhanced material performance occurs without a significant increase in the density of the polymer, and also without any reduction in the materials potential recycle ability. The development and study of nanocomposite hybrid material's in the field of materials science is a multi-disciplinary research activity generating both academic and industrial interest. Applications for PLSNs have been proposed for use in the materials, construction, aerospace and food-packaging sectors as displayed later, in Table 1–9.

The property improvements resulting from the formation of a nanocomposite most notably occur at extremely low concentrations of aluminosilicate (1-5 wt%) as compared to conventional phase-separated composites of a filler material in a polymer (20-30 wt%). The observed property enhancements result from the extremely large surface area available for interaction with a polymer, coupled with a relatively large aspect ratio [1-22].

The intercalation chemistry of polymers when mixed with appropriately modified layered silicate and synthetic layered silicates has long been known [1-23], however the topic of polymer clay nanocomposites has gained momentum only recently. The revival of interest in these materials is due to two major findings. Firstly a report from the Toyota research group working on Nylon-6 (N6)/montmorillonite (MMT) nanocomposites, demonstrated that small amounts of layered silicate result in pronounced improvements of thermal and mechanical properties [1-24], and secondly further work by Vaia *et al.* [1-25] who established the possibility of melt mixing polymers with layered silicates without the use of organic solvents.

To impart thermal stability/flame retardancy current trends favour the use of fillers like metal-trihydrate/hydroxide and halogenated compounds; however, the use of these systems has definite environmental and safety concerns [1-26]. An example of the impracticality of these systems comes from the application of aluminium hydroxide (ATH) in wires and cables [1-27]. This application requires loadings in excess of 60 wt% to achieve a suitable level of flame retardancy, which leads to an inflexible product and can cause processing problems. Whereas, halogenated flame retardants are expensive and may release biologically harmful toxins into the environment under combustion conditions [1-28, 1-29]. Nanocomposites minimise the disadvantages of these traditional flame retardant systems.

The use of mineral based systems had not been considered for flame retardancy until recently. However, reports of the improved thermal stability of siloxane polymer-clay composites [1-30] and a polyimide-clay composite [1-31] has generated new interest in the use of these mineral based systems.

1.2   Commercial Market for Polymer-Clay Nanocomposites

With further research polymer-clay nanocomposite materials have the potential to bring about a revolution in the plastics industry that would be beneficial to both the production industry (reduced costs and better processibility) and the consumer market (reduced cost and improved functionality). Figure 1–1 demonstrates the global market analysis of nanocomposite growth in different commodity sectors, predicted to 2009.
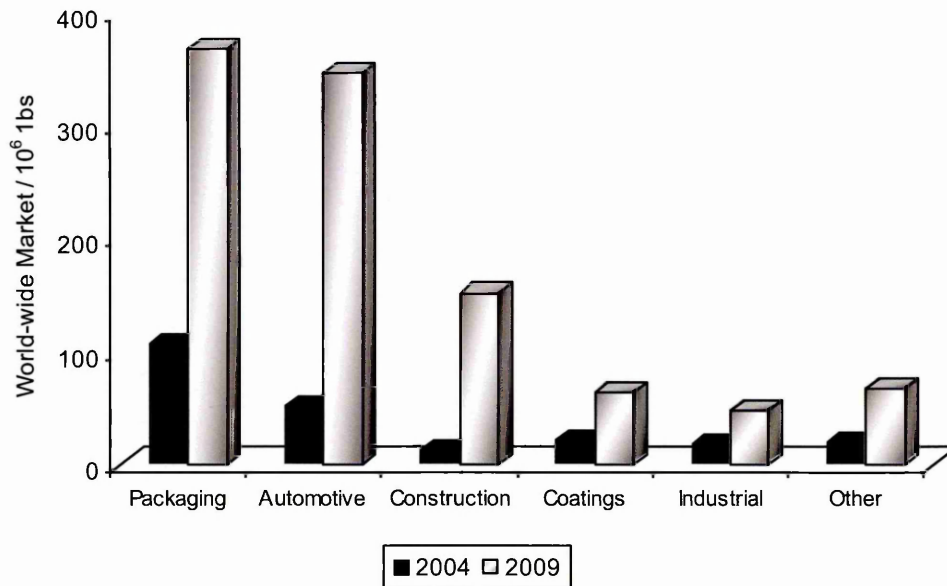
Figure 1–1 Global market analysis of nanocomposite growth in different commodity sectors, predicted to 2009 [1-32].

1.3   Classification of Minerals

All minerals are divided into several classes, of which the silicates were the main focus for this research. The silicates are divided into several sub-classes based on the number of linkages between the basic units of their structure (i.e. SiO_4 tetrahedra). The sub-classes found in sedimentary rocks are the tectosilicates (silica and feldspars) and the phyllosilicates (kaolinites, smectites, illites and chlorites) [1-33, 1-34] displayed in Table 1–2.

Table 1–2 The sub-division of the silicate class.

Class	Subclass	Group	Subgroup
Silicates	tectosilicates	silica	quartz
		feldspars	alkali series
			plagioclase series
	phyllosilicates	Kaolinites 1:1	
		Smectites 2:1	
		Illites 2:1	
		Chlorites 2:1	

1.4 Clay and Nanocomposite Structure

1.4.1 Structure of layered Silicates

Clay minerals (phyllosilicates) are among the most important industrial materials. Their physical and chemical properties are closely related to their structure and composition [1-35]. Clay minerals are often used as filler materials because of their properties in products such as dry wall finishing's, wallboard compounds or joint treatment compounds providing thickening properties and thixotropic characteristics [1-36].

The structure of clay minerals has been determined largely by X-ray diffraction (XRD) methods. In order to understand the importance of clay minerals, it is necessary to describe the compositional and molecular unit arrangements. Clay minerals are comprised of continuous two-dimensional tetrahedral sheets of the composition Si_2O_5, with SiO_4 tetrahedrons (Figure 1–2) linked by sharing three corners of each tetrahedron to form a hexagonal mesh pattern (Figure 1–3A).
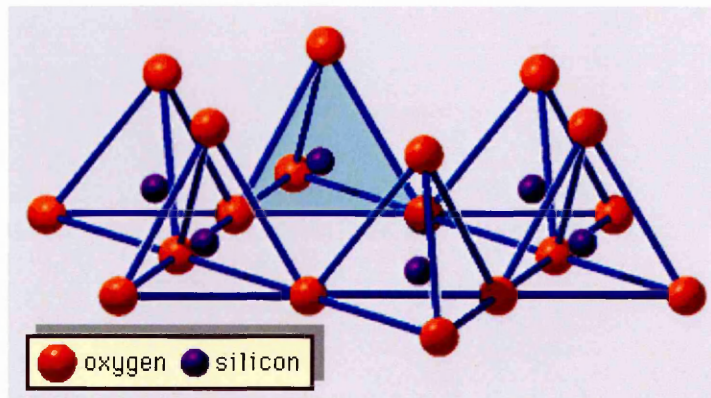
Figure 1–2 Schematic representation of the single silica tetrahedron (shaded) and the sheet structure of silica tetrahedrons arranged in a hexagonal network [1-37]
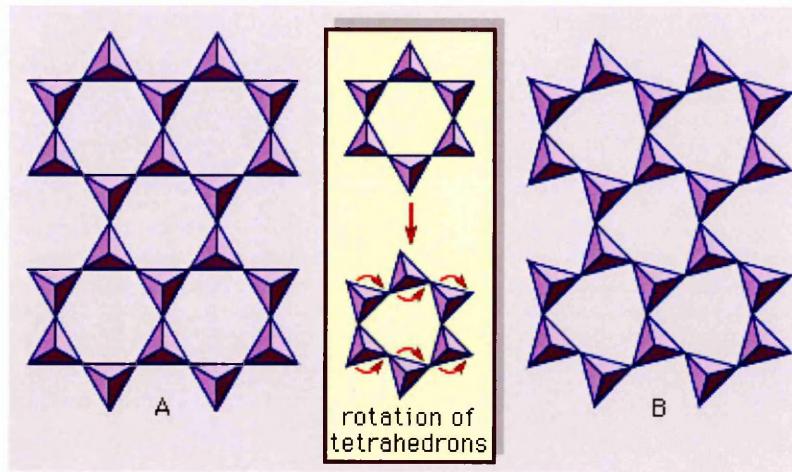
Figure 1–3 (A) Ideal hexagonal tetrahedral sheet. (B) Contracted sheet of ditrigonal symmetry owing to the reduction of mesh size of the tetrahedral sheet by rotation of the tetrahedrons [1-37].

Silicon atoms of the tetrahedrons are frequently, partially substituted by aluminum and, to a lesser extent, ferric iron. The apical oxygen at the fourth corner of the tetrahedrons, which is usually directed normal to the sheet, forms part of an adjacent octahedral sheet in which octahedrons are linked by sharing edges (Figure 1–4).
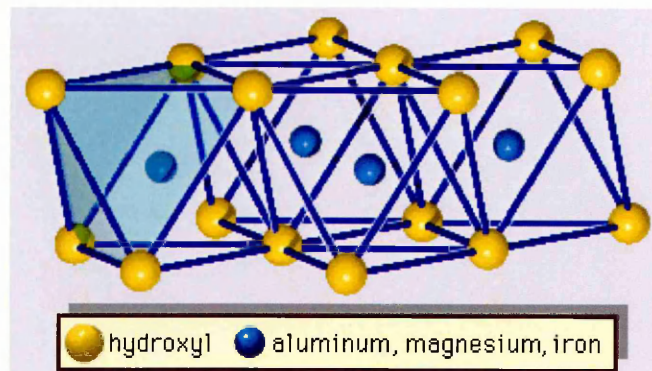
Figure 1–4 Schematic representation of the single octahedron (shaded) and the sheet structure of octahedral units [1-37]

The junction plane between the tetrahedral and octahedral sheets consists of shared apical oxygen atoms of the tetrahedrons and unshared hydroxyls that lie at the centre of each hexagonal ring of tetrahedrons and at the same level as the shared apical oxygen atoms (Figure 1–5). Common cations that coordinate the octahedral sheets are Al, Mg, Fe^{3+}, and Fe^{2+}; but occasionally Li, V, Cr, Mn, Ni, Cu, and Zn substitution occurs. If divalent cations (M^{2+}) are in the octahedral sheets, all the positions are filled to balance the charge ($Mg_3(OH)_6$), however, if trivalent cations (M^{3+}) are in the octahedral sheets, only two thirds of the positions need to be filled to balance the charge, ($Al_2(OH)_6$).

When all three octahedra have cations (Mg^{2+} and Fe^{2+}) at their centre the sheet is known as trioctahedral and dioctahedral (Al^{3+} and Fe^{3+}) when only two are occupied.
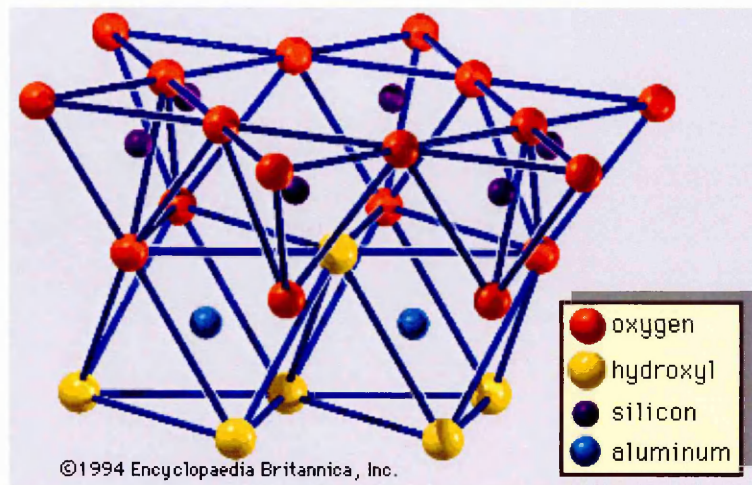
Figure 1–5 Structure of 1:1 layer silicate (kaolinite) illustrating the connection between tetrahedral and octahedral sheets [1-37].

In the composition of octahedral sheets, if all the anion groups are hydroxyl ions, the resulting sheets may be expressed by $M^{2+}(OH)_2$ and $M^{3+}(OH)_3$, respectively. Such sheets, called hydroxide sheets, occur singly, alternating with silicate layers in some clay minerals. Brucite, $Mg(OH)_2$, and gibbsite, $Al(OH)_3$, are typical examples of minerals having similar structures. There are two major types for the structural "backbones" of clay minerals called silicate layers. The unit silicate layer formed by aligning one octahedral sheet to one tetrahedral sheet is referred to as a 1:1 silicate layer, and the exposed surface of the octahedral sheet consists of hydroxyls. In another type, the unit silicate layer consists of one octahedral sheet sandwiched by two tetrahedral sheets that are oriented in opposite directions and is termed a 2:1 silicate layer (Figure 1–6). These structural features, however, are limited to idealized geometric arrangements.
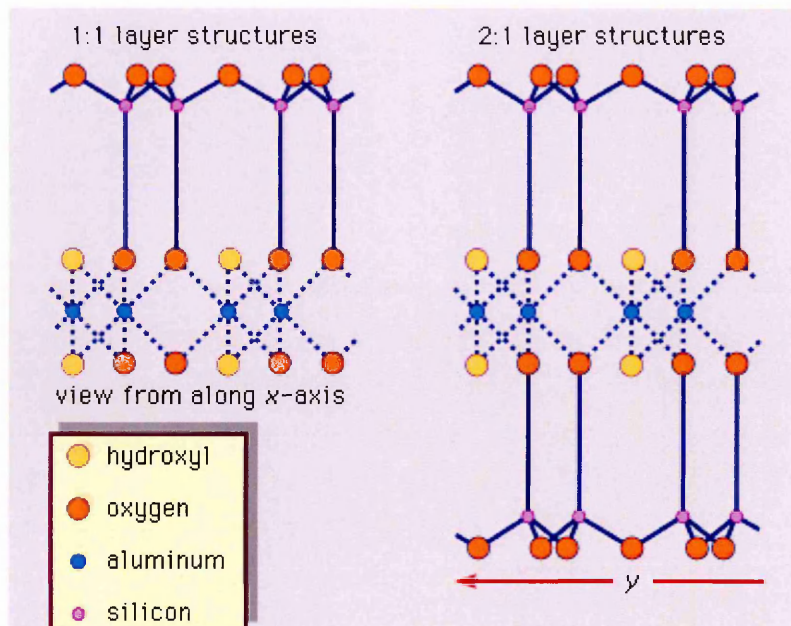
Figure 1–6 Schematic presentation of (A) 1:1 layer structures and (B) 2:1 layer structures [1-37].

Real structures of clay minerals contain substantial crystal strains and distortions, which produce irregularities such as deformed octahedrons and tetrahedrons rather than polyhedrons with equilateral triangle faces. Ditrigonal symmetry modified from the ideal hexagonal surface symmetry, and puckered surfaces instead of the flat planes made up by the basal oxygen atoms of the tetrahedral sheet can occur. One of the major causes of such distortions is dimensional "misfits" between the tetrahedral and octahedral sheets. If the tetrahedral sheet contains only silicon in the cationic site and has an ideal hexagonal symmetry, the longer unit dimension within the basal plane is 9.2 Å, which lies between the corresponding dimensions 8.6 Å of gibbsite and 9.4 Å of brucite. To fit the tetrahedral sheet into the dimension of the octahedral sheet, alternate SiO_4 tetrahedrons rotate (up to a theoretical maximum of 30°) in opposite directions to distort the ideal hexagonal array into a doubly triangular (ditrigonal) array (Figure 1–3B). By this distortion mechanism, tetrahedral and octahedral sheets of a wide range of compositions resulting from ionic substitutions can link together and maintain silicate layers. Among ionic substitutions, those between ions of distinctly different sizes most significantly affect geometric configurations of silicate layers.

Commonly used in nanocomposites are smectites, from the structural family known as the 2:1 phyllosilicates. A 2:1 layer is constructed of an octahedral sheet sandwiched between two tetrahedral sheets. The space that is positioned between two adjacent

10

layers is known as the interlayer, interlamellar or gallery space. The term interlayer space will be used throughout this thesis. The complete assembly is known as a *structural* layer where the theoretical thickness of both sheets (assuming they are undistorted) is 5 Å for the octahedral sheet and 4.6 Å for the tetrahedral sheet, resulting in an overall thickness of 9.6 Å for a 2:1 sheet.

The thickness of the layers is around 1 nm with the diameter of the layers ranging from 300 Å to several microns, or larger depending on the particular layered silicate. These uncharged layers are organized into stacks and this leads to a regular van der Waals gap between the interlayer. Isomorphic substitution of Al^{3+} for Si^{4+} in the tetrahedral sheet or Fe^{2+}, Mg^{2+} for Al^{3+} in the octahedral sheet creates an excess of negative charge in the clay layers that is counterbalanced by cations (usually alkali or alkaline earth cations) in the interlayer space. The distance between sites of negative charge depends on the extent of isomorphic substitution. The principal exchangeable cations are calcium, magnesium, sodium and potassium [1-38, 1-39].

The most commonly used layered silicates are montmorillonite (MMT), hectorite and saponite, their chemical formula and characteristics are given in Table 1–3 and the structure of MMT is given in Figure 1–7.
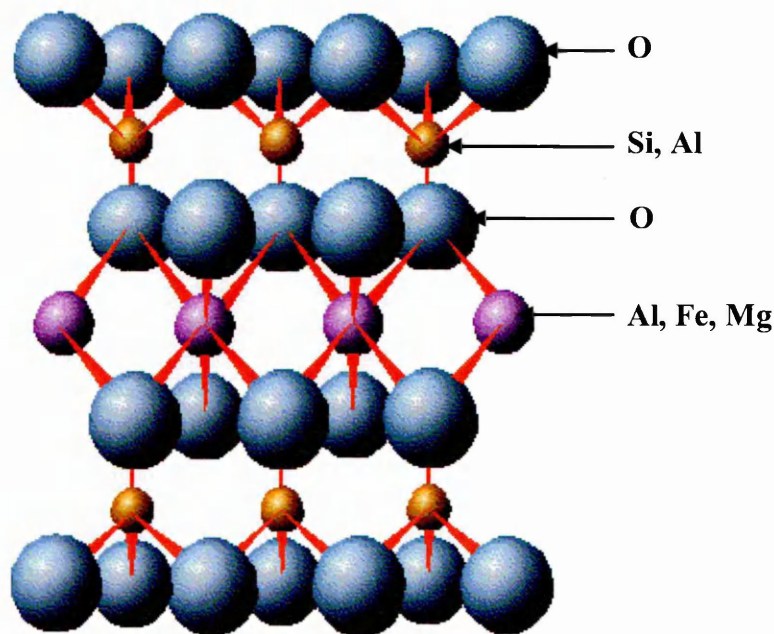
Figure 1–7 Schematic representation of the 2:1 phyllosilicate MMT [1-40].

The maximum amount of cations in a clay that can be exchanged by other cations is given by the cation exchange capacity (CEC) and is measured in milliequivalents (meq) per 100 grams of clay. The charge varies with 80 % of the CEC in the interlayer space and 20 % of the CEC at the edge of the layer and so the CEC is considered as an average value over the whole crystal.

Table 1–3 Chemical formula and characteristics of commonly used 2:1 phyllosilicates [1-41].

Class	Chemical Formula	CEC [meq/ 100g]
Montmorillonite	$M_x(Al_{4-x}Mg_x)Si_8O_{20}(OH)_4$	110
Hectorite	$M_x(Mg_{6-x}Li_x)Si_8O_{20}(OH)_4$	120
Saponite	$M_xMg_6(Si_{8-x}Al_x)O_{20}(OH)_4$	86.6

M=monovalent cation; x=degree of isomorphous substitution (between 0.5 and 1.3).

1.4.2 Clay Minerals of Relevance in This Thesis

1.4.2.1 Montmorillonite (MMT)

Montmorillonite (MMT) is the name given to the clay found first near Montmorillon in France, and is the most common phyllosilicate used for the production of commercial polymer clay nanocomposites. MMT composition varies across a relatively wide range not only with geographical location but also with the deposit strata [1-42]. A relatively high amount of isomorphous substitution leads to the composition of MMT deviating from the ideal formula, $Al_2Si_4O_{10}(OH)_2.xH_2O$. An idealised structural formula for MMT is $Na_{0.3}(Al_{1.7}Mg_{0.3})Si_4O_{10}(OH)_2$. Figure 1–7 displays the molecular structure of MMT [1-40], this model is the most widely accepted and was first proposed by Hofmann, Endel and Wilm [1-43] and modified by Magdefrau and Hofmann [1-44], and, Hendricks [1-45]. Water and polar molecules can easily enter between the layers of the montmorillonite structure. The electrostatic bonding between the layers and exchangeable cations is weak consequently the chances of swelling or intercalation are excellent.

1.4.3 Clay Mineral Properties and Characteristics

1.4.3.1 Isomorphous Substitution

Isomorphic substitution is the process in which octahedral or tetrahedral cations are substituted by other cations if they have the appropriate size to fit the structure (e.g. $Al^{3+} \rightarrow Si^{4+}$, $Mg^{2+} \rightarrow Al^{3+}$, $Li^{+} \rightarrow Mg^{2+}$). Since the substituting ions generally have a lower valency, then the initially neutral clay layer now carries a net negative charge. As a result, positively charged ions are adsorbed on the surface to electrically balance the layers. If isomorphic substitution occurs in the tetrahedral sheet then the negative charge is concentrated on the four surface oxygens at the base of the relevant tetrahedron. However, when isomorphic substitution occurs in the octahedral layer then the negative charge is spread out over ten of the oxygens and is diffuse. The extent of the net negative charge now carried by the clay sheets is measured by the CEC. Different clays have different CECs, and are displayed in Table 1–4:

Table 1–4 CEC values for selected clays (at pH 7).

	CEC Range meq/100g Clay
Kaolin	3-15
Chlorite	10-40
Illite	10-40
Smectite	80-120
Vermiculite	100-150

Cations that are common in clay minerals found in nature, e.g. Na^{+}, Ca^{2+}, Mg^{2+} or K^{+}, can be exchanged by other cations by dispersing the clay in a solution of the desired cation. Exchangeable cations can also be associated with the edges of silicate layers, where the structural ions have unsatisfied valences, because of broken bonds.

1.4.3.2 Swelling/Hydration of Clay

Clay is hydrophilic and water can usually be found in the interlayer spaces, solvating the exchangeable cations present [1-46]. Water molecules in the interlayer space can be present in different environments. They can either be directly co-ordinated to the exchangeable cations or they may be held in pores and removed by drying under ambient conditions. Water also may be adsorbed on the surface of clay mineral structures and in smectites, vermiculites, hydrated halloysite, sepiolite, and palygorskite; this water may occur in interlayer positions or within structural channels.
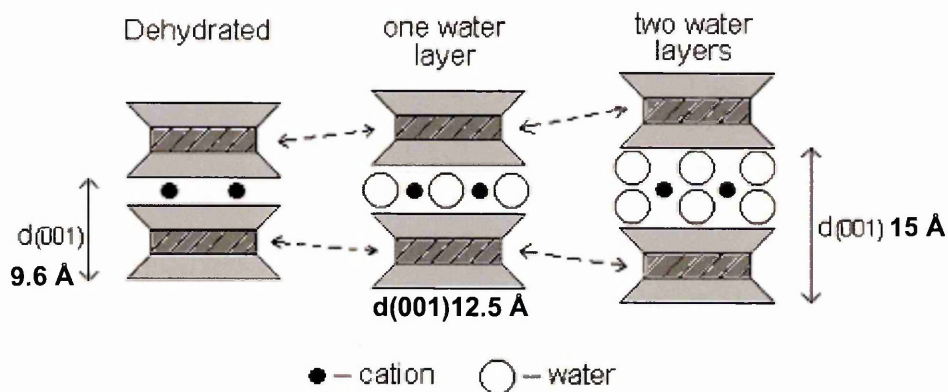
Figure 1–8 Swelling of clay in the presence of water [1-47].

When water is adsorbed between the layers, the distance between the layers (d_{001} spacing) increases in a pseudo stepwise manner. This is the result of a swelling of the clay layers and is represented in Figure 1–8. When an organic solvent is adsorbed between the layers it is referred to as intercalation. Another feature of the clay's structure that has a direct bearing upon the chemistry of the complexes is the acidic nature of the clay surface [1-48]. The clay can show Bronsted and Lewis acidity with the structure governing the degree to which these occur. For example, Lewis acidity is more commonly associated with exposed Al^{3+} and Fe^{3+} cations at the edges of the clay sheets and can be increased by the thermal treatment of the clay. Similarly, the Bronsted acid characteristics are usually governed by the availability of water in the interlayer around the cations and are the result of the dissociation of water molecules in a hydration space between the cations. The degree to which this effect is seen depends on the nature of the substitution, i.e. whether it is mainly from the tetrahedral or octahedral sheet, and on water content, the lower the water content the higher the acidity. Bronsted acidity is also very dependent on the polarising power of the interlayer cation.

1.4.4   Organic Mineral Interactions

For a number of years the interactions between clays and organic molecules have been of major interest to industry. Some of the industrial sectors that are specifically interested by such interactions include: geological [1-49], oil exploration [1-50], pharmaceutical [1-51], waste treatment [1-52], plastics [1-53], catalysis [1-54], laundry powders [1-55] and agricultural [1-56, 1-57, 1-58]. An example of this is the vital role that clay minerals play in the control of hazardous organic molecules. Organoclays are able to adsorb

hazardous organic pollutants (e.g. fuel contamination) within the interlayer spaces of the clay slowing down the migration of pollutants through soils and waterways [1-59, 1-60]. Sanchez-Martin *et al.* [1-61] studied the efficiency of a series of clay minerals (montmorillonite, illite, muscovite, sepiolite and palygorskite) modified with the cationic surfactant octadecyltrimetylammonium (ODTMA) in the adsorption of pesticides (penconazole, linuron, alachlor, atrazine and metalaxyl). They concluded that clay minerals could be used as barriers to prevent the mobility of certain hydrophobic pesticides from a point source of pollution.

1.4.4.1   Typical Smectite - Organic Molecule Interactions

Smectite clays interact with organic molecules in a very complex way. Lahav *et al.* [1-62,1-63] documented the interactions occurring between different cationic exchanged MMTs and the pesticide benzinine; the results indicated a variety of interactions were occurring. Other examples of complexes formed through organoclay interactions include; sulfolane adsorbed on cationic exchanged MMTs [1-64] and the interactions of alachlor (herbicide) with homoionic MMTs [1-65]. The five main types of interactions are described in Table 1–5 [1-38], it is also possible for positively charged organic molecules to be exchanged with the inorganic cations in the interlayer space [1-39]. The number and variety of organic compounds which can acquire a positive charge is limited, such compounds (e.g. alkylammonium ions) often contain nitrogen, of which the amines form the largest class. A fixed internal porosity is achieved by such cation exchanges since the pore size and shape depend on the alkylammonium ion.

Cation-exchange may also occur indirectly with organic molecules. Ruiz-Conde *et al.* [1-66] studied the interaction of aqueous solutions of formamide, acetamide and propionamide with vermiculite. Vermiculite is similar in structure to MMT but has a higher CEC (Table 1–4). These situations demonstrated that amides were hydrolysed to liberate NH_4^+.

Table 1–5 Types of interactions between organic molecules and (hydrated) cations [1-38].

Lewis Acidity - After thermal dehydration or at room temperature the exchangeable cations may serve as Lewis acids and adsorbed bases become co-ordinated directly to the cations. If M is an alkali metal cation, then the bond between it and B is mainly electrostatic, ion-dipole attraction.	$B\text{-}M^{n+}$
Protonation of Organic Molecules - Water coordinated to exchangeable metallic cations serves as a proton donor (Bronsted acid). Depending on the polarising power of the metal (M^{n+}) and the basic strength of the organic molecule (B), the organic molecule may be protonated by accepting a proton from a water molecule, thus gaining a positive charge.	$^{+}HB\text{---}(OH)^{-}\text{-}M^{n+}$
Water Bridges - The organic molecule may form a H-bond with the polar water molecule, i.e. the water acts as a bridging molecule.	$B\text{---}H\text{--}(OH)\text{-}M^{n+}$
Water Bridge Associations - Organic molecules may also be associated to molecules of the type opposite. The presence of these associations depends greatly on the size of the molecule.	$B\text{---}B\text{---}H(OH)\text{-}M^{n+}$
Other Associations - Organic molecules may also be associated with broken edges, external clay surfaces, with substitutions in the tetrahedral sheet or clusters between stacks of clay layers.	

1.4.4.2   Factors Affecting the Adsorption of Organic Molecules onto Minerals

The absorption process can be affected by a number of surface and organic molecular properties as displayed in Table 1–6:

Table 1–6 Surface and organo-molecular characteristics affecting adsorption.

Surface Properties	Organic Molecular Characteristics
Surface configuration	Size
Exchangeable ions on surface	Shape
Total surface area	Flexibility
Interlayer spacing	Charge
Surface Chemistry (O or OH)	Polarity
Particle size and crystallinity	

Certain reaction conditions are also significant in addition to these molecular factors:

- Temperature - The structure of the interacting liquid may be disrupted upon increased temperature due to greater thermal activity; increasing the relative number of free molecules and the rate of intercalation.

- Addition of water to the intercalating liquid - Too much water would result in the solvation of the intercalating molecules, resulting in relatively few un-solvated molecules being available to intercalate, therefore decreasing the intercalation rate.

- Reaction Solvent - Fujita *et* al. [1-67] investigated the interlayer structures of magadiite derivatives after alcohol adsorption. By changing the amount of modifying silylating regent, organic derivatives of magadiites with different adsorption capacities were prepared. After the adsorption of alcohols onto derivatives with different degrees of silylation, the samples with a lower degree of silylation exhibited larger basal spacings and adsorbed larger amounts of alcohols than did the samples with a higher degree of silylation.

1.4.4.3 Alkylammonium Ion Exchanged Clays

A variety of organic cations are able to replace the resident metal exchange cations on clays by a simple ion exchange process. [1-68]. The initial adsorption of organic molecules may lead to a change of the clay character from hydrophilic to organophilic and to an expansion of the interlayer d_{001} spacing. Both factors tend to facilitate further adsorption of organic substances by the interlamellar organic phase. Also the thermodynamic free energy of mixing must be able to compensate for the energy of increasing separation of the clay platelets. For example the adsorption of a base requires that the interlamellar phase comprises active acidic functionalities, while adsorption of non-ionic compounds requires that their solubility parameter is comparable to that of the interlamellar phase [1-69, 1-70]. *n*-alkylammonium derivatives of smectites have been extensively studied and the results obtained are summarised in numerous publications (e.g. Grim [1-71], Theng [1-72], Lagaly [1-73], Jones [1-74], Newman [1-75], Favre [1-76] and Xie [1-77]).
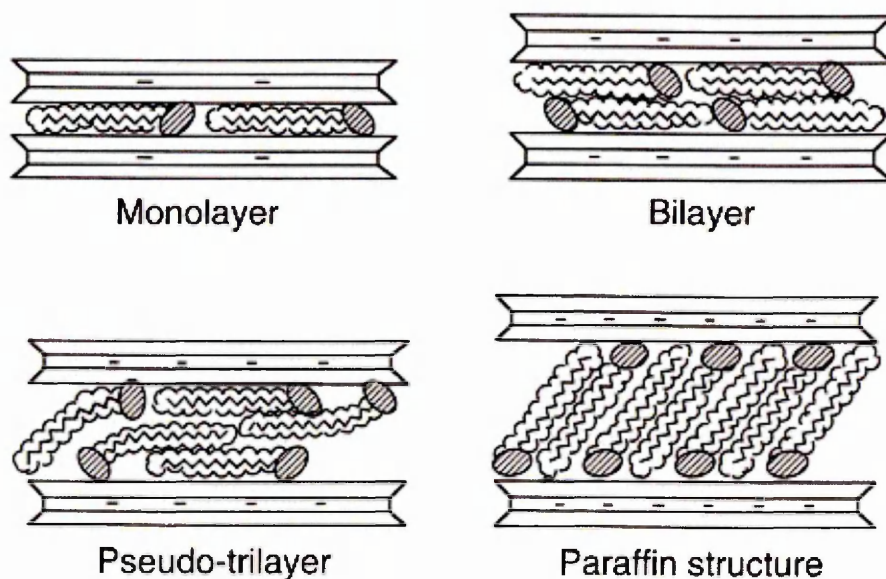
Figure 1–9 Orientations of alkylammonium ions in the galleries of layered silicates with different layer charge densities [1-79].

The orientations of the alkylammonium ion chains in organoclay were initially deduced based on infrared and X-ray diffraction (XRD) measurements [1-78] and depend on the layer charge density of the clay. The monolayer, bilayer, pseudo-trilayer, and paraffin type monolayer orientations are displayed in Figure 1–9. More recent modelling experiments by Hackett [1-79] have provided further insights into the packing orientations of the alkyl chains in organically modified layered silicates. Molecular dynamics (MD) simulations were used to study molecular properties such as density profiles, normal forces, chain configurations and trans-gauche conformer ratios.

A study by Vaia et al. [1-80] using Fourier transform Infrared (FTIR) spectroscopy has shown the structures in Figure 1–9 to be too simplistic. They monitored frequency shifts of the asymmetric CH_2 stretching and bending vibrations and found that the intercalated chains existed in states with varying degrees of order. Generally as the interlayer packing density or the chain length decreases (or temperature increases), the intercalated chains adopt a more disordered, liquid like structure, resulting from an increase in the gauche/ trans conformer ratio. As the available surface area per molecule reaches a certain range, the chains are not completely disordered but retain some orientational order similar to that in the liquid crystalline state demonstrated in Figure 1–10.
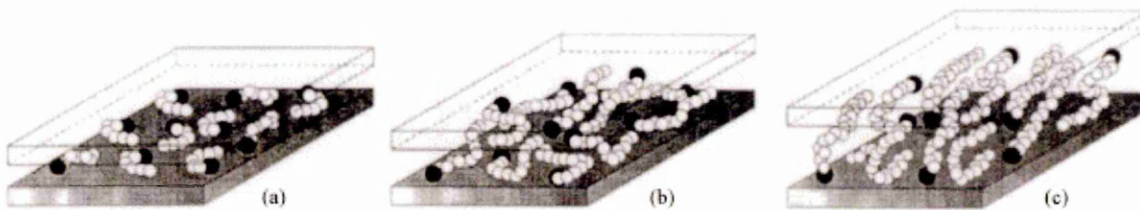
Figure 1–10 Alkyl chain aggregation models: (a) short alkyl chains: isolated molecules, (b) medium chain lengths: form quasi bilayers and (c) longer chain length: increased interlayer order, liquid-crystalline polymer environment [1-80].

1.4.5 Organically Modified Clays

Adsorption of organic cations renders the clay layer surface organophilic. Organo-modified clays can be used as gelling agents, fillers, thickeners, chromatography column packing materials and for sorption of hydrophobic pollutants [1-38]. Quaternary alkylammonium cations are the most common organic modifiers used to improve the compatibility between polymers and clay surfaces. This is because they readily exchange with the inorganic cations situated between the layers of clays like MMT. However, other compatibilising agents have recently been used to produce PLSNs, which either participate in or initiate the polymerisation process. Ethylene-vinyl alcohol (EVOH) copolymers have been shown to incorporate hydroxylated quaternary alkylammonium cations. These cations greatly improve the compatibility between the clay and the EVOH through the introduction of favourable hydroxyl group interactions. Other suitable compatibilising agents for the synthesis of nanocomposites with a variety of host polymers are listed by Ogawa *et al.* [1-81].

In other attempts to produce PLSNs, maleic anhydride grafted polypropylene has been shown to lead to the production of polypropylene-clay nanocomposites. The use of aminomethyl-styrene [1-82] and living free-radical initiators [1-83] has also been shown to have limited degrees of success in the formation of polystyrene-clay nanocomposites.

Jordan [1-84] was the first to discover that organoclays could be dispersed in polar organic liquids, when long-chain alkylammonium ions were cation exchanged onto MMT, resulting in the formation of gels with a high liquid content. The compatibility of clay interlayer spaces with various polymers can be accomplished by modifying the silicate surface with organocations via a cation exchange reaction [1-85]. The cationic head group of the alkylammonium molecule preferentially resides at the layer surface, while the

aliphatic tail radiates along or away from the surface. The nature of the interlayer space is altered by the presence of these aliphatic chains modifying it from its hydrophilic state to a hydrophobic/organophilic state. The organocations may also contain various functional groups, which could react with polymers and improve the adhesion between the clay platelets and a host matrix. Therefore, it is possible to obtain a good dispersion of organoclays in organic solvents and increase the *d*-spacing of a swelling clay by increasing the alkyl chain length and/or the charge density of the clay [1-86].

The most widely used alkylammonium ions are produced by protonation of the amine function of primary alkylamines in an acidic medium. The basic formula of an alkylammonium cation is $CH_3\text{-}(CH_2)_{n-1}NH_3^+$, where *n* is between 1 and 17. Interestingly the length of ammonium ions has a strong impact on the resulting structure of the nanocomposite. Alkylammonium ions based on secondary amines have also been successfully used [1-87].

In the early 1990's, Lan and Pinnavaia [1-86] used alkylammonium exchanged clays during a study of the formation of epoxy resin-clay nanocomposites. Three types of Na-MMT were cation exchanged with $CH_3(CH_2)_{n-1}NH_3^+$, where *n* = 7, 11, 17, which produced different results depending on the nature of the clay. XRD and composite testing showed that the synthesis of delaminated nanocomposites was favoured by exchange with alkylammonium cations with a chain length greater than $C_n = 8$ whereas alkylammonium cations with shorter chain lengths led to the formation of intercalated nanocomposites [1-85, 1-86]. This study was validated by Messersmith and Giannelis [1-88] who incorporated functionalised quaternary alkylammonium cations (i.e. $CH_3(CH_2)_{17}N^+CH_3(CH_2OH)_2$) in epoxy resin materials.

1.4.5.1   Hofmann Degradation of Alkylammonium Surfactants

The elimination reaction known as the Hofmann degradation reaction is able to convert ammonium salts to alkenes and ammonia. This reaction could be thermally driven in the case of *n*-alkylammonium cations, ammonia would be released as the temperature increased. Nucleophilic substitution reactions (SN^2) would occur between the hydrogen atoms on the alkyl chain's β-carbons and hydroxyl groups on the clay surface. The *n*-alkylammonium decomposition pathway would produce ammonia, while tertiary methyl

amino groups would be produced in the case of quaternary alkylamines, as well as alkenyl fragments and water.

The proximity of the Lewis base sites (i.e. hydroxyl groups) and the basic aluminosilicate surface to the intercalated alkylammonium molecules in organoclays would enhance (i.e. lower the activation energy of) the Hoffmann degradation. This has been shown by the lower onset temperature of the thermal desorption of alkylammonium cations in organoclays compared to their virgin state and increased alkene production [1-89]. The presence of branched alkanes also implies that secondary reactions, such as alkene addition, may occur between desorption products, complicating a simple explanation of product generation.

1.5   Polymers, Composites and Nanocomposite Principles

PLSNs are formed through the union of two very different materials namely organic polymers and specific clay minerals. A PLSN is a polymer that contains well dispersed nanometre sized (i.e. 10^{-9} m) clay particles.

1.5.1   Polymers

The polymer industry has been built with synthetic chemicals as its basis, however, this has begun to change in the past decade with the introduction of polylactic acid and other polymers derived from biomass [1-90, 1-91]. Polymers originated in the 1930s when polyvinyl chloride (PVC ~ originally reported by Baumann, 1870) was commercially developed (by BASF). Carothers [1-92] working at Du Pont synthesised polyesters, neoprene and the first polyamide - nylon 66, a replacement for silk patented in 1935. The need for commodity independence in times of war accelerated development in the synthetic polymer industry.

Other polymers developed during this period were; polyethylene (PE) by ICI, polymethylmethacrylate (PMMA) (trade name acrylic) also by ICI, Perspex, whose shatter-resistant properties were first applied to protective screens and aircraft canopies and polystyrene (PS) developed by BASF but originally reported by Simon (1839) and again by Staudinger (1922). PS was not mass produced until 1937. Since this early

period new polymers have been introduced every few years including polytetrafluoroethylene (PTFE/Teflon), polycarbonate (PC), polyethylene terephthalate (PET), polypropylene (PP), polyurethane (PU) and acetal [1-93].

During the period 1935-1945 other materials that were developed include silicones, used in heat resistant paints and as water repellents, epoxy resins which have excellent adhesion and chemical resistance properties and polyester resins which, when combined with glass fibre offer a structural material for boat and car bodies. Due to many of these polymers becoming malleable when heated, they became generically referred to as "plastics", a term taken from the Greek word "plastikos" meaning "to be moulded". Plastics are classified as either being Thermoplastic or Thermoset:

- *Thermoplastics* – Are polymers that soften when heated. Examples include Polyamides (PA), Polyolefins, (PO), PTFE and nylons.
- *Thermosets* – Are plastics that become hard with the application of heat. A chemical reaction is usually the heat source, generating heat in the liquid plastic, causing it to become hard. Examples include unsaturated polyester resin, epoxy resin and polyurethanes.

Preparation of polymer clay nanocomposites with a thermoset matrix is simpler for two reasons: (1) the monomers or oligomers show low viscosity, and (2) they are polar. Thus there are many publications and patents, especially for epoxy-based nanocomposites [1-87, 1-94, 1-95].

1.5.2   Polymer Additives

Polymers and polymer derivatives have been applied to an increasingly varied range of products and components particularly in the food packaging industry where traditional glass, metal and paper continue to be replaced by polymers. To reduce the weight of cars and improve manufacturing methods the automotive industry has replaced some under the bonnet parts with plastics. Polymers however, have certain limitations in both the food packaging and the automotive industries. In the packaging industry, certain oxygen sensitive foods (e.g. beer and tomato products) cannot be stored in polymer containers due to the oxygen permeability of the polymer. The use of polymers in

automotive applications is limited due to the tendency of plastics to warp and creep under heat and load pressure because of low stiffness and tensile strength.

Polymer disadvantages include;

- Poor mechanical properties, such as strength, stiffness, Young's modulus, hardness, shear strength etc;
- Poor processing properties including complex viscosity.
- Poor stability in oxygen, light and flame.
- High heat generation under curing and dynamic conditions.
- Easy crack initiation and crack propagation.
- Expensive.

Polymer materials are usually reinforced with fillers (fibres and metals) to improve mechanical properties. One of the most common reinforcing materials is a fibrous filler in a randomly dispersed state. Theories by Cox [1-96] and Kelly [1-97] are commonly employed to estimate the reinforcing effect of fibrous fillers. These fillers, fibres and metal are classified into a large number of groups depending on their function, some of these are presented below [1-98]:

- Fillers (30-150 wt%), used to increase bulk, modulus, stiffness, tensile strength, fatigue strength, shear strength, abrasion resistance and to reduce crack initiation/propagation. e.g. silica, clay, and zinc oxide.
- Extenders (10-30 wt%), tolerated by the polymer up to a certain extent, to reduce the product cost. e.g. refinery oil and chlorinated wax.
- Antioxidants (0.1-10 wt%), to prevent oxidation of the polymer in the presence of oxygen/air. e.g. acetone-diphenylamine-acetone-amine, and 4,4'-dioctyldiphenylamine.
- Cross-linking agents (0.1-5 wt%), used to increase hardness, modulus, stiffness, tensile strength, fatigue strength, shear strength, abrasion resistance and reduce crack initiation/propagation. e.g. sulphur and hydrogen peroxide.
- Coupling agents (10 wt% of filler), used for good adhesion between the filler and polymer. e.g. coating $CaCO_3$ with stearic acid.
- Fire Retardants (0.1-5 wt%), used to reduce polymer degradation against flame. e.g. triethyl phosphate, dimethyl methylphosphonate and brominated flame retardants.

Composite materials exhibit a number of improved properties in comparison with pure polymers. Composites have become very popular for structural applications and are sold in million tonne quantities [1-99]. From these quantities it has been shown that modified polymers already command a large market share in the plastics industry.

Interest in nanometre-size materials has increased in recent years owing to advances in synthetic techniques and the ability to readily characterise materials at the atomic level. Nanometre-size plates, grains and fibres have a considerably increased surface area and different chemistry when compared to traditional polymer additives. Carbon black/acetylene black (for the improvement of rubber) is produced by thermal decomposition of acetylene gas and known to have surface areas that are >1000 m^2/g, and have particle sizes <50 nm [1-100]. Carbon black also imparts UV protection, enhanced conductivity and structural reinforcement [1-101].

1.5.3 Polymer Flammability

Most plastics are carbon based materials and will burn producing gases and smoke when subjected to a flame. Plastics are excellent fuels and are generally classed as ordinary combustibles falling into the same category as wood, leather and many other common materials. All of these materials will degrade at very high temperatures into volatile and gaseous combustion products.

1.5.3.1 The Polymer Combustion Process

The actual process of combustion for plastics is very complex, however it generally follows 6 separate stages:

1. Primary Thermal - The ignition source heats the bulk plastic to create a rise in temperature depending on the product and the ignition source energy output.
2. Primary Chemical - Under the influence of the ignition source the heated plastic starts to degrade, through the formation of free radicals.
3. Polymer Decomposition - The plastic starts to rapidly degrade into a range of lower molecular weight decomposition products. Typical products at this stage are combustible gases and liquids, charred solids and possibly smoke.

4. Ignition - The combustible gases ignite and start to combust in the presence of sufficient oxygen and the ignition source. It is the combustible gases and liquids that burn and not the bulk material.

5. Combustion - The burning gases produce combustion at or near the surface of the bulk plastic. If the process produces sufficient energy it can become self-sustaining.

6. Flame Propagation - Depending on the plastic, the combustion stage produces flames (which can propagate) and charred surface layers. This can be accompanied by the emission of smoke and toxic gases.

The response of plastics in the combustion process also depends on the type of plastic. Thermoplastics tend to soften and flow at high temperatures, often before ignition takes place whereas thermosetting materials do not soften but undergo localized surface charring (sometimes with flaming) and the charred residue can either fall off or remain in place to form an insulating layer.

1.6 Polymer/Clay Nanocomposites

The first material to be commercialised was a nylon-6/montmorillonite hybrid developed at the Toyota Research Laboratory in 1988 [1-102] however, as far back as 1976 Unichika (Japan) filed a patent for a nylon-6/montmorillonite nanocomposite. Melt intercalation failed to disperse alkylammonium exchanged clays, so in-situ polymerisation of ε-caprolactam into C_{12}–ammonium exchanged montmorillonite was employed and was found to produce a composite with largely improved properties [1-103]. Publication of these findings sparked a worldwide interest in these materials and many polymer/ clay systems have been developed.

Nanocomposites are two phase materials with one phase whose dimensions are on the nanometer (10^{-9} m) scale being dispersed in a second [1-46]. Classification of nanofillers is in accordance with the number of dimensions of the material that are on a nanometer scale as summarised in Table 1–7.

Table 1–7 Types of Nanofiller Materials [1-20]

Number of dimensions on nanometer scale	Type of Nanofiller
One	Layered Crystals, e.g. Clay
Two	Nanotubes or Whiskers
Three	Spherical Silica Nanoparticles

PLSNs present a radical alternative to conventional filled polymers [1-15]. Owing to the nanometre-size particles obtained by dispersion of the clay, these nanocomposites exhibit markedly improved mechanical, thermal, barrier, optical and physico-chemical properties when compared with the pure polymer or conventional (microscale) composites as first demonstrated by Kojima *et al.* [1-104] for nylon-clay nanocomposites.

1.6.1   Structure of PLSNs

Layered silicates generally have layer thickness in the order of 1nm and have a high aspect ratio (e.g. 10-1000) and 1g of completely dispersed clay has a surface area of 760 m^2g^{-1}. Therefore if a few weight percent of clay is properly dispersed throughout a polymer matrix then a much higher surface area for polymer/filler interaction is created as compared to conventional composites. There are three main types of composites that can be obtained when a layered clay is associated with a polymer, and is dependent on the nature of the components used (layered silicate, organic cation and polymer matrix) as displayed in Figure 1–11.
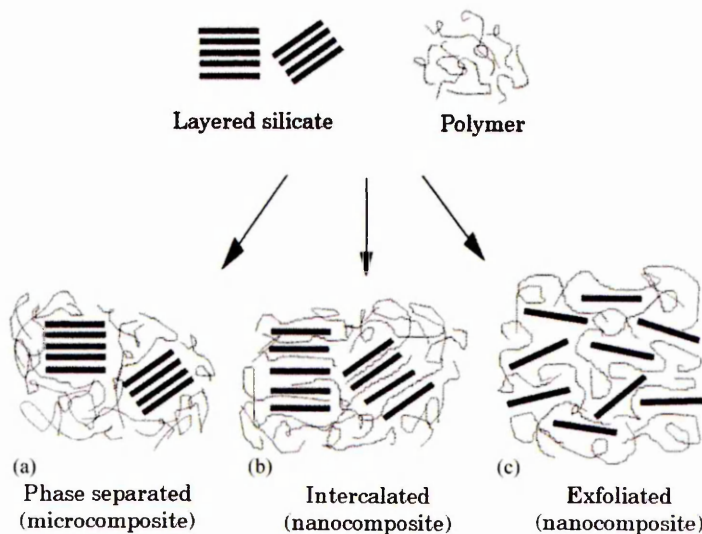
Figure 1–11 Structures of polymer/clay nanocomposites (not to scale).

A phase separated composite (Figure 1–11 a) is obtained when the polymer is unable to intercalate between the silicate sheets, its properties stay in the same range as traditional microcomposites. An intercalated structure (Figure 1–11 b) results when a single (and sometimes more than one) extended polymer chain intercalates between the silicate layers resulting in a well ordered multi-layer morphology that is built up with alternating polymeric and inorganic layers. An exfoliated or delaminated (Figure 1–11 c) structure is obtained when the silicate layers are completely and uniformly dispersed in a continuous polymer matrix, both ordered and disordered exfoliated nanocomposites can be achieved. Aggregated nanocomposites (Figure 1–12) are also possible, these are virtually the same as intercalated nanocomposites. However, silicate layers are some times aggregated due to hydroxylated edge–edge interactions of the silicate layers.

Aggregation is a condition in which clays, polymers or other small charged particles become attached and form a fragile structure. In dispersed clay slurries, aggregation occurs after mechanical agitation ceases and the dispersed clay platelets spontaneously form aggregates because of attractions between negative face charges and positive edge charges.

| Intercalated | Intercalated/Aggregated | Exfoliated |
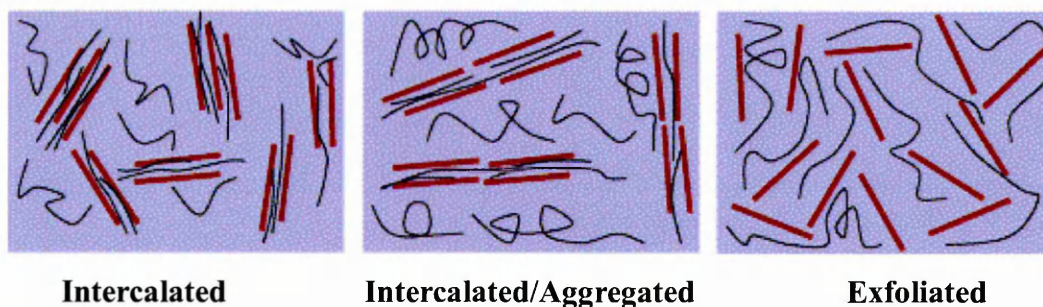
Figure 1–12 Schematic illustration of the three classes of thermodynamically achievable polymer/layered silicate nanocomposites [1-105].

To elucidate the structure of polymer/clay nanocomposites several methods are required to give complementary information. The most commonly used techniques are X-ray diffraction (XRD), which is used to give information on the spacing of the clay layers and crystallinity of the polymer and transmission electron microscopy (TEM), which allows the extent of clay dispersion to be observed. It is generally only used to confirm exfoliation after an 'XRD silent' trace has been obtained [1-41, 1-106]. Furthermore atomic force microscopy (AFM), nuclear magnetic resonance spectroscopy (NMR) and neutron scattering have been used to investigate the structure of polymer/clay hybrids [1-107].

Both XRD and TEM are essential tools for evaluating nanocomposite structures, however TEM is time-intensive and only gives qualitative information on a very small part of the sample, while low angle peaks in XRD allow quantification of changes in layer spacing. When the layer spacing exceeds around 80 Å in an intercalated nanocomposite or when the layers become significantly disordered in an exfoliated nanocomposite then XRD becomes less useful.

(a)   **(b)**
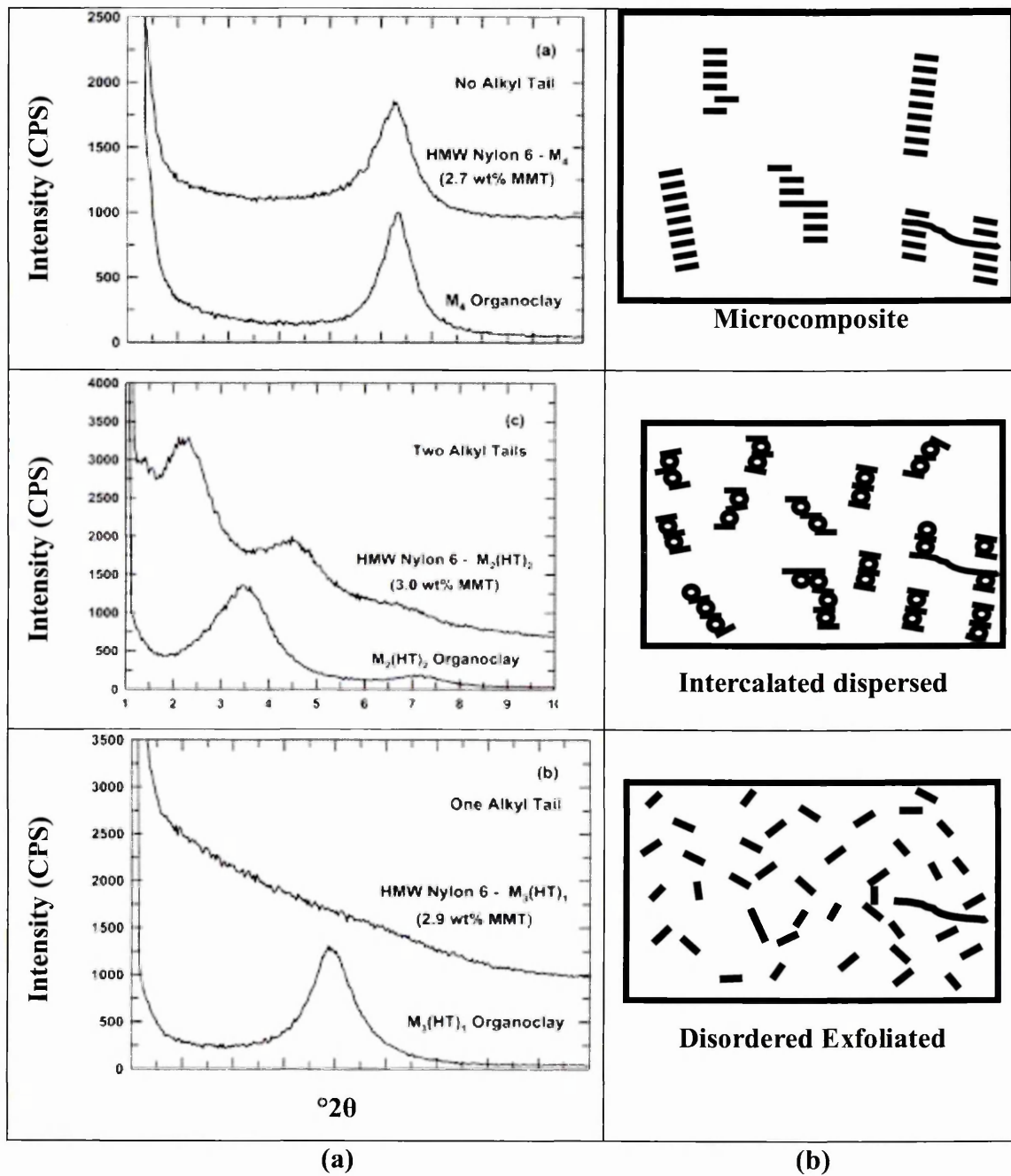
Figure 1–13 XRD traces for (a) Nylon-6 composites with different organoclays and (b) the corresponding arrangement of the clay layers [1-108].

Diffraction peaks are no longer visible in an exfoliated structure. Two possibilities for this are, (1) there is no clay in that part of the sample, or (2) the samples include clumps of disordered clay that do not diffract. Figure 1–13 displays the XRD traces and the corresponding arrangement of the clay layers within nylon-6/organoclay (nano) composites. Besides these well-defined structures, other intermediate organisations can also exist.

1.6.2   Nanocomposite Preparation

Nanocomposites can be prepared via different routes. There are four main preparation methods and the choice of method is dependent on the type of clay and the properties of the polymer matrix [1-109] utilised. In-situ polymerisation and solution intercalation are often limited in their use in technological applications as compatible clay/ monomer systems or clay/ polymer/ solvent systems are not always available [1-110].

1.6.2.1   In-Situ Intercalative Polymerisation

The first method used to synthesis PLSNs based on polyamide 6 [1-4] was in-situ polymerisation. The organosilicate is swollen with the liquid monomer (or monomer in solution) therefore allowing polymer formation to occur in between the intercalated sheets. Polymerisation can be initiated by heat, radiation, diffusion of a suitable initiator or by fixation of an organic initiator inside the galleries before the monomer swelling step. The key to this method is to control the rate of polymerisation occurring between the silicate layers (intragallery polymerisation). Polymer layered silicate nanocomposites based on thermosets such as epoxies, unsaturated polyester, and polyurethanes have been synthesised by this method as well as thermoplastic nanocomposites based on polyethylene terephthalate [1-111], polystyrene and polymethyl methacrylate (PMMA) [1-112].

1.6.2.2   Exfoliation-adsorption

By using a solvent in which the polymer (or prepolymer) is soluble the layered silicate can be exfoliated into single layers. Such layered silicates can be easily dispersed in an adequate solvent due to the weak forces that stack the layers together. The polymer is then adsorbed onto the delaminated sheets and when the solvent is evaporated (or the mixture precipitated) the sheets reassemble, sandwiching the polymer to form an

ordered multilayer structure. The major advantage of this method is that it is possible to synthesise intercalated nanocomposites based on polymers with low or even no polarity. However, due to the large quantities of solvent used in this approach, it is difficult to execute the exfoliation-adsorption process in industry. Nanocomposites based on high-density polyethylene, polyimide and nematic liquid crystal polymers [1-113] have been synthesised by this method.

1.6.2.3   Melt Intercalation

Melt intercalation was first reported by Vaia et al. [1-25] in 1993 and is applicable to a wide range of commodity polymers [1-114]. In order to optimise the polymer-layered silicate interactions the layered silicate is mixed with the polymer matrix in a molten state. The mixture is then annealed at a temperature that is above the glass transition temperature of the polymer to form the nanocomposite, and either an intercalated or an exfoliated nanocomposite can be formed. The melt intercalation process is increasingly popular due to its potential for application with rapid processing methods such as injection moulding. Silicate layers have been exfoliated and/or intercalated into a wide range of thermoplastics, from strongly polar nylon 6 to polystyrene using the melt intercalation process.

1.6.2.4   Template Synthesis

This method was first proposed by Carrado et al. [1-115] and is the in-situ hydrothermal crystallisation of silicate layers (hectorite) in an aqueous polymer gel. This method has been used for the synthesis of double-layer hydroxide-based nanocomposites [1-116] but is less advanced for layered silicates. Based on self-assembly forces, the polymer aids the nucleation and growth of the inorganic host crystals and gets trapped within the layers as they grow. This method is particularly suited to water soluble polymers such as poly(acrylonitrile) (PACN) and poly(aniline) (PANI). The driving force of this technique is the balance between the negatively charged sites on the silicate lattice with those on the cationic polymer chain. Unfortunately the size of the synthesised layers cannot compete with natural layered silicates for kinetic reasons and their average length is limited to around one third of their natural counterparts.

1.7   Nanocomposite Property Enhancements

Fukushima and Inagaki [1-117] proved that the surface chemistry of the clay could be made compatible with a hydrophobic polymer matrix, by the replacement of the inorganic cations in the clay galleries with alkylammonium cations. E-caprolactam was polymerised in the interlayer region of the organoclay to form a nylon(6)–clay nanocomposite [1-118]. With clay loading of only 4.2 wt%, the hybrid exhibited a doubling of modulus, a 50 % increase in strength, and an increase in the heat distortion temperature (HDT) of 85 °C compared to the pristine polymer (Table 1–8).

Table 1–8 Comparative physical data for Nylon-6, Nylon-6-MMT composite and Nylon-6-MMT nanocomposite [1-11, 1-118].

Sample	Clay (Wt%)	Tensile Strength (MPa)	Tensile Modulus (GPa)	Impact (KJ/m³)	HDT (°C @ 18.5 Kg/cm²)
Nylon-6-MMT Nanocomposite	4.2	107	2.1	2.8	152
Nylon-6-MMT composite	5.0	61	1.0	2.2	89
Nylon-6	0	69	1.1	2.3	65

Table 1–9 Nanocomposite suppliers, components and applications.

Company	Material	Application
Bayer AG (Durethan LPDU)	Nylon 6	Barrier films
Clariant	PP	Packaging
GE Plastics (Noryl GTX)	PPO/Nylon	Automotive painted parts
Honeywell (Aegis)	Nylon 6	Multi-purpose Bottles and film
Hyperion	PETG, PBT PPS, PC, PP	Electrically conductive
Kabelwerk Eupen of Belgium	EVA	Wire and cable
Nanocor (Imperm)	Nylon 6 PP Nylon MDX6	Multi-purpose Molding PET beer bottles
Polymeric Supply	Unsaturated polyester	Marine, transportation
RTP	Nylon 6, PP	Multi-purpose, electrically conductive
Showa Denko (Systemer)	Nylon 6 Acetal	Flame retardance Multi-purpose
Ube (Ecobesta)	Nylon 6, 12 Nylon 6, 66	Multi-purpose Auto fuel systems

It was also demonstrated that organoclays exfoliated in a nylon-6 matrix greatly improved the dimensional stability, the barrier properties and even the flame retardant properties [1-12, 1-119, 1-120]. The breakthrough with the nylon-6-MMT nanocomposite led to the first practical application as the material was used for the timing belt covers on Toyota Camry vehicles [1-121]. Table 1–9 displays a partial listing of companies marketing nanocomposite materials for different applications.

Polymers filled with nanometre-size materials have different properties than polymers filled with conventional materials. Some properties attributed to nanocomposites, such as increased thermal stability and tensile strength can be achieved by using higher conventional filler loadings. However, this is at the expense of increased weight of the material. Futhermore, properties like material clarity or improved barrier properties cannot be duplicated by filled resins at any loading. During delamination of the clay agglomerates, the clay structure reduces from cuboid agglomerates to flat platelets. The shape of clay platelets is usually expressed in terms of its aspect ratio, i.e. the ratio between the diameter and the thickness of a platelet. Mülhaupt et al. [1-122] summarised the advantages and disadvantages of nanocomposites compared to traditional fillers and pristine polymers, as displayed in Table 1–10.

Table 1–10 Advantages and disadvantages of polymer/ clay nanocomposites.

Advantages	Disadvantages
- improved gas/liquid barrier properties - increased thermal stability and fire resistance - improved abrasion resistance - altered electronic and optical properties - reduced shrinkage and residual stress - increased mechanical properties - low specific density - improved stiffness in flexible polymers - smooth surfaces - recyclable - control of biodegradation e.g. polylactic acid and starch - dispersion and fixation of pigments and fillers	- production costs - reduced extensibility in some thermoplastic blends - discolouration in cation activated bentonites - orientation and properties dependent on direction of shear - no adequate replacement of silica or carbon fibre reinforcement yet - high adhesive content in non-polar polyolefins

1.7.1 Flame Retardancy of Nanocomposites

Fire hazards result mainly from the combination of different factors. These include: ignitability, ease of extinction, flammability of generated volatiles, amount of heat released on burning, rate of heat release, flame spread, smoke obscuration and smoke toxicity. However, the most important fire hazards can be identified as heat, smoke and toxic gases [1-123]. A high heat release rate causes fast ignition and flame spread. It also controls the fire intensity and is therefore more important than ignitability, smoke toxicity or flame spread. The escape time for fire victims is also controlled by the heat release rate. Another important fire hazard is smoke production. People become disoriented in dark black smoke and therefore their escape from a burning building is hindered, also fire fighters have severe problems when rescuing people in smoke-darkened surroundings. The acute toxicity of fire gases is mainly controlled by the carbon monoxide content. Carbon monoxide is responsible for over 90% of people killed by fires [1-124].

Each year approximately 5000 people are killed by fire in Europe and more than 4000 people in the USA. Consequently it is important to develop well-designed flame retardant materials to minimise these fire hazards [1-125]. Polymers are increasingly used in new and varied applications, where specific mechanical, thermal and electrical properties are required. Another important property is the flame retardant behaviour of the polymers and this can be achieved through two routes:

- Use of intrinsically flame-retardant polymers like PVC or fluoropolymers.
- Use of flame retardants, such as aluminium trihydrate, magnesium hydroxide, brominated organic additives or intumescent systems to prevent the burning of polymers including PE, PP, UP.

However, these flame retardant systems can exhibit some significant disadvantages:
- The applications of aluminium trihydrate (ATH) or magnesium hydroxide requires very high loadings of the filler within the polymer matrix. Loading levels of more than 60 wt% are necessary to achieve a suitable flame retardancy, e.g. for cables and wires.
- In Europe, there are health and safety reservations about the general use of brominated additives as flame retardants.

- Intumescent systems are relatively expensive and electrical conductivity requirements can restrict the use of these products.

Nanocomposites avoid the outlined disadvantages of these traditional flame retardant systems. Nanocomposites have the ability to promote flame retardancy at very low filler levels (2-10 wt%) due to the formation of a thermally insulating char which has a low permeability to volatile combustion products caused by a fire [1-126]. The low filler contents in nanocomposites offering improvements in flame retardancy are highly attractive for the industry because the end-products can be made cheaper and are easier to process.

1.7.2 Thermal Stability

Thermogravimetric analysis (TGA) is generally used to study the thermal stability of polymeric materials. The weight loss, due to the formation of volatile products after degradation at high temperature, is monitored as a function of temperature. Heating under an inert gas flow results in a non-oxidative degradation (pyrolysis), while the use of air or oxygen allows oxidative degradation of the samples. Thermal stability is enhanced by the incorporation of silicate in the polymer matrix, the silicate acts as a superior insulator and mass transport barrier to the volatile products generated during decomposition [1-127]. Blumstein first indicated thermal stability improvements in nanocomposites [1-23], in a study on the thermal stability of poly (methyl methacrylate) (PMMA) intercalated with montmorillonite.

Burnside and Giannelis [1-30] used TGA (under N_2) to measure the thermal stability of cross-linked poly(dimethylsiloxane) (PDMS) in which 10 wt% of organo-MMT was exfoliated. When compared to unfilled cross-linked PDMS (Figure 1–14), the TGA displayed a large shift in weight loss towards higher temperature, with a stabilisation as high as 140 °C at 50 % weight loss. This was attributed to hindered out-diffusion of the volatile decomposition products (i.e. mainly cyclic silicates), as a direct result of the decrease in permeability predicted for exfoliated nanocomposites.
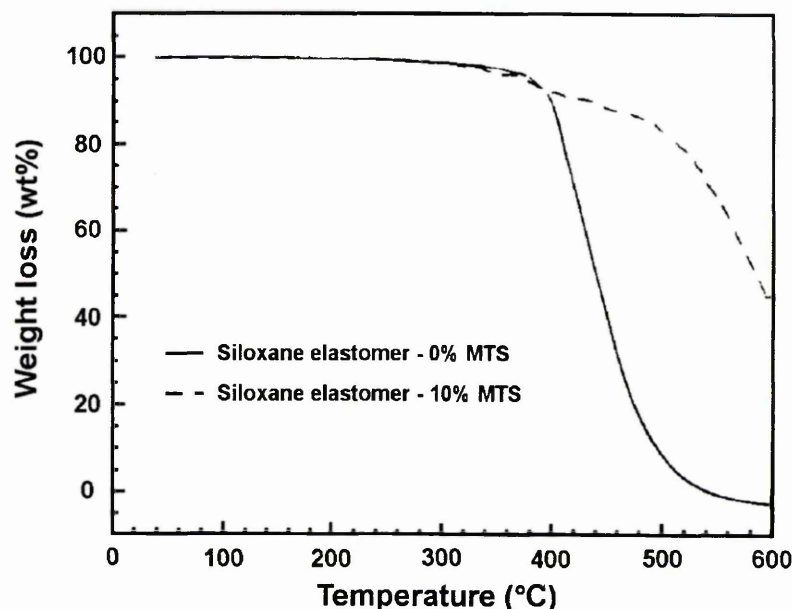
Figure 1–14 TGA traces for PDMS (solid line) and PDMS nanocomposite (dashed line) containing 10 wt% organo-modified MMT [1-30].

Another nanocomposite study based on cross-linked PDMS was conducted by Wang *et al.* [1-128] using slightly different processing conditions in order to produce mainly intercalated structures. These materials exhibited increased thermal stability for nanocomposites intercalated with 8.1 vol% of org-MMT but it was limited to about 60 °C at 50 % of weight loss. The increased thermal stability (also reported for silica-based nanocomposites in the same study) was attributed to the inactivation of the active centres in the main silicone chain, decomposition by interaction with the filler or by prevention of the unzipping degradation occurring through physical and chemical cross-linking points built up between polymer chains and filler particles.

A shift to a higher decomposition onset temperature was reported for intercalated nanocomposites of PMMA [1-129], PS [1-130] and Epoxy [1-131] when prepared by emulsion polymerisation in the presence of water swollen Sodium MMT (Na-MMT). The onset of thermal decomposition by TGA (under N_2) was measured by Doh and Cho [1-132] for intercalated PS-based nanocomposites produced by polymerisation of styrene containing various org-MMTs. The decomposition onset temperatures of PS-based nanocomposites with increasing filler content were collected together with a Na-MMT microcomposite for comparison. A large increase in the onset of decomposition occurred for nanocomposites at very low filler content and quickly levelled off at 430 °C. The threshold was reached for a filler content as low as 0.3 wt% when intercalating

35

an organoclay modified with a dimethylbenzyloctadecylammonium cation, which was considered to be compatible with PS. In contrast, Na-MMT did not modify the decomposition onset of the PS matrix. Another useful feature of nanocomposites in which the thermal property improvements occur at very low filler content, is that it often makes the final product cheaper, lighter and easier to process than more conventional microcomposites.

The extent of the thermal stabilisation in nanocomposites may also arise from the nature of the thermal degradation mechanism, which is often different from one polymer to another. When polyimide-clay nanocomposites were thermally degraded under N_2, their thermal stability was only enhanced by approximately 25 °C (at 50% of weight loss), which was much less than a shift of 140 °C observed in exfoliated PDMS nanocomposites [1-25, 1-133].

Zanetti et al. [1-134] conducted detailed TG analyses of nanocomposites based on ethylene-vinyl acetate (EVA). The inorganic phase used was either fluorohectorite (FH) or MMT, both exchanged with octadecylammonium cations. This study demonstrated that creation of nanocomposites by extrusion of EVA depended on both the type of silicate and the type of silicate modification. During thermal degradation, deacylation was accelerated and occurred at temperatures lower than those for the pure polymer due to catalysis by the strongly acid sites created by thermal decomposition of the silicate modifier. These sites were active when there was intimate contact between the polymer and the silicate. Slowing down volatilisation of the deacylated polymer in nitrogen may be due to the labyrinth effect of the silicate layers in the polymer matrix. In air, the nanocomposite presented significantly delayed weight loss derive from the barrier effect due to diffusion of both volatile thermo-oxidation products to the gas phase and oxygen from the gas phase to the polymer.

A significant delay in TGA weight loss has also been observed when heating under air, this may be attributed to barrier effects caused by diffusion of both volatile thermo-oxidation products to the gas phase and oxygen from the gas phase to the polymer. During volatisation the barrier effect increases due to the reassembly of the reticular layers of the silicate on the surface of the polymer [1-135]. Figure 1–15 displays the TGA

analysis of a polystyrene n-hexadecyl triphenylphosphonium clay nanocomposite (PS-P16) compared with virgin PS. The thermal stability of the nanocomposite is enhanced compared to that of the virgin polymer as the typical onset temperature of the degradation is around 50 °C higher for the nanocomposite than for virgin PS [1-136].
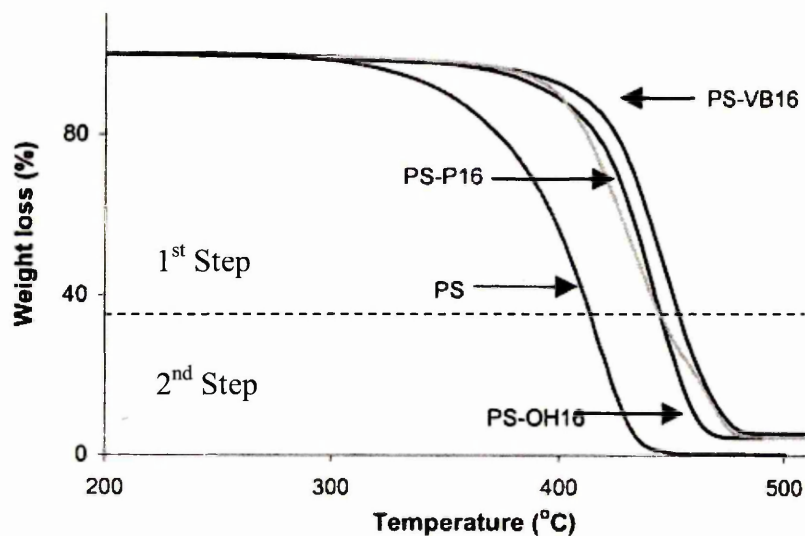
Figure 1–15 TGA curves for polystyrene, PS and the nanocomposites [1-136].

Figure 1–15 displays a difference in the degradation mechanism for phosphonium nanocomposites (PS-P16) as compared to ammonium nanocomposites (N,N-Dimethyl-n-hexadecyl-(4-vinylbenzyl) ammonium chloride (PS-VB16) and N,N-Dimethyl-n-hexadecyl-(4-hydroxymethylbenzyl) ammonium chloride (PS-OH16)). The nanocomposite made using PS-P16 appears to degrade by a two step process, with the second step accounting for approximately 30 % of the degradation of the phosphonium-PS nanocomposite and can be attributed to some interaction between the clay and the polymer assisting in stabilising the nanocomposite. A confident explanation for this phenomenon is that the increased decomposition temperature of the phosphonium clay provides the formation of char at an elevated temperature to retain the polymer [1-136]. However in the case of alkylammonium clays char formation occurs earlier and the char can be broken up by the time the polymer degrades.
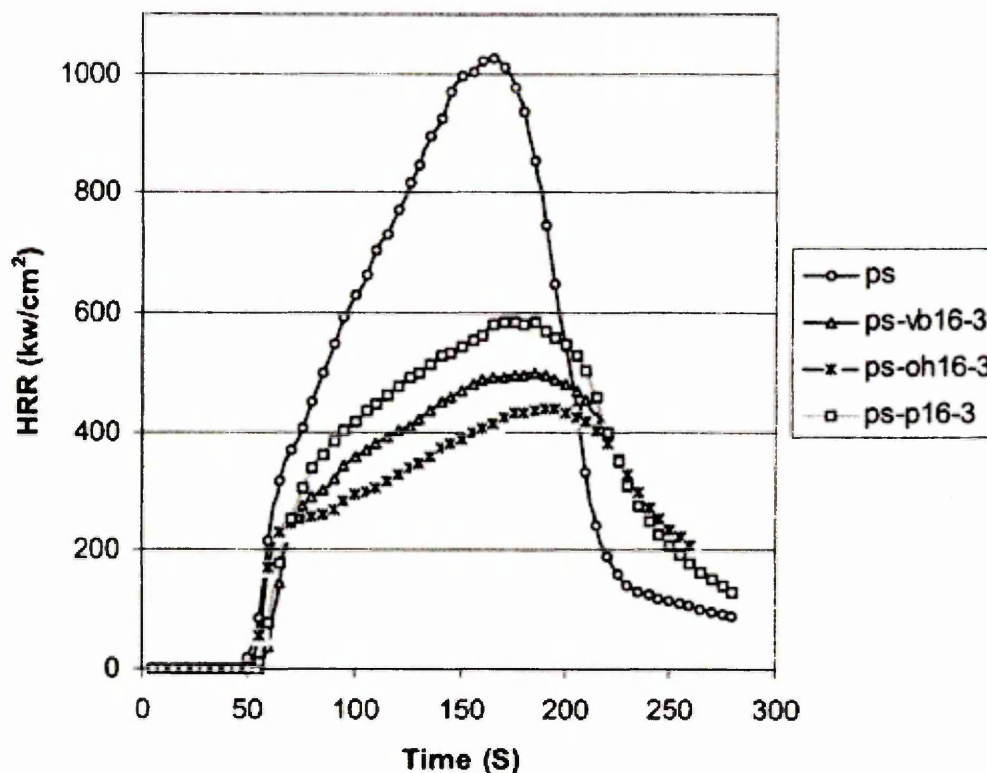
Figure 1–16 Peak heat release rates for polystyrene and the three nanocomposites [1-136].

The nanocomposites depicted in Figure 1–16 had much lower peak heat release rates (PHRRs) than the virgin polymer. Associated with the decrease in the rate of heat release was a decrease in the mass loss rate and the amount of energy released by the time at which polystyrene had entirely burned out and also a modest increase in the time at which the peak heat release was reached. The production of a char barrier served to retain some of the polymer and thus both the energy released and the mass loss rate decreased. The amount of smoke evolved and the specific extinction area, also decreased with the formation of the nanocomposite. It was apparent that phosphonium clays have greater thermal stability than the corresponding ammonium salts, which may be useful when polymer-clay mixtures are processed at relatively high temperatures.

1.7.3 Flame Retardancy

Gilman [1-12] reviewed the flame retardant properties of polymer-layered silicate nanocomposites using cone calorimetry (Figure 1–17). An improvement in flammability was revealed for many different types of PLSNs. Cone calorimetry is an effective bench scale method that measures fire relevant properties such as heat release rate (HRR), peak HRR, smoke production, and carbon monoxide yield. Typically the sample is exposed to a heat flux (often taken as 35 kW/m^2) and the HRR as well as the mass loss rate (MLR) are recorded as a function of time. Reduction of the peak HRR is the most clear-cut evidence for the efficiency of a flame retardant and is therefore the most important parameter in evaluating fire safety [1-137].
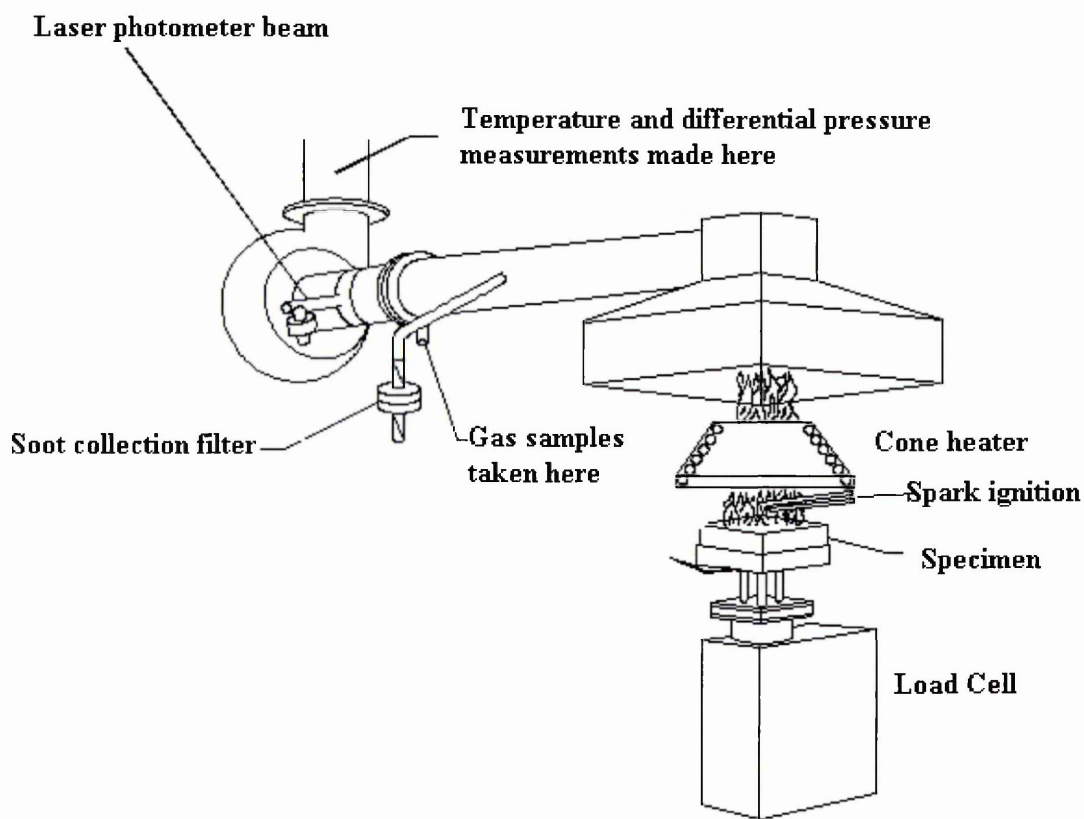
Figure 1–17 Cone Calorimeter [1-138]

A typical example is displayed in Figure 1–18 and peak HRR values in Table 1–11, where a HRR plot for nylon-6 was compared to that for a nylon-6 exfoliated nanocomposite (5 wt.% of exfoliated montmorillonite) at 35 kW/ m² heat flux. This plot is typical of those found for all the nanocomposites and shows a clear reduction in the peak HRR of 63 % as observed for a nylon-6 nanocomposite compared to pure nylon-6. The HRR is reduced in the nanocomposite, occurring over the temperature range of 280 to 1500 seconds as compared to between 300 and 1000 seconds for pure nylon-6. However, the time to ignition was also reduced by approximately 20 seconds in the nanocomposite sample as compared to nylon-6. The parameter that is primarily responsible for the lower HRR of nanocomposites is the MLR during combustion. The MLR obtained for nanocomposites is significantly reduced from the values obtained for the pure polymer [1-12].
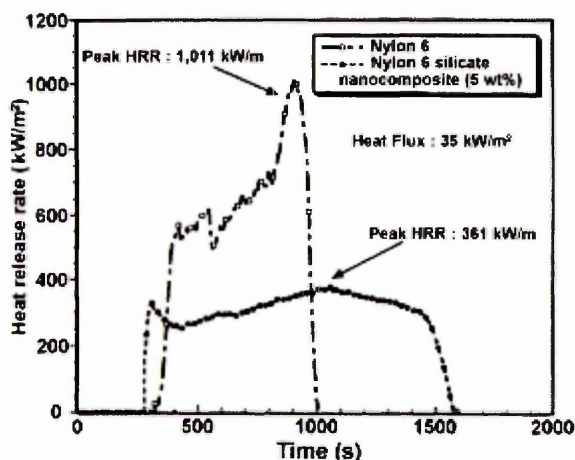
Figure 1–18 Comparison of the Heat Release Rate plot for nylon-6 and nylon-6 silicate nanocomposite [1-12].

Table 1–11 Peak HRR for Nylon-6 and Nylon-6 nanocomposites taken from cone calorimeter data [1-2]

	Peak HRR (kW/m²)
Nylon-6	1010
Nylon-6 nanocomposite 2%	686
Nylon-6 nanocomposite 5%	378

Comparison of cone calorimeter data for nylon-6, nylon-12, polystyrene (PS), and polypropylene (PP) nanocomposites revealed that the heat of combustion (H_c), and carbon monoxide yields were unchanged, suggesting that the source of the improved flammability properties of these materials is due to differences in the condensed phase decomposition process and not to a gas phase effect [1-139].

1.7.4 Fire Retardant Systems and Char Formation

The use of synthetic polymers in buildings or construction applications is steadily increasing and consequently more emphasis is placed on the hazards that result from the burning of such materials. The majority of polymer-containing end products must now pass regulatory tests and therefore considerable interest has arisen in the design of materials that can pass such tests. Although halogenated flame retardant systems have proven very effective, environmental concerns have prompted the development of alternative flame retardant systems [1-140]. Research into new fire-retardant systems covers a broad range of approaches, including the systematic investigation into combinations of additives that promote synergy [1-141], intumescent systems [1-135] and char formation [1-142]. Kashiwagi has identified char formation as the most promising of these and has reviewed the benefits of char formation in improving the fire resistance of polymers [1-143].

The advantages of char formation are:

- **Reduced mass of volatiles** - Part of the carbon (and hydrogen) stays in the condensed phase, reducing the mass of volatile combustible degradation fragments evolved.

- **Thermal insulation** - Polymer degradation results in a char layer forming over the remaining virgin polymer. This char layer has low thermal conductivity and enables it to act as thermal insulation therefore reducing the heat flux reaching the virgin polymer [1-144].

- **Obstruction of combustible gases** - A charred surface may act as a physical barrier, obstructing the flow of combustible gases generated from the degradation of the underlying un-burnt material [1-145].

- **Increased thermal capacity** - The formation of a char-polymer mixture increases the thermal capacity of the material relative to the scenario of no-char formation.

The flame retardant effect of a nanocomposite arises mainly from the formation of char layers obtained through the collapse of the exfoliated and/or intercalated structures during combustion. This multi-layered carbonaceous-silicate structure appears to enhance the performance of the char through structural reinforcement acting as an

excellent insulator and mass transport barrier, slowing down the escape of the volatile decomposition products as the polymer decomposes [1-146]. The most likely event occurring is the one illustrated in Figure 1–19 where a char layer has formed in between the clay layers giving an overall interlayer spacing of 12.6 Å.
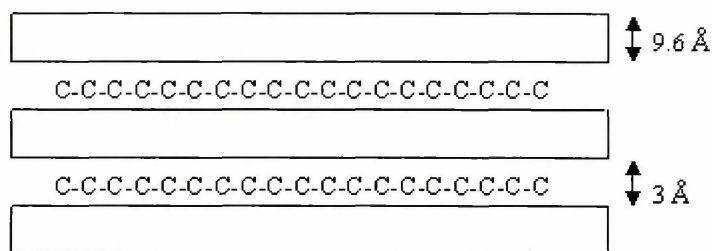
Figure 1–19 Illustration showing the formation of the char layer in between the clay layers.

Zanetti *et al.* [1-147] investigated the combustion behaviour of PLSNs based on ethylene co-vinyl acetate (EVA) using cone calorimeter experiments and demonstrated how the char layer forms after thermal degradation of the nanocomposite (Figure 1–20). A char layer forms on the surface of the nanocomposite as it burns, this layer insulates the material below and slows the mass loss rate of decomposition products. This residue layer is formed as the polymer burns away and the silicate layers reassemble into a multi-layer char, observed using TEM. It was found that the charring process was accelerated by acidic catalytic sites of the layered silicates, derived from the Hoffman reaction of the organic alkylammonium cation. Catalytic activity of zeolites (typically alluminosilicates) might depend on the presence of peroxides in their structure [1-148], generated during heat exposure in air. The role of catalysis in charring is indirectly supported by the fact that charring is only effective in the nanocomposite because the intimate contact between the polyene molecules and the atoms of the inorganic crystalline layers was so extensive that thermal bond scission was prevented. Only the surface of the nanocomposite, which is in contact with air, is charred and so this layer becomes an effective ceramic carbonaceous, thermally stable shield for the polymer, although they also prevent oxygen from diffusing into the bulk to extend its oxidative dehydrogenation carbonizing action.
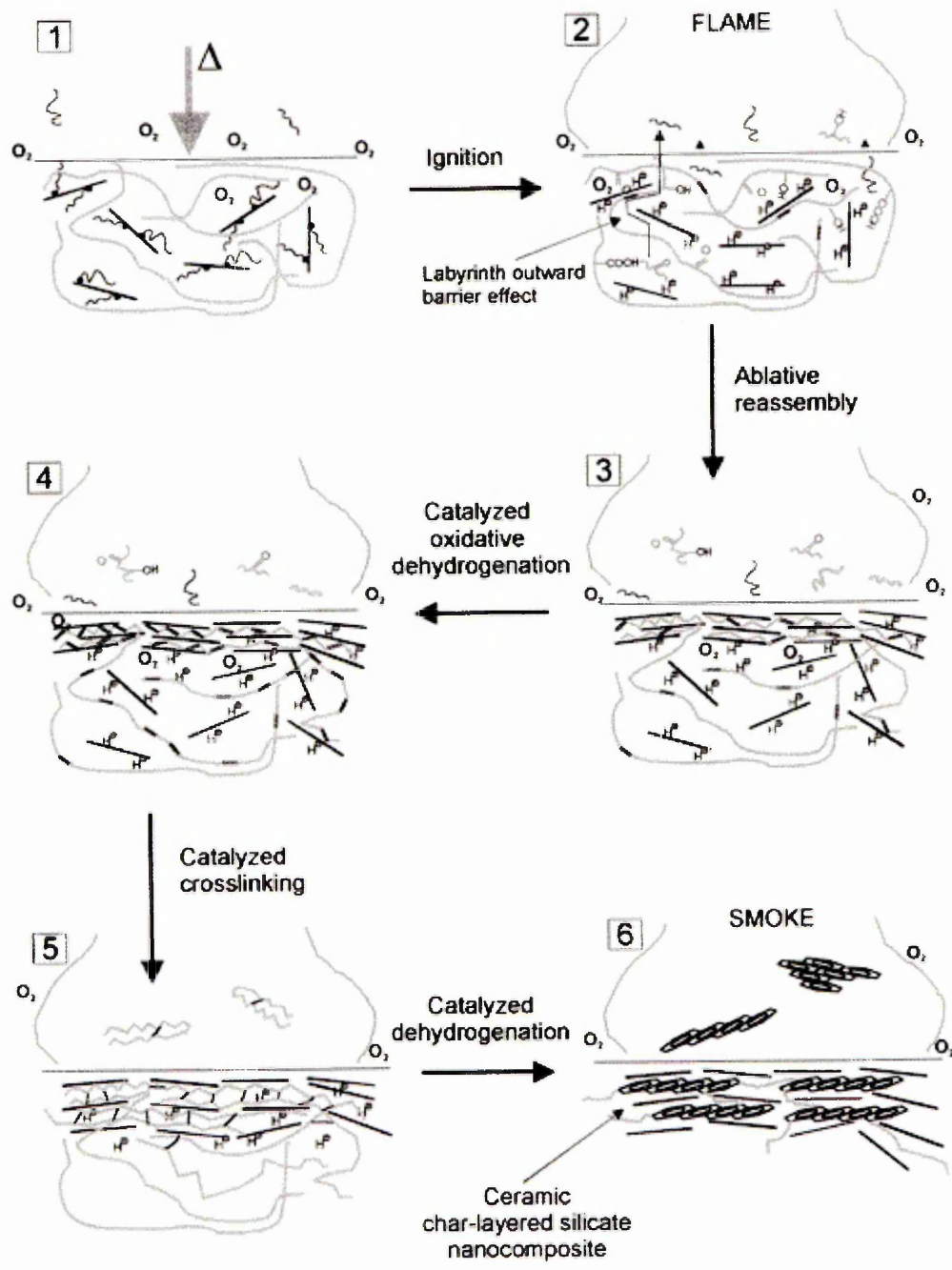
Figure 1–20 Schematic representation of combustion mechanism and ablative reassembly of a nanocomposite during cone calorimeter experiments [1-147].

A study by Gilman *et al.* [1-135] of the nylon-6 silicate nanocomposite pyrolysis process, under an atmosphere of nitrogen, revealed that a reduction in the MLR did not occur until the sample surface was partially covered with char. Visual observations of the pyrolysis demonstrated that when the MLR for nylon-6 silicate nanocomposite slowed, compared to the pure nylon-6, the surface of the silicate was over 50% covered by char.

1.7.5 Testing for Gases and Smoke

Toxic Gases - Toxic gases are the main source of death in many fires where high fuel loads of plastics are involved. However, there is no recognized standard for toxic gas emission testing, because the amount and type of toxic gas generated depends not only on the plastics involved but also on the additives used in the plastics and the details of the particular fire. For most conventional plastics the main gas risk is the generation of CO (exposure limit = 35 ppm, 40 mg/m^3), which at high concentrations is extremely toxic.

Smoke - A major hazard in real fires is the smoke given off when most plastics burn. The Smoke Box test developed by the National Bureau of Standards (NBS) is one of the most widely used laboratory-scale techniques to quantify the smoke generation from burning materials. This test measures the amount of smoke produced per unit area when a material is exposed to both flaming and radiant heat sources. The optical density of the smoke generated is measured as the smoke accumulates in a closed chamber system and test specimens can be burned in either the flaming or non-flaming (smouldering) mode.

1.7.6 Mechanical Property Enhancements of PLSNs

An unexpected large increase in the moduli (tensile or Young's modulus and flexural modulus) of PLSNs with organoclay loadings as low as 1 wt% has previously been revealed [1-119]. PLSN material stiffness was shown to be substantially enhanced whatever the method of preparation, polymerisation within protonated ε-caprolactam swollen MMT [1-16], and polymerisation of ε-caprolactam, an acid catalyst and natural MMT [1-17].

1.7.6.1 Tensile Modulus

The tensile or Young's modulus expresses the stiffness of a material. Remarkable improvements have been seen when nanocomposites are formed with layered silicates. Nylon-6 nanocomposites exhibit a dramatic increase in the tensile properties at relatively low filler content, when prepared through the in-situ intercalative ring opening polymerisation of ε-caprolactam using protonated aminododecanoic acid-exchanged MMT (ADA-MMT). The tensile modulus and other properties of exfoliated

nylon-6 PLSNs with various clay loadings were measured at 120 °C [1-119] (Table 1–12). The strong interaction between the matrix and silicate layers via the formation of hydrogen bonds is the main reason for this dramatic increase in tensile modulus.

Table 1–12 Property effects on Nylon-6-ADA-MMT with increased organoclay loadings [1-119].

Nylon-6- ADA-MMT (wt%)	Flexural Modulus (MPa)	Tensile Modulus (MPa)	HDT(°C)
0%	2836	2961	56
2%	4326 (53%)	4403 (49%)	125 (123%)
4%	4578 (61%)	4897 (65%)	131 (134%)
6%	5388 (90%)	5875 (98%)	136 (143%)
8%	6127 (116%)	6370 (115%)	154 (175%)

This remarkable improvement was first reported by the Toyota research group [1-4], an increase of 90% in which the modulus was found with the addition of only 6 wt% of exfoliated clay. They also found that the extent of the improvement to the modulus in their material was directly dependent upon the average length of the dispersed clay particles (i.e. the aspect ratio of the dispersed nanoparticles) [1-11].

A short review by Kornmann [1-109] concerning the moduli of PLSNs suggested that the stiffness of nanocomposites is related to the degree of exfoliation of the layered silicate in the polymer matrix. This is possibly because exfoliation increases the interaction between the silicate layers and the polymer by providing 360° access to the silicate layer by the polymer.

1.7.6.2   Impact Properties

The impact properties have been measured for nylon-6-based nanocomposites prepared either by in-situ polymerisation of ε-caprolactam using protonated aminododecanoic acid-exchanged MMT [1-119] or by melt intercalation of nylon-6 in octadecylammonium exchanged MMT [1-149]. Both methods lead to exfoliated nanocomposites especially at filler contents $\leq$ 10 wt% (at higher loadings, melt-intercalation provides partially exfoliated/partially-intercalated materials). An increase in the impact property of PLSN of Nylon-6-MMT was demonstrated (Table 1–8) as compared to the composite and pristine polymer.

1.7.6.3   Stress at Break

The stress at break expresses the ultimate strength that the material can bear before break. In intercalated and exfoliated PLSNs stress at break has been reported to vary greatly, depending upon the nature of the interactions between the matrix and the filler. In PS intercalated nanocomposites [1-130], the ultimate tensile stress was reported to be lower than the pristine polymer and the exfoliated PS nanocomposite, reducing further as the clay loadings were increased (Table 1–13).

Table 1–13 Tensile results for Nanocomposites of pure PS [1-130]

PS-MMT (wt%)	Stress at Max Load (Mpa)	Strain at Max Load (%)	Young's Modulus (Gpa)
0	28.7	2.87	1.21
5 (Exfoliated)	21.7	2.40	1.30
10	23.4	1.63	1.91
20	16.6	1.01	2.64
30 (Intercalated)	16.0	2.30	1.83

The benefit in strength for the strongly hydrophobic PS was not as great as that of the PMMA-clay hybrid. Suggesting that the reduced tensile strength in the nanocomposites was mainly attributed to poor interfacial adhesion between the PS matrix and the clay particles.

1.7.7   Barrier Property Enhancements of PLSNs

1.7.7.1   Permeability

A major advantage of PLSNs is the decrease in permeability brought about by the nanocomposites structure. This property was first reported by the Toyota research group, whose polyamide-6 clay hybrid had a water absorption rate that was reduced by 40% when compared to the pristine polymer. Phillip *et al.* [1-9] observed a dramatic decrease of water permeability with their poly(ε-caprolactone) layered silicate nanocomposite of up to 80% with only 5% volume of clay.

Enhancements in gas barrier properties are well known in PLSNs, however the dependence on factors such as the relative orientation of the sheets in the matrix and the state of aggregation and dispersion are not well understood. A study by Bharadwaj [1-8] has shed light on both of these issues by modifying a simple model, developed to

describe permeability in filled polymers on the basis of tortuosity arguments. By correlating the sheet length, concentration, relative orientation and state of aggregation, it was thought that better barrier materials could be designed using nanocomposites. The presence of fillers introduces a tortuous path for molecules that are diffusing through the composite. This reduces permeability by forcing the molecules to travel a longer diffusive path through the composite, as illustrated in Figure 1–21.
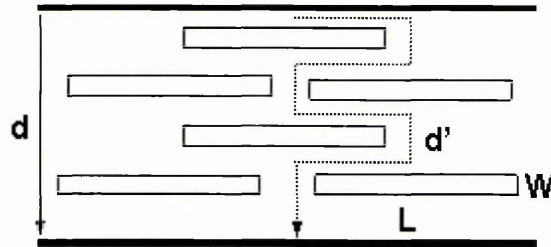
Figure 1–21 Tortuosity for a diffusing molecule introduced upon exfoliating layered silicates in a polymer matrix.

The sheet-like morphology of the silicate layers is particularly efficient at maximising the path length due to its large length to width ratio compared to other shapes such as spheres or cubes. The tortuosity factor (τ) is represented by the equation below and is defined as the ratio of the actual distance (d') that a penetrating molecule must travel to the shortest distance (d) that the molecule would have travelled in the absence of the layered silicate, this is expressed in terms of the length (L), width (W), and volume fraction of the sheets (ϕ_s):

$$\tau = \frac{d'}{d} = 1 + \frac{L}{2W}\phi_s \quad (1)$$

The effect of tortuosity on permeability is expressed as:

$$\frac{P_s}{P_p} = \frac{1 - \phi_s}{\tau} \quad (2)$$

where P_s and P_p represent the permeability of the PLSN and the pure polymer, respectively. In a study by Yano et al [1-10] H_2O permeability was measured for polyimide nanocomposites with 2 wt % of different silicates. Water permeability was reduced by a factor of 10 over the pure polyimide by dispersing 2 wt % of synthetic mica into the polyimide. The model predictions from equation 2 closely tracked the relative permeability as a function of the silicate sheet length. In addition equation 2

was found to accurately reproduce the observed concentration dependence of the relative permeability of H_2O in polyimide montmorillonite nanocomposites.

1.7.7.2   Effect of Sheet Orientation

Any movement away from the sheets orientating themselves perpendicular to the film plane would lead to deterioration in barrier properties. There is a range of possible orientations of the sheets with respect to each other as displayed in Figure 1–22, where 1 indicates perfect orientation i.e. parallel to film surface, - ½ indicates perpendicular or orthogonal orientation and 0 indicates random orientation. The two extremes planar and orthogonal alignment of the sheets can be treated simply by interchanging L and W in equation (1).
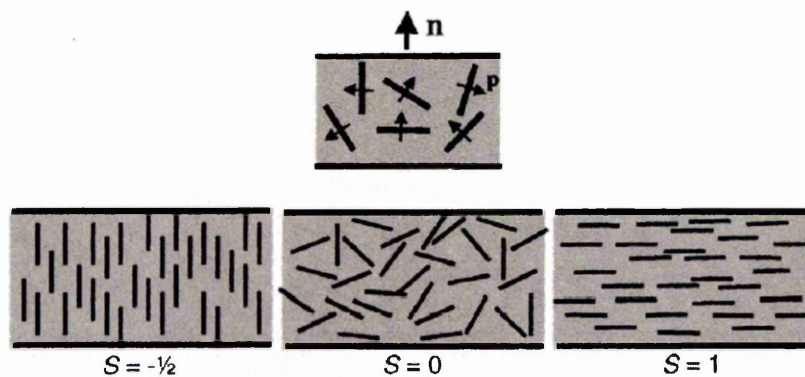
Figure 1–22 Definition of orientation of the direction of preferred orientation (n) of the silicate sheet normal's (p) with respect to the film plane. Three values of the order parameter (S) - ½, 0 and 1 are also displayed [1-8].

1.7.7.3   Solvent Resistance

The improved barrier properties of PLSNs also increase solvent resistance. A study by Heinemann et al [1-150] on epoxy clay nanocomposites demonstrated that these materials offered better resistance to organic solvents (such as alcohols, toluene and chloroform). This was even more apparent for solvent molecules that were small enough to penetrate into the polymer network and large enough so that once they were absorbed, they caused molecular damage to the epoxy matrix, as with propanol or toluene. This type of solvent molecule is prevented from diffusing into and damaging the bulk of the polymer network by the presence of the exfoliated silicate layers.

1.8 Nanocomposites and Conventional Flame Retardants

Flame retardants can be added to most conventional plastics to improve the ignition or burning performance. The disadvantage of the use of flame retardants is that many of the more common additives can also increase the amount of smoke generated during burning. The general approach starts with a conventional flame retarded polymer formulation, already showing good flammability properties. Then, incorporation of a nano dispersed layered silicate allows a significant portion of the conventional flame retardant to be removed from the formulation, therefore either maintaining or improving flammability performance and enhancing physical properties. These improvements result from reduction in the amount of conventional flame retardant used, which often degrades properties, and from the normal reinforcing effect of the nano dispersed layered silicate.

1.8.1 Nanocomposites and Intumescent Flame Retardants

Bourbigot *et al.* [1-151] studied the substitution of a PA-6 MMT (2% MMT) nanocomposite for pentaerythritol in a typical ammonium polyphosphate (APP) based intumescent flame retardant formulation. Measurable improvement in the mechanical and flammability properties of an ethylene vinyl acetate formulation (EVA-24, 24% vinyl acetate) were demonstrated. It was found that as much as one third of the APP could be removed whilst maintaining a V-0 rating (the V classification system is described in Chapter 2).

1.8.2 Phosphorus Containing Flame Retardants

Phosphates have long been known as fire retardants. Triphenyl phosphate has been used in cellulosic materials and dimethyl methylphosphonate has been used as a low viscosity liquid additive for ATH-filled polyester resins [1-152]. The fire retardant action of aromatic phosphates occurs mainly in the vapour phase leading to the production of incombustible carbonaceous char [1-153]. Consequently fewer toxic gasses are released into the atmosphere. Furthermore, the flame-retardant efficiency of phosphorus compounds has been reported to be better than equal-weighted halogenated compounds and could be further enhanced when phosphorus is covalently bound to the polymers [1-154, 1-155].

However, one of the less desirable features of the use of aromatic phosphates is that they tend to complex with cobalt-based cure promoters, and thereby slow down the cure. This problem can usually be overcome by increasing the amount of catalyst used. Another means is by heating, which for open mould applications may cause styrene emission problems. Akzo Nobel has found some novel cobalt catalysts which have pre-complexed cobalt cations, which are less prone to complexation and deactivation by the phosphate [1-156].

1.8.3 Nanocomposites and Melamine

A patent issued to Inoue and Hosokawa reports the use of silicate-triazine intercalation compounds in fire resistant polymeric composites [1-157]. V-0 ratings were achieved in the UL 94 flammability test through the combination of the known FR properties of triazine, melamine, and those of PLSNs. It was stated that the quaternary alkylammonium treatment, typically used to facilitate intercalation and delamination of layered silicates in polymers, increases the flammability of the nanocomposites. Their solution was to use the ammonium salt of melamine, which have known FR properties [1-158].

1.8.4 Other Nanostructured Flame retardants

Carbon nanotubes can also be used as nanofillers for the improvement of flame retardancy. Beyer [1-159] first investigated flame retardant properties of carbon nanotube based compounds by cone calorimetry. Flame retardant nanocomposites were also synthesised by melt blending ethylene vinylacetate copolymer (EVA) with multi-walled carbon nanotubes. Fire property measurements revealed that the incorporation of multi walled carbon nanotubes into EVA significantly reduced the peak heat release rates compared with virgin EVA. Char formation was considered to be the most important factor for these improvements. There was also a synergistic effect in the combination of carbon nanotubes and organoclays resulting in an overall more perfect closed surface responsible for the improved heat release values.

1.9   Unsaturated Polyesters

An unsaturated polyester (UP) is a long chain polymer containing a number of reactive double bonds. The unsaturated polyester is formed via a step polymerization reaction, the "polyester monomer" required for making cross-linked polyester is formed from ethylene glycol. An example of a polymerization reaction is shown in Figure 1–23.
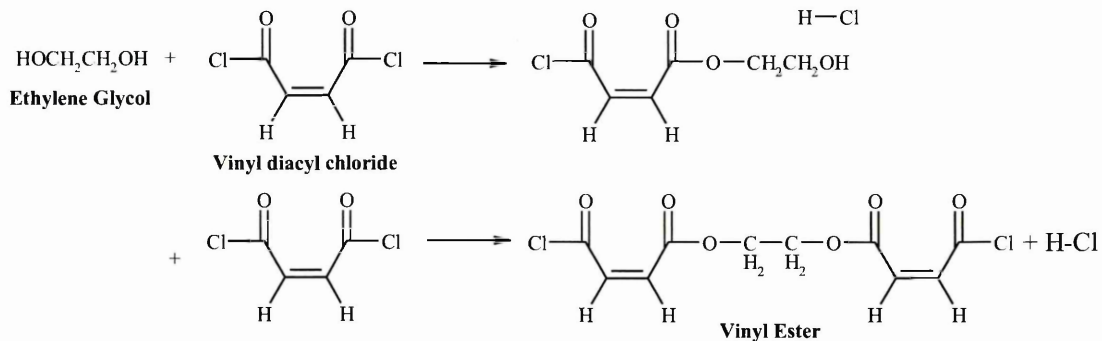
Figure 1–23 A step polymerization reaction forming unsaturated polyester.

Ethylene glycol acts as an organic base in this reaction, with the most important characteristic of the ethylene glycol being the hydroxyl groups at either end. The polyester reaction can therefore be thought of as an acid-base reaction. The organic acid is a vinyl diacyl chloride, which is also difunctional. The condensation polymerization reaction is simply the reaction of a base along with an acid to form an ester, with hydrochloric acid (HCl) being released as a condensation product. Each end continues to react to form polyester and this is the raw material for cross-linking. The actual cross-linked network is formed via a chain propagation reaction. An example is presented in Figure 1–24.
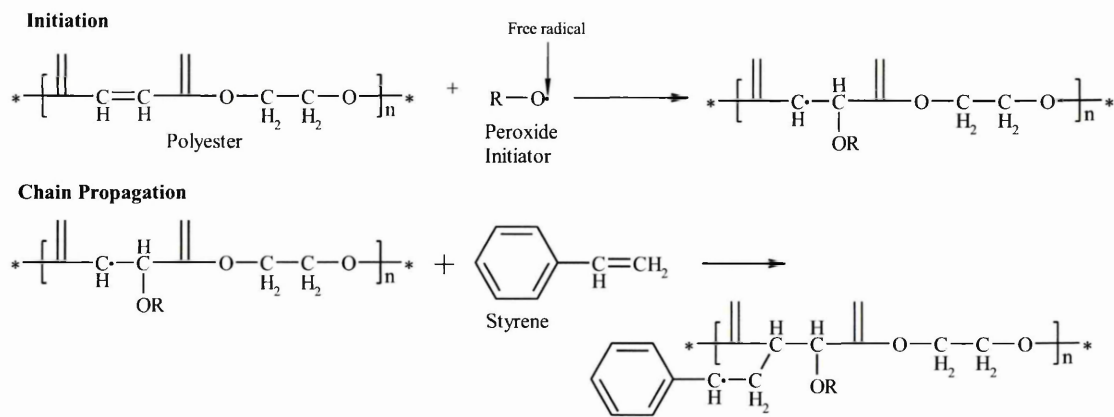
Figure 1–24 A chain propagation reaction forming cross-linked unsaturated polyester chains.

The unsaturated polyester formed by condensation polymerization is added to a mixture of styrene (a cross-linker) and peroxide (radical initiator). Radicals attack the unsaturation in the polyester or the styrene vinyl groups to initiate a chain polymerization reaction, which yields a cross-linked styrene-polyester copolymer. Styrene provides the crosslink's between the polyester chains to form a thermoset polymer. This is a chain addition reaction and so no additional products are formed. By connecting styrene monomers and unsaturated polyester molecules the free radicals grow and form long chain molecules, achieved by both inter- and intramolecular reactions. The styrene monomer, unsaturated polyester linear chain and organophilic-treated MMT exist together in the nanocomposite system resulting from the typical curing mechanism of unsaturated polyester. Therefore, it is very important how each component behaves in the formation of the nanocomposite.

Unsaturated polyester resins can be classified on the basis of their structure and can be grouped as follows: (1) ortho resins, (2) isoresins, (3) bisphenol-A fumarates, (4) chlorendics, and (5) vinyl ester (VE) resins [1-160]. Ortho resins are classed as general purpose resins, they are based on phthalic anhydride (PA), maleic anhydride (MA), or fumaric acid and glycols. Phthalic anhydride is relatively low in price and provides an inflexible link in the backbone, however, it has a tendency to reduce the thermal resistance of the laminate together with a limited chemical resistance and so processing problems can arise with ortho resins.

Iso resins are prepared using isophthalic acid, MA/ fumaric acid and glycol. These resins have considerably higher viscosities than ortho resins, therefore a higher proportion of the reactive diluent (styrene) is needed and the resin becomes more expensive. Due to the presence of higher quantities of styrene an improved water and alkali resistance is seen in the cured resin, isophthalic resins are hence of a higher quality since they demonstrate improved thermal, chemical resistance and mechanical properties.

1.9.1   Formation Mechanisms of Unsaturated Polyester Nanocomposites

Using MMT, Kornmann et al. [1-161] presented experimental evidence to support the formation of UP clay nanocomposites. Silane treatment was used in order to facilitate wetting of the silicate particles. However, Fourier Transform Infrared (FT-IR) results obtained with silane indicated that there were very few reactions with the silicate and therefore silane was not used to form the nanocomposites. It was also found that the toughness properties of the MMT-UP nanocomposite were improved significantly and at a MMT content of 1.5 wt% the fracture energy of the nanocomposite was 138 J/ m^2 as compared to the pure UP having fracture energy of 70 J/ m^2.

Suh et al. [1-162] reported the properties and formation mechanisms of unsaturated polyester nanocomposites using several preparation routes. Two mixing processes were used followed by a curing step, the crosslinking process began by decomposition of the initiators in the curing step. The first type of mixing used was simultaneous mixing, the UP chains, styrene monomers and organophilic-treated MMTs were simultaneously mixed for 3 h at 60°C. The second method, sequential mixing is a relatively new approach to preparing unsaturated polyester-layered silicate nanocomposites, in the first step the pre-intercalates of the UP and MMT were prepared and then in the second step the styrene monomer was added to the pre-intercalates, mixing times were varied.

The formation mechanisms, for samples prepared using the simultaneous and sequential mixing methods, were investigated using dynamic mechanical thermal analysis (DMTA). In the simultaneous mixing method, the styrene monomer was found to move more easily than uncured UP chains, generating a higher styrene monomer concentration in the MMT interlayer than in any other part of the simultaneously mixed system. If polymerisation were to occur under these conditions, the total cross linking density of the sample would decrease due to the low concentration of styrene in the uncured UP linear chains outside the interlayer space.

In the sequential mixing method the styrene monomer diffuses into the interlayer of the MMT that is intercalated with the UP, increasing the cross linking density of the UP-silicate nanocomposite. The styrene monomers that are acting as crosslinking curing agents are therefore better dispersed both inside and outside of the silicate layers with

increased mixing time. It was suggested that the crosslinking reaction takes place homogeneously inside and outside of the silicate layers, and crosslinking density reaches the degree of crosslinking density of the cured pure UP [1-162].

1.9.2 Mechanical Properties of Unsaturated Polyester Nanocomposites

In a study by Inceoglu [1-163] the effects of unmodified and modified MMT on the mechanical properties of polyester composites were investigated. The effect of ultrasonic mixing on the mechanical properties were also examined and the samples analysed using XRD, differential scanning calorimetry (DSC) and scanning electron microscopy (SEM). Organically treated Na-MMT (O-MMT (Cloisite 30B)) and non-treated Na-MMT were used at various weight percentages 3%, 5%, 7% and 10% respectively. The matrix used contained a relatively high styrene content of around 39%.

From the XRD patterns obtained it was found that the d-spacing of the organoclay expanded from 19.7 Å to 45 Å in the composites containing O-MMT, while the T_g values increased from 72°C in the unfilled unsaturated polyester, to 86°C in 10% O-MMT loaded unsaturated polyester. The SEM micrographs indicated that O-MMT exhibited a higher degree of exfoliation than Na-MMT, in which large agglomerates were present. In O-MMT composites a maximum value for the Young's Modulus was obtained at 5% clay content, which resulted in an improvement of 17% with respect to that of the neat polyester. At approximately 5% clay content the tensile strength exhibited a maximum and the strain at break values displayed a minimum. All these results indicated that the degree of exfoliation is at a maximum between 3%-5% of O-MMT content [1-163].

The degree of exfoliation in composites with Na-MMT was lower than that of O-MMT. Na-MMT also has a smaller effect on Young's Modulus, which increased by only 10% at 5% loading. The tensile strength did not change significantly and the impact strength values revealed a continual decrease with respect to increasing clay content. These results therefore indicated that there was a lower degree of exfoliation in the unmodified clay in comparison to the modified clay [1-163].

1-1 http://www.sure-fire.org.uk

1-2 Gilman, J.W., Jackson, C.L., Morgan, A.B., Harris, Jr, R., Manias, E., Giannelis, E.P., Wuthenow, M., Hilton, D. and Phillips, S.H., *Chem Mater* **12**, 1866 (2000)

1-3 Giannelis, E.P., *Adv Mater* **8**, 29 (1996)

1-4 Giannelis, E.P., Krishnamoorti, R. and Manias, E., *Adv Polym Sci* **138**, 17 (1999)

1-5 LeBaron, P.C., Wang, Z. and Pinnavaia, T.J. *Appl Clay Sci* **15**, 11 (1999)

1-6 Vaia, R.A., Price, G., Ruth, P.N., Nguyen, H.T. and Lichtenhan, J., *Appl Clay Sci.*, **15**, 67 (1999)

1-7 Xu, R., Manias, E., Snyder, A.J. and Runt, J., *Macromolecules*, **34**, 337 (2001)

1-8 Bharadwaj, R.K., *Macromolecules*, **34**, 9189 (2001)

1-9 Phillip, B, Messersmith, P.B. and Giannelis, E.P., *J Polym Sci, Part A: Polym Chem*, **33**, 147 (1995)

1-10 Yano, K., Usuki, A., Okada, A., Kurauchi, T. and Kamigaito, O., *J Polym Sci, Part A: Polym Chem.*, **31**, 2493 (1993)

1-11 Kojima, Y., Usuki, A., Kawasumi, M., Fukushima, Y., Okada, A., Kurauchi, T. and Kamigaito, O., *J Mater Res.*, **8**, 1179 (1993)

1-12 Gilman, J.W. Kashiwagi T. and Lichtenhan, J.D., *SAMPE J.*, **33**, 40 (1997)

1-13 Bourbigot, S., LeBras, M., Dabrowski, F., Gilman, J.W. and Kashiwagi, T., *Fire Mater* **24**, 201 (2000)

1-14 Gilman, J.W., Jackson, C.L., Morgan, A.B., Harris Jr, R., Manias, E., Giannelis, E.P., Wuthenow, M., Hilton, D. and Phillips, S.H., *Chem Mater*, **12**, 1866 (2000)

1-15 Giannelis, E.P., *Appl Organomet Chem*, **12**, 675 (1998)

1-16 Kojima Y., Usuki A., Kawasumi M., Okada A., Kurauchi T. and Kamigaito O., *J. Polym. Sci.*, **31**, 983 (1993)

1-17 Kojima Y., Usuki A., Kawasumi M., Okada A., Kurauchi T.and Kamigaito O, *J. Polym. Sci Part A: Polym. Chem.* **31**, 1755 (1993)

1-18 Vaia, R.A., Vasudevan, S., Krawies, W., Scanlon, L.G. and Giannelis, E.P., *Adv. Mater.*, **7**, 154 (1995)

1-19 Hutchison, J.C., Bissessur, R. and Shiver, D.F., *Chem. Mater.*, **8**, 1597 (1996)

1-20 Alexandre, M. and Dubois, P., *Mater Sci Engng R*, **28**, 1 (2000)

1-21 Sinha Ray, S., Yamada, K., Okamoto M. and Ueda, K., *Nano Lett*, **2**, 1093 (2002)

1-22 Bharadwaj, R.K., Mehrabi, A.R., Hamilton, C., Trujillo, C., Murga, M., Fan, R., Chavira A. and Thompson, A.K., *Polymer*, **43**, 3699 (2002)

1-23 Blumstein, A., *J Polym Sci A*, **3**, 2665 (1965)

1-24 Okada, A., Kawasumi, M., Usuki, A., Kojima, Y., Kurauchi, T. and Kamigaito, O., Schaefer DW, Mark J.E., editors. Polymer based molecular composites . MRS Symposium Proceedings, Pittsburgh, vol. **171**, 45 (1990)

1-25 Vaia, R.A., Ishii, H. and Giannelis, E.P., *Chem Mater*, **5**, 1694 (1993)

1-26 Bertalan, G., Marosi, G., Anna, P., Ravadits, I., Csontos, I. and Toth, A., *Solid State Ionics*, **141**, 211 (2001)

1-27 Canaud, C., Visconte, L.L.Y., Sens, M.A. and Nunes, R.C.R., *Polym. Deg. Stab.*, **70 (2)**, 259 (2000)

1-28 Murphy J., Flame Retardant Additives, *Plastic Additives and Compounding*, 16-20 April (2001)

1-29 Murphy, J., Flame retardant Additives, *Plastic Additives and Compounding*, 20-23 May, (2000)

1-30 Burnside S. and Giannelis, E., *Chem. Mater.*, **7**, 1597 (1995)

1-31 Lee, J., Yakekoshi, T. and Giannelis, E., *Mater. Res. Soc. Symp. Proc.*, **457**, 513 (1997)

1-32 Telford, C., Market Perspectives of Nanocomposites, Consultant: SRI Consulting Business Int.

1-33 Berry, L.G. and Mason, B., Mineralogy-concepts, descriptions, determinations, W. H. Freeman and Company (London), (1959)

1-34 Cox, K.G., Price, N. B. and Harte, D., *Introduction to the Practical Study of Crystals, Minerals and Rocks*, rev. 1st Ed., Mc-Graw-Hill (London), 127 (1974)

1-35 Murray, H.H., *Clay Miner.*, **34**, 39 (1999)

1-36 Chang, S.H., Ryan, M.E., Gupta, R.K. and Swiatkiewicz, B., *Colloid Surface*, **59**, 59 (1991)

1-37 **"clay mineral."** Encyclopædia Britannica. 2006. Encyclopædia Britannica Online. 19th October 2006 <http://www.britannica.com/eb/article-80127>.

1-38 Johnston, CT, *CMS Workshop Lectures*, **8**, 1 (1996)

1-39 Theng B.K.G., The chemistry of clay-organic reactions, Adam Helgier Ltd., 211-283 (1974)

1-40 Ball and Stick Model, Website: http//pubpages.unh.edu/~harter/crystal.htm Last accessed 03-03-06

1-41 Ray, S.S., Okamoto, M., *Prog. Polym. Sci.*, **28**, 1539 (2003)

1-42 Ross, C.S., *7th National Conference on Clays and Clay Minerals*, Pergamon Press London (1960)

1-43 Hofmann, U., Endell, K. and Wilm, D., *Z. Kristallogr.*, **86**, 340 (1933)

1-44 Maegdefrau, E. and Hofmann, U., *Z. Kristallogr.*, **98**, 299 (1937)

1-45 Hendricks, S. B., *J. Geol.*, **50**, 276 (1942)

1-46 Kornmann X, http://www.mb.luth.se/a_mpp/mpp_staff/xavier.Kornmann/Xavier.Kornmann.htm last accessed 07/2005.

1-47 Chipera, S.J. and Bish, D.L., *Clays Clay Miner.*, **49** 398 (2001)

1-48 Stackhouse, S., Coveney, P. V. and Sandre, E., *J. Am. Chem. Soc.*, **123**, 11764 (2001)

1-49 Hedges, J. I. and Oades, *J. M., Materials Today*, **6**, 20 (2003)

1-50 Chilingarian, G.V. and Vorabut,r P., *Drilling and Drilling Fluids*, Elsevier (Amsterdam), (1981)

1-51 Rodriguez, C. and Bugay D.E., *J. Pharm. Sci.*, **86**, 263 (1997)

1-52 Essington, M.E., *Soil Sci.*, **158**, 181 (1994)

1-53 Carrado, K.A., *Applied Polymer Science*, **17**, 1 (2000)

1-54 MacEwan, D.M.C., *Trans. Faraday Soc*, **44**, 349 (1947)

1-55 Sastry, N.V., Sequaris, J. M. and Schwuger, M. J., *J. Colloid Interface Sci.*, **171**, 224 (1995)

1-56 Gonzalez-Pradas, E., Villafranca-Sanchez, M. and Perez, M., *Agrochimica*, **37**, 104 (1993)

1-57 Luptakova, V., Horvath, I., Perjessy, A. and Pukyera, K., *Chem. Pap.*, **46**, 157 (1992)

1-58 Greenland D.J., *Soils Fert.*, **28**, 415 (1965)

1-59 Carrizosa, M. J., Koskinen, W. C., Hermosin, M. C. and Cornejo, J., *J. App. Clay Sci.*, **18**, 223 (2001)

1-60 Jaynes, W.F. and Boyd, S.B., *Soil Sci. Am. J.*, **55**, 43 (1991)

1-61 Sanchez-Martin, M.J., Rodriguez-Cruz, M.S., Andrades, M.S. and Sanchez-Camazano, M. *App. Clay Science*, **31**, 216 (2006)

1-62 Lahav, N., Lacher, M. and Yariv, S., *J. Thermal Anal.*, **39**, 1233 (1993)

1-63 Yariv, S., Lahav, N. and Lacher, M., *J. Thermal Anal.*, **42,** 13 (1994)

1-64 Lorprayoon, V. and Condrate, R.A., *Clays Clay Miner.*, **29**, 71 (1981)

1-65 Bosetto, M., Arfaioli, P. and Fusi, P., *Soil Sci.*, **155**, 105 (1993)

1-66 Ruiz-Conde, A., Ruiz-Amil, A., Perez-Rodriguez, J. L., Sanchez-Soto, P.J. and de la Cruz, F.A., *Clays Clay Miner.*, **45**, 311 (1997)

1-67 Fukita, I., Kuroda, K. and Ogawa, M. *Chem. Mater.* **15**, 3134 (2003)

1-68 McBride M., Surface chemistry of soil minerals: in Minerals in the Soil Environment, 2nd Ed., Soil Science and Society of America, Madison, Wisconsin, **35,** (1989)

1-69 Utracki, L.A. and Kamal, M.R., *Arabian J. Sci. Eng.*, **27**, 43(2002a)

1-70 Utracki, L.A., *J. Polym. Sci. Part B: Poly. Phys.*, **42**, 2909 (2004)

1-71 Grim R.E., *Clay Mineralogy*, McGraw-Hill, New York, (1968)

1-72 Theng, B.K.G., *The Chemistry of Clay Organic Reactions*, Adam Hilger, London, (1974)

1-73 Lagaly, G., *Clay Miner.,* **16**, (1981)

1-74 Jones, T.R., *Clay Miner.,* **18**, 399 (1983)

1-75 Newman A.C.D. (Ed.), *Chemistry of Clays and Clay Minerals*, Longman, London, (1987)

1-76 Favre, H. and Lagaly, G., *Clay Miner.*, **26**, 19 (1991)

1-77 Xie, W., Gao, Z., Pan, W.P., Hunter, D., Singh, A. and Vaia, R., *Chemistry of Materials*, **13 (9)**, 2979 (2001)

1-78 Lagaly, G., *Solid State Ionics*, **22**, 43 (1986)

1-79 Hackett, E., Manias, E. and Giannelis, E.P., *J. Chem. Phys.* **108**, 7410 (1998)

1-80 Vaia, R.A., Teukolsky, R.K. and Giannelis. E.P., *Chem Mater,* **6**, 1017 (1994)

1-81 Ogawa, M. and Kuroda, K., *Bull. Chem. Soc. Jpn.*, **70**, 2593 (1997)

1-82 Laus M., Camerani M., Lelli M., Sparnacci K., Sandrolini F. and Francescange O., *J. Mater. Sci.*, **33**, 2883 (1998)

1-83 Weimer, M.W., Chen, H., Giannelis, E.P. and Sogah, D.T., *J. Am. Chem. Soc.*, **121**, 1615 (1999)

1-84 Jordan J.W., *J. Phys. Colloid Chem.*, **53**, 294 (1949)

1-85 Lan T., Kaviratna, P.D. and Pinnavaia, T. J., *Chem. Mater.*, **7**, 2144 (1995)

1-86 Lan, T. and Pinnavaia, T.J., *Chem. Mater.,* **6**, 2216 (1994)

1-87 Wang, Z. and Pinnavaia, T.J., *Chem. Mater.*, **10**, 1820 (1998)

1-88 Messersmith, P.B. and Giannelis, E.P., *Chem. Mater*, **6**, 1719 (1994)

1-89 Qin, H., Zhang, S., Zhao, C., Hu, G. and Yang, M., *Polymer*, **46**, 8386 (2005)

1-90 Lunt, J., *Polymer Degradation and Stability*, **59**, 145 (1998)

1-91 Vink E.T.H., Rábago K.R., Glassner D.A. and Gruber P.R., *Polymer Degradation and Stability*, **80**, 403 (2003)

1-92 Mark H. and Whitby G.S. (Ed), Collected Papers of Wallace H. Carothers on High Polymeric Substances, High Polymers, Vol. I, Interscience Publishers, New York (1940)

1-93 British Plastics Federation, BPF History, Last accessed: 09-03-2006, URL: http://www.bpf.co.uk

1-94 Hussain, M., Varley, R.J., Mathys, Z., Cheng, Y.B. and Simon, G.P., *J. Appl. Polymer Sci.*, **91**, 1233 (2004)

1-95 Pinnavaia, T.J. and Lan, T., Pat. Application US005801216A (1998)

1-96 Cox, H.L., *Br. J. Appl. Phys.*, **3**, 72 (1952)

1-97 Kelly, A. and Tyson, W.R. *High Strength Materials*, John Wiley & Sons, 578 (1965)

1-98 Engelhardt, T., *Industrial Applications of Nanocomposite Fillers based on organic intercalated bentonites*, IMA 2002 Conference Proceedings, Brussels 6th June (2002)

1-99 Bentur A. *J Mater Civil Eng ASCE* , **14(1)**, 2 (2002)

1-100 Gerspacher, M., O'Farrell, C.P. and Yang, H.H., *Elastomerics*, **122**, 23 (1990)

1-101 Schroder, A., Kluppel, M., Schuster, R.H. and Heidberg, J., *Carbon*, **40**, 207 (2002)

1-102 Lawton, G. *Chem. Ind – London*, **6**, 174 (2001)

1-103 Kawasumi, M. *J. Polym. Chem.*, **42**, 819 (2004)

1-104 Kojima Y., Usuki A., Kawasumi M., Okada A., Fukushima Y., Karauchi T. and Kamigaito O., *J. Mater. Res.*, **6**, 1185 (1993)

1-105 Ray, S.S., Okamoto, K. and Okamoto, M., *Macromolecules*, **36 (7)**, 2355 (2003)

1-106 Zanetti M, Lomakin S, Camino G, *Macromol. Mater. Eng.*, **279**, 1 (2000)

1-107 Morgan, A.B. and Gilman, G.W., *J. Appl. Sci.*, **87** 1329 (2003)

1-108 Paul, D.R., Fornes, T.D. and Hunter, D.L., *Macromolecules*, **37 (5)**, 1793 (2004)

1-109 Kornmann, X., Doctoral Thesis, 17-21 (2001)

1-110 Giannelis EP, *Adv. Mater.*, **8**, 29 (1996)

1-111 Y. Ke, C. Long, and Z. Qi, *J. Appl. Polymer. Sci.,* **71**, 1139-1146 (1999)

1-112 Okamoto, M., Morita, S., Taguchi, H., Kim, Y.H., Kotaka, T. and Tateyama, H., *Polymer,* **41**, 3887 (2000)

1-113 Kawasumi, M., Hasegawa, N., Usuki, A. and Akane, O., *Mater. Eng. Sci. C,* **6**, 135(1998)

1-114 Giannelis EP, *Appl. Organomet. Chem.*, **12**, 675 (1998).

1-115 Carrado, K.A. and Xu, L., *Chem Mater*, **10**, 1440 (1998)

1-116 Wilson, Jr., O.C., Olorunyolemi, T., Jaworski, A., Borum, L., Young, D., Siriwat, A., Dickens, E., Oriakhi, C. and Lerner, M., *Appl. Clay Sci,* **15**, 265 (1999)

1-117 Fukushima, Y. and Inagaki, S., *J. Inclusion Phenom.*, **5**, 473 (1987)

1-118 Usuki A., Kawasumi M., Kojima Y. and Okada A., *J. Mater. Res.*, **8**, 1174 (1993a)

1-119 Kojima Y., Usuki A., Kawasumi M., Okada A., Fukushima Y., Kurauchi T. and Kamigaito O., *J. Mater. Res.*, **8**, 1185 (1993a)

1-120 Kojima Y., Usuki A., Kawasumi M., Okada A., Kurauchi T. and Kamigaito O., *J. Appl. Polym. Sci.*, **49**, 1259 (1993b)

1-121 Okada, A. and Usuki, A., *Mater. Sci. Eng.*, **C3**, 109 (1995)

1-122 Mülhaupt, R., Engelhardt, T. and Schall, N., *Kunststoffe*, **91**, 178 (2001)

1-123 Hirschler, M., *Polymeric Materials: Science and Engineering,* **83**, ACS Meeting Washington DC (2000)

1-124 Brabrauskas, V., *Fire and Materials*, **19**, 205 (1995)

1-125 Beyer.G., *Journal of Fire Sciences*, **23**, 75 (2005)

1-126 Beyer, G., *Fire and Materials*, **29**, 61 (2005)

1-127 Jash P. and Wilkie, C. A., *Polym. Degradation and Stability*, **88**, 401 (2005)

1-128 Wang S.J., Long C.F., Wang X.Y., Li Q. and Qi Z.N., *J. Appl. Polym. Sci,.* **69**, 1557 (1998)

1-129 Lee D.C. and Jang L.W., *J. Appl. Polym. Sci.*, **61**, 1117 (1996)

1-130 Noh M.W. and Lee D.C., *Polym. Bull.*, **42**, 619 (1999)

1-131 Lee D.C. and Jang L.W., *J. Appl. Polym. Sci.*, **68**, 1997 (1998)

1-132 Doh, J.G. and Cho, I., *Polym. Bull.*, **41**, 511 (1998)

1-133 Tyan H.L., Liu Y.C. and Wei K.H., *Polymer*, **40**, 4877 (1999)

1-134 Zanetti, M., Camino, G., Thomann, R. and Mulhaupt, R., *Polymer*, **42**, 4501 (2001)

1-135 Gilman J.W., Kashivagi T.C.L., Giannelis E.P., Manias E., Lomakin S., Lichtenhan J.D., Jones P., In: Le Bras M., Camino G., Bourbigot S. and Delobel R. editors. *Fire Retardancy of Polymer.* The Royal Society of Chemistry. (1998)

1-136 Zhu, J., Morgan, A.B., Lamelas F.J. and Wilkie, C.A., *Chem Mater*, **13**, 3774 (2001)

1-137 Babrauskas, V. and Peacock, R.D., *Fire Safety Journal* **18**, 255 (1992)

1-138 http://www.pslc.ws/macrog/mpm/analysis/cone.htm last accessed 19-10-06

1-139 Gilman, J.W., Kashiwagi, T., Lomakin, S., Giannelis, E.P., Manias, E., Lichtenhan, J.D. and Jones, P., *The Royal Society of Chemistry, Cambridge* (1998)

1-140 http://www.uow.edu.au/~mnelson/review.dir/char.html last accessed 11/05

1-141 Weil, E.D., Zhu, W., Patel, N. and Mukhopadhyay, S.M., *Polymer Degradation and Stability*, **54**, 125 (1996)

1-142 Horrocks, A.R., *Polymer Degradation and Stability*, **54**, 143 (1996)

1-143 Kashiwagi, T., *25th International Symposium on Combustion* (Pittsburgh PA: Combustion Institute), 1423 (1994)

1-144 Anderson Jr, C.E., Ketchum, D.E. and Mountain, W.P., *Journal of Fire Sciences,* **6**, 390 (1988)

1-145 Camino, G., Cota, L., Casorati, E., Bertelli, G. and Locatelli, R., *Journal of Applied Polymer Science*, **35**, 1863 (1988)

1-146 Gilman, J., *Appl. Clay Sci.*, **15**, 31 (1999)

1-147 Zanetti, M., Kashiwagi, T., Falqui, L. and Camino. G., *Chem Mater* **14 (2)**, 881 (2002)

1-148 Garces, J. M., Kuperman, A., Millar, D. M., Olken, M. M., Pyzik, A. J. and Rafaniello, W., *Adv. Mater.*, **12**, 1725 (2000)

1-149 Liu L.M., Qi Z.N., Zhu X.G., *J. Appl.Polym. Sci.* **71**, 1133 (1999)

1-150 Heinemann, J., Reichert, P., Thomann, R. and Mulhaupt. R., *Macromol. Rapid Commun.,* **20**, 423 (1999)

1-151 Bourgigot, S., Le Bras, M., Dabrowski, F., Gilman, J. and Kashiwagi, T. *Fire Mater.*,

1-152 Weil, E.D. and Levchik, S.V., *Journal of Fire Sciences*, **22**, 293 (2004)

1-153 Banks, M, Ebdon, J.R. and Johnson, M., *Polymer*, **35**, 3470 (1994)

1-154 Banerjee, S., Palit, S.K. and Maiti, S., *J Polym Sci Polym Chem*, **32**, 219 (1994)

1-155 Horrocks, A.R., Zhang, J. and Hall, M.E., *Polym Int*, **33**, 303 (1994)

1-156 Giovando, G. (1990). (to Akzo NV; Saint Peter S.r.L) PCT Int. Appl. WO 9012825 (Nov. 1, 1990; Chem. Abst. 115:209340.

1-157 Inoue, H. and Hosokawa, T., Japanese Pat. Application (Showa Denko K. K., Japan) Jpn Kokai Tokyo Koho 10 81,510 (98 81,510) (1998)

1-158 Weil, E.D. and Zhu, W. in Nelson, G. (Ed.), *Fire and Polymers*, ACS Symposium Series 599, American Chemical Society, Washington, DC, 199 (1995)

1-159 Beyer, G., *Fire and materials*, **26**, 291 (2002)

1-160 Malik, M., Choudhary, V. and Varma, I.K., *J.M.S.-REV. Macromol. Chem. Phys.,* **C40 (2&3)**, 139 (2000)

1-161 Kornmann, X., Berglund, L.A. and Sterte, J., *Polym Engng Sci,* **38**, 1351 (1998)

1-162 Suh, D.J., Lim, Y.T. and Park, O.O., *Polymer,* **41**, 8557 (2000)

1-163 Baran Inceoglu, A. and Yilmazer, U., *Polymer Engineering and Science,* **43**, 661 (2003)

In this section the materials, procedures and experimental techniques used in this thesis will be described.

2. Clay Preparation Procedures and Experimental Techniques

2.1 Sodium Ion Exchanged Cloisite

Sodium (Na^+) Cloisite is a natural, mainly Na^+ exchanged montmorillonite supplied by Southern Clay Products. The raw material was dispersed in 75g batches in an excess of deionised water (750 ml) in a large glass beaker (1.5 l). The clay/ water mixture was then stirred for 12 hours using a mechanical stirrer until a clay suspension was formed. Sodium hydroxide at 0.3 mole (12g in 250 ml deionised water) was added to the clay suspension and stirred for 48 hours. The mixture was then centrifuged and re-dispersed in deionised water between 8 and 10 times until the conductivity of the final supernatant reached below 50 μs. The exchanged clay was then air dried for 48 hours and ground manually using a pestle and mortar. The aim of this approach was to produce a homoionic sodium exchanged form of Na^+ Cloisite, into which it would be easier to exchange quaternary ammonium and alkylphosphonium cations and make the gallery surfaces organophilic.

2.2 Effect of Gallery Cations

The measured amount of cation varies with the charge on the exchange cation. The charge present on sites between the clay layers varies between 40-150 mEq/100g, however the charge on the external surface of clays is usually in the order of 5-10 mEq/100 g. This fact makes it possible to distinguish two kinds of clay, those with low exchange capacities (~10 mEq/100 g, e.g. Kaolinite) and those with high exchange capacities (40-150 mEq/100 g, e.g. Smectite) [2-1].

The arrangement of adsorbed water may be affected by the gallery cations in several ways. The gallery cations provide a bond of varying strength, which holds the layers together and controls the concentration of adsorbed water. The effectiveness of the exchange cations is dependent on their size and charge, i.e. Na^+, K^+ would develop a weak clay structure; clay slurry containing these ions would be capable of adsorbing

large concentrations of water. Ca^{2+}, Mg^{2+} would develop stronger links with the clay layer and clay slurry containing them would contain lower water concentrations. The replacing power of exchangeable cations increases with increasing valence and decreasing radius. A frequently quoted order of replacing power is sodium < potassium < calcium < magnesium < ammonia < hydrogen < iron < aluminium.

2.3 Quaternary Ammonium and Phosphonium Exchanged Na$^+$ Cloisite

By immersing quantities of Na$^+$ Cloisite in aqueous solutions containing various quaternary ammonium and phosphonium bromide salts, the replacement of the resident cations was performed. Na Cloisite samples were exchanged with decyltrimethylammonium bromide and alkyltriphenylphosphonium bromide cations of varying alkyl chain length, plus n-hexadecyl-tri-n-butyl phosphonium Bromide cations. Throughout subsequent chapters, the different organoclay species will be referred to with respect to the organocation headgroup and the alkyl chain length (Table 2–1).

The cation exchange capacity (CEC) is reported in terms of milliequivalents (mEq) of the molecular weight of surfactant cation per 100 g of the dry clay. The CEC of a clay species is a measure of the number of cations adsorbed on its surface once it has been washed free of excess salt solution. CEC is stated in milliequivalents per 100 g of dried material (mEq/100 g).

The cation loading of the surfactants (Table 2–1) offered to the clay was related to the CEC of Na$^+$ Cloisite (92.5 mEq/100 g). This was calculated from:

$$\text{Mass of Organocation Required} / g = \frac{\text{Mass of Clay/g x CEC of Clay/mEq/g x Multiple of CEC x } (M_w \text{ Organocation (amu) / Cation Charge})}{1000}$$

Table 2–1 Sample Identification for alkylammonium and alkylphosphonium exchanged Na$^+$ Cloisite

Organic Component	Abbreviation for Salt	Abbreviation for Cation	Abbreviation when exchanged onto Na$^+$ Cloisite
decyltrimethylammonium Bromide, $C_n = 10$	DTAB	DTA$^+$	DTA-MMT
ω-decyltrimethylammonium Bromide, $C_n = 10$	ω-DTAB	ω-DTA$^+$	ω-DTA-MMT
(1-octyl) triphenylphosphonium Bromide, $C_n = 8$	TP8B	TP8$^+$	TP8-MMT
decyltriphenylphosphonium Bromide, $C_n = 10$	TP10B	TP10$^+$	TP10-MMT
ω- decyltriphenylphosphonium Bromide, $C_n = 10$	ω-TP10B	ω-TP10$^+$	ω-TP10-MMT
n-dodecyl triphenylphosphonium Bromide, $C_n = 12$	TP12B	TP12$^+$	TP12-MMT
(1-tetradecyl) triphenylphosphonium Bromide, $C_n = 14$	TP14B	TP14$^+$	TP14-MMT
n-hexadecyltriphenylphosphonium Bromide, $C_n = 16$	TP16B	TP16$^+$	TP16-MMT
n-hexadecyl-tri-n-butyl phosphonium Bromide, $C_n = 16$	Bu16B	Bu16$^+$	Bu16-MMT

Na Cloisite was suspended in deionised water (10g clay in 100ml of H_2O), in a 250 ml beaker. The clay slurry was mixed for 1 hour to swell the clay galleries with water. The calculated mass of decyltrimethylammonium, alkyltriphenylphoshonium or n-hexadecyl-tri-n-butyl phosphonium salt was then pre-dispersed in 50 ml deionised water, added to the beaker, covered and stirred for 24 hr. These samples were repeatedly washed with deionised water and then centrifuged at 17,000 rpm for 1 hr and then air-dried for 48 hr to produce the organocation-exchanged samples for analysis. This method of preparation was also used to prepare the samples (using the salts in Table 2–1), which were used as the organoclay species in subsequent polymer-clay nanocomposite preparations.

2.4 Industrially Produced Organoclays; Cloisite 10A, Cloisite 15A, Cloisite 30B and Garamite.

Southern Clay Products were the suppliers of the industrially produced organoclays, Cloisite 10A, Cloisite 15A, Cloisite 30B and Garamite (Table 2–2). These organoclays were industrially prepared by cation exchanging Na-MMT with alkylammonium, hydrogenated tallow surfactants. Hydrogenated tallow is composed predominantly of octadecyl chains ($C_n = 18$) with small amounts of lower homologues, specifically 65 % - $C_n = 18$; 30 % - $C_n = 16$; 5 % - $C_n = 14$).

These organoclays were used in initial behaviour and characterisation experiments without further treatment or purification and were chosen to establish their compatibility with the unsaturated polyesters. The OH group on the Cloisite 30B headgroup was expected to be compatible with the ester on the oligomer, the benzene group on the Cloisite 10A headgroup was considered to be compatible with styrene, and it was anticipated that Cloisite 15A would be the least compatible with the polyester. These organomodifiers are displayed in Table 2–2:

Table 2–2 Structures of the organomodifiers on industrially produced organoclays
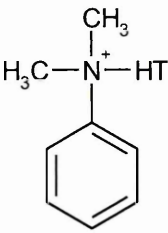
Cloisite 10A	Modifier concentration offered = 125 mEq / 100 g clay
$H_3C-N^+(CH_3)-HT$ with phenyl	Dimethyl hydrogenated tallowalkyl benzyl ammonium MMT d_{001} Spacing = 19.2 Å
Cloisite 15A	Modifier concentration offered = 125 mEq / 100 g clay
$H_3C-N^+(CH_3)-HT$ with HT	Dimethyl dihydrogenated tallowalkyl ammonium MMT d_{001} Spacing = 31.5 Å
Cloisite 30B	Modifier concentration offered = 90 mEq / 100 g clay
$H_3C-N^+(CH_2CH_2OH)-T$ with Cl^- CH_2CH_2OH	Methyl, tallow, bis-2-hydroxyethyl, quaternary ammonium MMT d_{001} Spacing = 18.5 Å
Na^+ Cloisite Na^+	Modifier concentration offered = 92.5 mEq / 100 g clay Na^+ d_{001} Spacing = 11.7 Å
Garamite	Modifier concentration offered = Unknown d_{001} Spacing = 12.2 Å
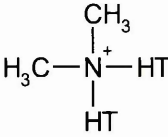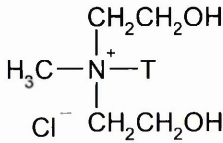
T = Tallowalkyl

Garamite is a mixture of organosmectite and sepiolite (i.e. a layered and a fibrous clay) also produced by Southern Clay Products and is a thixotropic additive for unsaturated polyester.

2.5 Unsaturated Polyester

Three commercially available resins were identified and provided by Scott Bader, Crystic 272, Crystic 189LV and Crystic R935. The main structural components are presented in Table 2–3. These are a representative selection of resins, ranging from high corrosion performance Crystic R935, high performance Crystic 272 and low viscosity general purpose resin Crystic 189LV. The product received is a polymeric oligomer dispersed in styrene, however the detailed composition of these resins were not divulged due to the commercial sensitivity of the resins.

Table 2–3 Main structural components of the commercially available resins

Crystic 189LV	Crystic 272	Crystic R935
Phthalic Anhydride	Isophthalic Acid	Isophthalic Acid
Ethylene Glycol	Propylene Glycol	Propylene Glycol
	Diethylene Glycol	1,5-pentane diol
		Neopentyl Glycol
Styrene (35 - 38 %)	Styrene (39 - 43 %)	Styrene (36 - 40 %)
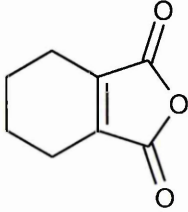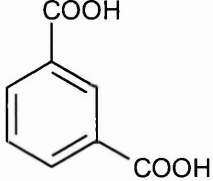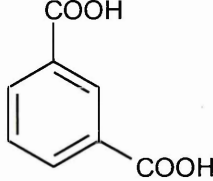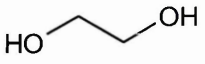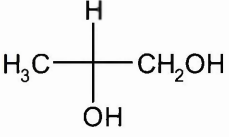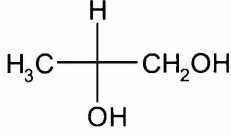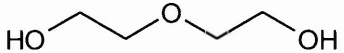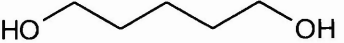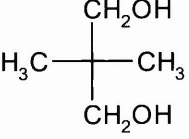
2.6 Characterisation Techniques

The following techniques were used in this thesis to characterise all clays, organoclays and nanocomposite materials.

2.6.1 X-Ray Diffraction (XRD)

2.6.1.1 XRD Theory

X-rays are a high frequency (around 10^{18} Hertz) form of electromagnetic radiation that is produced when atoms of any substance are struck by high-speed electrons. This form of radiation was first reported in 1895 by Wilhelm Röntgen and led to him being awarded the first Nobel Prize in Physics in 1901. He discovered, when experimenting with high-energy electrons, another type of radiation that had the following unique properties [2-2, 2-3]:

- it travelled in straight lines
- it was absorbed exponentially by matter and the exponent was proportional to the mass of the absorbing material
- it darkened photographic plates
- it created shadows of absorbing material on photosensitive paper

Max von Laue (1912) theorised that if crystals were composed of regularly spaced atoms acting as scattering centres for x-rays and if the wavelength of x-rays was about equal to the interatomic distance in crystals then it should be possible for a crystal to diffract x-rays. He devised an experiment in which x-rays were allowed into a lead box containing a crystal, with sensitive film behind the crystal. When the films were developed there was a large central point from the incident x-rays, but also many smaller points in a regular pattern. These points could only be due to the diffraction of the incident beam and the interference of many beams. By using a crystal as a diffraction grating, Von Laue proved that x-rays were not particles, but waves of light with very small wavelengths. W.L. Bragg and his father W.H. Bragg applied Von Laue's discovery to monochromatic radiation who demonstrated that diffraction could be treated geometrically like reflection. Bragg's law was derived allowing diffraction to

be treated in simple mathematical terms. The Bragg equation provides a simplified framework for diffraction that works for basic calculations:

$$n\lambda = 2d \sin \theta \qquad\qquad \text{Eq}^n \text{ 2-1}$$

where: n = integer, λ = wavelength of x-rays, d = d-spacing of crystal, θ = diffraction angle.

By re-arranging the equation the d-spacing may be calculated as follows:

$$d = n\lambda / 2\sin \theta \qquad\qquad \text{Eq}^n \text{ 2-2}$$

The terminology used for the d-spacing, i.e. d_{001}, is derived from the separation of the particular crystal planes in the unit cell that is being measured [2-4], and comprises the gallery spacing plus the platelet thickness e.g. for MMT: d_{001} = gallery spacing + 0.96 (nm) [2-5]. As the sample is rotated the incident beam encounters different planes of regular crystalline form and it is these planes that are given a set of indices according to their position in the unit cell.

In the early 1930's soil scientists Hendricks and Fry [2-6] and Kelley et al. [2-7] applied XRD to elucidate the crystalline structure of clay minerals. XRD is a powerful technique that can be used to identify the crystalline phases in materials [2-8, 2-9, 2-10] and has been used in the context of this thesis to monitor the position and intensity of the d_{001} basal reflection of clays or polymer clay nanocomposite materials to determine:

- that the clay treated with surfactant has been exchanged and the surfactant is intercalated into the gallery.
- the molecular orientation of surfactant molecules in the interlayer space of the organoclays.
- the level of dispersion of the organoclay within polymer matrix indirectly through peak broadening and loss of peak intensity (indicating a more disordered system).

XRD is dependent on many factors including sample length, alignment, sample homogeneity, thickness, position, and the quality of the calibration standards used making quantitative reproducibility difficult.

An important contributor to the performance of a polymer layered silicate nanocomposites (PLSN) is the extent of intercalation and exfoliation of the organoclay and XRD is the principal method that has been used to examine this. An example of X-ray scattering data obtained for an unsaturated polyester (UP)/ clay system is shown in Figure 2–1 as the scattering intensity versus 2θ, where 2θ is the angle of diffraction.
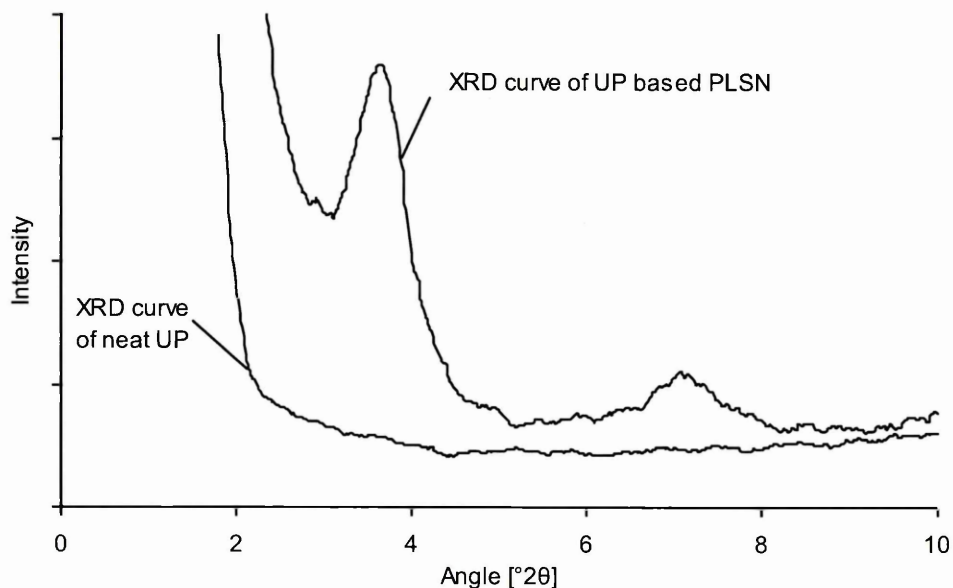
Figure 2–1 XRD traces of neat UP and a UP/ PLSN containing 5 wt% Cloisite 15A.

Below $2\theta < 10°$ the XRD trace of neat UP is featureless, yet, the PLSN containing 5 wt% Cloisite 15A exhibited distinct peaks. The positions and shapes of these peaks provide information on the dispersion/ agglomeration of the diffracting species, the organoclay. The presence of multiple peaks in the XRD traces was quite common. They often originated from different organoclay structures and their incomplete dispersion during incorporation in a polymeric matrix [2-11].

X-ray scattering instruments are divided into the more common wide angle and less common small-angle X-ray scattering instruments, WAXS and SAXS respectively. The scattering angle $2\theta = 2°$ is considered the boundary between the two however, newer WAXS instruments are frequently able to provide reliable scattering profiles down to $2\theta = 1°$.

2.6.1.2 XRD Analysis

X-rays are produced when high-speed electrons strike the atoms of another substance. The tube, which produces X-rays within the diffractometer, is under vacuum. Inside this tube electrons are generated by a glowing tungsten filament (cathode). The electrons are then accelerated by voltages (15-60 kV) in order to strike a metal target, which is acting as the anode. The accelerated electrons strike the inner more tightly bound electrons of the target knocking them out of their orbital positions, and away from the influence of their respective nuclei. Electron vacancies are produced, which are subsequently filled by higher orbit electrons dropping inwards to fill the vacancy. This drop involves the production of an X-ray photon, the energy of which is proportional to the difference between the energy levels of the orbitals. This energy difference is dependent on the number of protons in the nucleus attracting the electrons, and therefore depends on atomic number, z. The energy difference is related to the wavelength of the emitted x-ray via $\Delta E = hc/\lambda$.

The most commonly used material for the target and therefore the source of the x-rays is copper, although for the measurements presented in this thesis chromium is an important alternative. The wavelength of Cu $K\alpha$ radiation is 1.5418 Å while the wavelength of Cr $K\alpha$ radiation is 2.291 Å. The lowest angle of diffraction for both tubes is 2°. It is called the theta angle, and is measured in degrees. Therefore, using a theta angle of 2, the largest d-spacing that the copper tube can detect is 44.2 Å and the largest d-spacing that the chromium tube can detect is 65.6 Å. Other target materials include cobalt, molybdenum and iron, the wavelength for the $K\alpha$ lines of x-rays produced by these metals are summarised in Table 2–4.

Table 2–4 Summary of Wavelength of x-rays produced by various metals

Material	Wavelength $K\alpha$ line [Å]
Cobalt	1.790
Molybdenum	0.711
Chromium	2.291
Iron	1.937
Copper	1.542

In this thesis powder diffraction measurements in reflection were performed using a Bragg – Brentano geometry. Figure 2–2 illustrates the characteristics of Bragg-Brentano geometry.
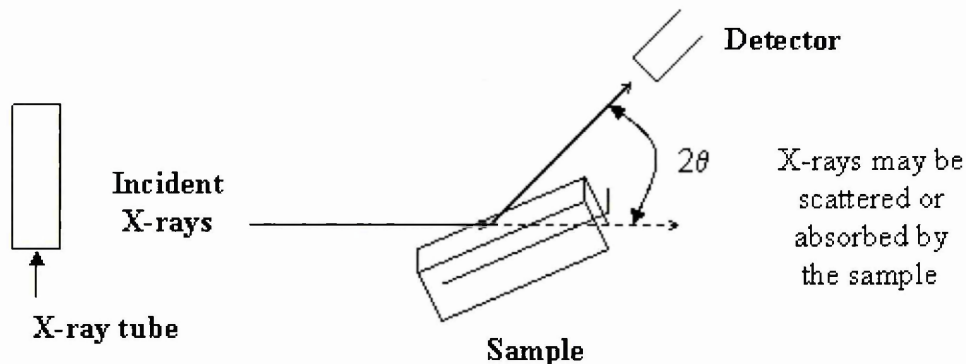
Figure 2–2 Schematic diagram of Bragg – Brentano geometry

As the X-rays pass through the sample matter, radiation interacts with the electrons in the atoms, resulting in the radiation becoming scattered. If the matter is crystalline and the atoms are organised in planes, with the distances between the atoms being of the same magnitude as the wavelength of the X-rays, then constructive and destructive interference will occur [2-3]. In a typical experiment the diffracted intensity (of the scattered x-rays that obey Bragg's Law) is measured as a function of the diffraction angle (2θ) and the orientation of the sample, which yields the diffraction pattern.

The use of powder diffraction in the analysis of PLSN's is largely based on the established procedures developed for the identification and characterisation of layered silicate minerals [2-12, 2-13]. XRD is used to monitor the position and the intensity of the d_{001} spacing corresponding to the repeat distance perpendicular to the layers. For clay nanocomposites within a polymer the 001 basal reflections are generally used to estimate the dispersion of the organoclay. The interlayer spacing of the layered silicates is usually calculated from the position of the 001 peak by employing Bragg's Law (equation 2-2).

Table 2–5 displays the diffraction profiles for selected examples of PLSNs. For immiscible mixtures the d-spacing does not change upon blending with the polymer, although the peak intensity may be reduced.

Table 2–5 Diffraction profiles for different types of intercalated and exfoliated nanocomposites

(a) Intercalated/Aggregated
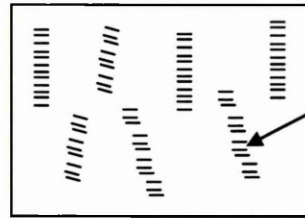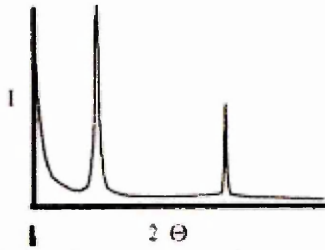
The finite layer expansion associated with intercalated structures results in a new basal reflection corresponding to a larger gallery height. If the clay layers are ordered then intense and sharp d_{001} and d_{002} reflections are visible.

(b) Intercalated/Dispersed
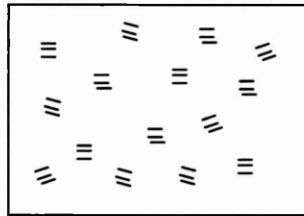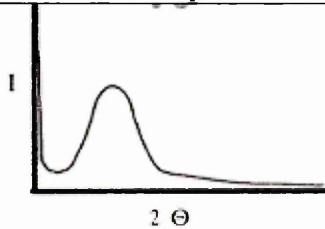
As the clay layers become less ordered (i.e. fewer large stacks), the peaks become broader and less intense and the d_{002} reflection is no longer visible.

(c) Partially Exfoliated
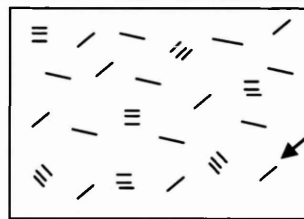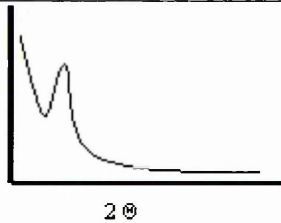
If a nanocomposite is made up of regions of exfoliated layers in amongst stacks of unexpanded clay, then this results in the d_{001} reflection shifting to lower angles for the unexpanded clay, than would be expected. This is as a result of the peak position and intensity being the sum of the d_{001} reflection for the unexpanded clay on top of scattering from the exfoliated, disordered platelets.
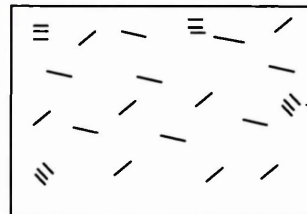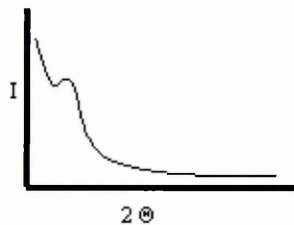
As the nanocomposite becomes more exfoliated and there are fewer unexpanded clay stacks then the intensity of the peak decreases and the breadth of the basal reflection increases.

(d) Exfoliated
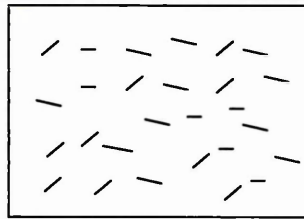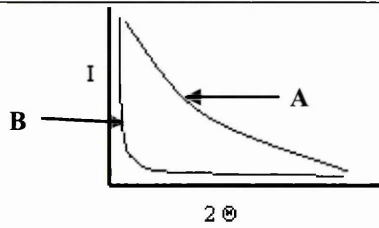
The extensive layer separation (beyond the resolution of Bragg-Brentano geometry) of exfoliated structures does not result in a new, observable d-spacing, but leads to loss of intensity and eventual disappearance of the d-spacing associated with the intercalated system [2-14]. An exfoliated nanocomposite displays a smooth scattering profile at low angle (trace A) indicating disruption of the once ordered clay layers. However, a scattering profile, which is similar to the one presented for trace B could indicate large packets of disordered layers separated by microns of polymer.

(e) Other Possible Diffraction Profiles

It is possible to achieve a combination of a number of profiles detailed above, which could lead to a diffraction trace, which is difficult to interpret. Other profiles are also possible such as disrupted stacks and card house structures. Disrupted stacks could give rise to an XRD pattern with a weak and broad d_{001} peak or no d_{001} at all as the clay layers are not optimally aligned, this could be misinterpreted as an intercalated/dispersed or exfoliated system. The clay layers in a card house structure are also not aligned correctly and would not give rise to an XRD pattern, however clay particles could possibly be visible by eye in the samples (as observed in some of the samples in Chapter 4 and Chapter 5, which did not diffract).
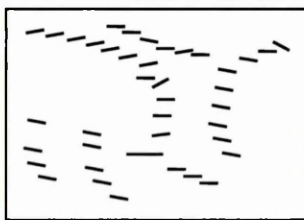
Disrupted stacks	**Card House Structure**
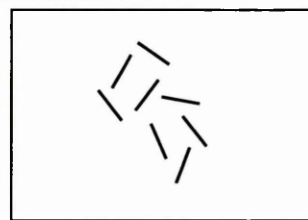
Vaia et al. [2-12] examined the kinetics of polymer melt intercalation and demonstrated the real-time evolution of these x-ray scattering patterns, providing detailed information on the dynamics of structure formation and intercalation.

It is especially critical to determine the presence of exfoliated layers because of their association with property enhancements although, the large d-spacings (d_{001} > 2.0 nm) and absence of *hkl* reflections requires the collection of data at scattering angles, 2θ, of less than 10°. However, contributions to the broadening and weakening of basal reflections occur as a result of (a) layer disorder, (b) silicate volume fractions less than 0.1 and (c) experimental conditions. Consequently special considerations are necessary when preparing samples, performing experiments and interpreting different traces from PLSNs.

The absence of basal reflections in powder diffraction spectra is often interpreted as evidence for an exfoliated PLSN. However, subsequent electron microscopic investigations reveal the presence of large quantities of disordered layers separated by microns of polymer devoid of layers, which is not the desired exfoliated morphology.

2.6.1.3 XRD Experimental Parameters

Samples were analysed on either a Philips PW3710 or a Philips PW1710 X-ray Diffractometer, which contained a Cu or Cr-tube, respectively. The instrumental settings that were used are summarised in Table 2–6.

Table 2–6 Settings for XRD measurements

Parameter	Cr Settings	Cu Settings
Generator tension [kV]	30	40
Generator current [mA]	40	40
Starting angle [°]	1.8	2
End angle [°]	12-75	12-75
Step size [°]	0.02	0.02
Time per step [sec]	1	1

For preliminary characterisation of clay minerals, scanning from 1.8-40 °2θ was considered adequate. The diffraction patterns for the modified organoclays were recorded over an angular range of 1.8-25 °2θ and the diffraction patterns for the unsaturated polyester clay nanocomposites were recorded from 1.8-12 °2θ. A scan rate of 2 °2θ per minute was used unless otherwise stated.

2.6.2 Thermogravimetric Analysis (TGA)

2.6.2.1 Thermal Analysis Techniques

A variety of thermo-analytical techniques may be used to investigate the thermal stability of organoclays and polymer-clay composites; these include thermogravimetric analysis (TGA), differential thermal analysis (DTA), differential scanning calorimetry (DSC) and thermo-mechanical analysis (TMA). In this thesis, the main thermal analysis technique used was TGA (also coupled with mass spectrometry (TG-MS)) and was used to measure changes in thermal stability and degradation temperature(s) as a function of the type or amount of additive in clay and polymer materials.

2.6.2.2 TGA Analytical Process

TGA involves the continual recording of a sample's weight when it is subjected to a precise, usually linear, temperature program [2-15]. The sample is contained in a refractory crucible within a furnace and suspended from a sensitive recording balance and therefore mass and temperature readings can be made simultaneously. Samples may be heated from room temperature up to 1000 °C using the metler system, 1100 °C using the Cahn system and 1650 °C using the Netzsch system. The TG weight loss curve plots weight loss on the y axis and increasing temperature to the right on the x axis. Subtle weight changes are often difficult to determine and so an alternative representation was regularly used which presents the negative 1st derivative of the TG weight loss curve i.e. the derivative thermogram (DTG) in which -dw/dT is plotted on the y-axis and temperature on the x-axis. The DTG curve presents the rate of change in mass, with respect to the rate of change in temperature (Figure 2–3).
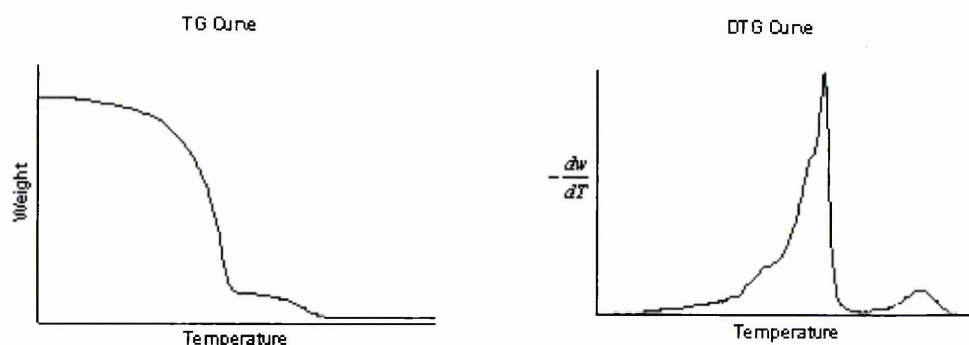
Figure 2–3 Diagrammatic representation of a typical TG curve and its associated DTG profile

Several experimental factors influence the shape of the TG curve, which include [2-15];

- **Sample size:** Large samples may produce poorly resolved events due to temperature gradients within the sample and/ or trapping of volatile materials.

- **Particle size distribution and packing density:** To optimise reproducibility these should vary as little as possible.

- **Purging atmosphere/ flow:** In this thesis nitrogen and air were used as a flow gas. The type of reaction occurring as the sample is heated is highly dependent on the choice of purge gas. The interaction of the sample and the gas involved with it is crucial. Under an inert nitrogen atmosphere pyrolysis is likely to occur, however under the reactive atmosphere of air oxidation is more likely to occur. An atmosphere rich in decomposition products would delay the corresponding decomposition of the heated material until a higher temperature. This principal is known as Le Chatelier's principal. So for the equilibrium:

$$X_{(solid)} \leftrightarrow Y_{(solid)} + Z_{(gas)}$$
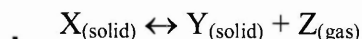
when an excess of Z is present it is less likely that X will decompose therefore fast flow rates of purge are an advantage, so that the reaction products are swept away upon release.

- **Heating rate:** The resolution of the TG curve decreases as the difference between the sample's actual and recorded temperature increases therefore a slow heating rate is used as standard to ensure the sample's recorded temperature and actual temperature remain as close as possible.

- **The sample holder:** To ensure conclusive results the sample container must not react with the sample and therefore alumina crucibles were used. The depth of the sample holder can also influence the degradation mechanism as the deeper the crucible then the poorer the purge flow to the sample, thus slowing down degradation.
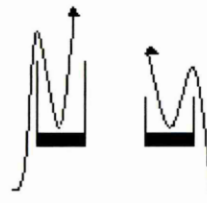
2.6.2.3 TGA Experimental Parameters

For all samples, TGA was performed on a Mettler-Toledo TA8000 thermogravimetric analyser where a nitrogen or air gas flow was maintained at a rate of 20 cm^3 min^{-1}. Standard 10 mg samples, which were sampled from the same area of the PLSN (5mm from the edge of the sample) were first conditioned at 35 °C for 15 minutes in order to remove weakly physisorbed components and obtain a stable weight reading. The temperature was then ramped at a rate of 20 °C min^{-1} up to 800 °C.

2.6.3 Evolved Gas Analysis (EGA) by Thermogravimetry-Mass Spectrometry TG-MS)

TG analysis is able to record weight changes occurring upon sample decomposition, but is unable to assign weight losses to specific components and must therefore be used in conjunction with other techniques (e.g. Mass Spectrometry or Fourier transform infrared spectroscopy), to provide corroborative evidence of the association of specific weight losses with particular components. Wie et al. [2-16] used TG-FTIR-MS for the thermal analysis of organically modified layered silicates (OLS) and compared them to pure montmorillonite. They examined the effect of chemical variation (alkyl chain length, number of alkyls and presence of C=C bonds) of the organic modifiers on the thermal stability and degradation products of the organically modified MMT. They found that TG-FTIR-MS provided useful information on the thermal decomposition of OLS such as decomposition products and that the release of organic compounds from OLS was staged and occurred via different mechanisms.

Another study by Wie et al. [2-17] examined the nonoxidative thermal degradation of MMT and OLS MMT using TG-FTIR-MS and pyrolysis/GC-MS. Analysis of products (GC-MS) indicated that the initial degradation of the surfactant in the OLS followed a Hoffmann elimination reaction and that the chain length, surfactant mixture, exchanged ratio, or preconditioning (washing) did not alter the initial onset temperatures. However, these factors were found to affect the initial mass loss.

In this thesis two different systems have been used a Unicam-Synergic Chemical Analysis System ('Synergy' system) and a NETZSCH STA instrument, both were used to perform evolved gas analysis (EGA). Both systems consisted of a thermobalance to record the weight loss of a sample and a mass spectrometer to detect and identify the fragment ions from the evolved gases. The MS output corresponds to different weight losses in real-time. This type of analysis is referred to as real time analysis, since time/temperature related weight losses observed in the TG are related to specific features seen in the total ion current trace from the spectrometer. EGA by real-time MS will be referred as TG-MS throughout this thesis.

2.6.3.1 TG-MS Interface

The Thermo Unicam system comprises an interface, which ensures that evolved gases are sampled (Figure 2–4) before they are allowed to diffuse throughout the entire volume of the TGA reaction cell [2-18].

The interface employs a 'sniffer' tube for MS sampling, it is constructed of a high temperature alloy and extends to a position just above the sample cup where it does not interfere with the TGA hang-down wire. The vacuum conditions that the MS unit is operated under serve to draw the evolved gases towards it along the transfer line. The transfer line temperature was optimised and run operated at 200 °C.
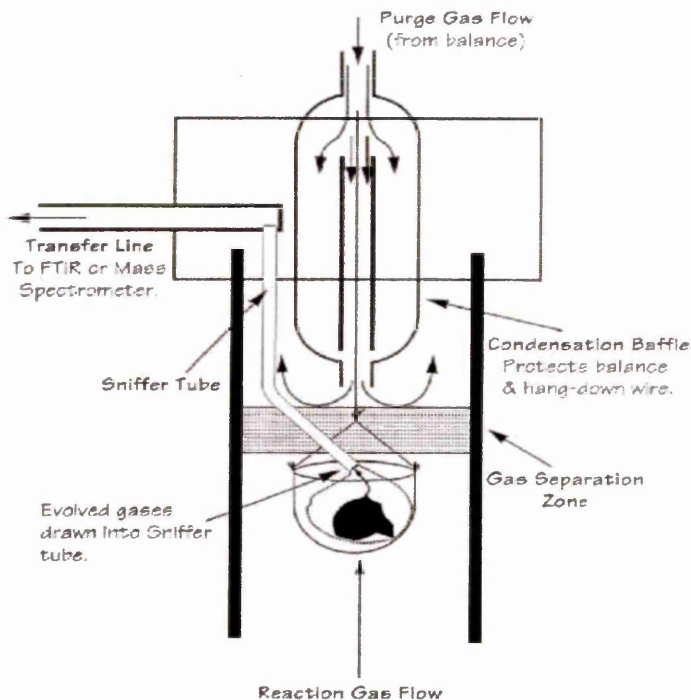
Figure 2–4 Schematic diagram of the Unicam TG-MS Interface System [2-19].
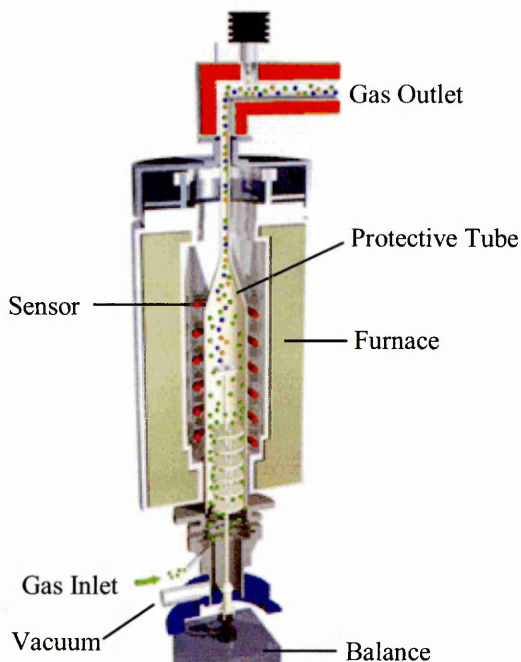
Figure 2–5 NETZSCH TG-MS Interface [2-20].

The NETZSCH STA instrument comprises an STA 409 PC *Luxx®* simultaneous thermal analyser and a QMS 403 C *Aëolos®* quadrupole mass spectrometer [2-20].

Figure 2–5 displays the TG-MS thermal analysis instrument for the NETZSCH STA system. Evolved gases are drawn under vacuum along the transfer line to the MS. The transfer line is set at 200 °C to ensure elimination of decomposition products during thermal analysis.

2.6.3.2 Mass Spectrometer

By coupling the thermal analysis instrument with a fast Quadrupole Mass Spectrometer (QMS) the detection and identification of gaseous components are possible in exact time correlation with the other thermal analysis signals. The mass spectrometer used in the 'Synergy system' was an ATI Unicam Automass System 2 quadrupole mass spectrometer, and the NETSCH STA system used a QMS 403 C made by *Aëolos®*. During this work the MS was operated in Electron Impact (EI), positive ionisation mode. It is composed of three main units:

- Ion source
- Quadrupole mass analyser
- Detector

2.6.3.3 Ion Source

The ion source is where the sample is introduced into the MS. In real time TG-MS the transfer line is directly interfaced with the ion source. The sample passes through an electron beam (70 eV) and ionisation occurs when an electron strikes a molecule and imparts enough energy to remove an electron from that molecule. The following example demonstrates the reaction methanol would undergo in the ion source:

$$CH_3OH + 1 \text{ electron} \rightarrow CH_3OH^{+\bullet} \text{(radical cation)} + 2 \text{ electrons}$$

Singly charged ions are usually produced by EI ionisation and contain one unpaired electron. This charged ion (i.e. $CH_3OH^{+\bullet}$) is called the molecular ion and remains intact. Energy imparted by EI is typically more than that required to produce the molecular ion and this excess energy causes instability in the molecular ion, causing it to break into smaller fragments to give a characteristic mass spectrum. The methanol ion may fragment in various ways, with one fragment carrying the charge and one fragment remaining uncharged. For example:

$$CH_3OH^{+\bullet} \text{ (molecular ion)} \rightarrow CH_2OH^+ \text{ (fragment ion)} + H^\bullet$$

Or

$$CH_3OH^{+\bullet} \text{ (molecular ion)} \rightarrow CH_3^+ \text{ (fragment ion)} + {}^\bullet OH$$
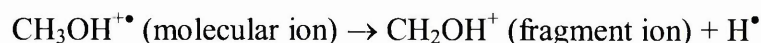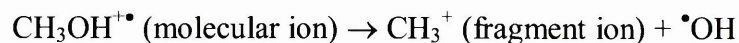
A typical EI fragmentation pattern of methanol is displayed in Figure 2–6, and mass to charge ratio (m/z) for each fragment are displayed in Table 2–7.

Table 2–7 Mass to charge ratio (m/z) for CH₃OH⁺˙ fragment ions

Fragment	Mass to Charge Ratio (m/z)
$CH_3OH^{+\bullet}$	32
CH_2OH^+	31
$CHOH$	30
CHO	29
CO	28
CH_3^+	15
$^\bullet OH$	17
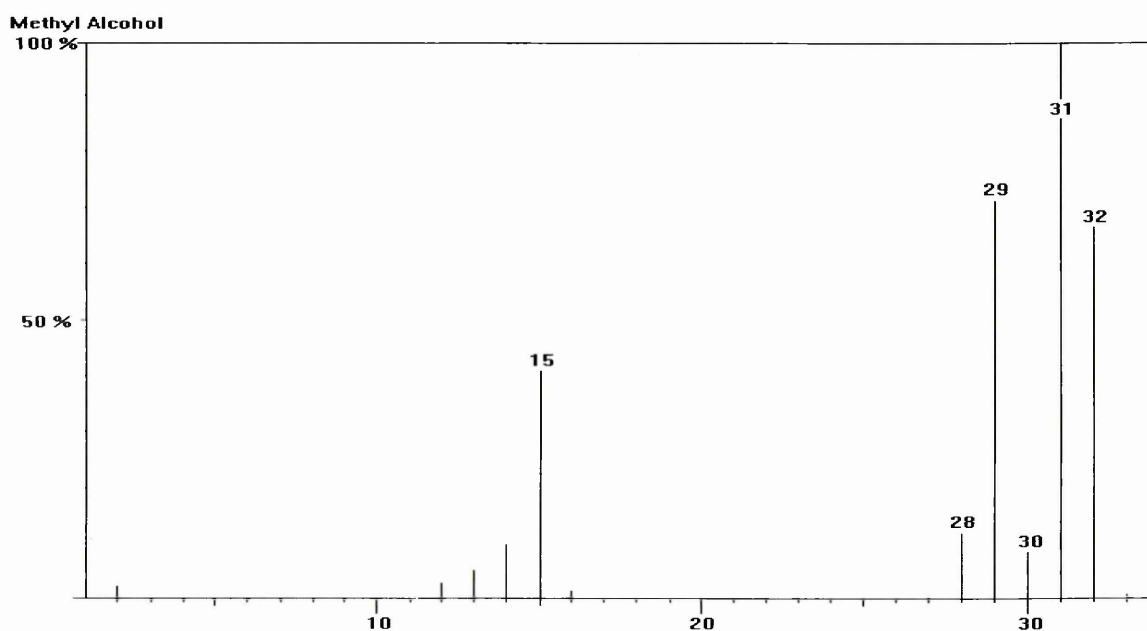
Figure 2–6 EI fragmentation pattern of Methanol

Qualitatively this type of spectrum demonstrates important features such as:

- The ions produced are singly charged and the m/z ratio corresponds to the 'weight' of the fragments produced. Not only is the elemental composition of each fragment ion accessible, but so are the molecular weight and molecular formula.

- The ions produced may be related to the structure of the intact molecule using well-understood principles.

- The mass spectra are reproducible. This is of crucial importance when libraries of reference spectra are used to aid structure determination.

However, there are two main disadvantages of EI, 1) there are limitations in the range of compounds which may be successfully ionised and 2) the utility of the resulting spectra. Samples must be volatile yet thermally stable to yield an EI spectrum and this prohibits the study of many unstable and thermally involatile analytes.

The utility of EI spectra may be reduced by the degradation/ breakdown of fragment molecules resulting from less than optimal transfer line temperatures before being analysed in the MS. This would result in no 'effective molecular ion' being detected, in these cases the molecular weight may not be determined and one of the single most valuable pieces of analytical information is lost. Therefore it is very important to optimise the transfer line temperature and introduction of the sample into the MS source, in this thesis the transfer lines were optimised at 200 °C.

2.6.3.4 Ion Analyser (Quadrupole)

Molecular ions and fragment ions produced during ionisation are accelerated by manipulation of the charged particles through the mass spectrometer, whereas uncharged particles and fragments are pumped away. Ion filters using positive and negative voltages control the path of ions through the quadrupole. Based on their mass to charge ratio (m/z) the ions travel down the path and the electric field triggers the ions to oscillate in the x and y directions. EI ionisation produces singly charged particles, so the charge (z) is one. Therefore, an ion's path through the quadrupole is dependent on its mass.

2.6.3.5 Mass Detector

The MS detector works by producing an electronic signal when struck by an ion. A series of timing mechanisms integrates the signal abundance and associates it with a particular rf/dc voltage ratio (m/z). By doing this the associated mass and signal abundance are correlated. The mass detector utilised in the Netzsch STA instrument was an SEV (Channeltron) detector.

2.6.3.6 Advantages of the STA 409 PC *Luxx*® when coupled to the QMS 403 C *Aëolos*®

Evolved gases are directed straight to the gas analyser along a heated transfer line, therefore eliminating condensation and decomposition products, via the absence of pressure reduction orifices. This achieves high detection sensitivity and facilitates quantitative detection of all identified gas components. The QMS 403 C *Aeolos*® EGA instrument can analyse a mass range between 1 and 300 amu.

2.6.4 X-ray Fluorescence (XRF) Spectrometry

An XRF spectrometer was used for quality assurance by quantitatively analysing the chemical composition of exchanged organo-clays, through the determination of the quantity of elemental oxides present in all samples, using pressed powders. X-rays are directed towards a sample and elements present in the sample produce characteristic fluorescence radiation at specific wavelengths. The amount of fluorescence at a specific wavelength is then related to the concentration of the element in the sample.

2.6.5 ^{1}H and ^{31}P NMR

^{1}H and ^{31}P NMR spectra were obtained using a Buker B-ACS 60, 200 MHz instrument. The spectra were used to determine the product purity and to monitor any chemical shifts in the different methacrylate functionalised phosphonium-organomodifiers that were synthesised. By monitoring the chemical shifts in the signal it was possible to determine whether intermediate products were still present or whether the reaction had gone to completion.

2.6.6 Infrared Spectroscopy

Infrared (IR) radiation is electromagnetic radiation with a wavelength positioned between the visible and the microwave regions of the electromagnetic spectrum. Information on the vibrational (and rotational) changes within molecules can be obtained from the molecular energies found within this region. The IR region can be divided into three sub-regions, the near IR region which covers the range of 14,000-4000 cm^{-1}, the mid-IR region between 4000-400 cm^{-1} and the far IR region between 200

and 20 cm^{-1}. An infrared spectrum is formed as a consequence of the absorption of electromagnetic radiation at frequencies that correlate to the vibration of specific sets of chemical bonds within a molecule [2-21].

Fourier Transform Infrared Spectroscopy (FT-IR) for the characterisation of PLSNs has been used initially in studies of the polymer matrix morphology, e.g., conformation and crystallisation behaviour of polystyrene (PS) [2-22] or α- to γ-crystalline form transition of PA-6 [2-23]. By comparing the experimental and calculated spectra, the type and intensity of interactions can be identified [2-24]. FT-IR has been utilised in this thesis to determine surface effects between the front and back surfaces of PLSNs and to determine whether methacrylate-functionalised phosphonium-organomodifiers have remained exchanged onto Na$^+$ Cloisite, after the washing process.

2.6.6.1 Fourier Transform Infrared Spectroscopy (FT-IR)

FT-IR spectroscopy is based on a Michelson interferometer and a mathematical procedure developed by Fourier to transform the time domain to the frequency domain [2-25, 2-26, 2-27]. Figure 2–7 presents a schematic illustration of a Michelson interferometer. In such a system the radiation from the light source (a mercury lamp or a silicon carbide rod) is sent to a beam splitter made from infrared transparent material (e.g. KBr). The beam splitter reflects approximately half the light onto a fixed mirror (reference mirror) that in turn reflects the light back to the beam splitter. The light that is not reflected of the beam splitter passes through onto a continuously moving mirror (objective mirror). The objective mirror is moving at a constant, known velocity, the light is reflected off this mirror and recombined with the light reflected off the fixed mirror at the beam splitter. The radiation is then passed through the sample and onto the detector (Figure 2–7 represents this as a screen). Commonly used detectors are the liquid nitrogen cooled mercury cadmium telluride (MCT) detector (used in this thesis) or the (less sensitive) deuterated triglycine sulphate (DTGS) detector.
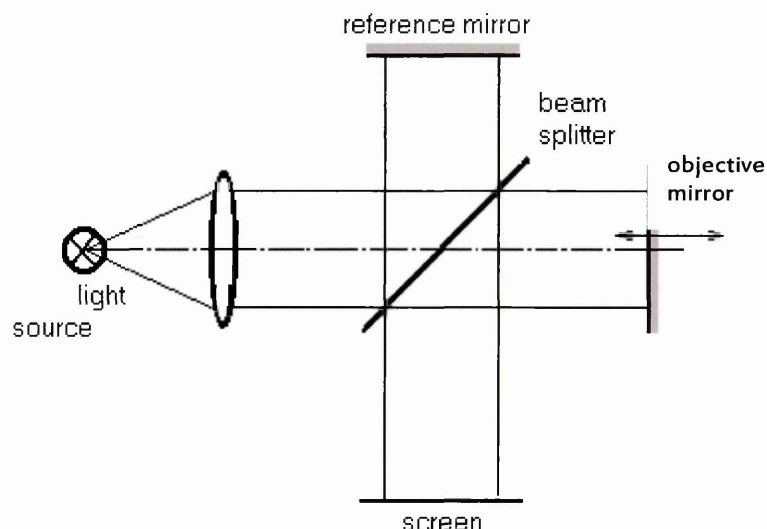
Figure 2–7 Schematic illustration of a Michelson Interferometer [2-28].

FT-IR has three major advantages over the traditional dispersive approach to record an infrared spectrum:

1. **Throughput (Jacquinot) advantage**: No slits are needed in this set-up, therefore the amount of radiation that reaches the detector is higher and an increased signal to noise ratio can be obtained.

2. **Multiplex (Fellgett) advantage**: All frequency elements reach the detector simultaneously in this set-up, therefore the spectrum can be obtained in a very short time.

3. **Laser reference (Connes) advantage**: Derived from the sampling method, the time interval at which information is sampled is determined by utilising a laser with a fixed wavelength (usually 632.8 nm). As the time interval can be measured very accurately the frequency domain spectrum obtained from the Fourier transformation is also very accurate. This allows the averaging of scans to reduce the signal to noise ratio of the final spectrum.

A disadvantage of the FT-IR system is that unwanted bands in the spectrum, from CO_2 or water vapour absorption, can only be removed by purging the instrument with a dry, infrared inactive gas such as nitrogen or subtraction of a spectrum of the sample compartment in the absence of a sample.

The most basic sampling technique in infrared spectroscopy is the transmission set-up. Here the light from the source is passed through the sample onto the detector as depicted in Figure 2–8.
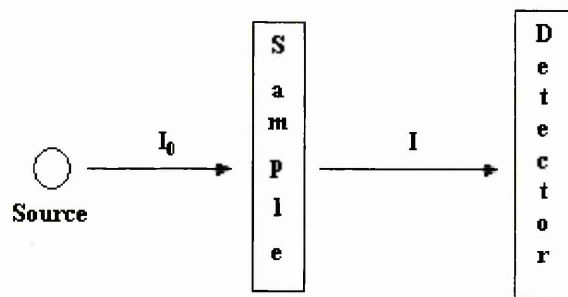
Figure 2–8 Schematic Representation of transmission Set-up

Information on the bulk of the sample can be obtained with this technique. The thickness of the samples that can be analysed by this method depends on their absorption properties. Only thin films can be analysed for strongly absorbing samples.

2.6.6.2 Attenuated Total Reflectance Fourier Transform Infrared Spectroscopy (ATR-FTIR)

Attenuated total reflectance (ATR) spectroscopy, also known as internal reflection spectroscopy (IRS), is especially suitable for the analysis of samples that are difficult to investigate by transmission measurements such as physically thick samples and strongly absorbing solids or liquids. The sample is placed in contact with an ATR crystal. The IR radiation sent through this crystal undergoes total reflection at the sample/crystal interface. The number of total reflections occurring is dependent on the size and geometry of the crystal as well as the angle of incidence of the incoming light [2-29].

ATR spectroscopy is a surface technique and the most important theoretical feature is associated with the properties of the evanescent field created at the surface of the ATR crystal. An evanescent field is created when light (in this case infrared radiation) travelling at an angle greater than the critical angle through a medium with a high refractive index (the ATR crystal or infrared element, IRE) undergoes total internal reflection at the interface with a material of lower refractive index.

The evanescent field decays exponentially with increasing depth from the interface. The rate of decay of the evanescent field depends on the wavelength, the angle of incidence of the light and the refractive indices of the denser and uncommon medium (ATR crystal and sample). The depth at which the field has dropped to 1/e ($\approx$36.8 %) of its original value has been defined as the depth of penetration. Harrick has arbitrarily defined this parameter, however, the naming has caused some confusion. The depth of penetration can be calculated using the following equation [2-30].

$$d_p = \frac{\lambda_1}{2\pi(\sin^2\theta - n_{21}^2)^{0.5}} \qquad \text{Eq}^n \text{ 2-3}$$

where:

θ: Angle of incidence, $n_{21}=n_2/n_1$, n_1: refractive index of the IRE, n_2: refractive index of the sample,

$\lambda_1=\lambda/n_1$

A major problem with ATR is the excellent sample contact required to obtain quantitative spectra. To achieve good sample contact the surface of the sample must remain, as flat as possible and therefore the pressure applied to the sample must be powerful enough to press the sample against the crystal but not damage the crystal or the sample. To obtain reproducible results the applied pressure has to remain constant [2-31].

The detection range depends on the type of detector and the material of the beam splitter. For ATR measurements a more sensitive detector needs to be used than for transmission as the energy reaching the detector is much lower because of absorption during reflection and losses in the optical system.

2.6.6.3 ATR-FTIR Experimental Parameters

ATR-FTIR spectra were recorded on a Nicolet Nexus FTIR spectrometer equipped with a Graseby – Specac Golden Gate™ accessory, a mercury cadmium telluride (MCT) detector and a single reflection diamond crystal. Spectra were recorded using the instrument settings summarised in Table 2–8.

Table 2–8 Settings for ATR-FTIR measurements on the Nicolet Nexus

Parameter	Setting
Number of Scans	10
Mirror Speed [cm/sec]	1.8988
Resolution [cm^{-1}]	4
Apodisation Function	Triangular
Spectral Region [cm^{-1}]	4000 - 650

2.6.7 Testing For Flammability

Within this thesis the UP nanocomposites were subjected to several tests for flammability namely the Underwriters Laboratory (UL94) and the Limiting Oxygen Index (LOI) tests. As with any test procedure, the tests for flammability are designed for the laboratory and quality control. In real fires plastics may behave significantly differently and the results of laboratory testing cannot predict the actual performance of a particular plastic or product.

2.6.7.1 Underwriters Laboratory (UL94)

UL testing is a method of classifying a material's tendency to either extinguish or spread a flame once it has been ignited and although originally developed by UL, it has now been incorporated into many National and International Standards (ISO 9772 and 9773). The testing involves applying a flame to a sample in various orientations and assessing the response of the material after the flame is removed. Materials that burn slowly or self extinguish and do not drip flaming material, rank highest in the UL classification scheme.

Horizontal Burning Test (94HB) - This is the easiest test to pass and materials that pass the vertical burning test will usually be acceptable for applications that require a horizontal burn, HB, only. The test involves applying a flame to one end of a horizontal bar of the plastic for 30 seconds or until the flame front reaches the specified mark. Figure 2–9 illustrates the horizontal burning test, and depicts a typical sample setup including dimensions. If burning continues then the time taken for the flame to travel between two set points is measured. If burning stops then the time of burning and the damaged length are measured.
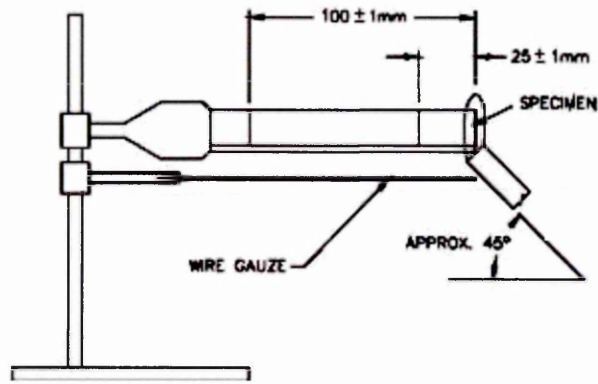
Figure 2–9 Schematic illustration of the Horizontal Burning Test (94HB)

A material will be classified 94HB if the time taken to reach the second mark is greater than the specified minimum or if burning stops before the second mark.

Vertical Burning Test (94V) - This is a more demanding test than the HB test because the specimen is tested in the vertical orientation and the material burning at the lower end of the sample preheats the material in the upper portion of the specimen. Figure 2–10 illustrates the vertical burning test, and depicts a typical sample setup including dimensions. A test flame is applied to the lower end of the test specimen and the material is classified according to Table 2–9. UL94V requires materials to be self-extinguishing to pass the test.
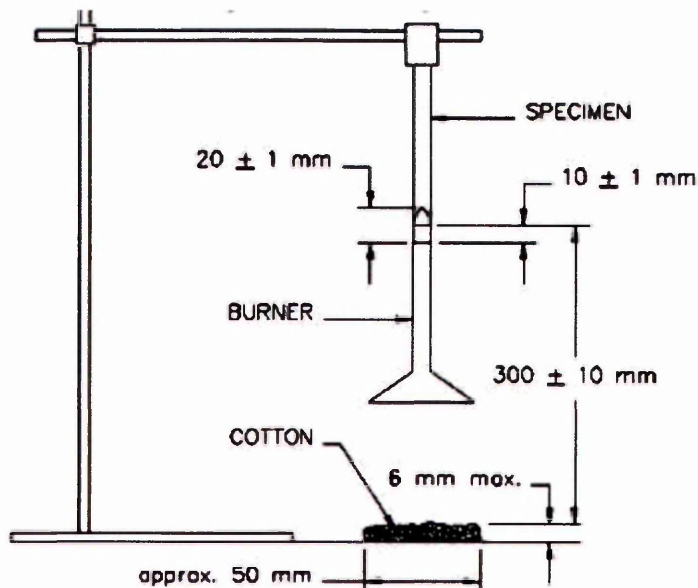
Figure 2–10 Schematic illustration of the Vertical Burning Test (94V)

There are 12 flame classifications specified in UL94 that are assigned to materials based on the results of these small-scale flame tests. These classifications, listed below in descending order of flammability (Table 2–9), are used to distinguish a material's burning characteristics after test specimens have been exposed to a specified test flame under controlled laboratory conditions [2-32].

- Six of the classifications relate to materials commonly used in manufacturing enclosures, structural parts and insulators found in consumer electronic products (5VA, 5VB, V-0, V-1, V-2, HB).

- Three of the remaining six classifications relate to low-density foam materials commonly used in fabricating speaker grills and sound-deadening material (HF-1, HF-2, HBF).

- The last three classifications are assigned to very thin films, generally not capable of supporting themselves in a horizontal position (VTM-0, VTM-1, VTM-2). These are usually assigned to substrates on flexible printed circuit boards.

To achieve either V-0, V-1 or V-2 ratings the criteria displayed in Table 2–9 have to be met:

Table 2–9 UL94 Ratings and Criteria [2-33]

UL94-V Rating	Duration of flaming for total flame application (Sec)	Total duration of flaming for 5 samples (10 flame applications) (Sec)	Dripping of Flaming Material
V-0 (Best)	Less than 10 sec	Less than 50 sec	None Allowed
V-1 (Good)	Less than 30 sec	Less than 250 sec	None Allowed
V-2 (Drips)	Less than 30 sec	Less than 250 sec	Dripping of flaming material which ignites the cotton placed below the specimen

2.6.7.2 Sample Specification

All samples were analysed using an in-house version of the UL94 vertical burning test. The samples were 1.5 mm thick, with dimensions of a standard microscope slide (75 x 25 mm). A standard butane gas 'crème brulee' torch (purchased from a local department store) was utilized with a set flame size of 40 mm. The samples were clamped in the vertical position, and then a flame applied to the bottom right hand corner of the sample for 10 seconds, the time it took for the flame to extinguish was recorded. 30 seconds after the flame had extinguished, the flame was re-applied in the same position for a further 10 seconds and the time recorded for the flame to extinguish. Both extinguish times were combined to give the total duration of flaming and the UL94-V rating.

2-1 Grim, R.E., Clay Mineralogy: McGraw-Hill, New York, 596 (1968)

2-2 Cullity, B.D. and Stock, S.R. 'Elements of X-Ray Diffraction' 3rd Edition, Prentice Hall, London (2001)

2-3 Moore D.M, Reynolds C (JR), 'X-ray Diffraction and the Identification and Analysis of Clay Minerals', 2nd ed., Oxford University Press, (1997)

2-4 Guy A., *Essentials of Materials Science*, McGraw-Hill Kogakusha Ltd (1976)

2-5 Utracki, L.A., 'Clay Containing Polymeric nanocomposites' Rapra Technology Ltd., 7-8 (2004)

2-6 Hendricks S.B, Fry W.H. *Soil Science*, **29**, 457 (1930)

2-7 Kelley W.P, Dore W.H and Brown S.M. *Soil Science*, **31**, 25 (1931)

2-8 Berry L.G, Mason B, 'Mineralogy-concepts, descriptions, determinations', W.H Freeman & Company, London, (1959)

2-9 Brindley G.W, Brown G, 'Crystal Structures of Clay Minerals and their X-ray identification', Mineralogical Society, Monograph No: 5, Spottiswoode Ballantyne Ltd, London, (1980)

2-10 Cullity B.D, 'Elements of X-ray Diffraction' Addison Wesley, Reading, (1978)

2-11 Polzsgay, A., Fráter, T., Százdi, L., Müller, P., Sajó, I. and Pukánszky, B. *Eur. Polym.*, **40**, 27 (2004)

2-12 Vaia, R.A., 'Polymer-Clay Nanocomposites' John Wiley & Sons Ltd 229-249 (2000)

2-13 Vaia RA, Liu WD, *J. Polym. Sci. Pt. B Polym. Phys.*, **40**, 1590 (2002)

2-14 Vaia, R.A. and Giannelis, E.P., *Macromolecules*, **30**, 8000 (1997)

2-15 Dodd J.W, Tonge K.H, Thermal Methods (Currell, B.R, ed.) John Wiley & Sons, London, 44 (1987)

2-16 Wei, Xie, Gao, Z., Liu, K., Pan, W.P., Vaia, R., Hunter, D. and Singh, A., *Thermochimica Acta*, **367-368**, 339 (2001)

2-17 Wei, Xie, Gao, Z., Pan, W.P., Vaia, R., Hunter, D. and Singh, A., *Chemistry of Materials*, **13** (9), 2979 (2001)

2-18 Green, A., MWTF Minneapolis, Minnesota, (1994)

2-19 Czarnecki J, Thumin D, Gas Flow Separation: The Sniffer Interface, NATAS conference proceedings, Toronto, Canada (1995)

2-20 Taken From http://www.ngb.netzsch.com/en/products/sta/ last accessed 23-03-06.

2-21 Coates J., *Encyclopaedia of Analytical Chemistry*, 10815 (2000)

2-22 Wu, H.D., Tseng, C.R. and Chang, F.C., *Macromolecules*, **34**, 2992 (2001)

2-23 Wu, Q., Liu, X. and Berglund, L.A., *Polymer*, **43**, 2445 (2002)

2-24 Aranda, P. and Ruiz-Hitzky, E., *Appl. Clay Sci.*, **15**, 119 (1999)

2-25 Griffiths, P. and de Haseth, J.A., Fourier Transform Infrared Spectrometry, Wiley & Sons, New York, (1986)

2-26 Materials and Engineering Research Institute webpage, last accessed: 05-12-05, URL: http://www.shu.ac.uk/schools/research/mri/pcas/

2-27 Maddams, B., *Int. J. Vibr. Spec.*, **5**, 3 (2001)

2-28 White Light Interferometry webpage, last accessed 05-12-05
http://images.google.co.uk/imgres?imgurl=http://rco.upol.cz/optics/research/witelite.old/pic1.gif&imgref url=http://rco.upol.cz/optics/research/witelite.old/witelite.htm&h=310&w=413&sz=4&tbnid=rbSe7Bh68 bwJ:&tbnh=90&tbnw=121&hl=en&start=18&prev=/images%3Fq%3DMichelson%2BInterferometer%2 6svnum%3D10%26hl%3Den%26lr%3D%26sa%3DG

2-29 Mirabella, M., *Appl. Spec. Rev.*, **21**, 45 (1985)

2-30 Garton, A., Infrared Spectroscopy of Polymer Blends, Composites and Surfaces', Hanser Publishers, Munich, (1992)

2-31 Buffeteau, T., Desbat, B. and Eyquem, D. *Vib. Spectrosc.*, **11**, 29 (1996)

2-32 From http://www.ul.com/plastics/flame.html last visited 12-01-06

2-33 From http://www.zeusinc.com/pdf/Zeus_Flammability.pdf last visited 16-01-06

3. Preparation and Characterisation of Commercial Organoclays and their Nanocomposites

3.1 Introduction

This chapter aimed to assess the commercially available nanofillers (Table 2-2 of Chapter 2) and to optimise mixing conditions for their dispersion into different unsaturated polyester resins (namely Crystic 272, Crystic 189LV and Crystic R935 (Table 2-3 of Chapter 2)). This was a scoping exercise carried out in the early stages of the project, before Cloisite 15A and Crystic 189LV were chosen as the optimal materials. It was also hoped to prepare experimental resins containing small amounts (<2%) of phosphonium groups in the unsaturated polyester backbone. It was anticipated that this small number of phosphonium groups would bind to the clay nanolayers and promote the dispersion of the clay throughout the resin. All organoclays and their resulting nanocomposites were characterised using XRD and TGA. The XRD and TGA experimental parameters can be found in sections 2.8.3 and 2.9.3 of Chapter 2. A summary of the nanocomposite preparation parameters can be found in Table 3–2.

3.2 Preparation and Formulation

Unsaturated polyester-clay (UP-clay) nanocomposites were prepared with variations in the sample composition and mixing procedure.

3.2.1 Preparation

The unsaturated polyester-clay nanocomposites (UPCN) were prepared by in-situ polymerisation. This method was chosen as it provided a straightforward means of casting the films once the nanocomposites had been prepared. The thermal stability and dispersion of the nanocomposites into the unsaturated polyester was investigated through the production of a wide range of samples. The samples were prepared using different organically modified montmorillonites and unsaturated polyesters, by varying the stirring time (to help expand the clay layers) and mixing speed (to investigate the effect of shear and clay loading) as displayed in Table 3–2.

Initially to be able to observe how the base resins behaved when cast under the manufacturers instructions, a series of experiments were carried out in which Crystic 272, 189LV and R935 were cast under the conditions recommended by Scott Bader, the manufacturers. Accelerator E (a cobalt accelerator containing 0.45% cobalt) provided by Scott Bader was added to 40g of Crystic 272 at 2 wt% and mixed at 1000 rpm for 15 minutes, Catalyst M (50% methyl ethyl ketone peroxide (MEKP)), also provided by Scott Bader, was then added at 2 wt% and the blend poured onto glass slides to gel.

3.2.2 Formulation

Organoclay, accelerator and 40 g of resin (provided by Scott Bader) were added together in a 100 ml waxed paper cup. A variety of organoclays were used at a range of concentrations between 1 and 5 wt% of the total weight of resin used. The accelerator (2 wt%) was mixed manually with a wooden spatula into the resin before the organoclay was added. The mixture was then blended together using a dispermat mixer equipped with a circ toothed dispersing impeller with a diameter of 2cm. The mixing speed and mixing time were varied during initial experiments. After the mixing step was complete the catalyst (2 wt%), was mixed manually into the resin with a wooden spatula and then the resin cast into a mould to produce samples with dimensions of 75 x 25 x 1.5 mm. The cast resins were then postcured, which consisted of a cure at room temperature for 24 hours and then heating to 80 °C for 3 hours. Table 3–1 displays the mixing regime adopted.

Table 3–1 Mixing regime adopted

1) Resins -	Crystic 272	2) Organoclays -	Cloisite 30B
	Crystic R935		Cloisite 10A
	Crystic 189LV		Cloisite 15A
			Garamite

3) Mixing Procedure - Resin + Accelerator E (2 wt%)
+ 5 wt% organoclay
(mixed for 15 or 30 minutes at 1000, 8000 or 14,000 rpm)
+ Catalyst M (2%)
(stirred with wooden spatula for 1 min)
(poured onto glass slide and levelled after resin began to thicken)

4) Postcuring - 24 Hours at room temperature followed by 3 hours at 80 °C

Table 3–2 Summary of the nanocomposite preparation parameters

wt% clay (with respect to UP)	Clay	UP	Mixing Speed (rpm)	Mixing Time (min)
---	---		1000	15
5	Cloisite 30B		1000	15
5	Cloisite 30B		1000	30
5	Cloisite 30B		8000	15
5	Cloisite 30B		8000	30
5	Na$^+$ Cloisite		1000	15
5	Cloisite 10A		1000	15
5	Cloisite 10A	Crystic 272	8000	15
5	Cloisite 15A		1000	15
5	Cloisite 15A		8000	15
5	Garamite		1000	15
5	Garamite		8000	15
1	Cloisite 30B		1000	15
3	Cloisite 30B		1000	15
5	Cloisite 30B		1000	15
10	Cloisite 30B		1000	15
---	---		1000	15
5	Cloisite 30B		1000	15
5	Cloisite 30B		8000	15
5	Cloisite 30B		14000	15
5	Cloisite 30B		1000	30
5	Cloisite 30B		8000	30
5	Cloisite 30B		14000	30
5	Sodium Cloisite		1000	15
5	Sodium Cloisite	Crystic R935	1000	30
5	Sodium Cloisite		8000	30
5	Cloisite 10A		1000	15
5	Cloisite 10A		8000	15
5	Cloisite 15A		1000	15
5	Cloisite 15A		8000	15
5	Garamite		1000	15
5	Garamite		8000	15
---	---		1000	15
5	Cloisite 30B		1000	15
5	Cloisite 30B		8000	15
5	Cloisite 30B		1000	30
5	Cloisite 30B		8000	30
5	Sodium Cloisite		1000	15
5	Sodium Cloisite	Crystic 189LV	8000	15
5	Cloisite 10A		1000	15
5	Cloisite 10A		8000	15
5	Cloisite 15A		1000	15
5	Cloisite 15A		8000	15
5	Garamite		1000	15
5	Garamite		8000	15

3.3   Results and Discussion

3.3.1   Effect of Organic Modifier on the Clay

The dispersion of four commercially available organically modified clays (at 5 wt% organoclay) in Crystic 272 were investigated (Cloisite 10A, Cloisite 15A, Cloisite 30B and Garamite).

3.3.1.1 XRD Analysis of the Effect of Organic Modifier on the Clay
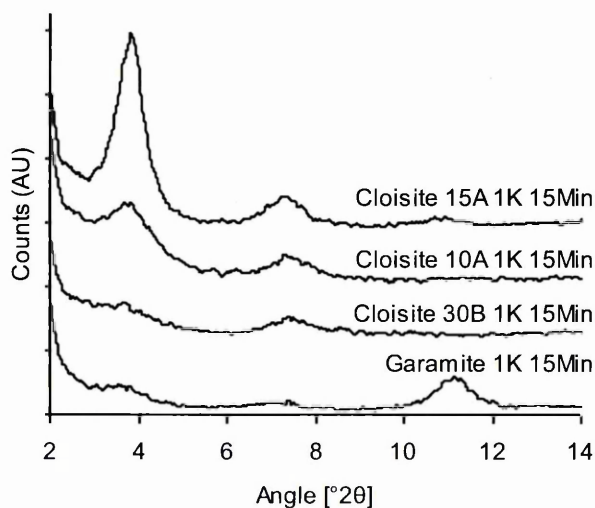
Figure 3–1 XRD traces (Cr tube) for Crystic 272 composites containing 5 wt% of various organoclays – Traces are offset for clarity
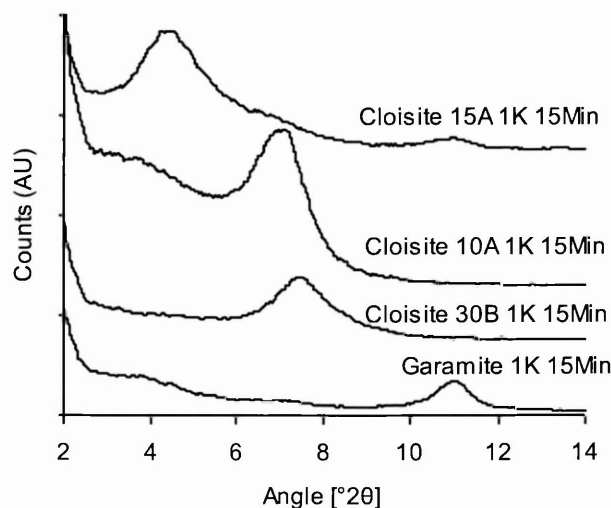
Figure 3–2 XRD traces (Cr tube) of various organoclays – Traces are offset for clarity

An increase in the layer spacing was observed in the XRD traces presented in Figure 3–1 compared to those in Figure 3–2, indicating that intercalated nanocomposites were produced. Cloisite 30B demonstrated the largest increase in layer spacing upon intercalation of Crystic 272 (from 17.2 Å to 34.4 Å (+ 100 %)) however, all clays reached a similar 'final spacing' near 34 Å (Cloisite 15A = 34.0 Å and Cloisite 10A = 33.7 Å). The increase in spacing between these samples and the pure clay was 76 % for Cloisite 10A (19.2 to 34.0 Å) but only 8 % for Cloisite 15A (31.5 to 34 Å), Cloisite 15A was very well ordered in Crystic 272.

The intense d_{001} peaks for the composites containing Cloisite 15A and Cloisite 10A indicated intercalated/aggregated composites as illustrated in Table 2-5 (a) of Chapter 2, in comparison the other composites displayed less intense peaks, which could be due to non-diffractioning clay aggregates or less organoclay in the beam. Cloisite 30B, Cloisite 10A and Cloisite 15A demonstrated intercalated/exfoliated composites when blended with Crystic 272. This was evident in the XRD traces by an increase in low angle scattering (indicating some exfoliation) and from the presence of less intense and broader d_{001} and d_{002} reflections (representing intercalation). The XRD trace for Garamite when blended with Crystic 272 was very similar to that of Garamite organoclay.

Cloisite 30B contained an hydroxyl group which was expected to be compatible with the ester on the oligomer, therefore allowing Cloisite 30B to disperse more readily into the UP. From the d_{001} spacing, derived from the XRD traces presented in Figure 3–1, Cloisite 30B displayed the largest increase in d-spacing (+15.9 Å) when dispersed in Crystic 272. Less Crystic 272 was able to penetrate into the clay layers of Cloisite 15A compared to Cloisite 10A, due to the surfactant on Cloisite 15A consisting of two alkylammonium chains as compared to Cloisite 10A which only has one. This made it physically harder for Crystic 272 to enter between the clay layers as there was less available space. The organocations in Cloisite 30B and Cloisite 10A change orientation upon dispersion into Crystic 272, going from lying parallel to the basal surface in a monolayer arrangement to orientating themselves perpendicular to the basal surface in a paraffin like arrangement (as depicted in Figure 1-9 of Chapter 1). This change in orientation accounts for the large increase in d-spacing upon dispersion into Crystic 272, however upon dispersion of Cloisite 15A into Crystic 272 the organocations were already orientated in a paraffin like arrangement and therefore Crystic 272 was not able to enter between the clay layers and cause significant layer expansion.

3.3.1.2 TGA Analysis of the Effect of Organic Modifier on the Clay
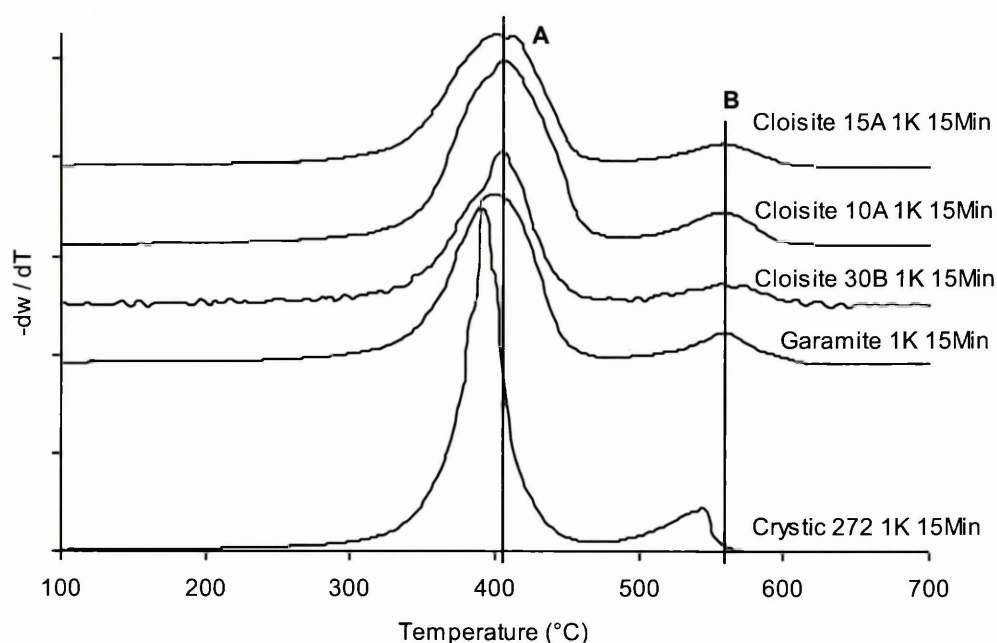
Figure 3–3 DTG traces (Air) for Crystic 272 prepared using 5 wt% of elected organoclay – Traces are offset for clarity

The DTG traces presented in Figure 3–3 displayed two thermal desorption events, occurring over two stages, for the nanocomposites and for Crystic 272. The nanocomposites displayed a temperature maximum (T_{max}) (A) at 409 °C and T_{max} (B) at 562 °C. Crystic 272 displayed T_{max} (A) at 393 °C and T_{max} (B) at 547 °C, therefore the addition of organoclay increased the maximum thermal decomposition temperature of Crystic 272 by approximately 20 °C. The addition of 5 wt% organoclay increased the peak width of the resulting nanocomposites by a maximum of 16 °C in the sample containing Cloisite 10A.

3.3.2 Effect of Clay Loading

Higher clay loadings can affect the dispersion of clay in a polymer matrix, increasing the number of intercalated or even agglomerated clay layers. To investigate the effect of clay loading on the thermal properties of UP nanocomposites, Crystic 272 was loaded with Cloisite 30B (the weakest trace in Figure 3–1) at 1, 3, 5 and 10 wt% and mixed at 1000 rpm for 15 minutes.

3.3.2.1 XRD Analysis of the Effect of Clay Loading
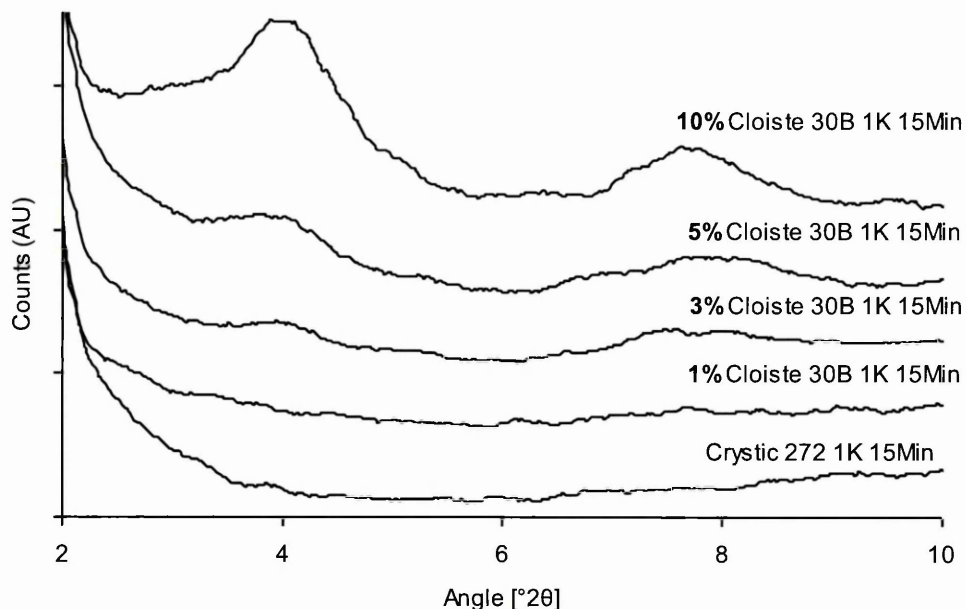
Figure 3–4 XRD traces (Cr Tube) for Crystic 272 nanocomposites prepared using Cloisite 30B at different clay loadings – Traces are offset for Clarity

The XRD results presented in Figure 3–4 demonstrated that at low clay loadings (1 to 3 wt%) the d_{001} peak could not be observed, which could indicate an exfoliated nanocomposite. However, an exfoliated nanocomposite should exhibit increased scattering at low angle, which the XRD traces for the 1-3 wt% samples do not show and therefore the traces are comparable to that for pure Crystic 272, possibly indicating poor scattering (Table 2.5 (e) of Chapter 2) or little/no clay in the beam. At 5 and 10 wt% the d_{001} and d_{002} peaks were clearly visible at 33.3 and 17.1 Å in the 5 wt% sample and 32.8 and 16.9 Å in the 10 wt% sample. As the amount of clay in the sample decreased from 10 to 5 wt% then a shift in the d_{001} and d_{002} spacings to a slightly lower angle was observed, the distance between the d_{001} and d_{002} peaks remained the same at approximately 16.0 Å and confirmed that the second peak was in fact the d_{002} reflection. If the second peak was not the d_{002} reflection but the d_{001} reflection of Cloisite 30B organoclay then the spacing between the first and second peak would not have remained the same and a peak at 17.2 Å would have been observed in both samples. An increase in low angle scattering coupled with a broader less defined d_{001} peak, indicated that intercalated/exfoliated nanocomposites had been formed when 5 or 10 wt% Cloisite 30B was dispersed in Crystic 272.

3.3.2.2 TGA Analysis of the Effect of Clay Loading
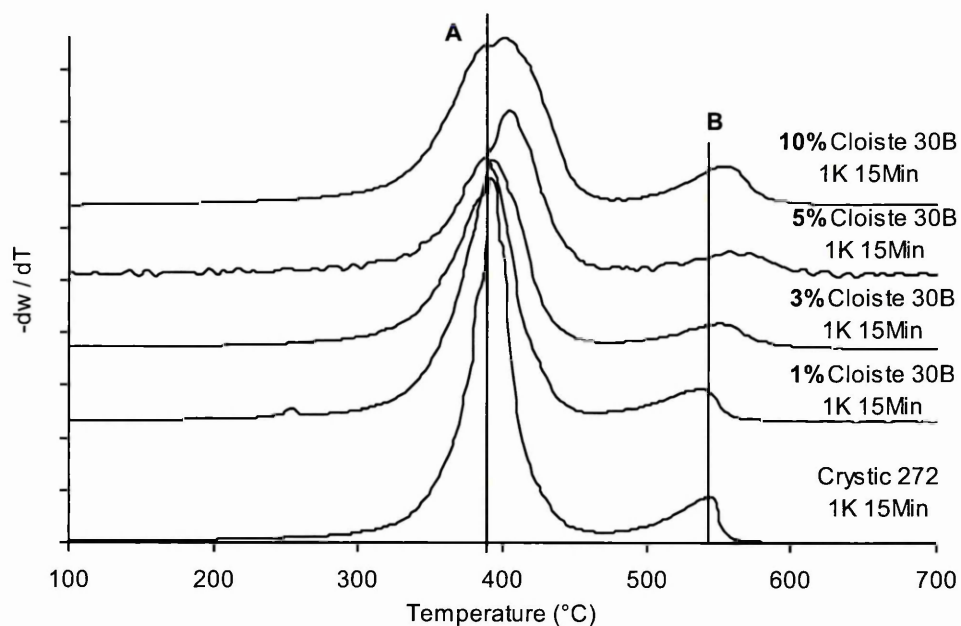
Figure 3–5 DTG traces (Air) for nanocomposites prepared using Crystic 272 with 0-10 wt% Cloisite 30B – Traces are offset for Clarity

The DTG traces presented in Figure 3–5 displayed two thermal desorption events (A and B), occurring over two stages for Crystic 272 incorporating between 0 and 10 wt% Cloisite 30B. T_{max} (A) occurred during stage 1 (200-477 °C) at 390 °C for Crystic 272 and the 1 wt% sample and 393, 409 and 404 °C for the 3, 5 and 10 wt% samples, respectively. T_{max} (B) occurred during stage 2 (478-625 °C) at 544 °C for Crystic 272 and, 540, 554, 568 and 558 °C for the 1, 3, 5 and 10 wt% samples, respectively. The peak width increased with increasing clay content, increasing by a maximum of 14 °C in the 10 wt% sample.

3.3.3 Effect of Stirring Time and Mixing Speed.

Experiments were carried out using Crystic R935 and Cloisite 30B in order to determine the optimum mixing speed and time required to obtain maximum clay dispersion in the final samples. The samples were mixed using 5 wt% Cloisite 30B for 15 or 30 minutes and at 1000, 8000 or 14, 000 rpm. Cloisite 30B was used as it gave the most XRD silent trace in Figure 3–1, which was thought to reflect the most dispersion.

3.3.3.1 XRD Analysis of the Effect of Stirring Time and Mixing Speed.
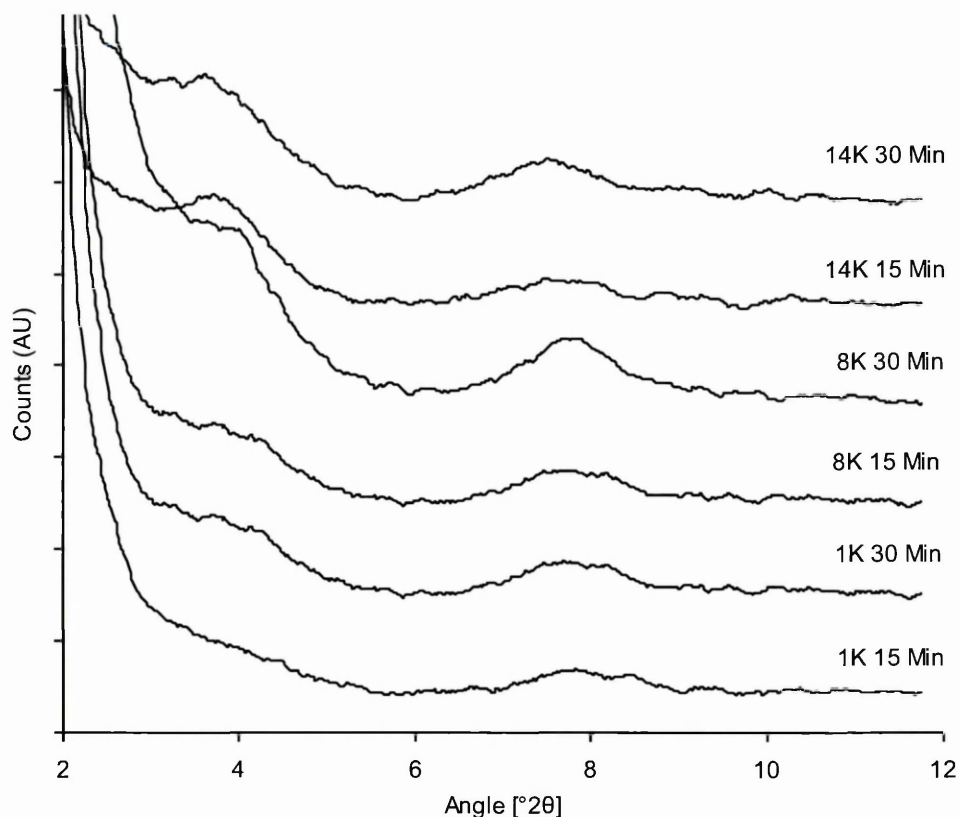
Figure 3–6 XRD traces (Cr Tube) for composites prepared using Crystic R935 and Cloisite 30B at different mixing times and speeds – Traces are offset for clarity

The XRD traces presented in (Figure 3–6) demonstrated a broad, weak d_{001} peak centred around 31.7 Å, and a second peak at approximately 16.8 Å, which is representative of the d_{002} of unexpanded Cloisite 30B as observed in Figure 3–2, where Cloisite 30B organoclay exhibited a d_{002} spacing of 17.2 Å. Cloisite 30B when mixed at 14 000 rpm for 15 or 30 minutes exhibited a d_{001} peak at a slightly lower angle and higher d-spacing (34.2 Å), however almost the same spacings (31.7 and 16.8 Å) were obtained when mixed at 1000 or 8000 rpm. All peaks were of similar intensity suggesting that all samples had a similar degree of exfoliation/intercalation, with the exception of the composite prepared at 8000 rpm for 30 minutes, which showed evidence of low angle scattering and therefore more exfoliated clay layers within the sample, leading to a more exfoliated/intercalated composite.

3.3.3.2 TGA Analysis of the Effect of Stirring Time and Mixing Speed.
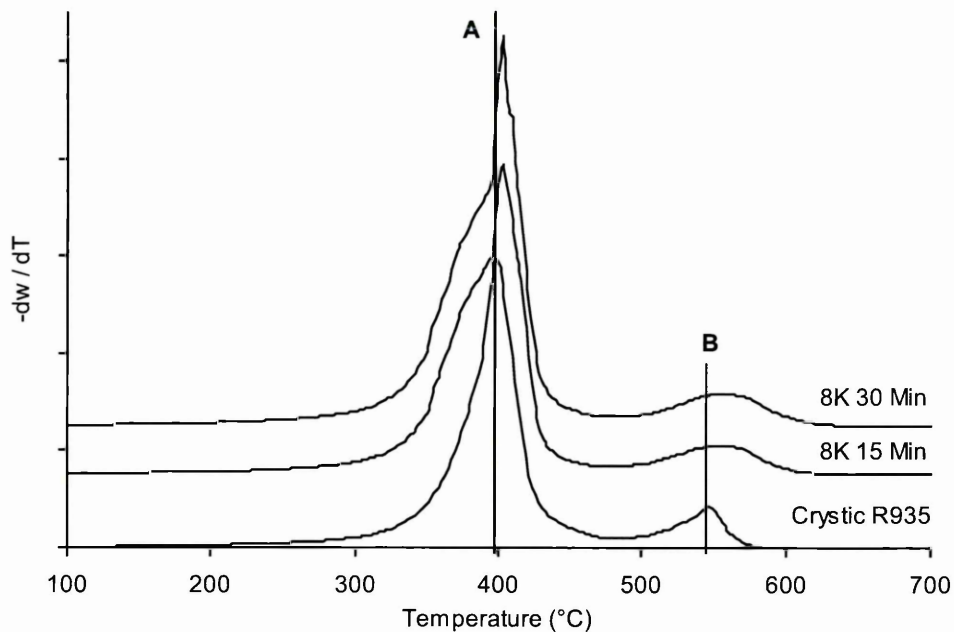
Figure 3–7 DTG traces (Air) for composites prepared using Crystic R935 and Cloisite 30B at 8000 rpm for 15 and 30 minutes – Traces are offset for clarity

The DTG traces presented in Figure 3–7 display a two stage thermal decomposition for both Crystic R935 and its nanocomposites containing Cloisite 30B. T_{max} (A) occurred at 395 °C for pure Crystic R935 increasing to 402 °C upon addition of Cloisite 30B. T_{max} (B) occurred at 551 °C in pure Crystic R935 increasing again by 7 °C upon addition of Cloisite 30B to give T_{max} (B) at 558 °C. This thermal degradation pattern was also observed in nanocomposites made at 1000 and 14000 rpm. At this stage it was decided to carry out further experiments at 1000 rpm for 15 minutes as it was thought that these mixing conditions resulted in an exfoliated nanocomposite. However, further understanding of the interpretation of the XRD spectra revealed that the composites (including composites prepared using Cloisite 10A and Cloisite 15A) prepared at 1000 rpm for 15 minutes were actually intercalated, and resembled the XRD traces displayed in Table 2.5 (b) of Chapter 2. An exfoliated nanocomposite would resemble the XRD trace displayed in Table 2.5 (d) of Chapter 2.

3.3.4 Effect of Polymer Structure

The original criterion for identifying the most appropriate organoclay was based on the extent to which the organoclay dispersed into different resins based on how silent the XRD traces were, however oven tests (performed by a colleague) and rudimentary flame tests clearly identified an intercalated structure as offering the most effective fire retardant properties. The oven tests were conducted to obtain information about the physical structure and chemical composition of the residues remaining after the samples were heated. The samples were heated in air in an oven at 500 °C for 5 minutes, and then the residue investigated using optical microscopy and scanning electron microscopy (SEM). The SEM studies indicated that intercalated nanocomposites produced large chunks of a solid and dense clay/graphite hybrid, while XRD silent nanocomposite produced small pieces of a solid clay/graphite hybrid dispersed in free graphite. The highly intercalated structure arising from Cloisite 15A dispersed in resin (Figure 3–1), produced the most integral and dense char which could be the best type of insulation layer for enhanced fire retardant properties. Therefore, Cloisite 15A was chosen over the largely XRD silent nanocomposites produced when Cloisite 30B was mixed with resin. A simple fire test, which utilised a horizontal burning position, was then set up. During these fire tests, the pure resin evolved massive quantities of smoke and the flame did not self extinguish. The same was observed with an XRD silent nanocomposite (Cloisite 30B and Crystic 189LV). However, the highly intercalated nanocomposite (Cloisite 15A and Crystic 189LV) produced less smoke when the sample burned, and self-extinguished within 26 seconds.

The three different types of unsaturated polyester used for nanocomposite preparation have different structures, which may influence the packing of the polymer chains within the clay layers. Cloisite 15A was mixed with the three unsaturated polyesters to investigate whether the polymer structure would influence the arrangement of the clay layers in the resulting nanocomposite material.

3.3.4.1 XRD Analysis of the Effect of Polymer Structure
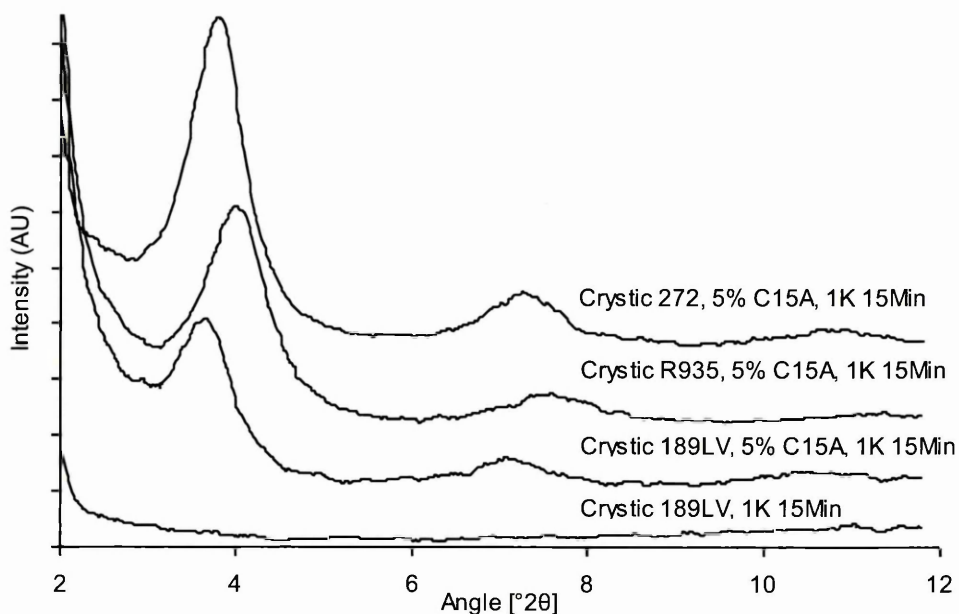
Figure 3–8 XRD traces (Cr tube) for composites prepared using Crystic 272, R935 and 189LV and Cloisite 15A. Crystic 189LV has been added as a comparison – Traces are offset for clarity

The XRD traces presented in Figure 3–8 display comparisons for nanocomposites of Crystic 272, Crystic R935 and Crystic 189LV containing 5 wt% Cloisite 15A. Crystic 189LV has been added as a comparison and displayed neither d_{001} nor d_{002} peaks. Both d_{001} and d_{002} peaks were present in all samples containing Cloisite 15A however, an increase in scattering at low angle in the Crystic 189LV composite compared to the Crystic 272 and R935 composites, coupled with a less well defined d_{001} peak indicated that the Crystic 189LV composite contained an increased amount of dispersed clay layers. The d_{001} spacings for composites prepared using Crystic 272, Crystic R935 and Crystic 189LV plus 5 wt% Cloisite 15A were 33.7 Å, 31.7 Å and 34.9 Å, respectively. The d_{001} and d_{002} spacings remained approximately 16 Å apart in all resins, confirming the identity of the d_{002} peak. Cloisite 15A displayed a d_{001} spacing of 31.5 Å (Figure 3–2), therefore it was apparent that the interlayer space of Cloisite 15A had not expanded when dispersed into Crystic R935. However, Cloisite 15A did expanded slightly when dispersed into Crystic 272 and Crystic 189LV.

3.3.4.2 TGA Analysis of the Effect of Polymer Structure
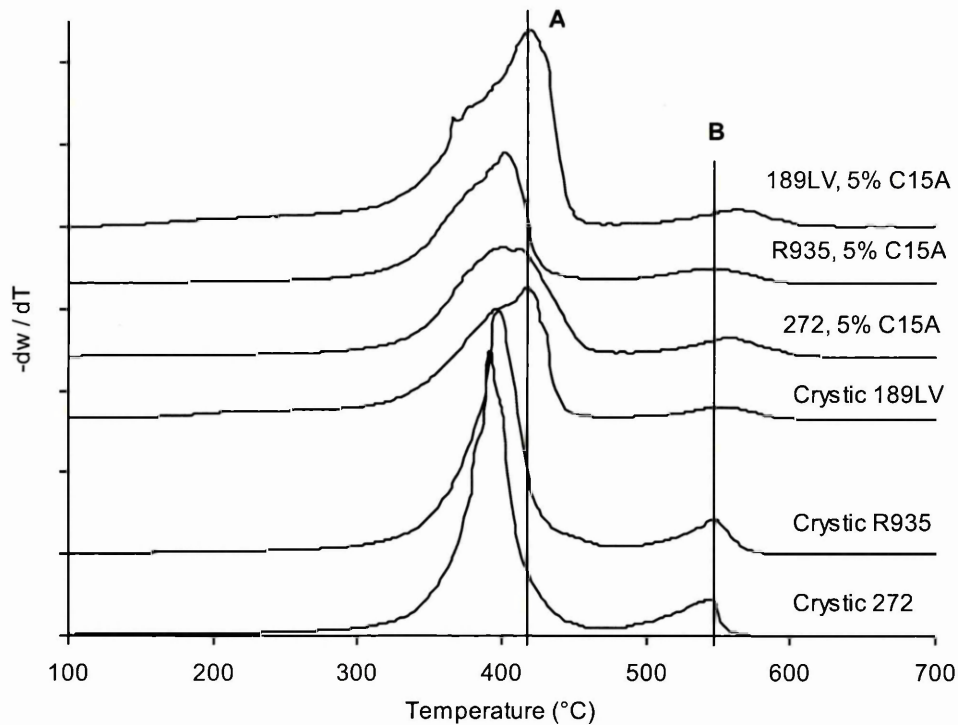
Figure 3–9 DTG traces (Air) for composites prepared using Crystic 272, R935 and 189LV and Cloisite 15A, mixed at 1000 rpm for 15 minutes – Traces are offset for clarity

The DTG results presented in Figure 3–9 displayed a two step thermal decomposition for both nanocomposites and pure resin. Upon comparison of the maximum temperature for the nanocomposites and pure resin it was apparent that T_{max} (A) increased from 393 to 407 °C in Crystic 272, however T_{max} (A) remained unchanged in Crystic 189LV and Crystic R935 at 422 and 403 °C, respectively. T_{max} (B) increased from 547 to 561 °C in Crystic 272, from 556 to 568 °C in Crystic 189LV yet remained unchanged in Crystic R935 at 548 °C. The biggest difference between the nanocomposites and resins was the increased peak width upon addition of organoclay, as observed in Figure 3–3 and Figure 3–5.

3.3.5 Effect of Ultrasound

In an attempt to improve dispersion of the organoclay into Crystic 189LV the use of ultrasound (15 minutes) prior to mixing was employed. An ultrasonic bath supplies energy to the polymer chains and the clay layers enabling the polymer chains to enter more readily into the galleries between the silicate layers [3-1]. An ultrasonic bath can therefore promote exfoliation and prevent formation of agglomerates resulting in an increase in polymer-clay surface interactions.

It was found that ultrasound and mixing did not significantly change the extent of dispersion or thermal properties of Cloisite 30B when mixed with Crystic 189LV. These results contrast with those obtained by Inceoglu et al. [3-1], who obtained an increase in tensile strength (+ 8.9%), tensile modulus (+ 4.3%) and impact strength (+ 13%) of samples prepared in an ultrasonic bath using an orthophthalic unsaturated polyester resin and Cloisite 30B. Their results indicated that when an ultrasonic bath was used, higher values were obtained due to a higher degree of exfoliation.

3.3.6 Comparison of Results for the Preparation of Unsaturated Polyester/Organoclay Nanocomposites

Nanocomposites of unsaturated polyester and organically modified montmorillonite were prepared by in-situ polymerisation. Several preparation parameters were investigated (e.g. clay loading and polymer structure) in order to optimise mixing conditions into different unsaturated polyester resins. All nanocomposites were characterised fully using XRD and TGA.

Differences in organic modification of commercially available organoclays resulted in changes in the interlayer spacing of the organoclay when dispersed in Crystic 272. XRD data demonstrated an increased d-spacing from 17.2 Å to 34.4 Å (+ 100 %) for Cloisite 30B, from 19.2 to 34.0 Å (+ 76 %) for Cloisite 10A and from 31.5 to 34 Å (+ 8 %) for Cloisite 15A. Cloisite 30B, Cloisite 10A and Cloisite 15A demonstrated intercalated/exfoliated composites when blended with Crystic 272, however Cloisite 15A displayed the most order within the nanocomposites, displaying clear, sharp, d_{001} and d_{002} peaks. Cloisite 30B displayed the largest percentage increase in the d_{001} spacing upon intercalation, however all of the organoclays reached a similar 'final spacing' near

34 Å. From the d_{001} spacing, derived from the XRD traces presented in Figure 3–1, Cloisite 30B displayed the largest increase in d-spacing (+15.9 Å) when dispersed in Crystic 272. The relatively low percentage increase in the d_{001} spacing for Cloisite 15A can be attributed to the surfactant on the clay containing two alkylammonium chains which make it physically more difficult for the resin to enter into the gallery of the clay.

The organocations in Cloisite 30B and Cloisite 10A change orientation upon dispersion into Crystic 272, going from lying parallel to the basal surface in a monolayer arrangement to orientating themselves perpendicular to the basal surface in a paraffin like arrangement (as depicted in Figure 1-9 of Chapter 1). This change in orientation accounts for the large increase in d-spacing upon dispersion into Crystic 272, however upon dispersion of Cloisite 15A into Crystic 272 the organocations were already orientated in a paraffin like arrangement and therefore Crystic 272 was not able to enter between the clay layers and cause significant layer expansion. These results are similar to those published by other groups [3-1, 3-2, 3-3] for the preparation of unsaturated polyester/clay nanocomposites.

An increase in low angle scattering in the XRD traces for Cloisite 30B, coupled with a decrease in intensity of the d_{001} and d_{002} reflections indicated that the composites were very likely to have regions of exfoliated clay layers co-existing with intercalated regions, very much like the XRD traces illustrated in Table 2.5 (c) in Chapter 2. XRD patterns exhibiting the absence of basal reflections are often initially interpreted as evidence for an exfoliated nanocomposite. However, Bharadwaj *et al.* [3-4] found that what appeared to be exfoliated nanocomposites using XRD, were actually intercalated/exfoliated nanocomposites when TEM was utilised. It was observed that regions of delaminated sheets dispersed individually existed amongst regions, where the regular stacking arrangement was maintained with a layer of polymer between the sheets. The diffraction profiles for different types of intercalated and exfoliated nanocomposites can be found in Table 2-5 of Chapter 2.

Increasing the clay loading of Cloisite 30B from 0 to 10 wt% into Crystic 272, resulted in the XRD traces for the samples containing 1 to 3 wt% Cloisite 30B resembling that of the XRD trace for pure Crystic 272. The absence of the d_{001} reflection did not indicate an exfoliated nanocomposite but rather a composite which was intercalated

(confirmed through the absence of low angle scattering), but had little/no clay in the beam. At 5 and 10 wt% the d_{001} and d_{002} peaks were clearly visible indicating an intercalated/exfoliated structure, confirmed through an increase in low angle scattering coupled with a broad and less intense d_{001} reflection. As the amount of clay in the sample decreased from 10 to 5 wt% then a shift in the d_{001} and d_{002} spacings to a lower angle was observed, the distance between the d_{001} and d_{002} peaks remained the same at approximately 17 Å, therefore confirming that the second peak was in fact the d_{002} reflection. If the second peak was not the d_{002} reflection but the d_{001} reflection of Cloisite 30B organoclay, then the spacing between the first and second peak would not have remained the same and a peak at 17.2 Å would have been observed in both samples. The DTG traces indicated an increase in the thermal decomposition temperature maxima (T_{max} (A)) of 19 °C as the clay loading of Cloisite 30B increased from 0 to 5 wt%. The peak width increased with increasing clay content, increasing by a maximum of 14 °C at 10 wt% Cloisite 30B. Based on these XRD and TGA results it was decided to carry out further experiments using 5 wt% organoclay as this produced a more exfoliated/intercalated composite with an increased thermal decomposition temperature maximum.

The dispersion of Cloisite 30B into Crystic R935 decreased as the mixing speed increased, probably due to shear forces causing the clay particles to re-aggregate. The reproducibility of the XRD traces also decreased as the mixing speed increased due to air bubbles trapped within the sample. Changing the stirring time from 15 to 30 minutes at each mixing speed did not decrease the level of dispersion at that mixing speed. All peaks were of similar intensity suggesting that all samples had a similar degree of intercalation/exfoliation, with the exception of the composite prepared at 8000 rpm for 30 minutes, which showed evidence of low angle scattering and therefore more exfoliated clay layers within the sample, leading to a more exfoliated/intercalated composite. The DTG traces indicated that the addition of Cloisite 30B into Crystic R935 increased the thermal decomposition temperature maxima by 5 °C for both T_{max} (A) and T_{max} (B) compared to pure Crystic R935, however T_{max} (A) and (B) remained the same when samples were prepared under all mixing conditions. Based on XRD results it was decided to use 1000 rpm for 15 minutes as the standard conditions because they produced what was thought to be an exfoliated nanocomposite, however further

understanding of the interpretation of the XRD spectra revealed that these composites were actually intercalated.

These experiments were carried out in the early stages of the project and the original criterion for identifying the most appropriate organoclay was based on the extent to which the organoclay dispersed in different resins. However oven tests and rudimentary flame tests clearly identified an intercalated structure as offering the most effective fire retardant properties. The highly intercalated structure arising from Cloisite 15A dispersed in Crystic 189LV, produced the most integral and dense char which is the best type of insulation layer for enhanced fire retardant properties. Therefore, Cloisite 15A and Crystic 189LV were chosen over the other organoclays and resins.

Upon dispersion of Cloisite 15A into the unsaturated polyesters Crystic 272, 189LV and R935 intercalated/exfoliated composites were formed. The d_{001} and d_{002} reflections were visible in all organoclay/resin mixtures, however an increase in the scattering at low angle in the Crystic 189LV composite, coupled with a less well defined d_{001} reflection indicated that this composite contained an increased amount of exfoliated clay layers. Cloisite 15A did not expand upon dispersion into Crystic R935 and expanded by approximately 2 Å, when dispersed into Crystic 272 and 189LV. Cloisite 15A also displayed minimal expansion upon dispersion into other resin systems such as polyvinylester (PVE) [5] and polymethylmethacrylate/poly(styrene-co-acrylonitrile) (PMMA/SAN) [6].

3.4   The Synergistic Effect between Halogenated Resins and Clays

In the early stages of the project it was hoped to prepare experimental resins containing small amounts (<2%) of phosphonium groups in the unsaturated polyester backbone. It was anticipated that this small number of phosphonium groups would bind to the clay nanolayers and disperse them throughout the resin in a similar manner to the use of maleated polypropylene [7, 8]. However, initial evaluation of this phosphorus monomer identified some issues with the chosen synthetic route regarding stability. Therefore, a range of unsaturated polyesters already incorporating chlorine (Crystic D3644LV) or bromine (Crystic PD7343) were provided by Scott Bader. In this thesis, the halogenated resins are denoted as Cl-resin and Br-resin. These halogen resins were blended with the

standard UP resin (Crystic 189LV) at different concentrations. Cloisite 10A was identified as a standard commercially available organoclay for this work. Cloisite 10A was chosen for this work before Cloisite 15A was set up as the optimum clay to be used throughout the project. The standard mixing regime outlined in Table 3–1 was used and blends of Crystic 189LV, which are outlined in Table 3–3 were prepared. XRD was used to evaluate the influence on organoclay dispersion when incorporating halogen resins, TGA measurements were also performed.

Table 3–3 Clay and halogenated clay additions to Crystic 189LV

Blend	C10A (wt%)	Cl-resin (wt%)	Br-resin (wt%)
1	1	-	-
2	3	-	-
3	5	-	-
4	1	10	-
5	1	20	-
6	1	40	-
7	1	-	10
8	1	-	20
9	1	-	40
10	3	10	-
11	3	20	-
12	3	40	-
13	3	-	10
14	3	-	20
15	3	-	40
16	5	10	-
17	5	20	-
18	5	40	-
19	5	-	10
20	5	-	20
21	5	-	40

3.4.1 XRD Analysis of the Synergistic Effect between Cl-resin and Clay
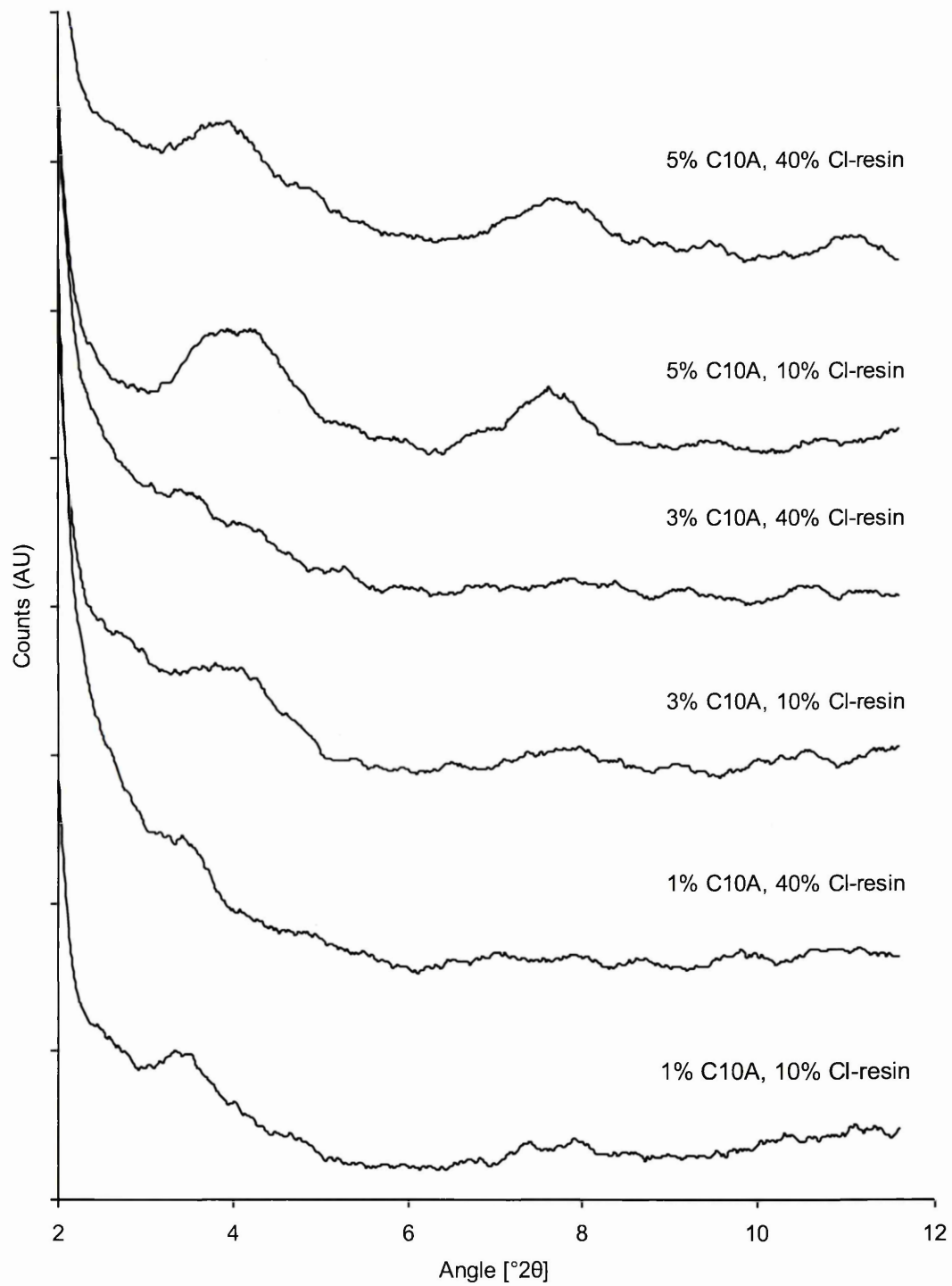
Figure 3–10 XRD traces (Cr Tube) for composites prepared using Crystic 189LV and 1 to 5 w% C10A, plus 10 or 40 wt% Cl-resin – Traces are offset for clarity

The XRD traces presented in Figure 3–10 display Crystic 189LV blended with Cloisite 10A at 1, 3 or 5 wt% and either 10 or 40 wt% Cl-resin. The XRD traces were very weak in all samples and therefore a significant amount of error ($\pm$ 2Å) had to be taken into consideration upon determination of the d-spacings. From the absence of low angle scattering in the XRD traces, all nanocomposites are presumed to be intercalated, however there was little/no clay in the beam to produce a d_{001} reflection in the samples containing less than 5 wt% Cloisite 10A. The traces at 5 wt% displayed d_{001} and d_{002} reflections, representing d-spacings of 29.8 and 16.8 Å, respectively. The XRD results for the Br-resin system indicated the same intercalated structure and degree of dispersion as the Cl-resin containing nanocomposites.

Table 3–4 Parameters of the diffraction peaks (Cl-resin system)

Composition	Peak Position (°2θ)	d-spacing (Å)
C10A-1 Cl-0	3.26	34
C10A-1 Cl-10	3.68	36
C10A-1 Cl-20	3.84	34
C10A-1 Cl-40	3.78	35
C10A-3 Cl-0	3.85	34
C10A-3 Cl-10	4.22	31
C10A-3 Cl-20	4.14	31
C10A-3 Cl-40	-	-
C10A-5 Cl-0	3.88	34
C10A-5 Cl-10	4.32	30
C10A-5 Cl-20	4.26	30
C10A-5 Cl-40	4.02	33

The diffraction peak parameters for the Cl-resin system are presented in Table 3–4. At each clay content (1, 3 or 5 wt%) as the halogen-resin increased from 0 to 40 wt% the d-value increased and the peak intensity decreased. At each Cl-resin content the d-value decreased with increasing clay content, also the degree of clay dispersion decreased with increasing clay content. These results correspond to the common knowledge that clay disperses more readily into mixtures containing more of a polar component.

Several studies have been conducted on the preparation and characterisation of poly(vinyl chloride) (PVC)/organically modified MMT nanocomposites [3-9, 3-10, 3-11]. It was noted that as the clay content increased (1-5 wt%), the characteristic diffraction peak of the organically modified MMT (OMMT) in PVC/OMMT nanocomposites decreased significantly in intensity and shifted to a lower angle. This indicated that the

PVC chains had intercalated into the interlayer of OMMT, and also confirmed that reducing the loading of OMMT was favourable for the intercalation of PVC chains into the silicate layers. TEM results suggested that partially exfoliated and partially intercalated structures had formed in PVC/OMMT nanocomposites. The PVC systems in the literature correspond to the Cl-resin systems in this thesis as a significant loss of intensity was also observed upon addition of the organic MMT Cloisite 10A and also a shift in the d_{001} spacing to a lower angle was observed. As the clay loading decreased from 5 to 1 wt% then the d_{001} spacing increased to approximately 35 Å in the 1 wt% sample, compared to approximately 31 Å in the 5 wt% samples.

3.4.2 TGA Analysis of the Synergistic Effect between Cl-resin and Clay
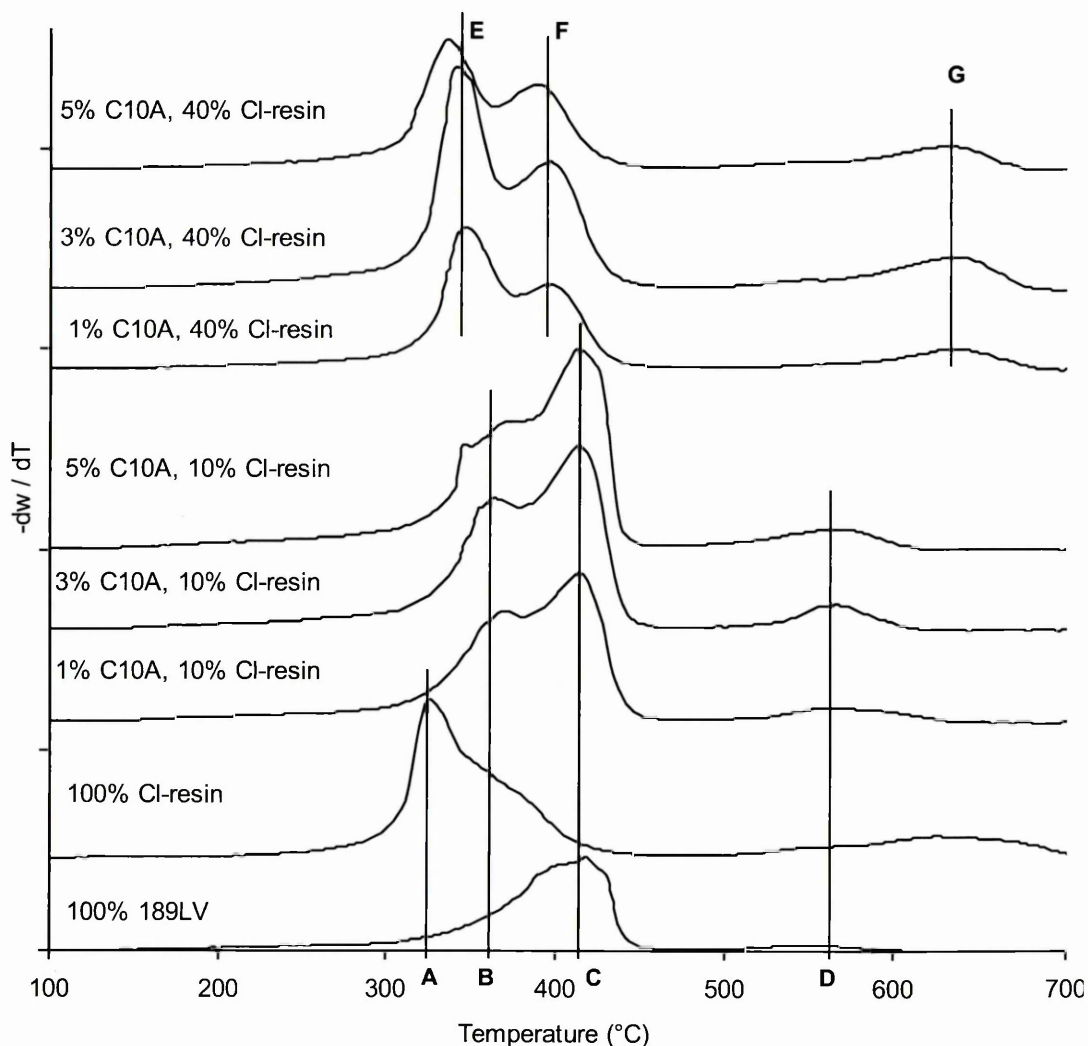
Figure 3–11 DTG traces (Air) for composites prepared using Crystic 189LV and 1 to 5 w% C10A, plus 10 or 40 wt% Cl-resin – Traces are offset for clarity

The DTG traces presented in Figure 3–11 display seven thermal desorption events (T_{max} (A), (B), (C), (D), (E) (F) and (G)) occurring over two stages (Stage 1 260-460 °C and stage 2 461-700 °C), which are listed in Table 3–5. Crystic 189LV displayed a two step decomposition with T_{max} (C) occurring at 422 °C and T_{max} (D) occurring at 556 °C, the Cl-resin displayed a three step decomposition with T_{max} (A) occurring at 323 °C, T_{max} (B) occurring at 369 °C and T_{max} (D) occurring at 631 °C. Three maxima were observed in the DTG traces for the composite samples (B, C and D for the 10% samples and E, F and G for the 40% samples). T_{max} (B), (C), (E) and (F) occurred over the region of 270-460 °C with T_{max} (B) occurring at 367 °C and T_{max} (C) occurring at 417 °C in the 10 wt% Cl-resin samples and T_{max} (E) occurring at 351 °C and T_{max} (F) occurring at 395 °C in the 40 wt% Cl-resin samples. T_{max} (D) and T_{max} (G), which were representative of the decomposition of the char layer formed upon burning, occurred at 568 °C (T_{max} (D)) in the 10 wt% Cl-resin samples and 638 °C (T_{max} (G)) in the 40 wt% Cl-resin samples. In Crystic 189LV and Cl-resin blends the two maxima representing thermal decomposition of the resin move closer in temperature with increasing Cl-resin content. The corresponding DTG traces for the Br-resin system (not illustrated) indicated the same thermal degradation profile as the Cl-resin containing nanocomposites.

Table 3–5 TG results of Crystic 189LV, Cl-resin and Crystic 189LV/Cl-resin/Cloisite 10A composites

	Stage 1 10 wt% Sample			Stage 2 10 wt% Sample	Stage 1 40 wt% Sample		Stage 2 40 wt% Sample
	A (°C)	B (°C)	C (°C)	D (°C)	E (°C)	F (°C)	G (°C)
Crystic 189LV			422	556			
Cl-resin	323	369					631
1% C10A, 10% Cl-resin		367	417	568			
3% C10A, 10% Cl-resin		367	417	568			
5% C10A, 10% Cl-resin		367	417	568			
1% C10A, 40% Cl-resin					351	395	638
3% C10A, 40% Cl-resin					351	395	638
5% C10A, 40% Cl-resin					339	390	638

Yang *et al.* [3-10] also observed three maxima in their DTG traces for the thermal decomposition of PVC/OMMT nanocomposites. In the presence of silicate layers a decrease in the T_{max} under stage 1 was observed, however a slight increase in the T_{max} under stage 2 was observed. This trend was also observed in the samples listed in Table 3–5, the temperature maxima under stage 1 decreased by 2 °C for T_{max} (B) and 5 °C for T_{max} (C), however under stage 2 T_{max} (D) (T_{max} (G) in the 40 wt% Cl-resin sample) increased by 12 °C in the 10 wt% Cl-resin samples and 7 °C in the 40 wt% Cl-resin samples.

3.5 The Effect of Clay on Char Formation

All flame retardants act either in the vapour phase or the condensed phase through a chemical and/or physical mechanism to interfere with the combustion process during heating/pyrolysis, ignition or flame spread. It is unlikely that organoclay plays a significant retarding role in the vapour phase. Hence the improvement in fire retardant performance is attributed to the insulating barrier 'char'. Consequently, the composition, quantity and quality of the char formed in a nanocomposite have been investigated. The amount of char, the onset temperature for char decomposition and char decomposition temperature range were evaluated using TG results. Decomposition of an UP occurs in two steps; thermal decomposition of the resin and decomposition of the char formed (Figure 3–12).
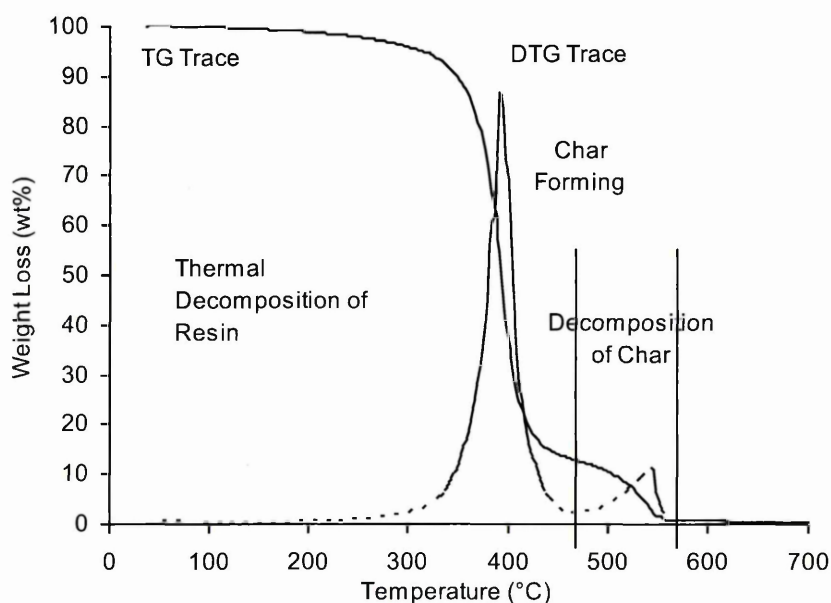
Figure 3–12 Typical TG and DTG traces (air) for UP decomposition

3.5.1 Effect of Clay on Amount of Char Formed

Generally, the incorporation of clay into a polymer matrix enhances its thermal stability by acting as a superior insulator and mass transport barrier to volatile products generated during decomposition. The clay acts as a heat barrier, which enhances the overall thermal stability of the system, as well as assisting in the formation of char after thermal decomposition of the resin. This high performance carbonaceous-silicate char builds up on the surface of the nanocomposite during burning, therefore insulating the underlying material [3-12]. As the fraction of clay increases, the amount of char that can be formed increases, and the rate at which heat is released decreases, provided an integral, coherent char is formed. There are many methods to evaluate the flame retardant properties of polymers, a convenient and useful method to evaluate char at the research and development stage is TGA, however it must be noted that a real combustion situation is more complicated and severe than that in a 'static' heating environment.

The TG and DTG traces presented in Figure 3–13 display nanocomposites of the Cl-resin with increasing clay content (0-5 wt%). The corresponding parameters are calculated and listed in Table 3–6 and Table 3–7. In the thermal decomposition section of the DTG trace (i.e. before char forming) two peaks were observed, two maximum weight loss temperatures were presented in the mixture of Cl-resin and UP resin. The addition of 10 wt% Cl-resin to Crystic 189LV decreased the 5% weight loss temperature from 256 °C for Crystic 189LV to 247 °C, however increasing the Cl-resin content above 10 wt% increased the 5% weight loss temperature, until a maximum of 284 °C was reached at 100 wt% Cl-resin. The 30% weight loss temperature decreased upon addition of Cl-resin from 375 °C for Crystic 189LV to 331 °C for the Cl-resin. The maximum weight loss temperature decreased from 418 °C for Crystic 189LV to 325 °C at 100% Cl-resin.

The addition of Cloisite 10A into 10 wt% Cl-resin increased the 5% weight loss temperature from 247 °C to 260, 271 and 261 °C in the 1, 3 and 5 wt% Cloisite 10A samples. The temperature at 30% weight loss also increased from 357 °C to approximately 365 °C upon addition of Cloisite 10A. The maximum weight loss temperature did not vary significantly when Cloisite 10A was added to the Cl-resin.

The char forming ability is very important for flame retardancy. Although halogens act mainly in the vapour phase, the mixture of Cl-resin and UP resin formed more char with increasing Cl-resin content. The char formation and char decomposition range presented very similar behaviour in both Br- and Cl-resin systems however, variations that occurred in the Br-system were weaker than those that occurred in the Cl-system. The char decomposition onset temperature and maximum char decomposition temperature remained unchanged by the addition of clay or halogenated resin alone; however a synergistic effect existed between clay and the halogenated resin, more clay and more halogenated resin created more char and an increased decomposition range (Table 3–7).

Table 3–6 Parameters from TG for the Cl-Resin System

Composition	5% Weight Loss Temperature (°C)	30% Weight Loss Temperature (°C)	Maximum Weight Loss Temperature (°C)
C10A-0 Cl-0	256	375	418
C10A-0 Cl-10	247	357	374, 414
C10A-0 Cl-50	273	343	345, 391
C10A-0 Cl-100	284	331	325
C10A-1 Cl-0	264	379	423
C10A-1 Cl-10	260	364	369, 411
C10A-1 Cl-20	277	359	358, 409
C10A-1 Cl-40	272	347	346, 393
C10A-3 Cl-0	239	373	414
C10A-3 Cl-10	271	364	365, 414
C10A-3 Cl-20	274	358	353, 412
C10A-3 Cl-40	273	343	342, 395
C10A-5 Cl-0	235	371	418
C10A-5 Cl-10	261	366	370, 412
C10A-5 Cl-20	267	356	351, 404
C10A-5 Cl-40	260	337	334, 386
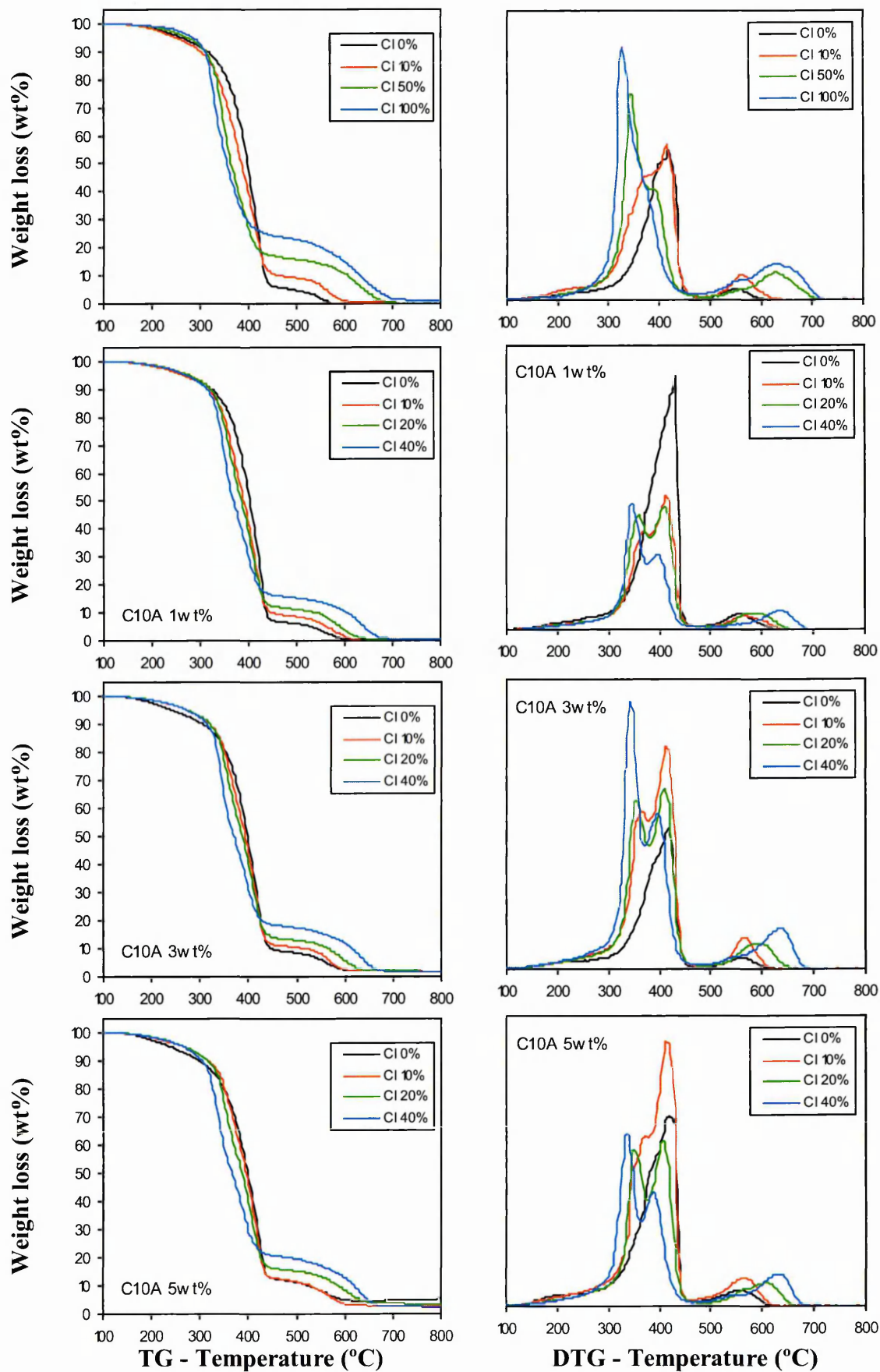
Figure 3–13 TG and DTG traces (air) of the Cl-resin nanocomposites

Table 3–7 Parameters from TG for the Cl-Resin System

Composition	Char Content (wt%)	Max. Char Decomposition Temp (°C)	Char Decomposition Range (°C)
C10A-0 Cl-0	4.9	552	483-619 (136)
C10A-0 Cl-10	9.7	560	476-644 (168)
C10A-0 Cl-50	16.3	628	476-711 (235)
C10A-0 Cl-100	23.7	625	468-736 (268)
C10A-1 Cl-0	6.3	556	485-632 (147)
C10A-1 Cl-10	8.9	563	483-653 (170)
C10A-1 Cl-20	11.9	584	476-661 (185)
C10A-1 Cl-40	15.8	633	485-705 (220)
C10A-3 Cl-0	9.0	561	470-619 (149)
C10A-3 Cl-10	11.0	563	468-636 (168)
C10A-3 Cl-20	13.3	594	478-667 (189)
C10A-3 Cl-40	18.0	633	470-707 (237)
C10A-5 Cl-0	12.1	558	466-621 (155)
C10A-5 Cl-10	12.5	565	462-634 (172)
C10A-5 Cl-20	15.6	607	476-678 (202)
C10A-5 Cl-40	20.2	631	466-699 (233)

From Table 3–7 it is clear that the amount of char formed upon addition of clay is more than the wt% of clay added into the system. For example the sample containing 0 wt% Cl-resin has a char content of 4.9 wt%, therefore the addition of 1 wt% Cloisite 10A should result in a char content of 5.9 wt%, however 1 wt% Cloisite 10A contains approximately 0.6g of inorganic silicate layers and 0.4g of surfactant and so the char content should equal 4.9 + 0.6 = 5.5 wt%. From Table 3–7 the actual char content for the 1 wt% Cloisite 10A sample was 6.3 wt% which was above the calculated value of 5.9 wt%. This synergistic effect on char formation was also apparent in the 3 and 5 wt% Cloisite 10A samples. The addition of an extra 2 wt% of Cloisite 10A to make the 3 wt% sample was calculated to achieve a char content of 7.5 wt% (6.3 + (0.6 x 2) = 7.5), however the actual char content was 9.0 wt%. The addition of a further 2 wt% of Cloisite 10A to make the 5 wt% sample was calculated to achieve a char content of 10.2 wt% (9.0 + (0.6 x 2) = 10.2), however the actual char content was 12.1 wt%.

A similar pattern was also observed in the samples containing Cl-resin and Cloisite 10A, the higher the wt% of Cl-resin in the system then the higher the char content, doubling the wt% of Cl-resin in the system lead to an increase of between 4 and 5 wt% char. These increases in char content are plotted in Figure 3–14. Without the addition of Cl-resin, clay improved the formation of carbonaceous char, with the amount of

carbonaceous char being almost doubled upon addition of 5 wt% clay. The organic part of the silicate has been omitted as the organic part primarily degrades and is desorbed from the sample.
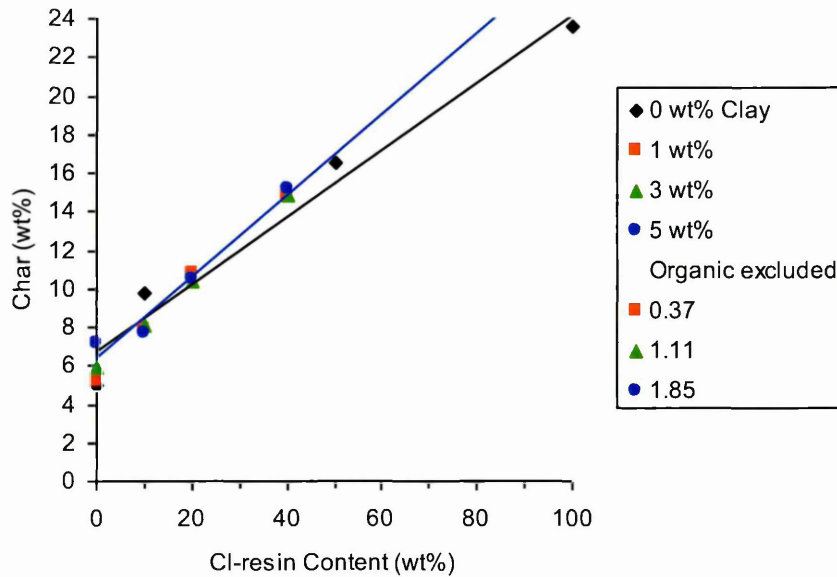
Figure 3–14 Char content formed in Crystic 189LV composites containing Cl-resin (with and without clay)

Table 3–8 Char characteristics for Br- and Cl-resin systems

Specimen	Char type	Dense char dimension
Pure resin Crystic 189LV	Loose char only	
Cl-resin	Mostly dense char	5mm-1cm, same thickness as the original sample
Cl-resin + 5wt% C10		5mm-1cm
Cl-resin + 5wt% C15		2cm or larger, whole sample present as 2 pieces
Br-resin	Mostly dense char	
Br-resin + 5wt% C10		The char was a single, whole piece. It was, laterally expanded, much thinner than the original sample and was net-like.
Br-resin + 5wt% C15		Integral, almost the same thickness as the original sample, no expansion in lateral direction

Oven tests (performed by a colleague) were conducted on the Br- and Cl-resin systems and are summarised in Table 3–8. The incorporation of clay promoted the formation of more integral insulation layers. Samples were subjected to the in-house version of the UL-94 horizontal burning test (see section 2.6.7.1 of Chapter 2 for description of test), and all samples self extinguished in 3 seconds irrespective of how much clay had been added or which halogenated resin was used.

3.6 Conclusions

The addition of Cloisite 30B, Cloisite 10A and Cloisite 15A into Crystic 272 increased the d-spacing of the organoclays from 17.2, 19.2 and 31.5 Å, respectively, to a similar 'final spacing' of 34 Å. Intense d_{001} peaks were observed for the composites containing Cloisite 15A and Cloisite 10A, therefore indicating intercalated/aggregated composites. In comparison Cloisite 30B displayed less intense peaks, which could be due to non-diffractioning clay aggregates or less organoclay in the beam. The d-spacing of Garamite did not increase upon addition into Crystic 272. The thermal decomposition temperature maxima (T_{max} A and T_{max} B) increased by 16 °C upon addition of all four commercially available organoclays into Crystic 272.

Increasing the loading of Cloisite 30B from 1 to 10 wt% in Crystic 272 resulted in a more intercalated/exfoliated nanocomposite in the 5 and 10 wt% samples, the greatest peak intensity was seen in the 10 wt% sample. The thermal decomposition temperature maximum (T_{max} A) increased as the clay loading increased from 390 °C in Crystic 272 and the 1 wt% sample to 393, 409 and 404 °C in 3, 5 and 10wt% samples, respectively. Therefore, the optimal clay loading was reached at 5 wt% as this loading gave the desirable intercalated/exfoliated morphology plus the most elevated thermal decomposition temperature maximum.

Increasing the stirring time and mixing speed did not result in an increase in the d-spacing of Cloisite 30B when mixed in Crystic R935, however the 8000 rpm sample at 30 minutes displayed a more exfoliated/intercalated nanocomposite. Increasing the mixing time from 15 to 30 minutes in the 1000, 8000 and 14,000 rpm samples increased the thermal decomposition temperature maximum (T_{max} A) by 7 °C in all samples. At this stage it was decided to carry out further experiments at 1000 rpm for 15 minutes as

it was thought that these mixing conditions resulted in an exfoliated nanocomposite. However, further understanding of the interpretation of the XRD spectra revealed that the composites (including composites prepared using Cloisite 10A and Cloisite 15A) prepared at 1000 rpm for 15 minutes were actually intercalated.

The d-spacing of Cloisite 15A when dispersed in Crystic 189LV, Crystic 272 and Crystic R935 increased from 31.5 Å to 34.9, 33.7 and 31.7 Å, respectively. Therefore, Crystic R935 did not intercalate into the gallery of Cloisite 15A, however Crystic 272 and Crystic 189LV did increase the d-spacing of Cloisite 15A slightly. The thermal decomposition temperature maximum did not increase upon addition of Cloisite 15A into Crystic 189LV and Crystic R935, however, an increase of 14 °C was observed when Cloisite 15A was dispersed in Crystic 272. The biggest difference between the nanocomposites and resins was the increased peak width upon addition of organoclay, with the largest increase observed in the Crystic 189LV/Cloisite 15A sample.

It was found that the use of ultrasound and mixing did not significantly change the extent of dispersion or thermal properties of Cloisite 30B when mixed with Crystic 189LV.

The addition of halogen resins did provide better flame retardant properties. As the amount of Cl-resin increased from 10 to 40 wt% the XRD traces indicated a more exfoliated/intercalated nanocomposite, the thermal decomposition temperature maxima also shifted to a lower temperature as the amount of Cl-resin increased. The amount of char formed upon addition of clay was more than the wt% of clay added into the system, for example the addition if 3 wt% clay formed 4.1 wt% char in the 0% Cl-resin sample. A synergistic effect occurred upon addition of Cloisite 10A in Crystic 189LV plus Cl-resin, in the 3 wt% Cloisite 10A samples the amount of char formed increased from 9 to 11% when 10 wt% Cl-resin was incorporated into the system and the amount of char increased from 9 to 18 % when 40 wt% Cl-resin was incorporated into the system. The maximum char decomposition temperature increased by a maximum of 70 °C upon incorporation of 40 wt% Cl-resin, and the char decomposition range also increased as the amount of Cl-resin and clay in the system increased.

Crystic 189LV was identified as the polymer system of choice at this stage as it contained no additional additives such as pigments, thixotropes and stabilisers. Crystic 189LV displayed the broadest peak width and increased temperature maximum (T_{max} (A)) compared to the other UP resins, also rudimentary horizontal burning tests identified Crystic 189LV as displaying the most promising fire retardant properties when clay was added. The mixing speed of 1000 rpm and time of 15 minutes were chosen as the standard mixing conditions because they produced what was thought at this stage to be an exfoliated nanocomposite. Based on XRD and TGA results it was decided to carry out further experiments using 5 wt% organoclay as this produced a more exfoliated/intercalated composite with an increased thermal decomposition temperature maximum.

Based on oven tests the intercalated composites formed using Cloisite 15A and Crystic 189LV offered the most effective fire retardant properties and were chosen over the exfoliated/intercalated composites incorporating Crystic 189LV and Cloisite 30B. The highly intercalated structure arising from Cloisite 15A dispersed in Crystic 189LV, produced the most integral and dense char which is the best type of insulation layer for enhanced fire retardant properties. Cone calorimetry data collected for the halogenated resin systems resulted in a predicted Euroclass rating of D. The promising fire retardant system incorporating Crystic 189LV/Cloisite 15A (Surefire hand lay-up resin (Cloisite 15A at 1 wt%)) also reached a Euroclass rating of D, in the cone calorimetry test results and therefore reinforce comparability to the halogenated resin systems and could possibly eliminate the need for halogenated resins in the future.

Unfortunately, the aim of the project was to formulate halogen free resin systems, however the performance of the halogenated resins in the horizontal burning test proved to be a benchmark value to which the other flame retardant systems within this thesis were compared. Therefore, unsaturated polyester/clay nanocomposites containing small amounts of non-halogenated flame retarding agents, which offer superior flame retardant properties became the ultimate target for this project.

3-1 Inceoglu, A.B. and Yilmazer, U., *Polymer Engineering and Science*, **43**, 661 (2003)

3-2 Kornmann, X., Berglund, L.A. and Sterte, J., *Polym. Engineering and Sci.*, **38**, 1351 (1998)

3-3 Suh, D.J., Lim, Y.T. and Park, O.O., *Polymer*, **41**, 8557 (2000)

3-4 Bharadwaj, R.K., Mehrabi, A.R., Hamilton, C, Trujillo, C., Murga, M., Fan, R., Chavira, A. and Thompson, A.K., *Polymer*, **43**, 3699 (2002)

3-5 Kandare, E., Chigwada, G., Wang, D., Wilkie, C.A. and Hossenlopp, J.M., *Polym. Deg. Stab.*, **91**, 1209 (2006)

3-6 Lee, M.H., Dan, C.H., Kim, J.H., Cha, J., Kim, S., Hwang, Y. and Lee, C.H., *Polymer*, **47**, 4359 (2006)

3-7 Wong, S.C., Lee, H., Qu, S., Mall, S. and Chen, L., *Polymer*, **47**, 7477 (2006)

3-8 Toth, R., Coslanich, A., Ferrone, M., Fermeglia, M., Pricl, S., Miertus, S. and Chiellini, E., *Polymer*, **45**, 8075 (2004)

3-9 Chen, C.H., Teng, C.C., Tsai, M.S. and Yen, F.S., *J. Polym. Sci. Part B: Polym. Phys.*, **44 (15)**, 2145 (2006)

3-10 Yang, D.Y., Liu, Q.X., Xie, X.L. and Zeng, F.D., *J. Thermal Analysis and Calorimetry*, **84**, 355 (2006)

3-11 Ren, T., Yang, ., Huang, Y., Ren, J. and Liu, Y., *Polymer Composites*, **27 (1)**, 55 (2006)

3-12 Gilman, J.W., Jackson, C.L., Morgan, A.B., Harris, Jr.R., Manias, E., Giannelis, E.P., Wuthenow, M., Hilton, D. and Phillips, S.H., *Chem. Mater*, **12**, 1866 (2000)

4 Organoclays Prepared Using Commercially Available Organophosphorus Cations

4.1 Introduction

In this chapter, a series of alkyltriphenylphosphonium cations, of variable carbon chain lengths, plus an n-hexadecyl-tri-n-butyl phosphonium cation were sourced and exchanged onto Na-MMT. The resulting phosphonium clays were, characterised using XRD, TGA and in some cases TG-MS, combined with the orthophthalic unsaturated polyester resin Crystic 189LV and tested using the UL94 vertical burning test for flammability (see section 2.6.7.1 of Chapter 2 for description of test). Special emphasis was placed on the determination of whether the different organocations and clay compositions that were produced lead to improved thermal stability of the organocation, and therefore the nanocomposite in which it was used.

The gas phase fire retardant dimethyl methyl phosphonate (DMMP) was added into the unsaturated polyester resin system to try and improve the fire retardant properties of the resulting nanocomposites incorporating these phosphonium organoclays. Individual components of the nanocomposite systems (DMMP and styrene) were analysed to determine which was responsible for the increased dispersion of the organoclay into the unsaturated polyester. An in-depth investigation into the role of DMMP as a fire retardant was carried out using TGA and TG-MS. The effect of increasing the loading of the organocation and also incorporating a washing step after organocation exchange were employed.

To try and improve the efficiency and reduce the cost of the nanocomposite preparation procedure, an efficient 'one-pot' method was explored in which all components of the nanocomposite were combined simultaneously in a mixture. The organoclay dispersion, thermal degradation pattern and fire retardancy of these systems was investigated and compared to samples prepared using the standard nanocomposite preparation method.

The exchangeable cations of natural clays can be replaced by various organocations through a simple ion exchange process. These organocations may, for example, have an ammonium (or phosphonium) head group, consisting of a nitrogen atom in an alkyl or quaternary ammonium complex, with a positive charge. When exchanged onto a clay surface these organocations replace the resident Na^+, Ca^{2+}, ions (i.e. they are adsorbed onto cation-exchange sites) and the free inorganic cations from the clay and halide ions from the ammonium can then be washed out [4-1].

Theng *et al.* [4-2] found that the affinity of a clay for the organic molecules was linearly correlated to the molecular weight of the alkylammonium ion, i.e. the greater the length of the alkyl chain, the greater the contribution to the physical forces of adsorption. The stability of alkylammonium montmorillonite (MMT) complexes has been partly attributed to the Van der waals attraction of hydrocarbon chains with their neighbouring chains and with the clay surface. Other contributions are believed to be due to the thermodynamic stabilisation of the alkylammonium ion at the clay surface when compared with the same ion hydrated in aqueous solution [4-3]. As a result, organoclay complexes are generally thermally stable up to at least 175 °C. However the thermal stability of alkylphosphonium exchanged clays in nitrogen has been noted to increase above that of alkylammonium complexes. This is because the thermal stability of an exchanged MMT is related to the thermal stability of the parent salts. The higher decomposition temperature of the alkylphosphonium clay provides the formation of char at a more opportune time, preventing further degradation of the polymer. However, in the case of alkylammonium clays char formation occurs earlier and can be broken up by the time that the polymer degrades. The incorporation of ammonium and phosphonium-clay into a polystyrene clay nanocomposite causes a decrease in the degradation onset temperature [4-4], however the degradation products of a phosphonium-clay further react with aromatic carbon in the system to form a complex phosphorus-carbon structure, by grafting on, or linking different aromatic carbons, which are hard to degrade [4-5].

Traditionally, the main use of alkylammonium-exchanged clays has been to produce thixotropic effects in aqueous or non-aqueous systems, e.g., to improve paper coating, lubricant thickening or to prevent sedimentation of dispersed solids. Organoclays are also effective adsorbents for removing organic contaminants from water. When non-polar molecules and dissolved organic compounds encounter organoclay particles with their alkyl chains protruding into the polar solvent (e.g. H_2O), these species are attracted by the alkyl chains (i.e. because they are chemically similar). Since this partitioning activity takes place in the clay galleries, no stable binding of the contaminant to the surface of the clay occurs. Their use as adsorbents for organic compounds in water was mentioned as early as the 1960's [4-6, 4-7], but most work has been conducted since the 1980's. The hydrophobic interactions that occur between non-polar organic pollutants and the alkyl chains of organoclays reduces the mobility of organic pollutants (i.e. in soil and waterways), such as benzene derivatives (benzene, toluene and xylene (BTX)) and phenols (i.e. non-ionic chemicals with low water solubility). This extends to the use of organoclays to remediate groundwater and industrial wastewater in underground storage tank sites, oil storage terminals, oil drilling sites and refineries, where the groundwater may be contaminated with oil, grease, phenolic compounds, aromatic and halogenated hydrocarbons [4-8, 4-9].

Depending on the size of the organic cations and the layer charge of the mineral, the alkyl chains of the organocations can adopt different configurations within the gallery space (Figure 1-7), and so, may impart steric/ size exclusion thresholds for the adsorption of organic molecules.

Organocation exchange of a, normally hydrophilic, silicate surface renders it organophilic, this makes it possible to intercalate many different engineering polymers into the clay gallery. The role of alkylammonium cations in an organoclay for the production of nanocomposites is to lower the surface energy of the inorganic host, and so, improve its wetting characteristics with respect to the polymer, by reducing platelet-platelet interactions and increasing the compatibility with polymers. Also, the alkylammonium and alkylphosphonium cations may have functional groups that can either react with the polymer [4-10] or initiate the polymerisation of monomers [4-11] to improve the strength of the interface between the inorganic guest and the polymer.

4.2 Organo-Modification of Clays

Successful incorporation of MMT into a polymer requires the surface of the hydrophilic MMT to be rendered more organophilic. This can be achieved through exchange of the hydrated interlayer cations with cationic surfactants such as alkylammonium cations. A problem however is that commonly used surfactants have limited thermal stability [4-12]. A number of concepts have been proposed that offer alternatives to conventional ammonium-modified montmorillonite, these include alkylimidazolium as the surfactant to increase the initial decomposition temperature [4-13] and phosphonium-based surfactants to improve thermal stability [4-14, 4-15].

4.3 Phosphonium Based Surfactants on Clays

Phosphonium compounds are widely used as stabilizers in many applications and offer unique additional opportunities for polymer layered silicate nanocomposites (PLSNs) [4-16]. Examples include mono and bisphosphonium salts (e.g. mono and bisalkyltriphenylphosphonium salts) that are used as flame retardants for textiles and paper, stabilization agents for polyacrylonitrile fibres exposed to sunlight, heat stabilizers for nylon and condensation additives to organic dyes to produce wash fast colours [4-12]. Therefore the use of phosphonium salts as organic modifiers for layered silicates may further enhance the thermal properties of polymer nanocomposites. Xie et al [4-12] conducted a study in order to provide a better understanding of the thermal behaviour of phosphonium salts and the modified MMTs (P-MMT) produced using them. The thermal stability and degradation mechanism of phosphonium-modified MMTs (P-MMT) were discussed and compared directly to ammonium-modified MMTs (N-MMT).

Nonisothermal decomposition of quaternary phosphonium modified MMT (e.g. tetraoctylphosphonium modified MMT (P-4C8)) occurred in four stages, which were similar to those observed for the corresponding quaternary ammonium modified MMT (e.g. tetraoctylammonium modified MMT (N-4C8)) (Figure 4–1).
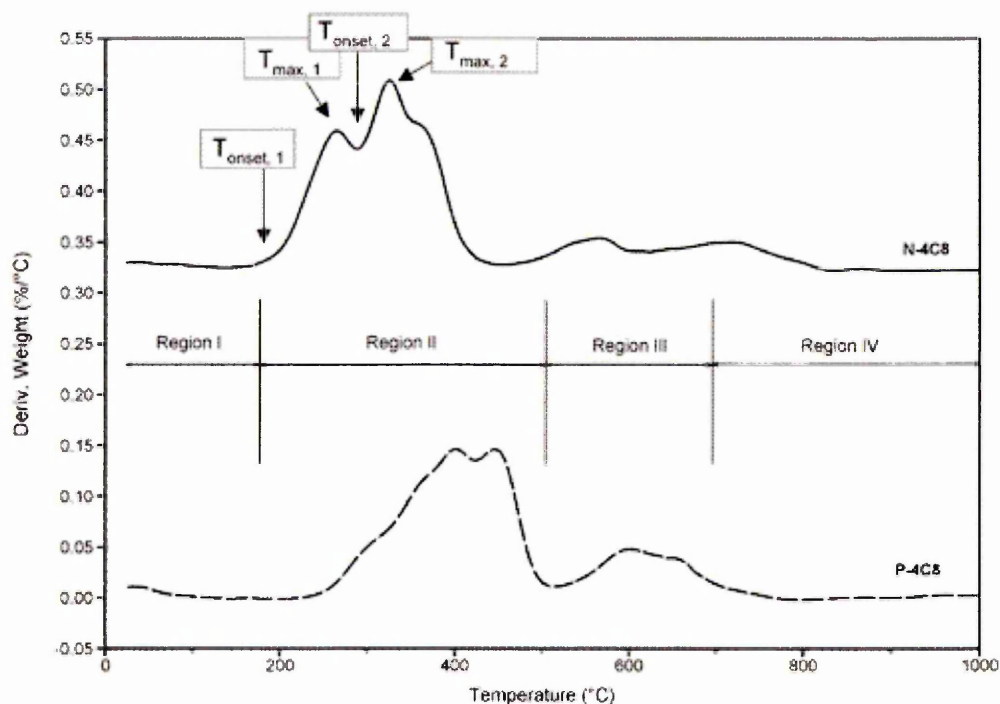
Figure 4–1 DTG traces (N₂) comparing quaternary ammonium MMT (N-4C8) and quaternary phosphonium MMT (P-4C8) [4-12].

In summary, evolution of adsorbed water occurred below 180 °C (Region I). Organic substances evolved between 250 °C and 500 °C (Region II). Dehydroxylation of the aluminosilicate occurred between 500 °C and 700 °C (Region III), and evolution of products associated with residual organic carbonaceous residue occurred between 700 °C and 1000 °C (Region IV).

The major difference between the thermal decomposition behaviour of P-4C8 and N-4C8 under N₂ was that the maximum rate of mass loss and onset temperature (T_{onset}) for neat phosphonium salts were consistently 70-80 °C higher than that observed in the corresponding P-MMT, compared to a 15-25 °C difference observed between neat ammonium salts and the corresponding N-MMT. Therefore, indicating that the influence of the layered silicate was more substantial for phosphonium than ammonium surfactants [4-12]. To conclude it can be said that the superior improvement in thermal stability (i.e. increase in T_{onset}) for P-MMT compared to that of N-MMT under N₂, along with the well-known properties of phosphorus compounds, such as flame retardancy and heat stabilization represent advantages to the utilization of P-MMT in various polymer composites.

4.4 Commercially Available Phosphonium Cations

4.4.1 Preparation

The gallery cations of Na^+ Cloisite were exchanged with alkyltriphenylphosphonium (TP) cations with chain lengths ranging from $C_n = 8$ to $C_n = 16$ ($TP8^+$ to $TP16^+$) and an alkyltributylphosphonium ($Bu16^+$) cation. They were exchanged at a concentration that was equivalent to 1 x CEC of Na^+ Cloisite (92.5 mEq/100g). XRD and TGA were carried out on all exchanged clays, the specific trends within which are discussed below. The organoclay samples prepared will be referred to with respect to their organocation species (Table 4–1).

Table 4–1 Sample identification for alkyl phosphonium exchanged Na^+ Cloisite

Organic Component	Abbreviation for Salt	Abbreviation for Cation	Abbreviation when exchanged onto Na^+ Cloisite
(1-octyl) triphenylphosphonium Bromide, $C_n = 8$	TP8B	$TP8^+$	TP8-MMT
decyltriphenylphosphonium Bromide, $C_n = 10$	TP10B	$TP10^+$	TP10-MMT
n-dodecyltriphenylphosphonium Bromide, $C_n = 12$	TP12B	$TP12^+$	TP12-MMT
(1-tetradecyl) triphenylphosphonium Bromide, $C_n = 14$	TP14B	$TP14^+$	TP14-MMT
n-hexadecyltriphenylphosphonium Bromide, $C_n = 16$	TP16B	$TP16^+$	TP16-MMT
n-hexadecyl-tri-n-butyl phosphonium Bromide, $C_n = 16$	Bu16B	$Bu16^+$	Bu16-MMT

4.4.2 XRD Analysis of TP8^{+} - TP16^{+} and Bu16^{+} Exchanged Na^{+} Cloisite
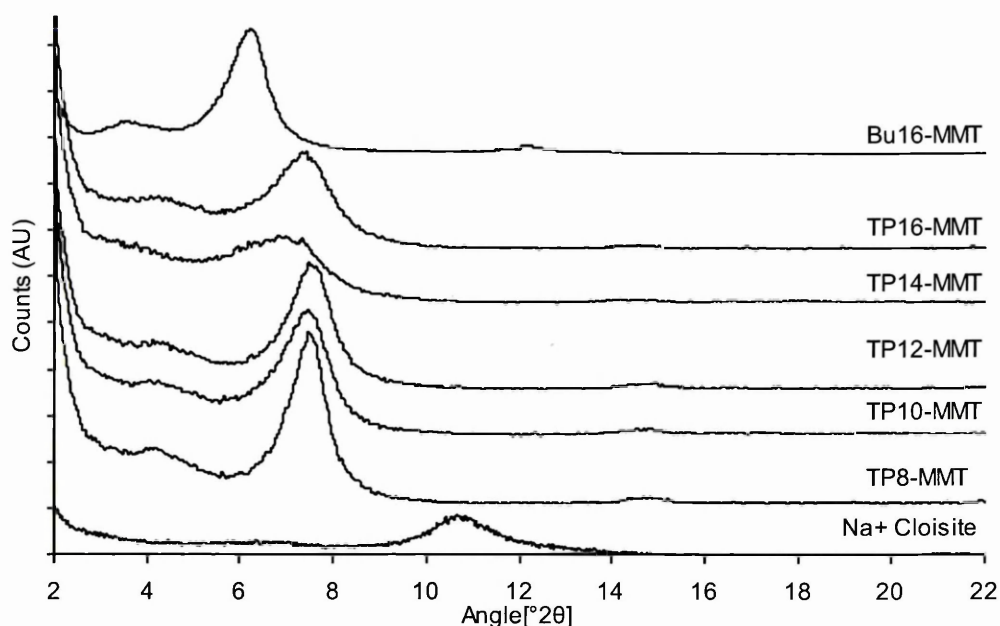
Figure 4–2 XRD traces (Cr Tube) for TP8^{+} - TP16^{+}, Bu16^{+} exchanged Na^{+} Cloisite. Together with that for Na^{+} Cloisite – Traces are offset for clarity

The XRD traces presented in Figure 4–2, displayed an increase in the d_{001} spacing from 12.1 Å for Na^{+} Cloisite to 17.4 Å in TP8-, TP10- and TP12-MMT, respectively. As the length of the carbon chain increased the d_{001} spacing increased up to 18.7 Å in TP14-MMT and 17.7 Å in TP16-MMT. The d_{001} spacing in Bu16-MMT was 20.9 Å, this can be attributed to the bulkier head group further expanding the clay layers. A smaller peak occurred at lower angle representing d-spacings of 30.5 Å in TP8-, TP10-, TP12-, and TP16-MMT and 36.5 Å in Bu16-MMT.

4.4.3 TGA Analysis of TP8$^+$ - TP16$^+$ and Bu16$^+$ Exchanged Na$^+$ Cloisite
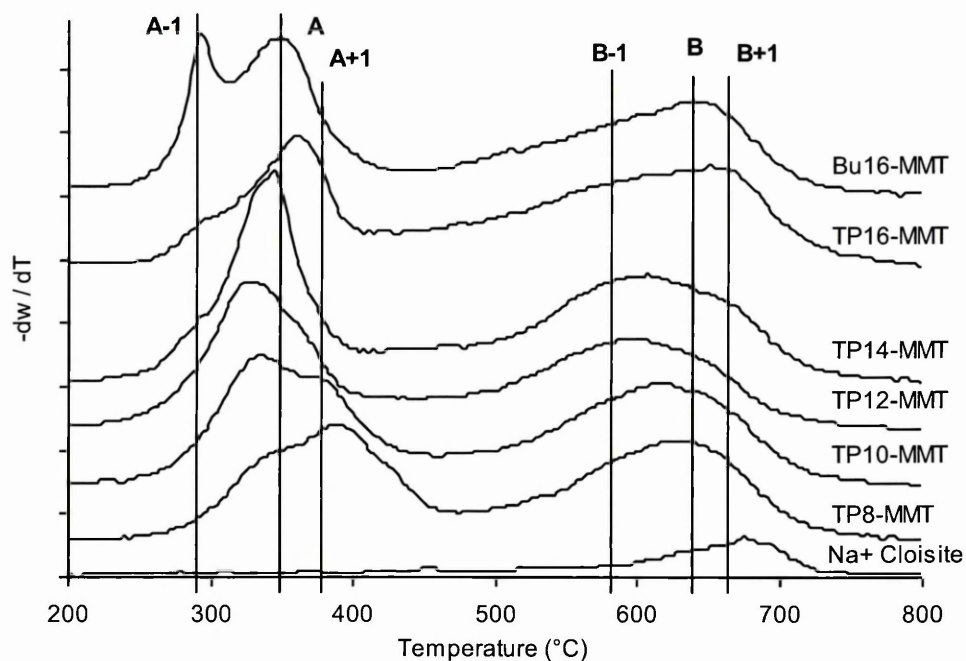
Figure 4–3 DTG traces (Air) for Na$^+$ Cloisite exchanged with TP8$^+$-TP16$^+$ and Bu16$^+$ – Traces are offset for clarity.

The DTG traces presented in Figure 4–3 exhibited several thermal desorption events, these can be grouped to form temperature ranges within which the thermal desorption maxima varied 35-200 °C, 200-450 °C and 450-800 °C. An assignment of the events occurring within these temperature ranges are presented in Table 4–2.

Table 4–2 Assignment of desorption maxima occurring within specific temperature ranges of TG traces for TP8- to TP16-MMT and Bu16-MMT

Stage	Desorption Temperature (°C)	Assignment
1	35 - 200	evolution of adsorbed water
2	200 - 450	decomposition of organocations producing aliphatic species, ring compounds, ammonia, water and CO_2
3	451 – 800	clay dehydroxylation and CO_2 evolution

The DTG traces for TP8$^+$ - TP16$^+$ and Bu16$^+$ exchanged Na$^+$ Cloisite (Figure 4–3) display two maxima in the decomposition process (A and B), however several smaller peaks occurred (A-1, A+1, B-1 and B+1), which decomposed over three stages (1, 2 and 3). Three peaks (A-1, A and A+1) were present over the temperature range 200 – 450 °C

130

(stage 2), and were representative of decomposition of the alkylphosphonium cations from the Na^+ Cloisite galleries. Three peaks (B-1, B and B+1) were also present over the temperature range 451 – 800 °C (stage 3), and were representative of clay dehydroxylation and CO_2 evolution. The decomposition temperatures for peaks A and B, and the smaller peaks either side of A and B are displayed in Table 4–3.

Table 4–3 Decomposition peak temperatures for TP8- to TP16-MMT and Bu16-MMT

	A-1 (°C)	A (°C)	A+1 (°C)	B-1 (°C)	B (°C)	B+1 (°C)
TP8-MMT		351	388		631	
TP10-MMT		334	369		619	638
TP12-MMT		327	351		598	626
TP14-MMT	299	341			610	645
TP16-MMT	309	360		612	645	
Bu16-MMT	292	348		610	640	
Na Cloisite					675	

T_{max} (A) represented the main decomposition peak during stage 2, however the position of this peak varied across the TP series. T_{max} (A) occurred at a higher temperature of 351 °C in TP8-MMT, then as the alkyl chain length increased from $C_n = 8$ to $C_n = 12$, a progressive decrease in the desorption temperature (351 to 327 °C) of T_{max} (A) was observed. T_{max} (A) then increased to 341 and 360 °C in TP14- and TP16-MMT, respectively. T_{max} (A-1) was present in TP14-, TP16- and Bu16-MMT, while T_{max} (A+1) was present in TP8-, TP10- and TP12-MMT, all peaks were present as shoulders on the main decomposition peak A, with the exception of Bu16-MMT which displayed a clear sharp A-1 peak. T_{max} (B) occurred during stage 3 and displayed the same temperature pattern as stage 2. T_{max} (B-1) was present in TP16- and Bu16-MMT, while T_{max} (B+1) was present in TP10-, TP12- and TP14-MMT, however it was difficult to determine the actual peak positions of the shoulders under T_{max} (B) due to the increased peak width of peak (B). Below 200 °C (stage 1), the alkylphosphonium chains were thermally stable, and so, any weight loss was attributed to adsorbed water being thermally desorbed (Table 4–4).

Table 4–4 Comparison of weight losses for TP8$^+$ - TP16$^+$ and Bu16$^+$ exchanged Na$^+$ Cloisite (air) at different temperature ranges with increasing chain length.

	Stage 1	Stage 2	Stage 3	
	35-200 °C (%)	201-450 °C (%)	451-800 °C (%)	Total (%)
Na$^+$ Cloisite	5.4	1.0	4.8	11.2
TP8-MMT	0.7	12.6	18.1	31.4
TP10-MMT	0.8	14.1	19.1	33.9
TP12-MMT	1.4	16.3	21.0	38.7
TP14-MMT	0.6	15.2	21.7	37.5
TP16-MMT	2.2	10.9	20.1	33.1
Bu16-MMT	0.8	16.1	18.2	35.1

Weight losses across stage 2 (201 – 450 °C) followed the pattern TP12>Bu16>TP14>TP10>TP8>TP16. Weight losses across stage 3 (451 – 800 °C) followed a similar pattern to the previous segment, which resulted in the total weight loss following the pattern TP12>TP14>Bu16>TP10>TP16>TP8.

Table 4–5 Possible organic exchange against actual organic exchange for TP8- to TP16-MMT and Bu16-MMT at 1 x CEC

	TP8-MMT	TP10-MMT	TP12-MMT	TP14-MMT	TP16-MMT	Bu16-MMT
Possible Organic Exchange (mg/g)	372.8	385.7	398.7	411.6	424.6	394.9
Actual Organic Exchanged (mg/g)	234.2	254.8	289.5	286.4	238.8	265.2
Percentage Exchanged (%)	63	66	73	70	56	67

* All exchange amounts are ± 5%

Table 4–5 presents the actual amount of organic exchange in comparison with the possible amount of organic exchange for the TP series and Bu16-MMT. The actual amount or organic exchange was similar for TP8-, TP10-, TP12-, TP14- and Bu16-MMT at 68% ± 5% of the possible organic exchange, however the actual amount exchanged for TP16-MMT was slightly lower at 56%, of the possible organic exchange amount. These exchange amounts did appear rather low, and so Bu16$^+$ was exchanged onto Na$^+$ Cloisite at 1.5 and 2.0 x CEC of Na$^+$ Cloisite to try and increase the percentage exchange. The percentage exchange was calculated to be 90 and 84% at 1.5 and 2.0 x CEC (± 5%), respectively, confirming that the original Bu16-MMT sample and most probably the TP$_n$-MMT samples had not been fully exchanged at 1 x CEC.

132

4.5 Crystic 189LV Composites Prepared Using TP8$^+$ - TP16$^+$ and Bu16$^+$ Exchanged Na$^+$ Cloisite – Preliminary Studies

In order to assess the influence of the carbon chain length and head group on the dispersion of alkylphosphonium modified clays into an unsaturated polyester resin nanocomposites were made using Crystic 189LV and TP8$^+$ - TP16$^+$ and Bu16$^+$ exchanged Na$^+$ Cloisite. The mixing regime outlined in section 2.6.2 of Chapter 2 was employed.

4.5.1 XRD Analysis of Nanocomposites
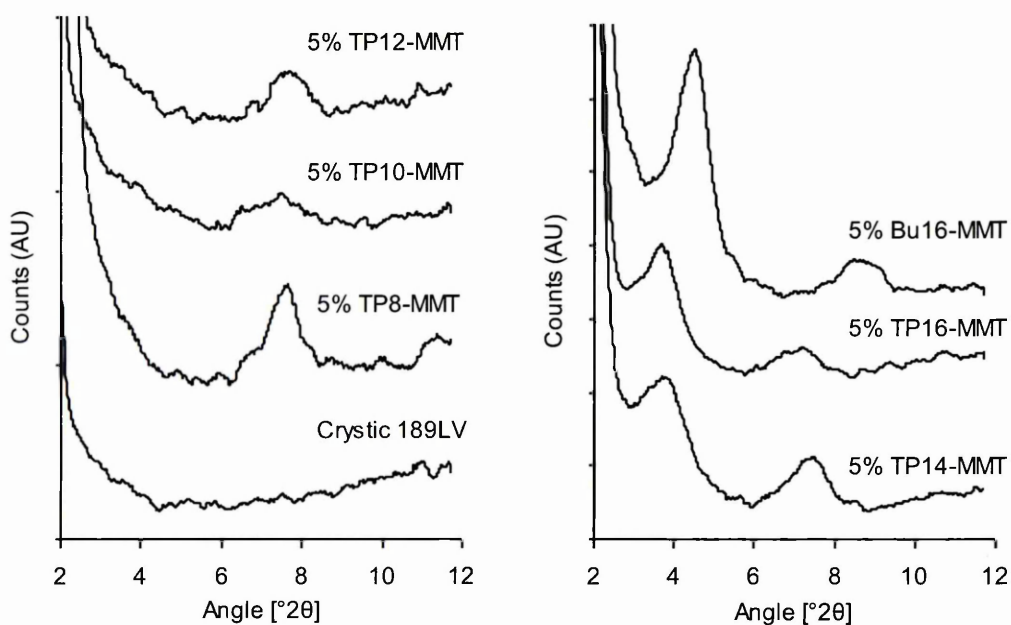
Figure 4–4 XRD traces (Cr Tube) for Crystic 189LV composites containing 5wt% of TP8- to TP16-MMT and Bu16-MMT – Traces are offset for clarity

The XRD traces presented in Figure 4–4 display TP8- to TP16-MMT and Bu16-MMT mixed with Crystic 189LV. When mixed with Crystic 189LV, the d_{001} spacing of TP14-, TP16- and Bu16-MMT increased from 18.7, 17.7 and 20.9 Å, to 33.1, 33.7 and 27.8 Å, respectively. A partially exfoliated/intercalated composite was achieved when Crystic 189LV was mixed with TP14- and TP16-MMT, evident from an increase in background at lower angle (due to fewer intercalated stacks) and from the presence of a less intense d_{001} peak (from remaining intercalated stacks in the composite). Bu16-MMT when mixed with Crystic 189LV displayed an intercalated/aggregated composite, this was evident from the presence of an intense d_{001} peak and a clear d_{002} peak. The smaller

peaks which appeared between 7 and 8 °2θ in the traces for TP14- and TP16-MMT nanocomposites could be representative of the d_{002} spacings of the composites or possibly unexpanded TP14- and TP16-MMT. The XRD traces for composites containing TP8-, TP10- and TP12-MMT displayed very weak d_{001} peaks at 16.8 Å, which were very similar to the d-spacings of $TP8^+$, $TP10^+$ and $TP12^+$ exchanged Na^+ Cloisite. The weak d_{001} peaks in the XRD traces, indicated that no intercalation has occurred and a microcomposite was achieved. Organoclay dispersion within the TP8-, TP10- and TP12-MMT samples was very poor as organoclay particles were clearly visible within the films, this further confirmed the formation of a microcomposite.

4.5.2   TGA Analysis of Nanocomposites
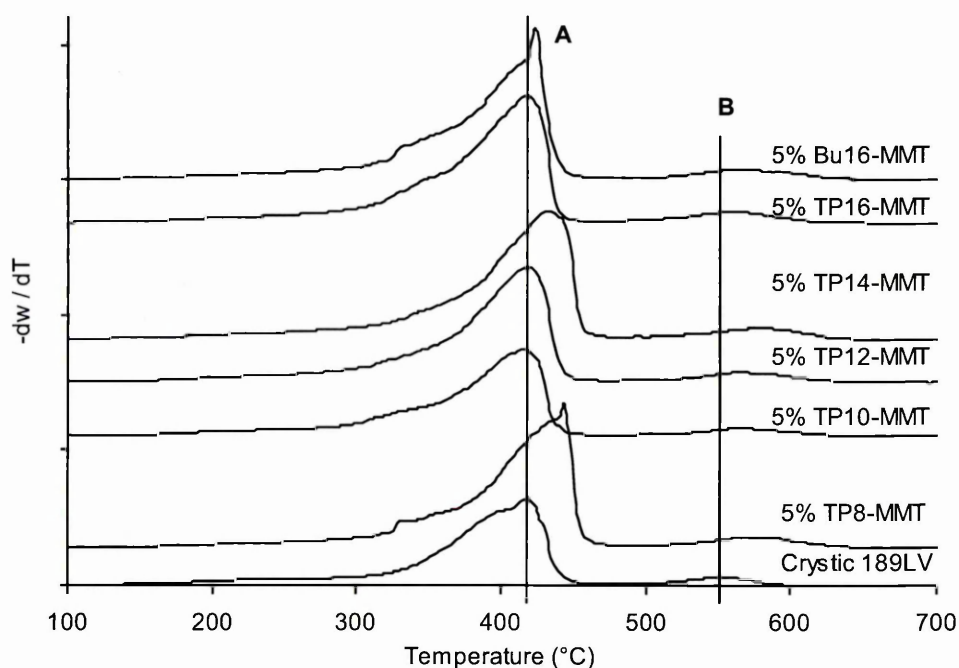
Figure 4–5 DTG traces (Air) for Crystic 189LV composites containing 5wt% of TP8- to TP16-MMT and Bu16-MMT – Traces are offset for clarity.

The DTG traces presented in Figure 4–5 display two maxima in the decomposition process (A and B), decomposing over two stages. Stage 1 occurred between 121 and 480 °C and exhibited T_{max} (A) at 422 °C for pure Crystic 189LV and samples made using Crystic 189LV and 5 wt% TP10-, TP12-, TP16-, and Bu16-MMT. TP8- and TP14-MMT displayed T_{max} (A) at the slightly higher temperature of 444 and 437 °C, respectively. However, when comparing the %wt loss for all nanocomposites (Table 4–6) the weight loss over the ranges 121-480 °C and 481-800 °C were very similar for all

samples and the total %wt loss was approximately 97 % (± 2 wt%). T_{max} (B) occurred at 556 °C for pure Crystic 189LV, increasing to 568 °C for the nanocomposites containing TP10-, TP12-, TP16- and Bu16-MMT, respectively. T_{max} (B) occurred at 582 °C for nanocomposites containing TP8- and TP14-MMT. T_{max} (B) is probably a degradation product that decomposes at a higher temperature (e.g. the char that forms when organoclay and resin decompose in stage 1). From the DTG traces it was apparent that composites containing TP8- and TP14-MMT were more stable than composites containing TP10-, TP12-, TP16- and Bu16-MMT, however these composites were not carried forward as they proved unsuccessful in the in-house version of the UL94 Vertical Burning tests (Table 4–15).

Table 4–6 Comparison of the weight losses for Crystic 189LV composites containing 5wt% of TP8-to TP16-MMT and Bu16-MMT at different temperature ranges between 35 and 800 °C.

	35-120 °C (%)	Stage 1 121-480 °C (%)	Stage 2 481-800 °C (%)	Total (%)
Crystic 189LV	0.04	92.8	6.8	99.6
TP8	0.05	88.0	7.9	95.9
TP10	0.3	88.4	9.0	97.6
TP12	0.2	88.0	8.4	96.6
TP14	0.1	88.3	8.4	96.8
TP16	0.3	88.8	8.2	97.3
Bu16	0.2	88.5	8.4	97.2

4.6 Comparison of Data of $TP8^+$ - $TP16^+$ and $Bu16^+$ Exchanged Na^+ Cloisite and Nanocomposites of Crystic 189LV/ $TP8^+$ - $TP16^+$ and $Bu16^+$ Exchanged Na^+ Cloisite

4.6.1 Comparison of XRD Data for Alkylphosphonium Clays and their Composites with Crystic 189LV

The basal spacings for $TP8^+$ - $TP16^+$ and $Bu16^+$ exchanged Na^+ Cloisite, are displayed in Table 4–7, and indicate that expansion of the gallery occurred when exchanged with the full range of alkylphosphonium cations. For the organoclays the gallery was expanded to the highest degree when exchanged with $TP14^+$ and $Bu16^+$.

Table 4–7 Comparison of d_{001} for Na^+ Cloisite exchanged with $TP8^+$-$TP16^+$, $Bu16^+$ and their corresponding Crystic 189LV nanocomposites

	TP8-MMT	TP10-MMT	TP12-MMT	TP14-MMT	TP16-MMT	Bu16-MMT
Organoclay d_{001} (Å)	17.4	17.4	17.4	18.7	17.7	20.9
Nanocomposite d_{001} (Å)	16.8	16.8	16.8	33.1	33.7	27.8

The basal spacings of Crystic 189LV composites containing 5 wt% TP8- to TP16-MMT and Bu16-MMT, are also displayed in Table 4–7, and indicate that expansion of the gallery occurred when nanocomposites of Crystic 189LV were made. Crystic 189LV mixed with TP8-, TP10-, and TP12-MMT displayed weak d_{001} peaks at 16.8 Å, which were very similar to the d-spacing for $TP8^+$, $TP10^+$ and $TP12^+$ exchanged Na^+ Cloisite.

A small peak at lower angle (corresponding to d-spacings of 30.8 Å for TP8- to TP16-MMT and 36.5 Å for Bu16-MMT) occurred in the XRD traces for the alkyltriphenylphosphonium and alkyltributylphosphonium exchanged Na^+ Cloisite. The presence of this peak does not appear to effect the nanocomposite formation but an attempt is made to explain its presence. Ijdo and Pinnavaia [4-17] have attributed this to the formation of several products when the inorganic cations in the gallery are only partially replaced by organic cations (Figure 4–6). Phase segregation can occur, yielding starting material and newly formed organoclay (a). Figure 4–6 illustrates that mixing of the two ions at exchange sites can lead to the formation of a single homostructured phase (b) or two types of heterostructured phase (c). The mixed ion homostructure (b) has all the interlayers occupied by both metal ions and the onium ions, whereas the heterostructures (c) have two types of segregated galleries, one occupied by inorganic cations and the other by organic cations. The two galleries of the heterostructure may be stacked either in a disordered, interstratified manner or in a regularly alternating fashion.

136
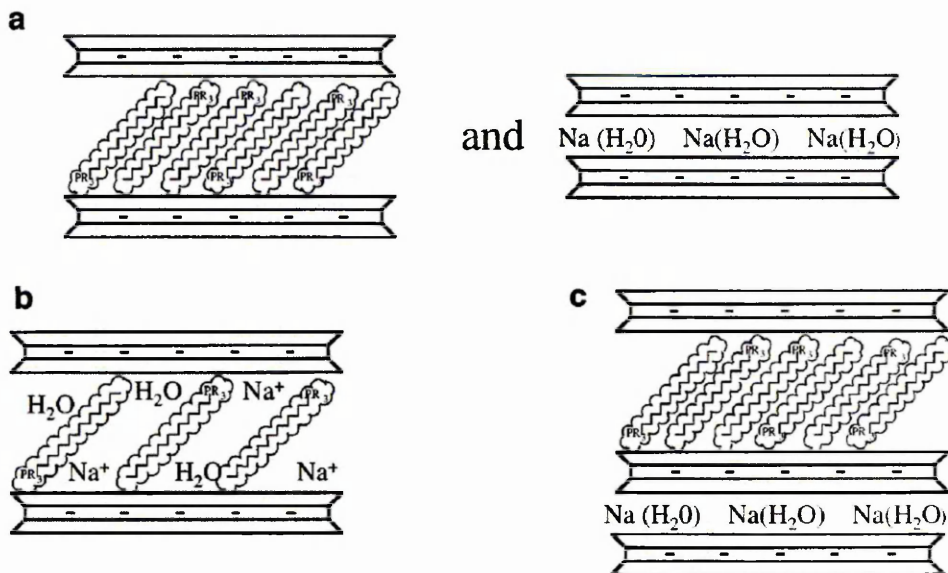
Figure 4–6 Three possible structures formed when the exchange sites of smectite clays are occupied with two different cationic species, alkylammonium and hydrated sodium ions [4-17].

The regular stacking of the distinguishable organic and inorganic galleries has also been observed in the staging behaviour in graphite [4-18]. The peaks at lower angle associated with spacings of 30.8 Å and 36.5 Å were most likely due to the formation of a mixed ion heterostructure (Figure 4–6 (c)) with the TP8$^+$ - TP16$^+$ and Bu16$^+$ cations and Na(H$_2$O) cations segregated into two interlayers (Figure 4–7) in a regular alternating fashion.
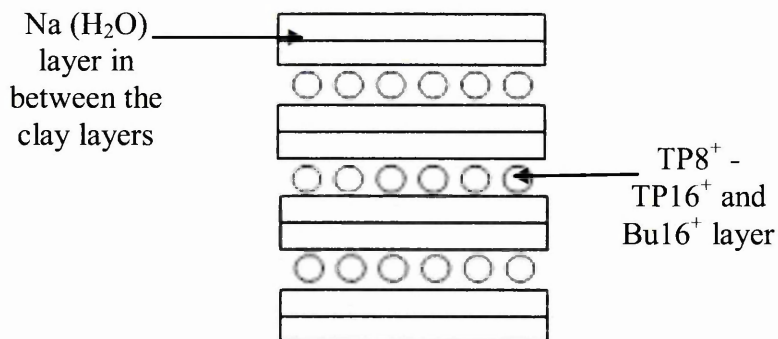
Figure 4–7 Schematic illustration of the possible structure for TP8$^+$ - TP16$^+$ and Bu16$^+$ exchanged Na$^+$ Cloisite

In the early stages of the project, the aim was to produce a fully sodium exchanged form of montmorillonite, into which it would be easier to exchange quaternary ammonium and phosphonium cations and make the gallery surfaces organophilic. To make this possible, it was necessary to convert Na$^+$ Cloisite (with its various hydrated gallery cations (E.g. majority Na$^+$, Ca^{2+}, Mg^{2+})) into sodium clay by exchange with sodium

137

hydroxide (NaOH). The exchange process required the exchanged clay to be washed many times (between 8 and 10) until the conductivity of the final supernatant reached below 50 μs (5-10), therefore from an industrial perspective fully exchanged clays are very time consuming and expensive to produce. Due to the industrially driven nature of the project the NaOH exchange procedure was discontinued and as received Na^+ Cloisite was utilized. However, differences in the XRD traces were seen between the fully Na-exchanged and as received forms, an example using Bu16-MMT is displayed in Figure 4–8, which demonstrated a clear peak at lower angle (this peak was also seen in the TP_n-MMT series), which was only visible when the as received form of Na^+ Cloisite was used.

Bu16-MMT prepared using the Na^+ exchanged form of Na^+ Cloisite displayed a slightly higher d_{001} spacing than Bu16-MMT prepared using the as received form of Na^+ Cloisite, this could be attributed to varying states of hydration between the two forms of Bu16-MMT. One possibility is that Na^+ Cloisite (as received) contained a small, fixed amount of clay with high layer charge, accounting for the small fixed amount of the heterostructure observed. The separation distance between the d_{001} peak and the small peak at lower angle for TP8- to TP16-MMT and Bu16-MMT (as received form) are presented in Table 4–8.
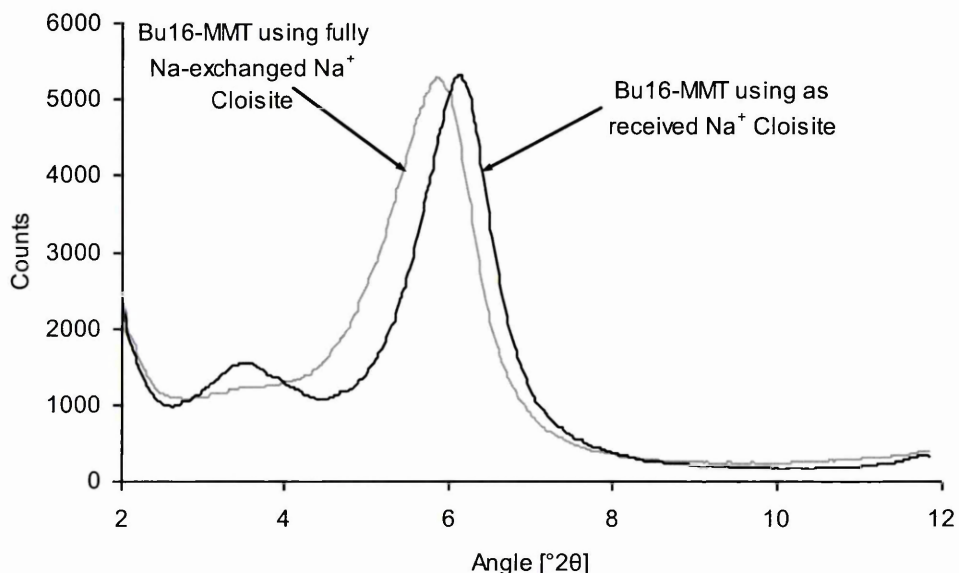
Figure 4–8 XRD traces (Cr tube) displaying the differences between fully Na-exchanged and as received forms of Bu16-MMT

138

Table 4–8 Separation distances between d_{001} and small peak at lower angle

	TP8-MMT	TP10-MMT	TP12-MMT	TP14-MMT	TP16-MMT	Bu16-MMT
Distance between d_{001} and small peak (Å)	13.4	13.4	13.4	-	12.5	14.7

The distance between the layers was approximately the same distance as that found in the hydrated form of Na^+ Cloisite (12.4 Å) (Figure 4–9) and therefore supports the formation of a mixed ion heterostructure as displayed in Figure 4–6 (c). In comparison the exchanged form of Na^+ Cloisite formed a mixed ion homostructure as displayed in Figure 4–6 (b).
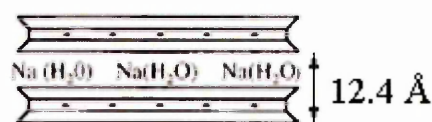
Figure 4–9 Distance between layers in a hydrated Na^+ Clay

Table 4–9 exhibits the possible amount of organic exchange against the actual amount of organic exchange (using TG data) for Bu16-MMT prepared using fully Na-exchanged Na^+ Cloisite as compared to Bu16-MMT prepared using as received Na^+ Cloisite. In the fully exchanged form, Calcium (Ca^{2+}) has been removed from the exchange sites, therefore more exchange sites were available for organic exchange with $Bu16^+$ cations. Therefore, an increase in the percentage exchange was observed from 67.1 to 83.8 % in the fully exchanged form, compared to the as received form.

Table 4–9 Possible organic exchange against actual organic exchange for Bu16-MMT prepared using fully Na-exchanged Na^+ Cloisite as compared to Bu16-MMT prepared using as received Na^+ Cloisite – At 1 x CEC.

	Bu16-MMT using fully Na-exchanged Na^+ Cloisite	Bu16-MMT using as received Na^+ Cloisite
Possible Organic Exchange (mg/ g)	394.9	394.9
Actual Organic Exchanged (mg/ g)	331.1	265.2
Percentage Exchanged (%)	83.8	67.1

* All exchange amounts are ± 5%

4.6.2 Comparison of TGA Data for Alkylphosphonium Clays and their Composites with Crystic 189LV

The total weight loss from standard 10 mg samples increased as the length of the alkyl chain in the alkyltriphenylphosphonium cation increased from $C_n = 8$ to $C_n = 12$ (Table 4–10), above this chain length a steady decrease in the total weight loss was observed. The weight loss < 200 °C, which was believed to be due to loss of water associated with the surfactant head group, remained relatively constant throughout the series of samples, with the exception of TP12- and TP16-MMT which demonstrated a slightly higher weight loss (Table 4–4). The alkyltriphenylphosphonium cations decomposed and the products desorbed from the Cloisite galleries between 201 °C and 450 °C (stage 2), three decomposition peaks were present over this temperature range (T_{max} (A-1) T_{max} (A) and T_{max} (A+1)). T_{max} (A) was the main decomposition peak during stage 2, however two shoulders on T_{max} (A) occurred in the decomposition pathway. TP8-, TP14-, TP16-, and Bu16-MMT displayed T_{max} (A-1) as a shoulder before the main decomposition peak (A), while TP10- and TP12-MMT demonstrated T_{max} (A+1) as a shoulder after the main decomposition peak (A). As the length of the alkyl chain increased, the profile of the thermal events changed, the majority of the thermal desorption occurred at a maximum of 388 °C when $C_n = 8$, decreasing to 360 °C when $C_n = 16$. The weight loss > 451 °C was attributed to clay dehydroxylation and CO_2 formation as the carbonaceous coke was gasified.

Table 4–10 Comparison of total weight losses for Na^+ Cloisite exchanged with $TP8^+$-$TP16^+$, $Bu16^+$ and their corresponding nanocomposites

	$TP8^+$	$TP10^+$	$TP12^+$	$TP14^+$	$TP16^+$	$Bu16^+$
Organoclay Total %wt Loss	31.4	33.9	38.7	37.5	33.1	35.1
Nanocomposite Total %wt Loss	95.9	97.6	96.6	96.8	97.3	97.2

Crystic 189LV nanocomposites containing TP8-, TP16- and Bu16-MMT displayed a total %wt loss of approximately 97 % (± 2 wt%) compared with 99.6 % for pure Crystic 189LV. This weight loss should reflect the amount of inorganic added, however when the amount of inorganic is calculated (2.8, 2.7, 2.7, 2.6, 2.5 and 2.7 wt% for TP8-, TP10-, TP12-, TP14-, TP16- and Bu16-MMT, respectively) the %wt of the sample remaining is higher than the amount of inorganic in the system. Therefore, it is believed that a synergistic effect occurred between the organoclay and the unsaturated polyester,

which lead to the formation of an increased amount of carbonaceous char and decreased total %wt loss. The nanocomposites containing TP8- and TP14-MMT displayed a slightly higher temperature thermal decomposition maxima (T_{max} (A) = 444 and 437 °C, respectively) compared to pure Crystic 189LV, TP10-, TP12- and TP16-MMT (T_{max} (A) = 422 °C). Crystic 189LV nanocomposites containing TP8- and TP14-MMT displayed a shift in the desorption maxima towards a higher temperature, demonstrating a stabilising effect on the entire system until the upper thermal limit of the material was reached. This shift could possibly be due to which part of the nanocomposite was sampled (centre or edge), however care was taken to ensure all nanocomposites were sampled from the same area (section 2.6.2.3 of chapter 2).

It was not clear why this shift occurred, Yang et al. [4-19] believed that this shift could be attributed to an increase in the formation of the protective barrier layer due to the surface accumulation of clay platelets held together by carbonaceous char. This barrier would have thermally insulated the UP matrix. Also, a highly tortuous path to mass transport produced by layering of the clay platelets would have created a diffusion barrier to gases and fumes [4-20]. These two mechanisms, described more fully in section 1.6.4 of Chapter 1, are the most likely to retard the combustion of the polymeric materials.

4.7 Difficulties Optimising the Dispersion of the Organophosphonium Clays in Crystic 189LV

Initially self aggregation occurred when preparing nanocomposites using the organomodified clays based on $TP8^+$-$TP16^+$ and $Bu16^+$ exchanged Na^+ Cloisite. Mechanical milling was used in an attempt to overcome this problem, however large particles could still be visually identified. Dimethyl methylphosphonate (DMMP) is a liquid phosphonate that has been identified as a fire retardant agent in many polymers [4-21, 4-22]. DMMP was originally added to the polymer systems to reduce the extinguish times of samples when subjected to the fire tests, the liquid fire retardant additive DMMP, which acts primarily in the gas phase reduced the extinguish times of samples prepared using Crystic 189LV. The fire retardant performance improved as the DMMP level increased; addition of 10 wt% DMMP to Crystic 189LV achieved a borderline V-1 pass. DMMP was added at various stages in the mixing procedure (i.e. before/after the

organoclay and resin had been mixed together) and it was noted that the addition of DMMP to the organoclay before mixing into Crystic 189LV improved the dispersion of the organoclay into Crystic 189LV, by acting as a pre-swelling agent. Therefore, pre-swelling of the organophosphonium modified clays with DMMP was identified as the preferred method to overcome dispersion issues. To investigate the effect of individual components in the nanocomposite systems (DMMP and styrene (from the unsaturated polyester matrix)), on the d-spacing of organophosphonium clays, XRD analysis was carried out on organophosphonium clays, organophosphonium clays dispersed in DMMP, organophosphonium clays dispersed in styrene, and organophosphonium clays dispersed in DMMP, dried and then dispersed in styrene.

4.7.1 XRD Analysis of Organophosphonium Clays Dispersed in DMMP

XRD analysis was carried out on organophosphonium clays dispersed in DMMP, to investigate the effect that DMMP had on the d-spacings of the organophosphonium clays. 1 g of each organophosphonium clay (TP8- to TP16-MMT and Bu16-MMT plus Na^+ Cloisite) was dispersed in DMMP, and then dried in an oven at 80 °C overnight.
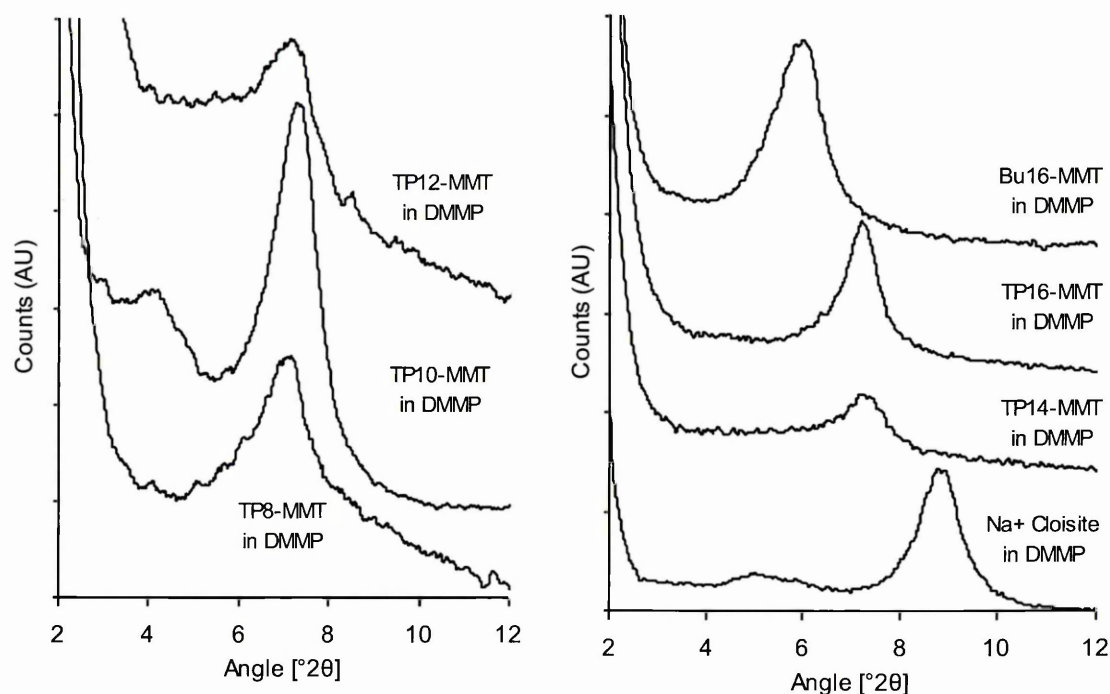
Figure 4–10 XRD traces (Cr tube) for TP8- to TP16-MMT, Bu16-MMT and Na^+ Cloisite, dispersed in DMMP – Traces are offset for clarity

The XRD traces presented in Figure 4–10 display TP8- to TP16-MMT, Bu16-MMT and Na$^+$ Cloisite, treated with DMMP. The dispersion of these organophosphonium clays into DMMP did not appear to increase the d_{001} spacings, however it did increase the d_{001} spacing of Na$^+$ Cloisite from 12.5 to 14.6 Å. A decrease the d_{001} spacing of Bu16-MMT from 20.9 to 17.7 Å was observed, which could suggest that excess surfactant has been washed out or that Bu16$^+$ had re-orientated within the interlayer space. The d-spacings are displayed in Table 4–11, compared to the d-spacings for organophosphonium clays, and organophosphonium clays dispersed in styrene.

4.7.2 XRD Analysis of Organophosphonium Clays Dispersed in Styrene

XRD analysis was carried out on organophosphonium clays dispersed in styrene, to evaluate the effect of styrene from the unsaturated polyester matrix, on the d-spacings of organophosphonium clays. 1g of each organophosphonium clay was dispersed in styrene, and then dried in an oven at 100 °C overnight, the lower temperature of 80 °C used to dry the DMMP samples was not sufficient to dry the styrene samples.
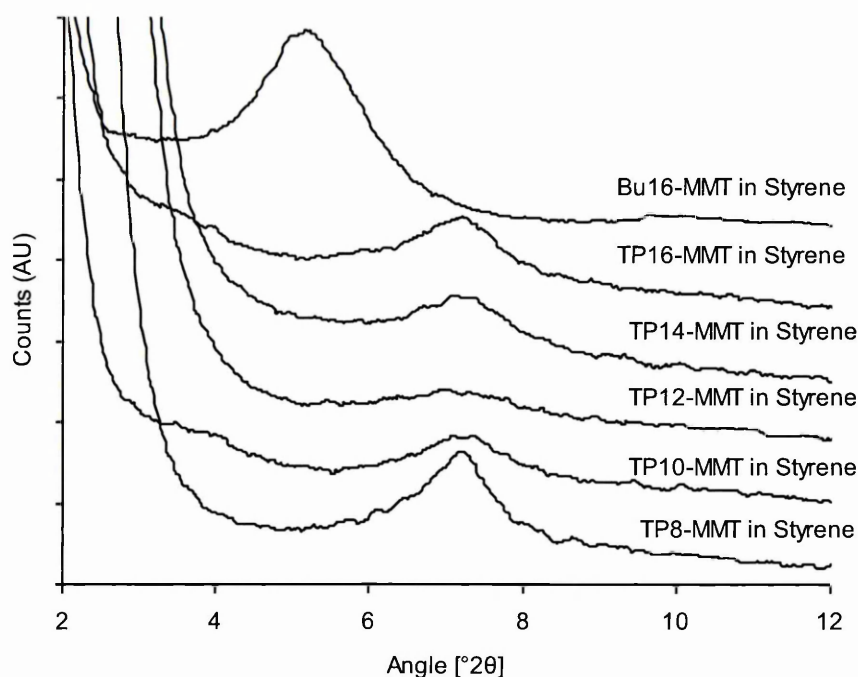
**Figure 4–11 XRD traces (Cr tube) for TP8- to TP16-MMT and Bu16-MMT, dispersed in styrene –**
Traces are offset for clarity

The XRD traces presented in Figure 4–11 display TP8- to TP16-MMT and Bu16-MMT, dispersed in styrene. The XRD traces for all organophosphonium clays dispersed in styrene displayed a clear d_{001} spacing of 17.8 Å, with the exception of Bu16-MMT, which displayed a d_{001} spacing of 24.8 Å. A small peak at lower angle (33.0 Å) is visible in the XRD traces for TP10- and TP16-MMT dispersed in styrene. The d-spacings are displayed in Table 4–11, compared to the d-spacings for organophosphonium clays, and organophosphonium clays dispersed in DMMP. The increase in background at a lower angle in the TP8-, TP12- and TP14-MMT samples could possibly be attributed to the polymerisation of styrene within the samples. There was strong evidence of polymerisation within these samples, after they had been dried overnight the samples had taken on a glassy appearance characteristic of polymerised styrene.

4.7.3 XRD Analysis of Organophosphonium Clays Dispersed in DMMP, then Dispersed in Styrene

The effect on the d-spacings of organophosphonium clays dispersed into DMMP and then dispersed into styrene were analysed using XRD. 1g of each organophosphonium clay (plus Na^+ Cloisite) was dispersed in DMMP, dried in an oven at 80 °C overnight, and then dispersed in styrene and dried in an oven at 100 °C overnight.
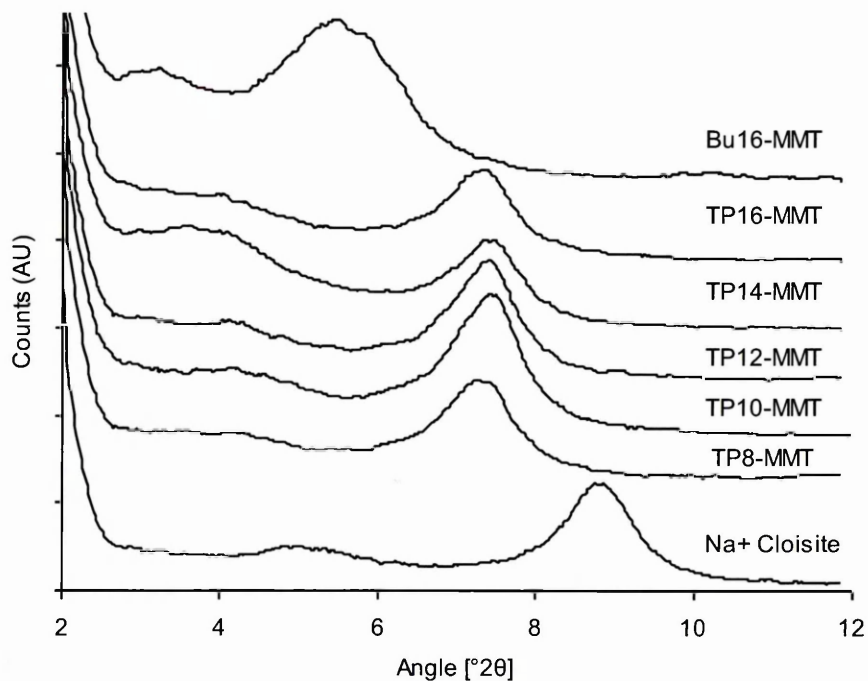
Figure 4–12 XRD traces (Cr tube) for TP8- to TP16-MMT, Bu16-MMT and Na^+ Cloisite, dispersed in DMMP, dried, then dispersed in styrene – Traces are offset for clarity

The XRD traces presented in Figure 4–12 display TP8- to TP16-MMT, Bu16-MMT and Na^+ Cloisite, dispersed in DMMP, dried, and then dispersed in styrene. The d-spacings are presented in Table 4–11, with comparisons of the d-spacings obtained for organophosphonium clays, organophosphonium clays dispersed in DMMP, and organophosphonium clays dispersed in styrene.

Table 4–11 Comparison of d_{001} spacings for organophosphonium clays and Na^+ Cloisite, dispersed in DMMP, dispersed in styrene and dispersed in DMMP, dried then dispersed in styrene

d_{001} (Å)	TP8-MMT	TP10-MMT	TP12-MMt	TP14-MMT	TP16-MMT	Bu16-MMT	Na^+ Cloisite
Organophosphonium clays	17.4	17.4	17.4	18.7	17.7	20.9	12.5
Organophosphonium clays dispersed in DMMP	17.9	17.6	17.9	17.7	17.7	17.7	14.6
Organophosphonium clays dispersed in styrene	17.8	17.8	17.8	17.8	17.8	24.8	-
Organophosphonium clays dispersed in DMMP, dried, then dispersed in styrene	17.5	17.5	17.5	17.5	17.5	23.4	14.7

The d-spacings for organophosphonium clays TP8- to TP16-MMT, did not appear to expand significantly upon dispersion into DMMP, styrene, or DMMP and then styrene. The d-spacing of Bu16-MMT decreased when dispersed into DMMP, increased when dispersed into styrene, and increased when dispersed in DMMP which was then dried and dispersed into styrene. It was observed that the small peak at lower angle, which was found in all organophosphonium clays, was not present when the clays were dispersed in DMMP and was only present in the TP10- and TP16-MMT samples when dispersed in styrene. However, when dispersed in DMMP, dried and then dispersed in styrene, the small peak at lower angle was once again visible in all organophosphonium clays plus Na^+ Cloisite. These experiments confirmed that the expansion in the d_{001} spacing observed when composites were prepared using these organophosphonium clays and Crystic 189LV, was due to polymerisation of Crystic 189LV in the gallery space, therefore expanding the clay layers further. The increase in the d_{001} spacing cannot be attributed to DMMP or styrene preferentially expanding the clay layers.

4.7.4 XRD Analysis of Composites Prepared Using DMMP

Modified organophosphonium clays once pre-dispersed in DMMP were then mixed with Crystic 189LV following the mixing regime outlined in section 3.2.2 of Chapter 3. The samples, described in Table 4–12, were based on those in section 4.5.2 which formed a microcomposite (TP12-MMT) and intercalated nanocomposite (TP16-MMT with Crystic 189LV plus an intercalated nanocomposite of Crystic 189LV/Bu16-MMT.

Table 4–12 Nanocomposite formulations involving DMMP

Organoclay	Carbon Chain Length	Organoclay Used (wt%)	DMMP (wt%)
Bu16-MMT	16	2.5	5
Bu16-MMT	16	5	10
TP16-MMT	16	5	0
TP16-MMT	16	2.5	5
TP16-MMT	16	5	10
TP12-MMT	12	5	0
TP12-MMT	12	2.5	5
TP12-MMT	12	5	10
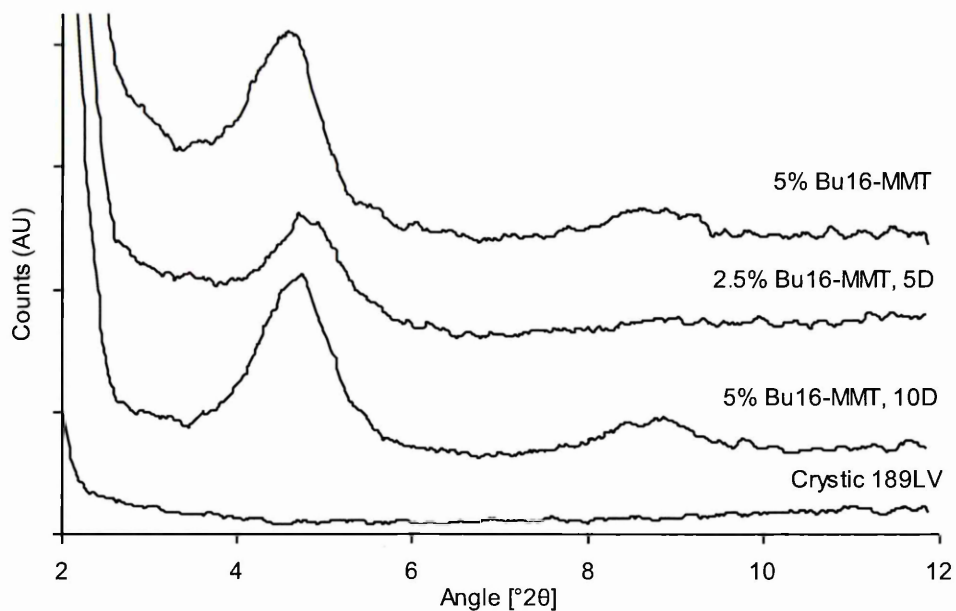
Figure 4–13 XRD traces (Cr Tube) for Crystic 189LV composites prepared by pre-mixing Bu16-MMT and different percentages of DMMP (e.g. 5D = 5% DMMP) – Traces are offset for clarity

146

This pre-swelling step using DMMP made it easier to physically combine the phosphonium-based organoclays with the resin. The XRD traces presented in Figure 4–13 display Crystic 189LV and Crystic 189LV mixed with 5 wt% Bu16-MMT, 2.5 wt% Bu16-MMT plus 5 wt% DMMP (5D) and 5 wt% Bu16-MMT plus 10D. Intercalated and aggregated nanocomposites were achieved in the 5 wt% Bu16-MMT and 5 wt% Bu16-MMT plus 10D samples, confirmed by the presence of clear d_{001} and d_{002} peaks. The XRD traces for composites prepared using 2.5 wt% Bu16-MMT plus 5D were less intense, possibly due to the decreased amount of clay in the sample. The d_{001} spacing increased from 20.9 Å in Bu16-MMT to 29.1 Å when mixed with Crystic 189LV/5 wt% Bu16 and 28.1 Å when mixed with Crystic 189LV/2.5 or 5 wt% Bu16 plus DMMP. Upon increasing the amount of DMMP in the Bu16-MMT samples from 5 to 10 wt%, the samples remained intercalated, therefore DMMP did not clearly influence the dispersion and size of the stacks within the Bu16-MMT samples.
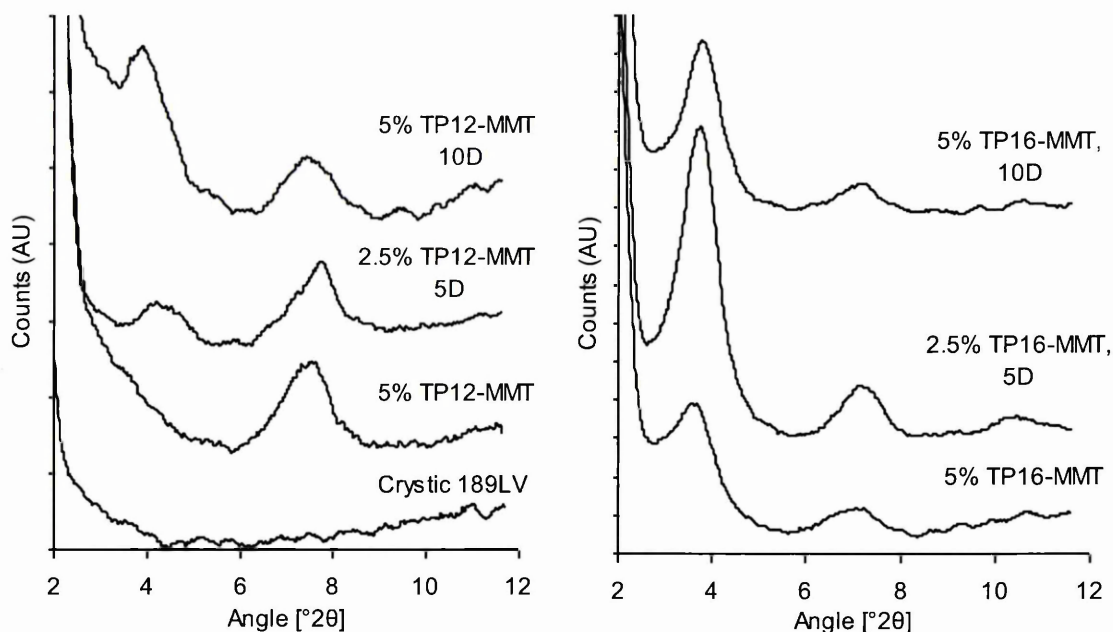
Figure 4–14 XRD traces (Cr Tube) for Crystic 189LV composites prepared by pre-mixing TP12- and TP16-MMT and different percentages of DMMP (e.g. 5D = 5% DMMP) - Traces are offset for clarity

The XRD traces presented in Figure 4–14 were obtained from Crystic 189LV nanocomposites containing TP12- and TP16-MMT, with and without pre-dispersion in DMMP. When mixed with Crystic 189LV and DMMP, an increase in the d-spacing of TP12-, and TP16-MMT occurred from 17.4 and 17.7 Å, to 30.1 and 31.7 Å, respectively. Crystic 189LV did not intercalate into TP12-MMT, this is evident from the d_{001} peak, which displayed a d-spacing of 17.4 Å, which was the same as that for unexpanded TP12-MMT (Figure 4–2). The addition of 5D into the TP12-MMT/Crystic 189LV system produced some intercalated nanocomposite, but lots of undispersed TP12-MMT remained. However a more exfoliated/intercalated nanocomposite was formed upon addition of 10D, which was observed through increased low angle scattering and intensity of the d_{001} peak. Therefore, there is clear evidence that the addition of DMMP did influence the dispersion of Crystic 189LV into TP12-MMT, however micrograins still remained in the sample. Intercalated and aggregated nanocomposites were formed when TP16-MMT was mixed with Crystic 189LV, occurring in the presence and absence of DMMP. The 2.5 wt% TP16-MMT/5D samples displayed a more intercalated/aggregated nanocomposite nature, observed through increased intensity of the d_{001} and d_{002} peaks. Table 4–13 exhibits the d_{001} spacings for TP12-, TP16- and Bu16-MMT/ DMMP/ Crystic 189LV nanocomposites (± 0.2 Å).

Table 4–13 Comparison of d_{001} spacings for Crystic 189LV composites prepared by premixing TP12-, TP16- and Bu16-MMT and different percentages of DMMP (e.g. 5D = 5% DMMP)

Organoclay	Organoclay (wt%)	DMMP (wt%)	d_{001} (Å)
TP12	5	0	-
TP12 (1)	2.5	5	27.4
TP12 (2)	5	10	30.1
TP16	5	0	33.2
TP16 (3)	2.5	5	32.9
TP16 (4)	5	10	31.7
Bu16	5	0	29.1
Bu16 (5)	2.5	5	28.1
Bu16 (6)	5	10	28.1

4.7.5 TG Analysis of Composites Prepared using DMMP
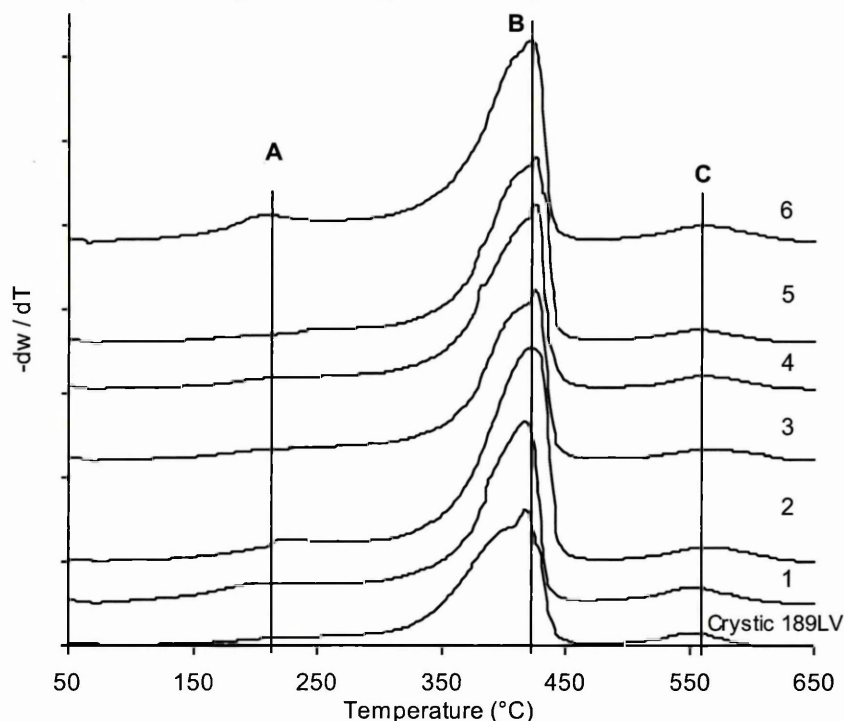
Figure 4–15 DTG traces (Air) of composites prepared using Crystic 189LV, TP12-, TP16- and Bu16-MMT and DMMP (formulations described in Table 4–13) – Traces are offset for clarity.

The DTG traces presented in Figure 4–15 are for the nanocomposite samples prepared using TP12-, TP16- and Bu16-MMT (labelled 1-6 in Table 4–13). They decomposed over three stages, with three maxima in the decomposition process (A, B and C). T_{max} (A) occurred at 215 °C, T_{max} (B) occurred at 425 °C, and T_{max} (C) occurred at 565 °C. The peak under T_{max} (A) most likely corresponds to the evaporation of DMMP, which boils at 181 °C, however this peak is not prominent in all samples. T_{max} (B) and T_{max} (C) correspond closely to the decomposition maxima for Crystic 189LV blended with modified organoclays.

Therefore, DMMP does not appear to affect the decomposition pathway of these systems, at this level of investigation, as well as having little effect on the d_{001} of the C16 chains. DMMP does however aid the dispersion of TP12-MMT, increasing the amount of intercalation by the UP.

4.8 One Pot Synthesis of Crystic 189LV-Clay Nanocomposites Incorporating TP8$^+$ to TP16$^+$ and Bu16$^+$, DMMP and Na$^+$ Cloisite

4.8.1   Introduction

This section describes the preparation of (nano) composites from an original 'one-pot' process, starting with Na$^+$ Cloisite. An efficient one-pot synthesis method would involve all the components for a UP-clay (nano) composite simultaneously in a mixture, which would permit the in-situ preparation of organophosphonium clays. Such a method would potentially provide an economic advantage through cost reduction, be more efficient and reduce environmental impact through reduced process manufacture.

4.8.2   Experimental Method

The usual method of preparing an organoclay is to pre-disperse inorganic cation exchanged clay in a large amount of water. The salt is then added into the suspension. After the ion-exchange reaction, the solids obtained are washed, dried and ground. Generally washing is the time intensive stage. In this simplified 'one-pot' method the inorganic clay and alkylphosphonium salt were mixed with UP resin and DMMP, simultaneously.

Bu16-MMT was studied first simply because it presented the best fire retardant results (Table 4–15) in the initial survey. For comparison Na$^+$ Cloisite was exchanged with Bu16$^+$, using the general method described in section 2.3 of Chapter 2. Three Crystic 189LV based composites containing 5 wt% organoclay were prepared: one from Bu16-MMT and 10 wt% DMMP (**1**), one from Na$^+$ Cloisite and 10 wt% DMMP (**2**) and the last one from a mixture of Na$^+$ Cloisite, Bu16$^+$ salt (Bu16B) and 10 wt% DMMP (**3**). In the 'one-pot' method, Bu16B was added at the beginning of the blending procedure, i.e. directly with the DMMP and Na$^+$ Cloisite before addition to Crystic 189LV. Most importantly, the nanocomposites produced by the 'one-pot' method were found to have comparable fire retardant properties to the nanocomposites produced by the standard method. In addition to Bu16B, samples containing TP8B to TP16B salts were also prepared using the 'one-pot' method.

4.8.3 XRD Analysis of 'one-pot' composites
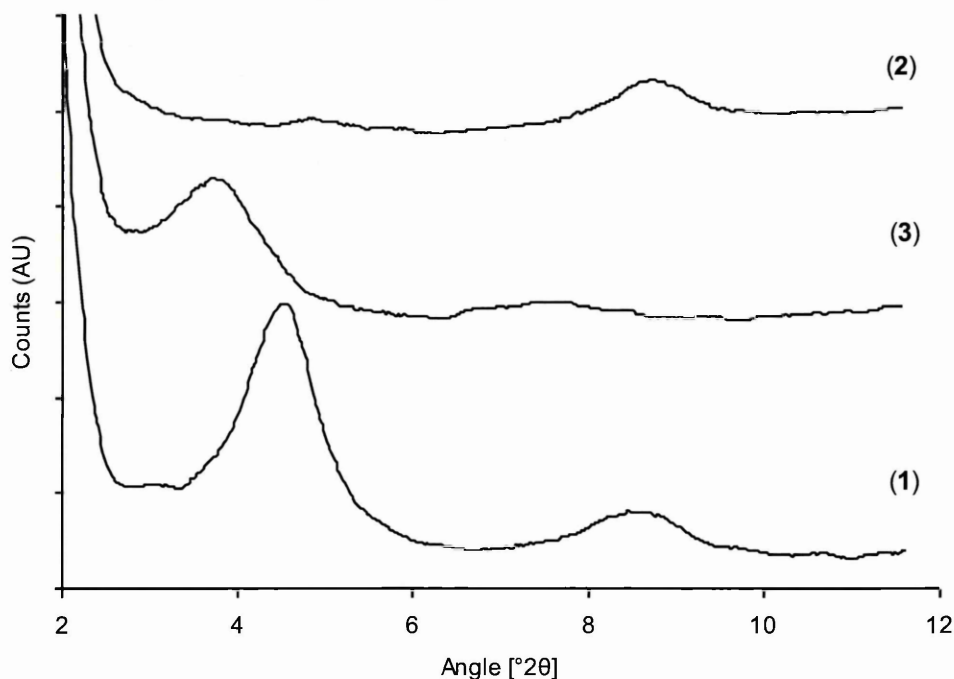
Figure 4–16 XRD traces (Cr Tube) for Crystic 189LV composites prepared using (1) Bu16-MMT and 10D (Standard Method), (2) Na$^+$ Cloisite and 10D and (3) Bu16B, Na$^+$ Cloisite and 10D (One Pot Method) – Traces are offset for clarity

The XRD traces presented in Figure 4–16 display traces for composites **1** to **3**. These results indicate an intercalated morphology for both compounds **1** and **3**, with d-spacings of 28.6 Å (**1**) and 34.4 Å (**3**), the second peak in composite **1** was representative of the d_{002} peak of the Crystic 189LV intercalated Bu16-MMT. Compound **2** exhibited only a weak peak corresponding to a d-spacing of 14.7 Å, which is in agreement with the d-spacing of the DMMP expanded Na$^+$ clay (Table 4–11).

Table 4–14 Comparison of d_{001} spacings for Bu16-MMT dispersed in DMMP and styrene, and its nanocomposites prepared using the standard and 'one-pot' methods

	d_{001} (Å)
Bu16-MMT	20.9
Bu16-MMT dispersed in DMMP	17.7
Bu16-MMT dispersed in styrene	24.8
Bu16-MMT dispersed in DMMP, dried, then dispersed in styrene	23.4
Standard method	28.6
'one-pot' method	34.4

Table 4–14 displays a comparison of the d_{001} spacings for Bu16-MMT dispersed in DMMP and styrene, and its nanocomposites prepared using the standard and 'one-pot' methods. The 'one-pot' method exhibited the largest increase in d-spacing, however upon comparison of the d_{001} spacings in Table 4–14 it was unclear at this stage whether the increase could be attributed to one/or a combination of components in the 'one-pot' system.

4.8.4 TGA Analysis of 'one-pot' composites
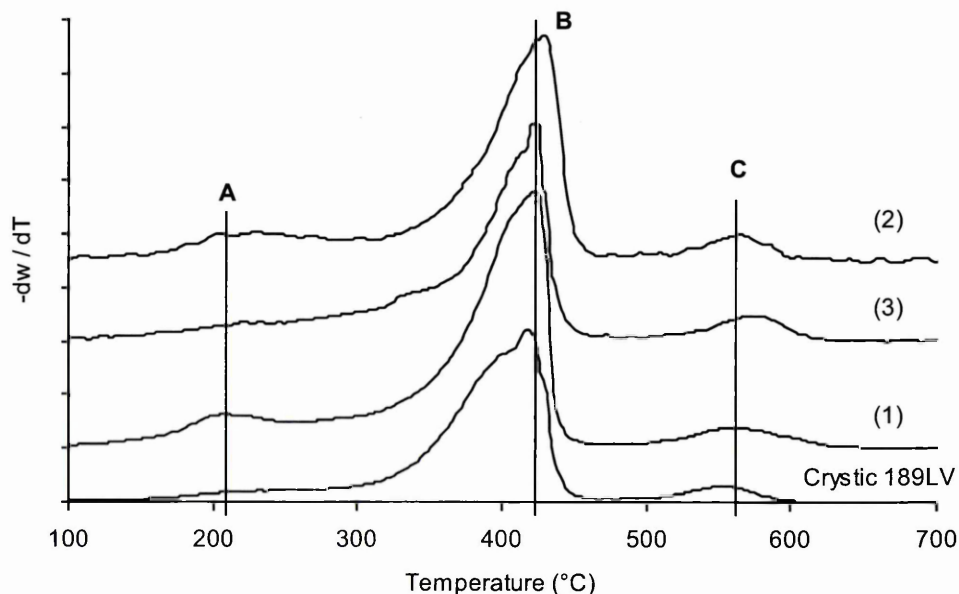
Figure 4–17 DTG traces (Air) for Crystic 189LV and composites prepared using Crystic 189LV and (1) Bu16-MMT and 10D (Standard Method), (2) Na$^+$ Cloisite and 10D and (3) Bu16B, Na$^+$ Cloisite and 10D (One Pot Method) – Traces are offset for clarity

The DTG traces presented in Figure 4–17 display three maxima in the decomposition process (A, B and C), occurring over three stages. T_{max} (A) occurred during stage 1 at 220 °C and represented the thermal desorption of DMMP, T_{max} (B) occurred during stage 2 at 421 °C for pure Crystic 189LV and at temperatures between 425 and 430 °C for compounds (1) to (3). T_{max} (C) occurred during stage 3 at 556 °C for pure Crystic 189LV, increasing to 568 °C for compounds (1) (standard method) and (2), and 577 °C for compound (3) (the 'one-pot' method).

152

Alexandre *et al.* [4-23] carried out a similar study and reported on the preparation of ethylene-vinyl acetate (EVA) nanocomposites in an original 'one-pot' reactive process, starting directly from natural, Na$^+$ exchanged clay. Dimethyl dioctadecylammonium bromide (DMDODABr) was studied as a potential clay/matrix reactive compatibiliser. Three EVA based composites were prepared: (**X**) using a standard method similar to the one used in this thesis, (**Y**) a control using Na$^+$ Cloisite, and (**Z**) using a 'one-pot' method. XRD analysis revealed an intercalated morphology for composite (**X**) and intercalated/exfoliated morphology for composite (**Z**). An increase in the Young's modulus, the stress at break and a decrease in the strain at break were observed in the composite made by the 'one-pot' method. These differences were explained by the difference in structure observed between nanocomposites (**X**) and (**Z**) (intercalated v. intercalated/exfoliated), as the amount of individual clay platelets responsible for the large increase in modulus is smaller in the case of the 'one-pot' nanocomposite. This behaviour might also result from a limited diffusion of the ammonium salts within the EVA, inducing a modification of the clay layer that was not sufficient to achieve the best compatibilisation.

Another property for which the nanocomposite morphology played an important role was the thermal stability under air. The DTG results observed for Bu16-MMT are similar to those found by Alexandre *et al.* [4-23] in that they also found an increase in T_{max} (C) for the nanocomposite made using the 'one-pot' method (**Z**), as compared to the microcomposite (**Y**), this is also in agreement with improvements reported for other partially intercalated and partially exfoliated nanocomposites [4-24, 4-25].

4.9 UL94 Vertical Burning Test Results using Dimethyl methyl phosphonate (DMMP) as a Flame Retardant

DMMP served a dual purpose, not only was it used as a flame retardant, it was also used as a pre-dispersing agent for the modified clays. Very interesting results on fire performance were produced that could remove the need for halogenated products to achieve increased fire retardancy. DMMP is a liquid phosphonate that has been used as a fire retardant agent in many polymers, and acts mainly in the vapour phase. Considering this knowledge the following question was addressed:

Could the combination of clay and DMMP provide better fire retardant performance given that clay forms much better insulation layers and that the evaporation or decomposition of DMMP would suppress the flame?

To evaluate the effectiveness of DMMP as a flame retardant agent a fire test similar to the UL94 vertical burning test (94V) (Section 2.13.1 of Chapter 2) was performed on the entire series of TP and Bu16$^+$ exchanged organoclay nanocomposites and DMMP. A comparison of samples made via the standard and one-pot routes were also included.

4.9.1   UL 94 Vertical Burning Test Results

TP8– to TP16-MMT and Bu16-MMT were mixed with Crystic 189LV and DMMP at 2000 rpm for 30 minutes, using the standard and 'one-pot' methods, postcured and then subjected to the vertical burning test. The results are displayed in Table 4–15 and a UL94-V classification was applied where possible.

A sample displaying good burning characteristics incorporated Crystic 189LV, 5 wt% Bu16-MMT and 10 wt% DMMP (10D) (highlighted in Table 4–15). Four different samples were burnt in total (Burn 1, Burn 2 etc.). Each sample, which was the size of a standard microscope slide, was secured in a clamp, before a flame with a length of approximately 5 cm was applied to the bottom corner of the sample for 10 seconds after the sample had extinguished. The sample was allowed to cool for 30 seconds and a second flaming applied. The time it took for the flame to extinguish after each flaming was recorded (e.g. 2, 11 etc.), the mean value for the total time for each flaming was taken, which resulted in a UL94-V classification being applied (criterion for each UL94-V classification can be found in section 2.6.7.1 of Chapter 2).

Crystic 189LV when mixed with 5 wt% TP14 displayed poor burning characteristics. After the first flaming the samples continued to burn beyond 60 seconds and consequently were extinguished manually (denoted as Ex, in Table 4–15), a second flaming was not applied and the samples failed to reach a UL94-V classification.

Table 4–15 UL94 Vertical Burning Test Results

	Burn 1	Burn 2	Burn 3	Burn 4	Total	UL94- V Classification
Original Method						
Crystic 189LV	Ex	Ex	Ex	Ex	-	Fail
Crystic 189LV, 10D	3, Ex	20, Ex	3, Ex	4, Ex	7.5, Ex	Fail
5% TP8-MMT	Ex	Ex	Ex	Ex	-	Fail
5% TP8-MMT, 10D	2, 5	3, 5	3, 9	2, 11	2.5, 7.5	V-0
5% TP10-MMT, 10D	3, 4	6, 9	2, Ex	Ex	-	Fail
5% TP12-MMT, 10D	3, Ex	Ex	Ex	Ex	-	Fail
5% TP14-MMT	Ex	Ex	Ex	Ex	-	Fail
5% TP14-MMT, 10D	4, 30	5, Ex	6, Ex	Ex	-	Fail
5% Bu16-MMT	Ex	25, Ex	28, Ex	Ex	-	Fail
5% Bu16-MMT, 10D	3, 8	4, 5	2, 5	1, 9	2.5, 6.75	V-0
One-pot Method						
5% TP8^{+} and MMT, 10D	5, 19	6, 14	3, 11	4, 15	4.5, 14.75	V-1
5% TP10^{+} and MMT, 10D	3, 8	12, 26	21, 22	-	5.6, 18.6	V-1
5% TP12^{+} and MMT, 10D	31, Ex	7, 24	-	-	-	Fail
5% TP14^{+} and MMT, 10D	15, 40	8, Ex	-	-	-	Fail
5% TP16^{+} and MMT, 10D	3, 8	12, Ex	-	-	-	Fail
5% Bu16^{+} and MMT, 10D	3, 12	3, 10	3, 7	-	3, 9.6	V-1

(Ex = Extinguished manually after 60 seconds)

The vertical burning test results in Table 4–15 indicated to some extent that the original and 'one-pot' methods were comparable, however the V-rating slipped from a V-0 in the case of the Bu16^{+} samples down to a V-1 rating, and this was also the case for the TP8^{+} samples. In some of the samples, organoclay particles were clearly visible in the films. When organoclay particles were visible, then the samples had a tendency to crack when subjected to the first flaming and had to be extinguished manually, this phenomenon was attributed to poor dispersion within the samples. As a result of poor dispersion, the addition of organophosphonium–clays alone did not result in significant

fire retardant improvement. However, using DMMP as a pre-swelling agent not only improved the dispersion but also caused the fire retardant properties to reach a much higher classification. The pure resins and samples without DMMP failed and had to be extinguished manually.

Based on the vertical burning test results in Table 4–15 it was decided not to pursue the TP series. Poor dispersion of these clays within the polymer lead to an increased incidence of cracking within the samples after they had been subjected to the first flaming. Consequently the sample continued to burn after the second flaming due to non-uniformity of the char layer and had to be extinguished manually. Bu16-MMT however, displayed comparable fire retardant properties to the halogenated resins in section 3.5 of Chapter 3. The halogenated resins self extinguished within 3 seconds after the first flaming, compared to Bu16-MMT composites, which self extinguished in approximately 2.5 seconds after the first flaming. As a result of these comparable fire retardant results it was decided to further pursue composites prepared using Crystic 189LV, Bu16-MMT and DMMP.

4.10 Variation in Bu16 Exchanged Na$^+$ Cloisite Batches and its Effect on Fire Retardant Properties of Crystic 189LV Composites Containing DMMP

The most promising fire retardant results were observed when Bu16$^+$ was exchanged onto Na$^+$ Cloisite and mixed with Crystic 189LV and DMMP. Consequently many different batches of this organophosphonium-clay were produced during the project. Fire retardant performance varied and although all batches were made using the same exchange procedure both batch-to-batch differences, and differences between samples made from the same batch, but on different days were seen. Table 4–16 displays different Bu16-MMT (5 wt%) batches mixed with Crystic 189LV and 10D, that were subjected to the in-house version of the UL94 Vertical Burning Test (where possible V-ratings have been applied).

Table 4–16 UL94 Vertical Burning Test results for different Bu16-MMT batches

	Burn 1	Burn 2	Burn 3	Burn 4	Burn 5	Burn 6	Total	UL94- V Rating
Batch 2	3, 8	4, 5	2, 5	1, 9	-	-	2.5, 6.8	V-0
Batch 4, Mix 1	1,8	3, 7	2, 5	3, 5	3, 6	3, 9	2.5, 6.7	V-0
Batch 4, Mix 2	3, 42	4, Ex	3, 12	3, Ex	6, 8	4, Ex	3.8, -	Fail
Batch 4, Mix 3	2, 11	3, Ex	2, Ex	3, 12	2, 6	4, Ex	2.7, -	Fail
Batch 4, Mix 4	3, 15	2, 10	2, 11	<1, 4	2, 7	2, 8	1.8, 9.2	V-1/ V-0
Batch 5	Ex, -	6, 11	7, 6	7, Ex	-	-	-	Fail
Batch 6	4, 30	2, 23	3, 16	2, 14	-	-	2.8, 20.8	V-1
Batch 8	4, 32	3, 20	4, 25	4, 13	-	-	3.8, 22.5	V-1

(Ex = Extinguished manually after 60 seconds)

4.10.1 XRD Analysis of Different Bu16-MMT Batches
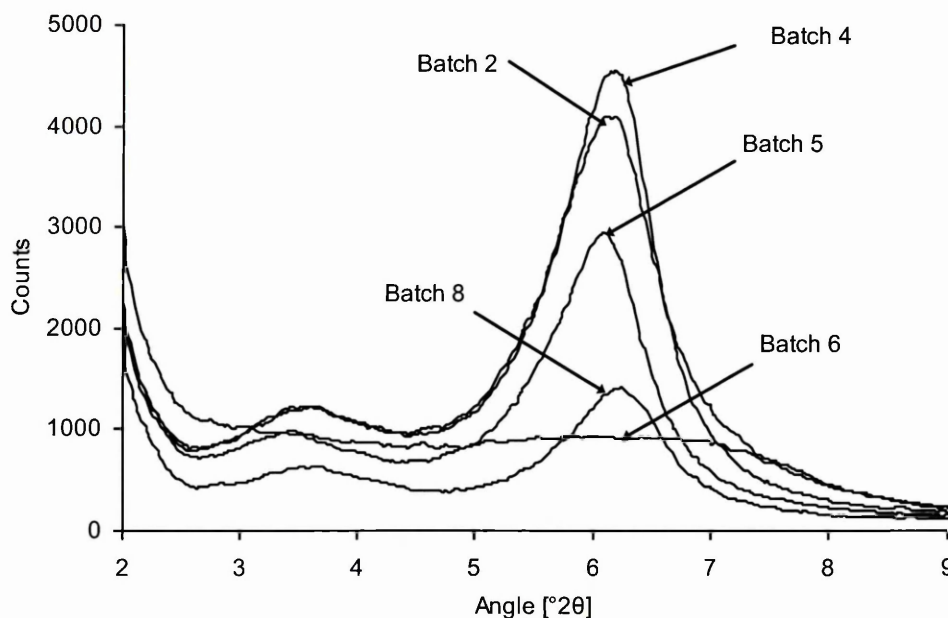
Figure 4–18 XRD traces (Cr Tube) for different Bu16-MMT batches

The XRD traces presented in Figure 4–18 display different Bu16-MMT batches. Table 4–17 displays the d_{001} spacing and the d-spacing for the smaller peak at lower angle for each batch. Differences were seen in the intensity of the d_{001} peak, batches 2 and 4 displayed the most intense d_{001} signals and were approximately twice as intense as batch 5 and three times as intense as batch 8. The ratio of the small peak at low angle to the d_{001} peak also differed, varying as 10:1, 9:1, 8:1 and 4:1 for batch 4, batch 2, batch 5 and batch 8, respectively.

Table 4–17 Comparison of d_{001} and small peak at lower angle spacings for Bu16-MMT batches

	d_{001} (Å)	d-spacing for small peak (Å)
Batch 2	21.2	36.3
Batch 4	21.2	36.3
Batch 5	21.5	37.7
Batch 6	-	-
Batch 8	20.9	35.7

The d_{001} spacings for the different Bu16-MMT batches presented in Table 4–17 are all similar at 21.2 Å ± 0.3 Å. However, the d-spacing for the small peak at lower angle varied by approximately 2 Å from batch to batch, which could indicate regular interstratification of Na^+ and $Bu16^+$, or it could indicate an increased amount of $Bu16^+$ in some of the samples.

4.10.2 TG Analysis of Different Bu16-MMT Batches
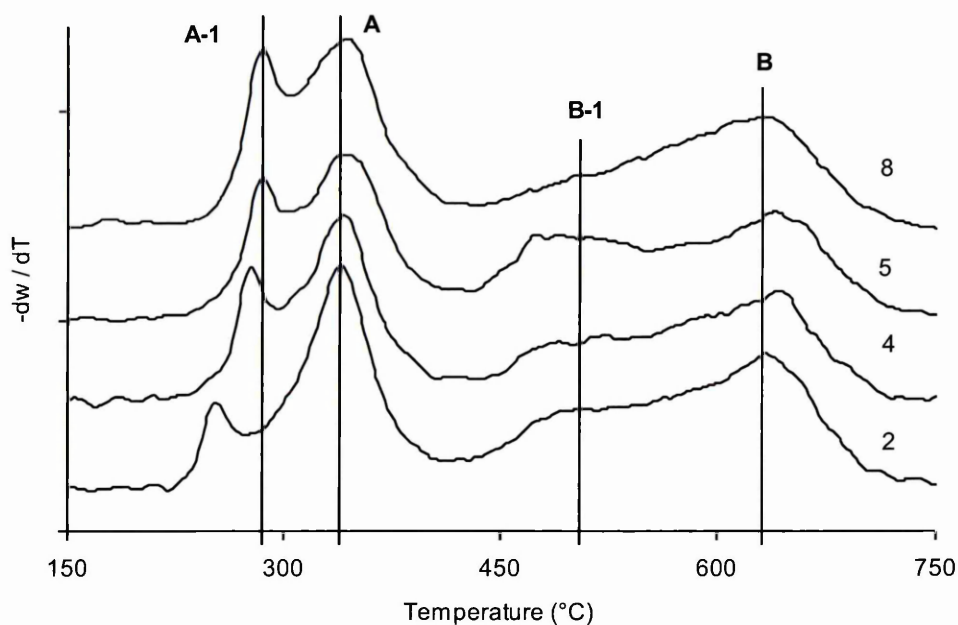
Figure 4–19 DTG traces (Air) for different Bu16-MMT batches – Traces are offset for clarity

The DTG traces presented in Figure 4–19 display two maxima in the decomposition process (A and B), decomposing over two stages. In batches 2, 4, 5 and 8, T_{max} (A) occurred at 344 °C and T_{max} (B) occurred at 652 °C, however, there were differences in the position and intensity of the minor peaks under T_{max} (A-1) and T_{max} (B-1) as displayed in Table 4–18.

Figure 4–20 displays the DTG trace for batch 6. Batch 6 displayed a different degradation pattern to the other batches. T_{max} (A) occurred at a lower temperature of 330 °C. However, T_{max} (A-1) occurred at 290 °C, which was the same temperature as batches 5 and 8. T_{max} B occurred at a lower temperature of 638 °C and T_{max} (B-1) occurred at 593 °C.
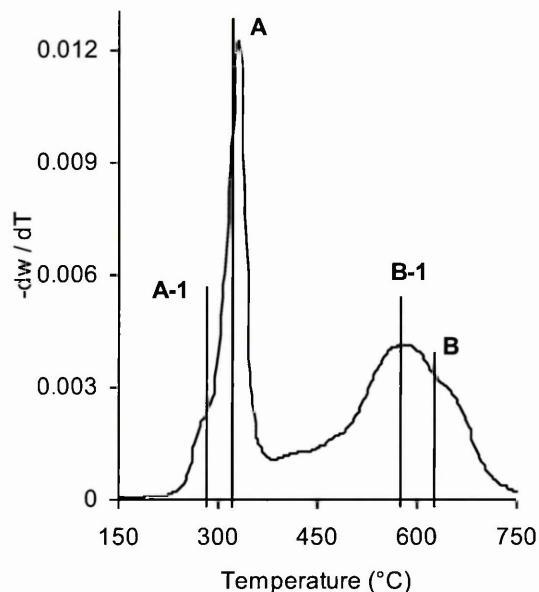
Figure 4–20 DTG trace (Air) for Bu16-MMT batch 6

From the UL94 vertical burning test results (Table 4–16) batches 2 and 4 displayed the most promising fire retardant properties reaching a V-0 classification, however batch 4 (mixes 2 and 3) along with batch 5 also displayed the least promising fire retardant properties. T_{max} (A-1) displayed a significant shift in temperature (up to 28 °C between batches 2, 5 and 8) and height between different batches.

Table 4–18 Differences in peak positions and intensity for different Bu16 batches

	Stage 1	Stage 2				
	T_{max} A (°C)	T_{max} B (°C)	T_{max} A-1 (°C)	T_{max} B-1 (°C)	Height A : A-1	Separation Between A and A-1 (°C)
Batch 2	350	645	262	-	1:0.4	88
Batch 4	350	645	283	510	1:0.7	67
Batch 5	350	645	290	510	1:0.88	60
Batch 6	330	638	290	593	1:0.2	40
Batch 8	350	645	290	510	1:1.05	60

It was unclear at this stage what was being released under T_{max} (A-1) and whether the peak shifts and peak heights played an important role in the fire retardant properties of Bu16$^+$ exchanged Na$^+$ Cloisite, when included in the Crystic 189LV composites with DMMP. It appeared that when there was a large difference in peak heights as for Batch 2 (plus a large separation between T_{max} (A) and (A-1)), then the fire retardancy changed from a V-1 to a V-0 classification. When the peak heights were in the mid range as for

Batch 4 and Batch 5, then the fire retardancy reached a V-0, V-1 or fail classification. To provide a better understanding of what was being released under T_{max} (A-1), TG-MS analysis was carried out and will be reported later in the Chapter.

4.10.3 XRF Analysis of Different Bu16-MMT Batches

X-ray fluorescence elemental analysis was carried out on the different Bu16 batches (Table 4–19) to give an indication of the amount of Na^+ displaced. For comparison the data for Na^+ Cloisite has been included in the table.

Table 4–19 XRF Elemental Analysis of Different Bu16-MMT batches and Na^+ Cloisite

	Batch 2 (%)	Batch 4 (%)	Batch 6 (%)	Batch 8 (%)	Na^+ Cloisite (%)
MgO	1.9	2.1	2.08	2.1	2.3
Na_2O	0.1	0.09	0.2	0.06	4.3
Al_2O_3	22.5	22.4	22.3	22.5	22.6
SiO_2	64.5	64.5	64.1	64.7	65.1
P_2O_5	5.7	5.8	6.4	5.6	0.01
SO_3	0.01	-0.02	-0.02	-0.01	0.7
K_2O	0.06	0.06	0.06	0.02	0.1
CaO	0.3	0.3	0.3	0.3	0.2
TiO_2	0.1	0.2	0.1	0.1	0.1
Fe_2O_3	4.7	4.6	4.5	4.6	4.7

As expected Na^+ Cloisite contained more Na_2O than the Bu16-MMT batches and very little P_2O_5. Batches 2, 4 and 8 all contained similar amounts of Na_2O and P_2O_5, suggesting that the exchange process had occurred to a similar extent in these batches. However, from the elemental analysis of Batch 6, it was clear that the exchange process had occurred differently. Batch 6 contained more Na_2O than the other batches, suggesting that less $Bu16^+$ had entered the gallery to replace the Na_2O. It is also possible that there was free phosphonium salt that had not ion exchanged onto the clay and that the washing process had not removed sufficiently. Batch 6 displayed a markedly different XRD pattern compared to the other batches.

4.11 Increasing the Loading of Bu16$^+$ onto Na$^+$ Cloisite

Batch 6 prepared using Bu16$^+$ exchanged Na$^+$ Cloisite displayed a different degradation pattern to the other batches and it was thought that the exchange process had occurred differently. To investigate whether variations in the loading of Bu16$^+$ onto Na$^+$ Cloisite affected the thermal degradation pattern and whether a trend could be established between a fully/partially exchanged batch and good/poor fire retardant properties Na$^+$ Cloisite was loaded with Bu16$^+$ at different percentages of the CEC (Table 4–20). Therefore, the effect of organocation excesses and deficiencies could be investigated.

Table 4–20 CEC exchange mass for Bu16$^+$ at 0.25 to 2 x CEC of Na$^+$ Cloisite

Mass of Clay (g)	CEC of Clay (mEq/g)	Multiples of CEC	Molecular Weight (g)	Cationic Charge	Mass Required (g)
1	0.925	0.25	507.6	1	0.12
1	0.925	0.5	507.6	1	0.23
1	0.925	1	507.6	1	0.47
1	0.925	1.5	507.6	1	0.70
1	0.925	2.0	507.6	1	0.94

## 4.11.1 XRD Analysis of Clay with Different Bu16$^+$ Loadings
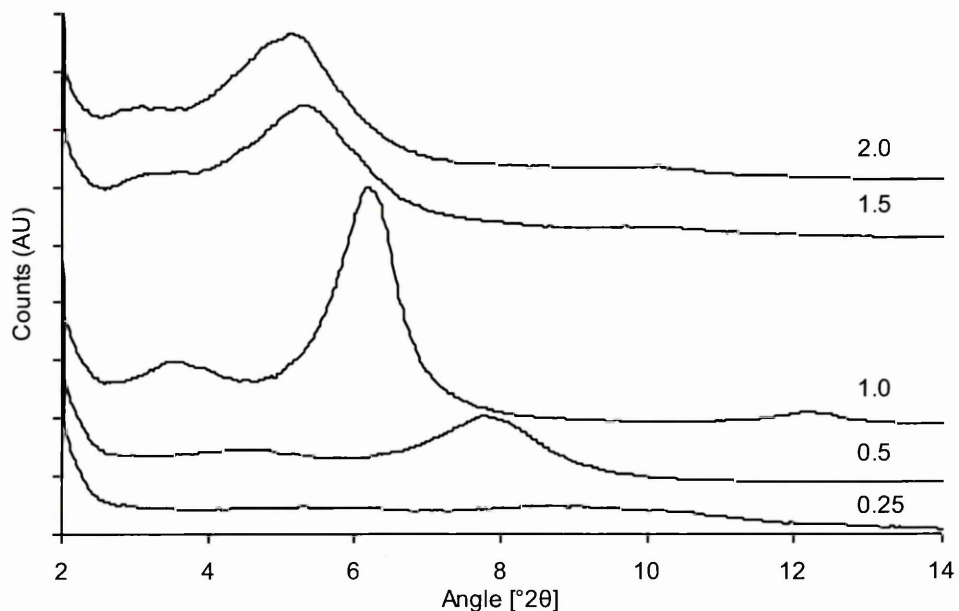
Figure 4–21 XRD traces (Cr-tube) for Na$^+$ Cloisite loaded with Bu16$^+$ at 0.25 – 2.0 x CEC – Offset for clarity

The XRD traces presented in Figure 4–21 displayed an increase in the d-spacing as the loading of Bu16$^+$ increased. The d_{001} peak in the XRD trace for 0.25 x CEC is difficult to see due to the higher intensity of the diffraction peaks in the other samples, however upon expansion of the y-axis the d_{001} spacing was visible at 14.8 Å. The d_{001} spacings and the d-spacing for the smaller peaks at lower angle are presented in Table 4–21.

Table 4–21 Variation in d-spacing with loading for the Bu16$^+$ exchanged clay

% CEC	d_{001}-Spacing (Å)	Small Peak (Å)	Difference between d_{001} and small peak (Å)
0	12.1	20.3	8.2
0.25	14.8	23.4	8.6
0.5	16.4	28.2	11.8
1.0	20.8	35.7	14.9
1.5	24.3	40.0	15.7
2.0	24.3	40.0	15.7

The d-spacings in Table 4–21 display some variability in the distance between the d_{001} spacing of Bu16-MMT and the smaller peak for the heterostructure. However, as the loading of Bu16$^+$ increased from 1.0 to 1.5 and 2.0 x CEC, the difference between the d_{001} spacing and the spacing for the small peak at lower angle remained the same at approximately 15 Å, and the values aligned with that in Table 4–8 for Bu16-MMT. These diffraction patterns could be further evidence for a staged intercalate, and variation in the basal spacing of the galleries containing the inorganic cations in the heterostructure defined by Figure 4–6 (c), have been tentatively attributed to variable hydration of the inorganic cations. Basal spacings from 12.5 to 15 Å are readily obtained at different relative humidities.

4.11.2 TGA Analysis of Clay with Different Bu16^{+} Loadings
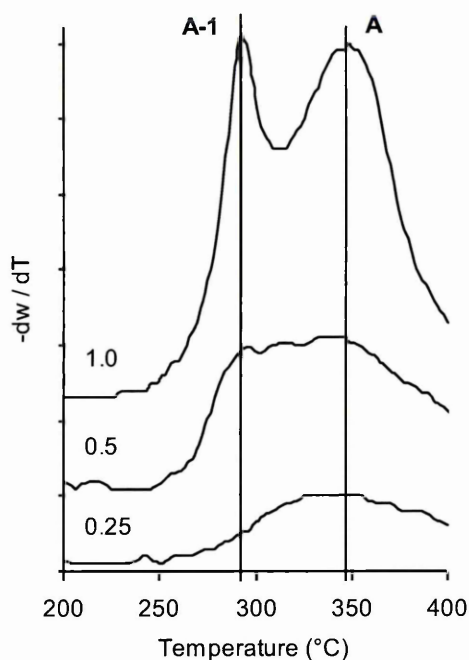
Figure 4–22 DTG traces (Air) Bu16^{+} at 0.25 to 1.0 x CEC of Na^{+} Cloisite – Traces are offset for clarity
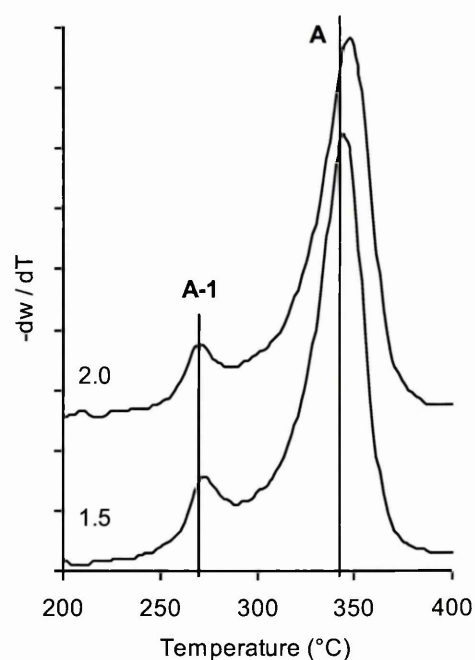
Figure 4–23 DTG traces (Air) Bu16^{+} at 1.5 and 2.0 x CEC of Na^{+} Cloisite – Traces are offset for clarity

The DTG traces presented in Figure 4–22 and Figure 4–23 display Bu16^{+} at loadings of 0.25 to 2.0 x CEC on Na^{+} Cloisite, over the temperature region (200 to 400 °C) in which differences were seen in the different Bu16-MMT batches (Figure 4–19). The peak under T_{max} (A-1) became less intense and moved to a lower temperature as the loading of Bu16^{+} on Na^{+} Cloisite increased. The peak positions and intensities are presented in Table 4–22. The sample exchanged at 0.25 x CEC behaved very much like Na^{+} Cloisite and did not exhibit T_{max} (A-1), however T_{max} (A) was visible at 348 °C which was the same temperature as in the other samples.

Table 4–22 Differences in peak positions and intensity for Bu16^{+} at 0.25 to 2.0 x CEC of Na^{+} Cloisite

	T_{max} A (°C)	T_{max} A-1 (°C)	Intensity A : A-1	Separation Between A and A-1 (°C)
0.25	348	-	-	-
0.5	348	299	-	-
1.0	348	292	1:1	56
1.5	344	273	1:0.2	71
2.0	348	273	1:0.2	75

From the data presented in Table 4–18 and Table 4–22 it was still unclear which factors could potentially link to the fire retardant properties of the sample. From the T_{max} (A-1) value it appeared that batches 5 and 8 were exchanged at 1.0 x CEC and that batches 2 and 4 were exchanged somewhere between 1.0 and 1.5 x CEC. It appeared however that as the separation between T_{max} (A) and T_{max} (A-1) increased then the fire retardant properties of the resulting composite also increased.

4.11.3 XRF Analysis of Clay with Different Bu16^{+} Loadings

X-ray fluorescence elemental analysis was carried out on Bu16^{+} at loadings of 0.25 to 2.0 x CEC on Na^{+} Cloisite (Table 4–23) to give an indication of the extent of exchange onto Na^{+} Cloisite as the loading increased. Data for Na^{+} Cloisite has been included in the table for comparison.

Table 4–23 XRF Elemental Analysis of Bu16-MMT at 0.25 to 2.0 x CEC of Na^{+} Cloisite

	0.25 (%)	0.5 (%)	1.0 (%)	1.5 (%)	2.0 (%)	Na^{+} Cloisite (%)
MgO	2.27	2.23	2.19	2.08	2.08	2.3
Na_2O	2.15	1.03	0.12	0.07	0.07	4.3
Al_2O_3	22.92	22.90	22.62	22.01	21.97	22.6
SiO_2	65.73	65.6	64.8	63.2	63.1	65.1
P_2O_5	1.6	3.1	5.3	7.9	8.1	0.01
SO_3	0.2	0.01	-0.01	-0.10	-0.08	0.7
K_2O	0.06	0.05	0.04	0.05	0.03	0.1
CaO	0.3	0.3	0.3	0.2	0.2	0.2
TiO_2	0.1	0.1	0.1	0.1	0.1	0.1
Fe_2O_3	4.6	4.7	4.6	4.4	4.4	4.7

The data in Table 4–23 indicated that as the loading of Bu16^{+} onto Na^{+} Cloisite increased from 0.25 to 2.0 x CEC of Na^{+} Cloisite, the wt% of Na_2O decreased and the wt% P_2O_5 increased significantly. The large decrease in Na_2O between Na^{+} Cloisite (4.3 %) and Bu16^{+} at 0.25 x CEC, is due to excess Na^{+} on Na^{+} Cloisite, which was removed during the washing process. As was expected Na^{+} Cloisite contained more Na_2O than Bu16-MMT and very little P_2O_5. However, the wt% of P_2O_5 did not increase proportionally to the amount of Bu16^{+} offered. Between 1.0 and 2.0 x CEC the wt% of P_2O_5 increased by only 65 %.

4.12 TG-MS Analysis of Bu16$^+$ Exchanged Na$^+$ Cloisite

Noticeable differences in the decomposition peak position of T_{max} (A-1) between different batches of Bu16$^+$ exchanged Na$^+$ Cloisite were found (Figure 4–19). Therefore to provide a better understanding of what was being released under T_{max} (A-1), TG-MS analysis was carried out on batch 2 and batch 5. These batches produced composites which displayed 'good' (batch 2) and 'bad' (batch 5) fire retardant properties, and so the decomposition ions were examined to confirm whether the species being released would render the material more or less fire retardant.

4.12.1 TG-MS Analysis of a Good vs. Bad Batch
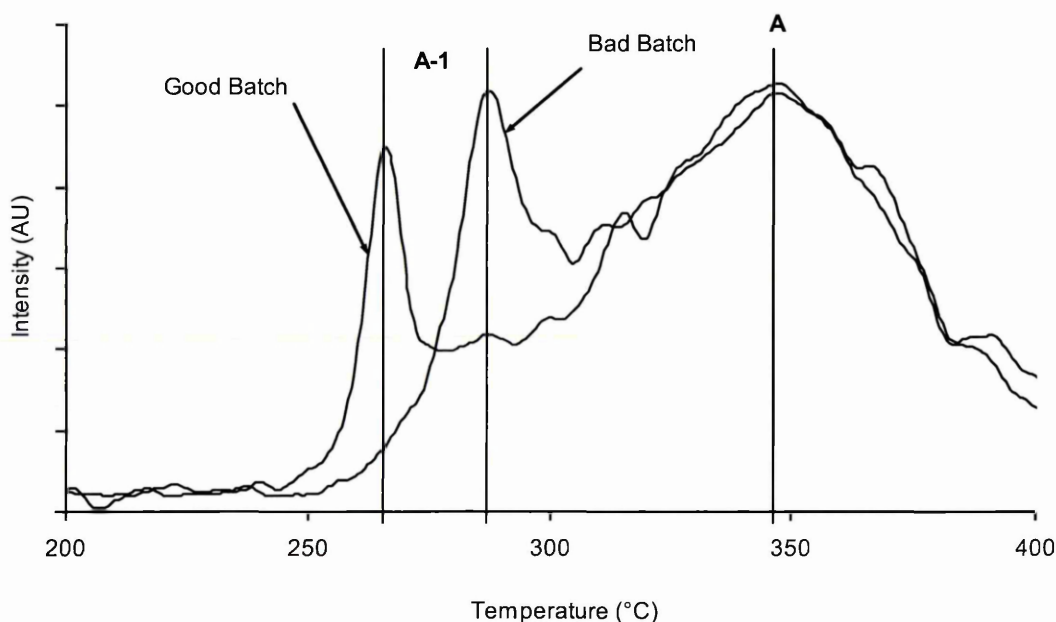
Figure 4–24 DTG (Air) of Good (batch 2) and Bad (batch 5) Bu16-MMT batches using Netzsch TG-MS Instrument

The DTG traces presented in Figure 4–24, obtained using the Netzsch TG-MS instrument, displayed T_{max} (A) at 347 °C in both the 'good' (batch 2) and 'bad' (batch 5) Bu16-MMT batches, however T_{max} (A-1) occurred at 266 °C in the 'good' and 287 °C in the 'bad' Bu16-MMT batch. This trend was also observed when batch 2 and batch 5 were run on the Mettler system. Consequently, the ions that were desorbed under the temperature region of interest (250 to 450 °C) were analysed for both samples.

After surveying the decomposition ions from several Bu16-MMT batches, three decomposition ions were chosen, m/z = 50, which is present in all Bu16-MMT samples and two strong Bu16-MMT decomposition ions m/z = 57 and 71. It is still unclear what m/z = 50 represents, it has been suggested to come from methyl chloride, however the mass spectrum did not contain peaks at m/z = 35 or 37, which are characteristic of the isotopes of chlorine and so it is still unclear what m/z = 50 represents. M/z = 50 was always present in the presence of Bu16-MMT. The decomposition ions m/z = 57 and 71 are thought to represent $-(CH_2)_3CH_3$ and $-(CH_2)_4CH_3$, respectively. T_{max} (A-1) always contained ions with m/z = 50, 57 and 71, which were independent on the peak position, therefore it can be confirmed that T_{max} (A-1) came from the organocation and was not due to water evolution as previously speculated. Figure 4–25 displays the MS data for 'good' (batch 2) and 'bad' (batch 5) Bu16-MMT batches. It was observed that the ions evolved with two temperature maxima, T_{max} (A-1) and T_{max} (A), T_{max} (A) occurred at the same temperature in both samples, however T_{max} (A-1) desorbed at a higher temperature in the 'bad' Bu16-MMT batch. It was observed that the peak under T_{max} (A-1) always desorbed 30-40 °C higher in the MS as compared to the DTG.

Differences in the intensity of the ions evolved were observed between the 'good' and 'bad' batches, with the 'good' batch being approximately one third more intense as the 'bad' batch. Therefore, TG-MS could be used as an early predictor of fire performance, in that the difference between 'good' and 'bad' fire performance could be related to the thermal desorption temperature of the peak under T_{max} (A-1) and the amount of Bu16$^+$ that was exchanged onto Na$^+$ Cloisite, which is proportional to the intensity of the ions evolved. However, at this stage it is still unclear which of these factors are the major contributors to the fire performance of the Bu16-MMT composites, or whether good fire performance is related to some other as yet unidentified contributing factor. After increasing the loading of Bu16$^+$ onto Na$^+$ Cloisite (section 4.11) and comparing the values for T_{max} (A-1), it indicated that batch 2 was exchanged at between 1.0 and 1.5 x CEC of Na$^+$ Cloisite, however batch 5 was exchanged at 1.0 x CEC of Na$^+$ Cloisite.
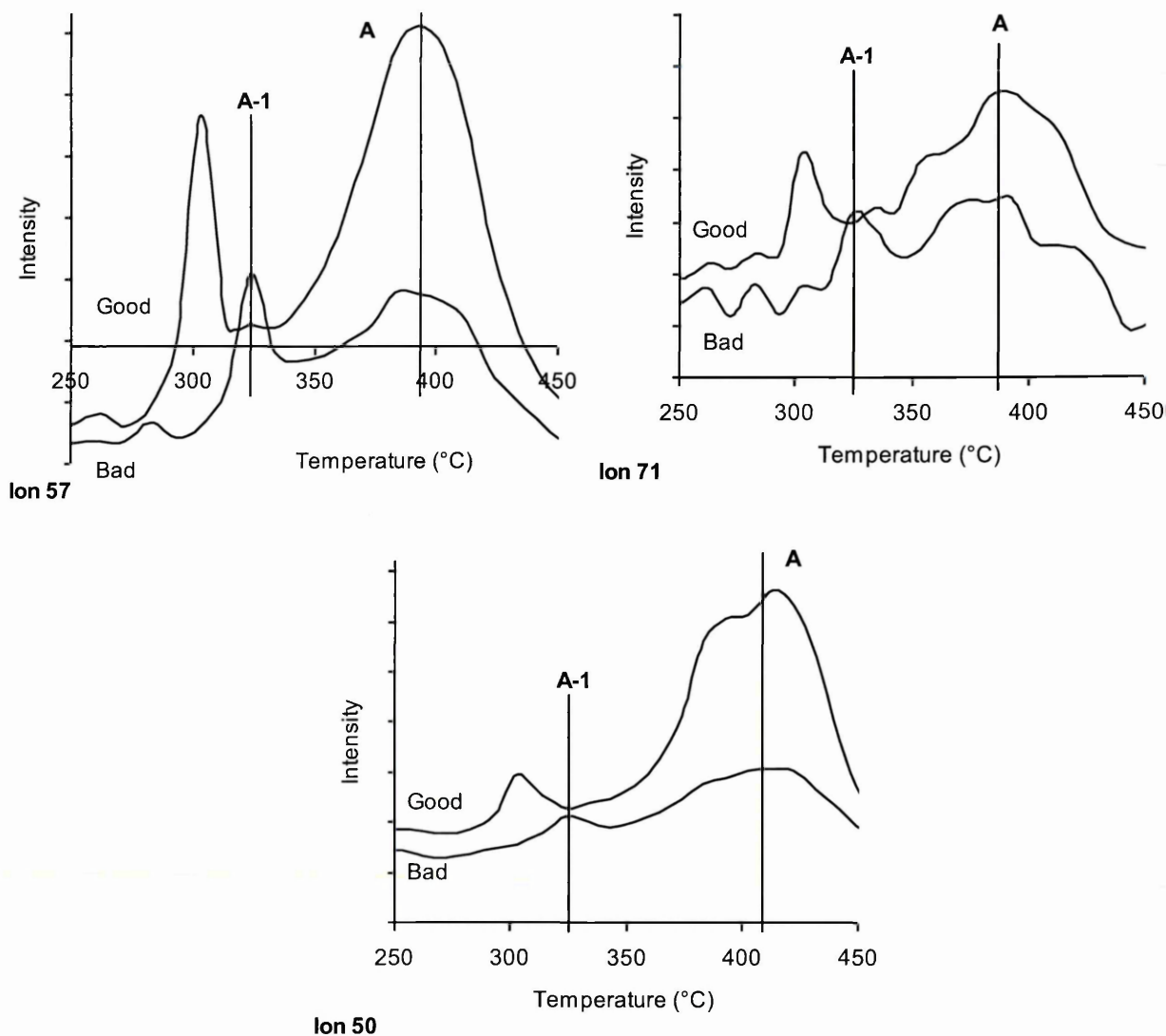
Figure 4–25 Ion comparisons for a Good (Batch 2) and Bad (Batch 5) Bu16-MMT Batch

4.13 Bu16-MMT Washed in 80:20 EtOH:H₂O

The organoclays used were layered silicates, which had been made organophilic by an ion exchange process. Due to natural defects/charge heterogeneity on the clay plates, some of the clay plates may not have been fully ion exchanged. Therefore, some of the organic treatment remained associated with the clay after the ion exchange process, but was not ionically bound to the surface, only physisorbed to the surface. This extra surfactant may possibly be removed by solvent washes [4-26], however, commercial organoclays are usually only washed with water. Therefore, the extra surfactant associated with these organoclays will be carried along into the preparation of a polymer nanocomposite. When the organoclay is mixed with a polymer, this surfactant may serve a beneficial role, in that it assists the dispersion of the clay plates into the

167

polymer matrix. However, the surfactant may also affect the polymer nanocomposite properties negatively by plasticizing the polymer or inhibiting crystal growth in crystalline polymers [4-27]. Furthermore, the excess organic treatment may remove some of the flammability benefits obtained from nanocomposites, by causing early ignition of the nanocomposite.

Therefore, Bu16-MMT prepared at 1.5 and 2.0 x CEC of Na^+ Cloisite, which were found to contain extra surfactant, were washed with a mixture of 80:20 $EtOH:H_2O$, to evaluate any detrimental effects due to this extra surfactant on organoclay dispersion and flammability properties of the composites prepared using the organoclay. Bu16-MMT samples (~1g) were dispersed in 80:20 $EtOH:H_2O$ (~20ml) and mixed overnight. They were then centrifuged for 1 hour at 16, 500 rpm and dried in an oven set at 50 °C overnight. The organoclays were then ground manually with a pestle and mortar and characterised using XRD and TGA.

4.13.1 XRD Analysis of Washed Bu16-MMT
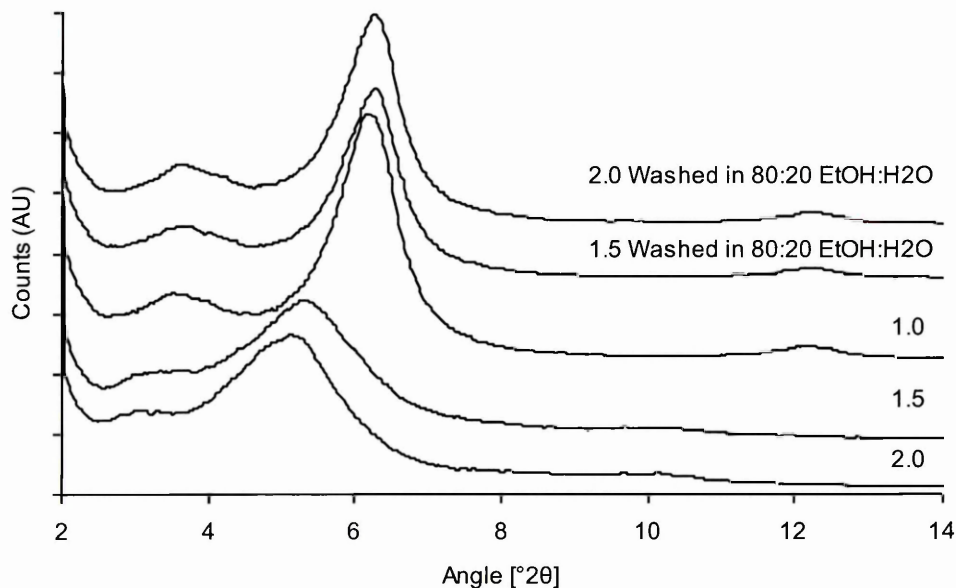
Figure 4–26 XRD traces (Cr Tube) for Bu16-MMT prepared at 1.5 and 2.0 x CEC of Na^+ Cloisite, washed in 80:20 $EtOH:H_2O$.

168

The XRD traces presented in Figure 4–26 indicate that after Bu16-MMT had been washed with ethanol and water, the excess surfactant was removed, and the d-spacing of organoclays originally exchanged at 1.5 and 2.0 x CEC of Na^+ Cloisite became comparable to the d-spacing of $Bu16^+$ prepared at 1.0 x CEC of Na^+ Cloisite (Table 4–25).

4.13.2 TGA Analysis of Washed Bu16-MMT
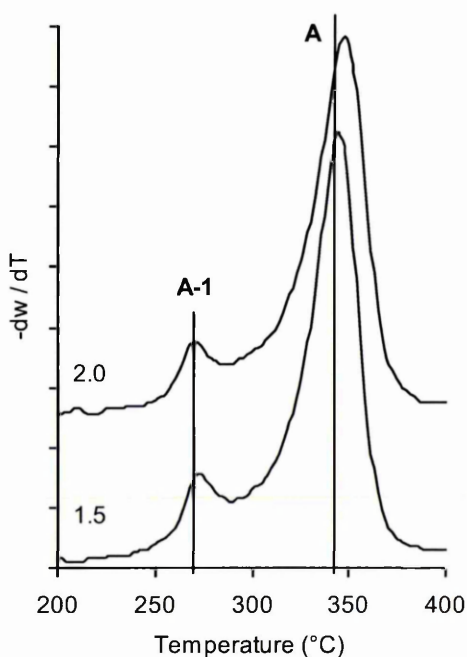
Figure 4–27 DTG traces (Air) $Bu16^+$ prepared at 1.5 and 2.0 x CEC of Na^+ Cloisite – Traces are offset for clarity
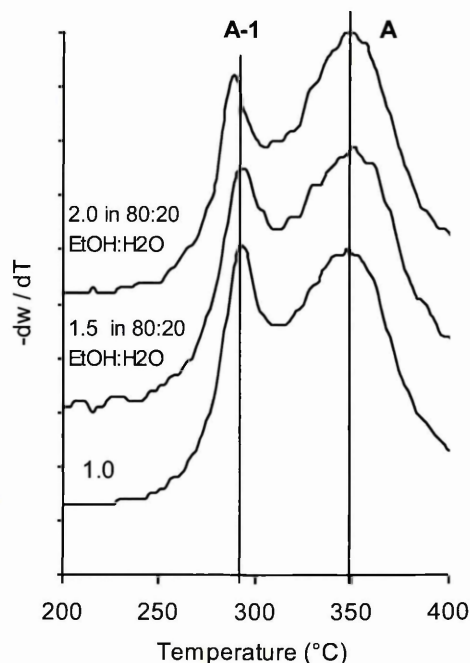
Figure 4–28 DTG traces (Air) $Bu16^+$ prepared at 1.0, 1.5 and 2.0 x CEC of Na^+ Cloisite (1.5 and 2.0 washed in 80:20 EtOH:$H_2$0) – Traces are offset for clarity

The DTG traces presented in Figure 4–27 and Figure 4–28 indicated that after washing with ethanol and water the thermal degradation pattern of Bu16-MMT prepared at 1.5 and 2.0 x CEC of Na^+ Cloisite (Figure 4–27) became very similar to that of Bu16 prepared at 1.0 x CEC of Na^+ Cloisite (Figure 4–28). T_{max} (A) remained the same at approximately 348 °C, however the value of T_{max} (A-1) increased from 273 to 290/292 °C after washing with ethanol and water (Table 4–24). Therefore incorporation of this washing step into the cation exchange process would ensure that excess surfactant was removed from the organoclays, which could reduce plasticization of the polymer or prevent early ignition of the nanocomposite.

169

The data presented in Table 4–24 demonstrates that after washing with 80:20 EtOH:H_2O the height of peak A in relation to peak A-1, for Bu16-MMT prepared at 1.5 and 2.0 x CEC, was comparable to that of Bu16-MMT prepared at 1.0 x CEC (without washing in 80:20 EtOH:H_2O). The separation distance between peaks A and A-1 were also very similar. Therefore, upon preparation of composites containing these washed Bu16-MMTs, it was expected that the washed Bu16-MMT would display a similar thermal degradation pathway, and also behave similarly in the UL-94 vertical burning test.

Table 4–24 Differences in peak positions and heights for Bu16$^+$ at 1.0, 1.5 and 2.0 x CEC of Na$^+$ Cloisite, plus Bu16$^+$ at 1.5 and 2.0 x CEC of Na$^+$ Cloisite, washed in 80:20 EtOH:H_2O

	T_{max} A (°C)	T_{max} A-1 (°C)	Height A : A-1	Separation Between A and A-1 (°C)
1.0	348	292	1:1	56
1.5	344	273	1:0.2	71
2.0	348	273	1:0.2	75
1.5 Washed in 80:20 EtOH:H_2O	348	292	1:0.9	56
2.0 Washed in 80:20 EtOH:H_2O	348	290	1:0.8	58

4.14 Nanocomposites Containing Bu16-MMT Prepared at 1.5 and 2.0 x CEC and washed in 80:20 EtOH:H_2O

To give an indication of whether excess surfactant affected the fire retardant properties of the resulting polymer nanocomposites, Bu16-MMT exchanged at 1.5 and 2.0 x CEC of Na$^+$ Cloisite after washing with 80:20 EtOH:H_2O, was dispersed in DMMP and then mixed with Crystic 189LV at 2000 rpm for 30 minutes. Nanocomposites were made as a comparison using Bu16-MMT prepared at 1.5 and 2.0 x CEC of Na$^+$ Cloisite, which had not been washed. All samples were postcured in the usual way, characterised using XRD and TGA and then subjected to the in-house version of the UL94 Vertical Burning Test (Table 4–26) (where possible V-ratings have been applied).

4.14.1 XRD Analysis of Nanocomposites Containing Washed Bu16 Clays
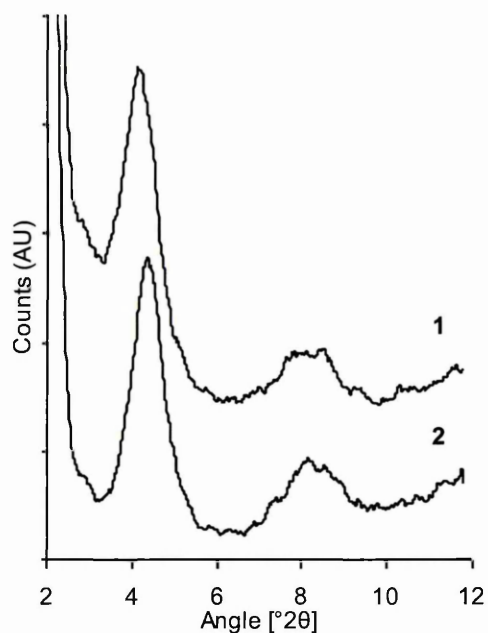
Figure 4–29 XRD traces (Cr tube) for Crystic 189LV and (1) 5 wt% Bu16-MMT prepared at 1.5 x CEC, 10D, (2) 5 wt% Bu16-MMT prepared at 2.0 x CEC, 10D – Traces are offset for clarity.
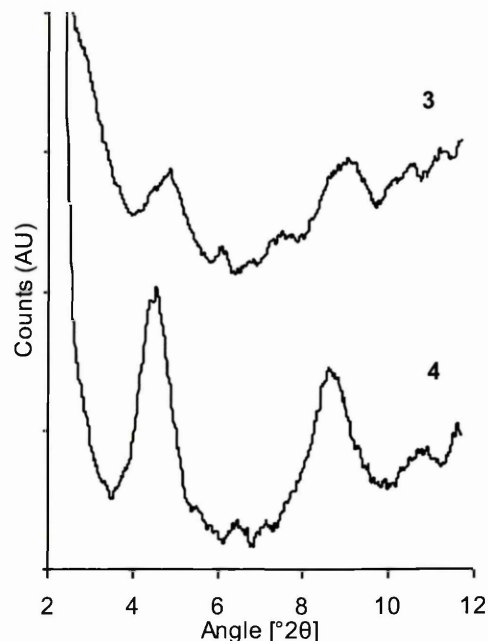
Figure 4–30 XRD traces (Cr tube) for Crystic 189LV and (3) 5 wt% Bu16-MMT prepared at 1.5 x CEC (washed in 80:20 EtOH:H$_2$O), 10D and (4) 5 wt% Bu16-MMT prepared at 2.0 x CEC (washed in 80:20 EtOH:H$_2$O), 10D – Traces are offset for clarity.

The XRD traces presented in Figure 4–29 and Figure 4–30 display nanocomposites of Crystic 189LV prepared using (1) 5 wt% Bu16-MMT at 1.5 x CEC, 10D, (2) 5 wt% Bu16-MMT at 2.0 x CEC, 10D, (3) 5 wt% Bu16-MMT at 1.5 x CEC (washed in 80:20 EtOH:H$_2$O), 10D and (4) 5 wt% Bu16-MMT at 2.0 x CEC (washed in 80:20 EtOH:H$_2$O), 10D. The XRD traces representing nanocomposites (1) and (2) displayed an intercalated/aggregated structure, confirmed through the presence of intense d$_{001}$ and d$_{002}$ peaks. However, after washing with methanol and water the XRD traces representing nanocomposites (3) and (4) also displayed intercalated nanocomposites, but the d$_{001}$ peaks were less intense, therefore indicating that there was less clay in the beam or that it was an intercalated/dispersed structure.

Table 4–25 displays the d$_{001}$ values obtained for Crystic 189LV composites prepared using 5 wt% Bu16-MMT prepared at 1.5 and 2.0 x CEC (washed and un-washed), which were pre-dispersed in 10 wt% DMMP.

Table 4–25 Comparison of d_{001} spacings for nanocomposites prepared using Crystic 189LV and 5 wt% Bu16-MMT prepared at 1.5 and 2.0 x CEC (washed and un-washed), pre-dispersed in 10D

	d_{001} Organoclay (Å)	d_{001} Nanocomposite (Å)
Original Bu16-MMT at 1.0 x CEC	20.8	27.1
(1) Bu16-MMT at 1.5 x CEC	24.3	31.1
(2) Bu16-MMT at 2.0 x CEC	24.3	30.0
(3) Bu16-MMT at 1.5 x CEC, Washed EtOH:H₂O	20.8	26.7
(4) Bu16-MMT at 2.0 x CEC, Washed EtOH:H₂O	20.8	28.5

The d_{001} values in Table 4–25 indicate that when Bu16-MMT was washed with 80:20 EtOH:H$_2$O, the layer spacing was comparable to that of Bu16-MMT (20.8 Å) prepared at 1.0 x CEC of Na$^+$ Cloisite. This was also the case when nanocomposites of Bu16-MMT were prepared at 1.5 and 2.0 x CEC of Na$^+$ Cloisite (washed in 80:20 EtOH:H$_2$O). Therefore, it could be anticipated that the fire retardant properties would also be similar to the original Bu16-MMT nanocomposites.

4.14.2 TGA Analysis of Nanocomposites Containing Washed Bu16 Clays
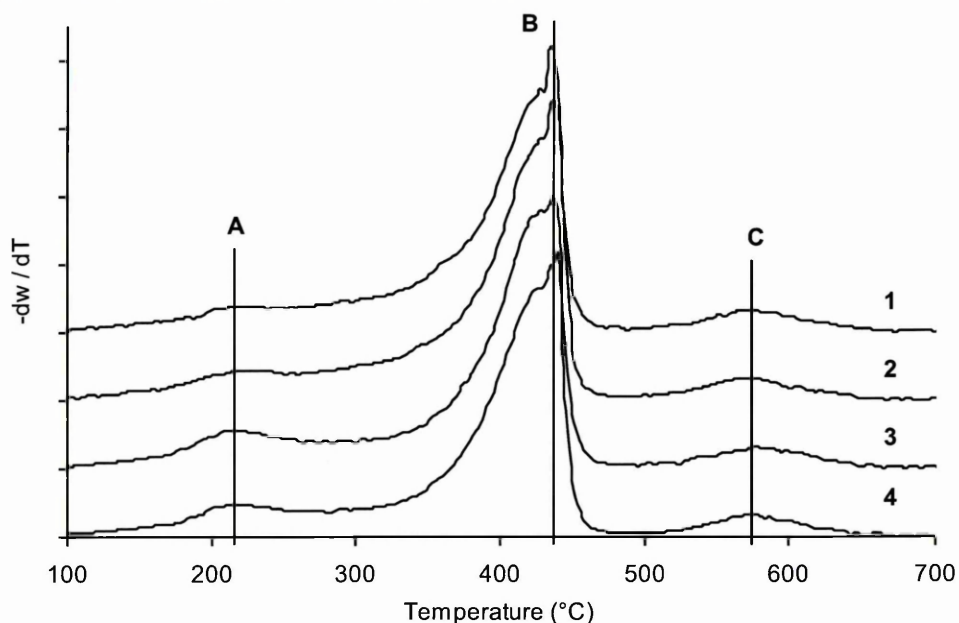
Figure 4–31 DTG traces (Air) for Crystic 189LV nanocomposites prepared using (1) 5 wt% Bu16-MMT prepared at 1.5 x CEC, 10D, (2) 5 wt% Bu16-MMT prepared at 2.0 x CEC, 10D, (3) 5 wt% Bu16-MMT prepared at 1.5 x CEC (washed in 80:20 EtOH:H₂O), 10D and (4) 5 wt% Bu16-MMT prepared at 2.0 x CEC (washed in 80:20 EtOH:H₂O), 10D – Traces are offset for clarity.

172

The DTG traces presented in Figure 4–31 display three thermal decomposition maxima (A, B and C) occurring over three stages. For all nanocomposites displayed in Figure 4–31, T_{max} (A) (evolution of DMMP) occurred during stage 1 at 220 °C, T_{max} (B) (decomposition of resin) occurred during stage 2 at 437 °C and T_{max} (C) (decomposition of carbonaceous char) occurred during stage 3 at 580 °C. Therefore, the removal of excess surfactant did not affect the thermal decomposition of the nanocomposites, however, the XRD traces presented in Figure 4–30 indicated that it did result in a less aggregated nanocomposite due to the loss of intensity of the d_{001} peaks.

4.14.3 UL94 Vertical Burning Test

Nanocomposites prepared using Crystic 189LV, washed and unwashed Bu16-MMT and 10D were subjected to the in house version of the UL94 vertical burning test. The results are presented in Table 4–26. Bu16-MMT at 1.0 x CEC of Na^+ Cloisite (batch 4, mix 1) from Table 4–16, has been displayed as a comparison.

Table 4–26 UL94 Vertical Burning Test Results for washed and un-washed organoclays

	Burn 1	Burn 2	Burn 3	Burn 4	Total	UL94-V Rating
Bu16-MMT at 1.0 x CEC	1,8	3, 7	2, 5	3, 5	2.3, 6.3	V-0
(1) Bu16-MMT at 1.5 x CEC	5, Ex	3, Ex	4, Ex	20, Ex	-	Fail
(2) Bu16-MMT at 2.0 x CEC	5, Ex	6, Ex	3, Ex	15, Ex	-	Fail
(3) Bu16-MMT at 1.5 x CEC, Washed EtOH:H$_2$O	Cracked, Ex	30, Ex	8, Ex		-	Fail
(4) Bu16-MMT at 2.0 x CEC, Washed EtOH:H$_2$O	Cracked, Ex	Cracked, Ex	17, Ex		-	Fail

(Ex = Extinguished Manually after 60 seconds)

From the XRD results it was expected that the vertical burning test results might be similar to those for Bu16-MMT prepared at 1.0 x CEC, as similar d-spacings were observed. The DTG results for the nanocomposites indicated a shift to a higher thermal decomposition temperature for samples containing Bu16-MMT at 1.5 and 2.0 x CEC of Na^+ Cloisite, T_{max} (A), (B) and (C) increased by 5, 12, and 15 °C, respectively.

However, poor dispersion of Bu16-MMT into the unsaturated polyester as the loading of Bu16$^+$ increased from 1.0 to 1.5 and 2.0 x CEC of Na$^+$ Cloisite led to an increased incidence of cracking after the first flaming, and consequently the samples had to be extinguished manually (Table 4–26).

A number of papers have reported on the influence of cationic surfactant on the thermal stability of organoclays. He *et. al.* [4-28] reported that there are three different molecular environments for surfactants within organoclays: (1) surface cations intercalated into the clay layers through cation exchange and bound to surface sites via electrostatic interaction, (2) surfactant physically adsorbed on the external surface of clay and (3) surfactant-anion ion pairs located within the clay gallery. The decomposition temperature for the surfactants with different molecular environments is different from each other. An increase in the concentration of surfactant physically adsorbed to the external-surface of an organoclay decreases the thermal stability of the organoclay and hence the resultant nanocomposite. This decrease was observed in both the Bu16$^+$ organoclays exchanged at 1.5 and 2.0 x CEC and the resultant nanocomposites, with a decrease of 7 °C for the organoclays and approximately 15 °C for the nanocomposites.

Xie *et. al.* [4-29] washed their alkyl quaternary ammonium modified MMTs with methanol and found that the organic content after washing corresponded to the CEC of the MMT. In this thesis after washing, the organic content of the samples corresponded closely to the organic content in the 1.0 x CEC samples, as displayed in Table 4–27.

They compared the d-spacing and total organic content and concluded that the majority of the excess surfactant is contained within the gallery and not physisorbed to the exterior of the crystallites. They concluded that MMT that has been exchanged beyond the CEC did not have a substantially greater fraction of surfactant residing outside the gallery than MMTs exchanged at their CEC equivalent. The d-spacing for Bu16-MMT increased significantly from 20.8 Å at 1.0 x CEC to 24.3 Å at 2.0 x CEC, above that of Bu16-MMT exchanged at the CEC equivalent of Na$^+$ Cloisite and therefore, suggests that excess surfactant in these systems resided in the gallery. If this was not the situation then expansion of the d-spacing would not have been observed.

Table 4–27 Possible organic exchange against actual organic exchange for Bu16-MMT at 0.25 to 2.0 x CEC, plus 1.5 and 2.0 after washing

	0.25	0.5	1.0	1.5	2.0	1.5 Washed	2.0 Washed
Possible Organic Exchange (mg/ g)	98.8	197.5	394.9	592.5	789.9	-	-
Actual Organic Exchanged (mg/ g)	89	156	270	354	330.6	259.5	281.1
Percentage Utilised (%)	90	79	68	60	42	44	36
Percentage of 1 CEC covered (%)	23	40	68	90	84	66	71

* All exchange amounts are ± 5%

Xie *et. al.* [4-29] associated initial decomposition events based on TGA analysis with degradation of the excess surfactant above the CEC that resides exterior to the layers. Therefore removal of this surfactant by repeated washings and the corresponding reduction in the magnitude of the initial event would then imply that the intercalated surfactants are stabilized by confinement within the interlayer and degrade during the higher temperature events. However, further examination of their results indicated that this initial hypothesis was not correct. The results for Bu16-MMT at 1.5 and 2.0 x CEC support their hypothesis, given that after washing with 80:20 EtOH:H$_2$O the initial event occurring under T$_{max}$ (A-1) increased in temperature from 271 to 292 °C.

4.15 The Role of Dimethyl methylphosphonate (DMMP)

Work has been carried out to try and understand the role of DMMP in combination with organoclays both as intercalated powders and as components of nanocomposites prepared using Crystic 189LV. 1g of TP8- to TP16-MMT and Bu16-MMT were dispersed in DMMP and then dried in an oven at 80 °C overnight. Any differences in the thermal decomposition of the organoclays after dispersion in DMMP were analysed using TGA and TG-MS, the XRD traces for the organoclays and organoclays dispersed in DMMP are displayed in Figure 4–2 and Figure 4–10, respectively.

4.15.1 TGA Analysis of TP8- to Bu16-MMT, and TP8- to Bu16-MMT Dispersed in DMMP

Figure 4–32 to Figure 4–37 display the thermal decomposition of TP8- to TP16-MMT and Bu16-MMT using TGA under air. The DTG results demonstrated two thermal decomposition maxima T_{max} (A) and T_{max} (B) for all organoclays, however under these main peaks multiple shoulders occurred. The peak temperatures and positions are displayed in Table 4–28:

Table 4–28 Peak position temperatures for TP8$^+$ to TP16$^+$ and Bu16$^+$ Exchanged Na$^+$ Cloisite

	A-1 (°C)	A (°C)	A+1 (°C)	B-2 (°C)	B-1 (°C)	B (°C)	B+1 (°C)
TP8-MMT	358	393	418	-	598	635	-
TP10-MMT	341	381	-	-	-	635	-
TP12-MMT	-	334	-	-	-	603	635
TP14-MMT	-	346	-	-	-	612	635
TP16-MMT	-	365	-	523	572	661	-
Bu16-MMT	269	337	-	-	528	631	-

Bu16-MMT displayed a slightly different decomposition pathway than the other organoclays. Two main peaks were observed however, there was a clear sharp peak under T_{max} (A-1) that was not seen in the other organoclays.

Figure 4–38 to Figure 4–43 demonstrate the thermal decomposition of TP8- to TP16-MMT and Bu16-MMT dispersed in DMMP, using TGA under air. The DTG traces demonstrated three thermal decomposition maxima (A, B and C), however multiple shoulders occurred under T_{max} (C). The peak temperatures and positions are displayed in Table 4–29:

Table 4–29 Peak position temperatures for TP8$^+$ to TP16$^+$ and Bu16$^+$ exchanged Na$^+$ Cloisite, dispersed in DMMP

	A (°C)	B (°C)	C-1 (°C)	C (°C)	C+1 (°C)
TP8-MMT	122	372	-	628	-
TP10-MMT	131	327	-	603	-
TP12-MMT	124	325	512	612	659
TP14-MMT	122	325	512	612	652
TP16-MMT	150	351	505	584	640
Bu16-MMT	148	320	521	591	652

TP8-MMT and TP10-MMT dispersed in DMMP demonstrated the same decomposition pathway with three clear decomposition peaks, TP12-, TP14-, TP16- and Bu16-MMT all displayed three main decomposition peaks (A, B and C), plus two shoulders under T_{max} (C) (displayed as T_{max} (C-1) and T_{max} (C+1) in Figure 4–40 to Figure 4–43).

Three major peaks (A, B and C) were observed in the decomposition pathway of the organophosphonium clays dispersed in DMMP, compared to two major peaks (A and B) in the decomposition pathway of the organophosphonium clays. TP8- and TP10-MMT dispersed in DMMP displayed an intense peak exhibiting a T_{max} (A) at 122 and 131 °C, respectively, however this peak was absent in the organophosphonium clays. Peaks A and B in TP8-/TP10-MMT and B and C in TP8-/TP10-MMT dispersed in DMMP were of similar intensity in both samples, however the peaks evolved at a slightly higher temperature in TP8-/TP10-MMT. Several shoulders occurred under the main decomposition peaks A and B in TP$_n$-MMT, and peak C in TP$_n$-MMT dispersed in DMMP.

Upon dispersion of Bu16-MMT into DMMP, the characteristic peak A-1 was no longer visible and the decomposition profile resembled that of the TP$_n$-MMT series.
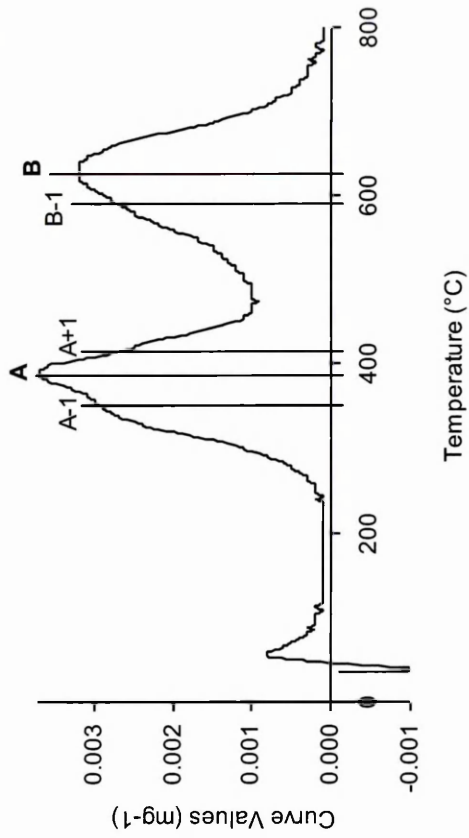
Figure 4–32 DTG traces (Air) TP8+ exchanged Na+ Cloisite
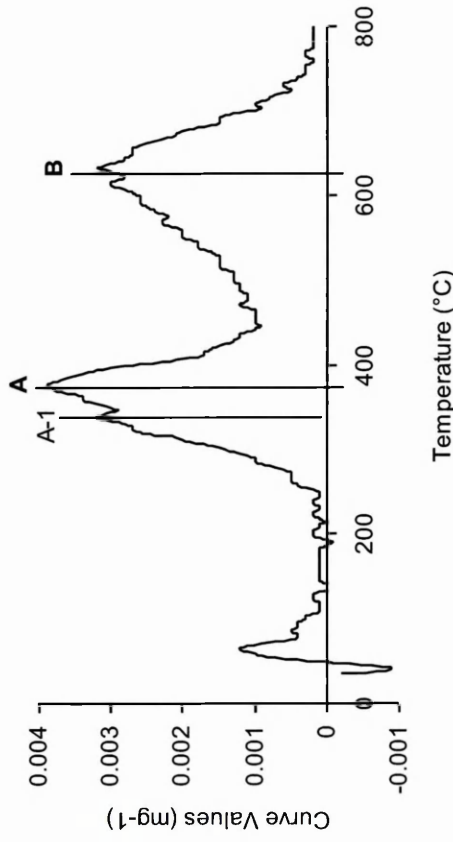
Figure 4–33 DTG traces (Air) TP10+ exchanged Na+ Cloisite
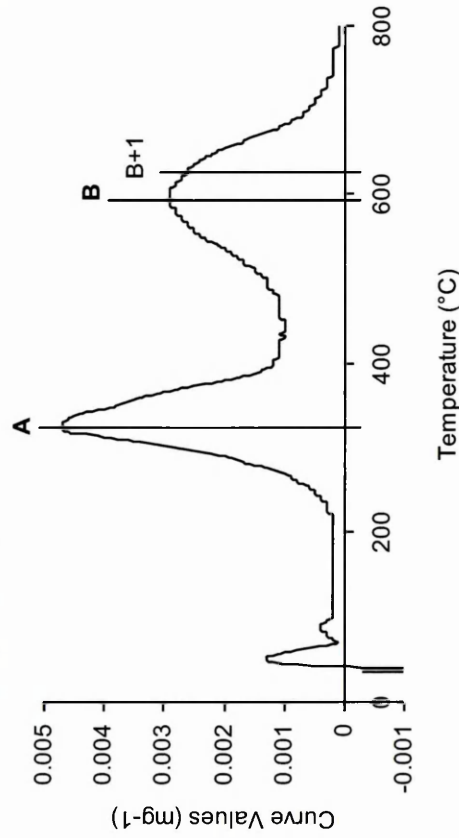
Figure 4–34 DTG traces (Air) TP12+ exchanged Na+ Cloisite
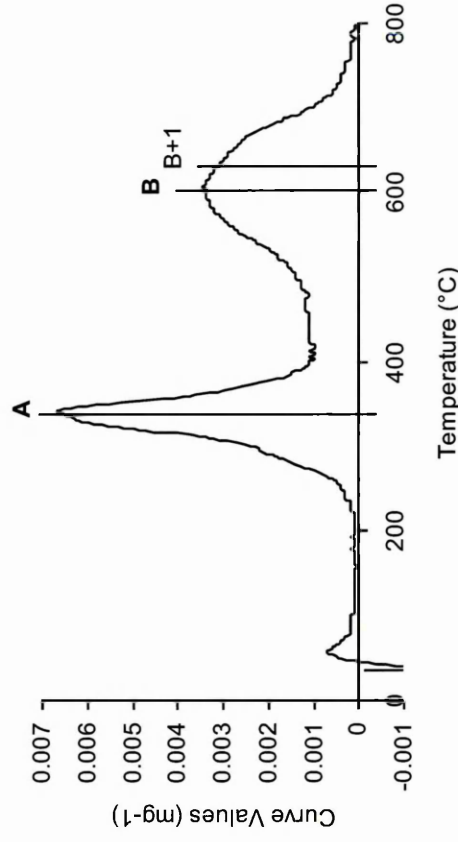
**Figure 4–35 DTG traces (Air) TP14+ exchanged Na+ Cloisite**
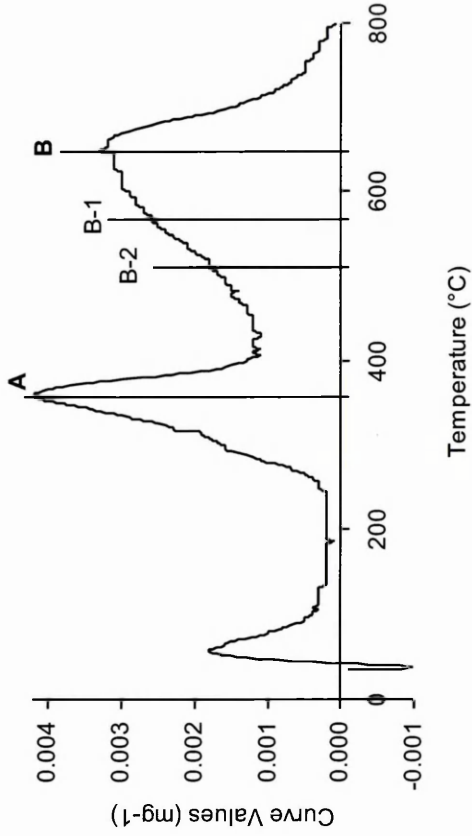
Figure 4–36 DTG traces (Air) TP16+ exchanged Na+ Cloisite
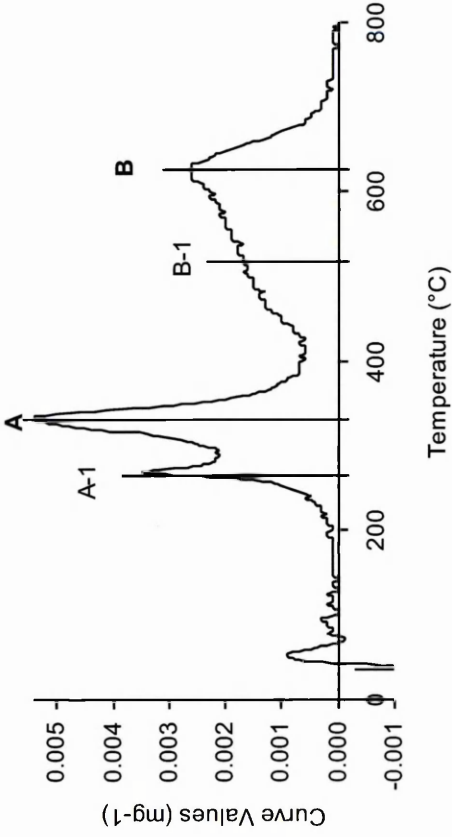
Figure 4–37 DTG traces (Air) Bu16+ exchanged Na+ Cloisite
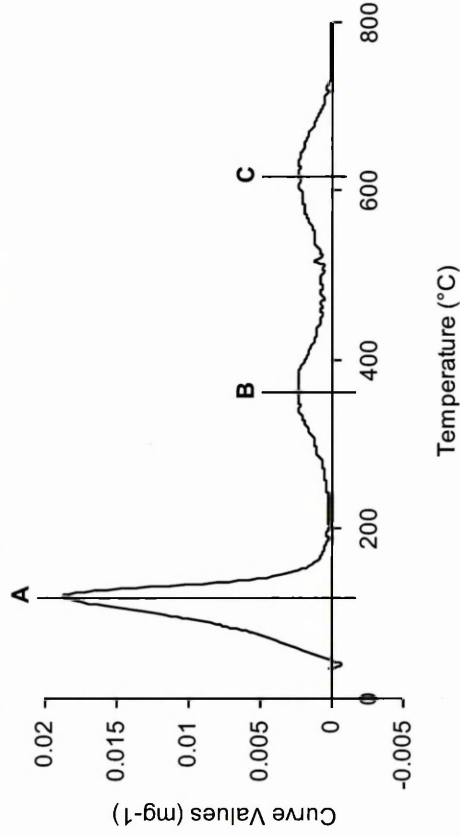
Figure 4–38 DTG traces (Air) TP8+ exchanged Na+ Cloisite - Dispersed in DMMP
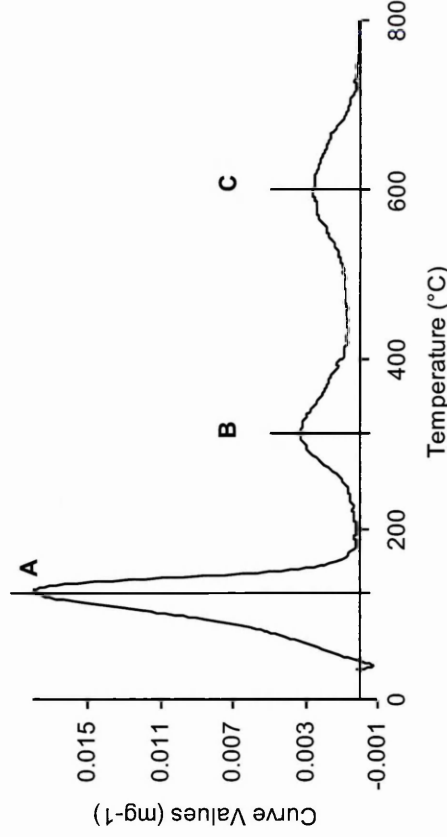
Figure 4–39 DTG traces (Air) TP10+ exchanged Na+ Cloisite - Dispersed in DMMP

179
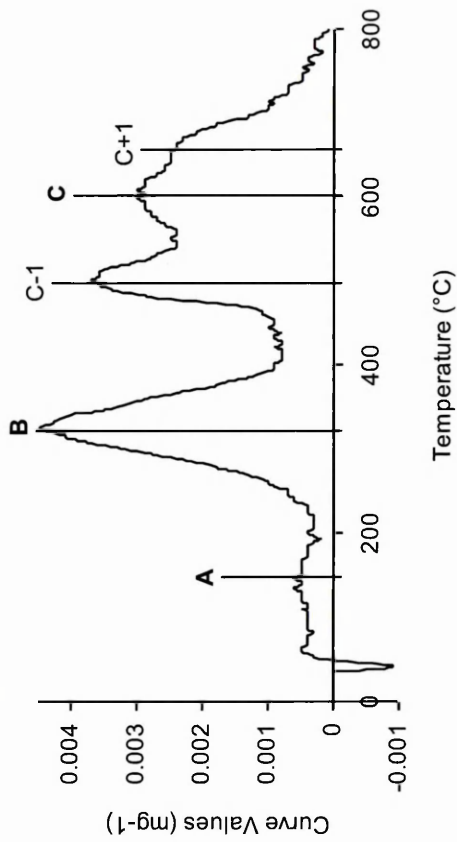
Figure 4-40 DTG traces (Air) TP12$^+$ exchanged Na$^+$ Cloisite - Dispersed in DMMP

Figure 4-41 DTG traces (Air) TP14$^+$ exchanged Na$^+$ Cloisite - Dispersed in DMMP
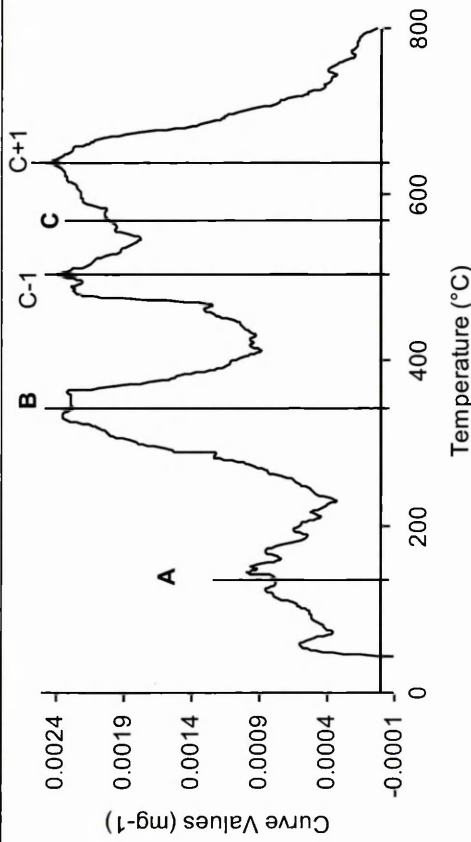
Figure 4-42 DTG traces (Air) TP16$^+$ exchanged Na$^+$ Cloisite - Dispersed in DMMP
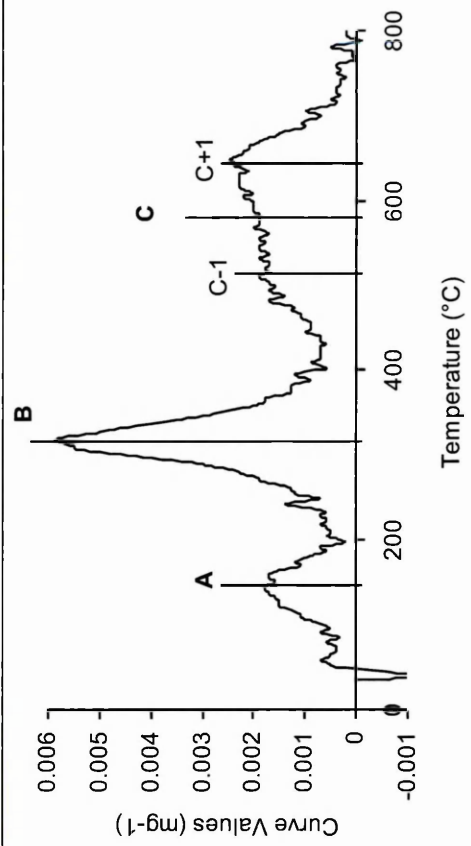
Figure 4-43 DTG traces (Air) Bu16$^+$ exchanged Na$^+$ Cloisite - Dispersed in DMMP

180

4.15.2 TG-MS Analysis of TP8- to Bu16-MMT Dispersed in DMMP
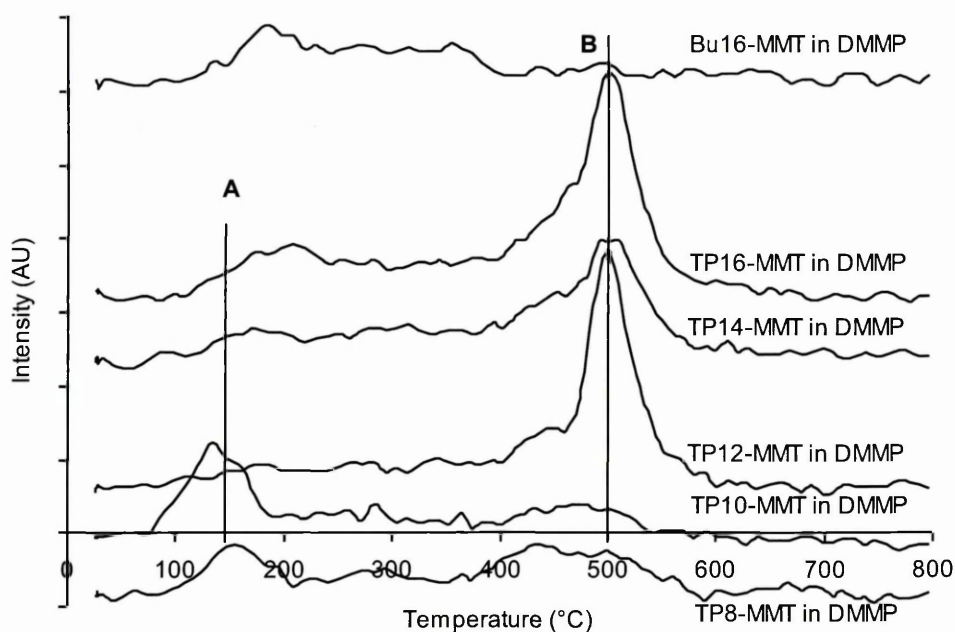
Figure 4–44 m/z = 79 (Air) – TP8- to TP16-MMT and Bu16-MMT dispersed in DMMP – MID – Traces are offset for clarity

Figure 4–44 displays m/z = 79 (main decomposition ion in DMMP) for TP8- to TP16-MMT and Bu16-MMT dispersed in DMMP. The traces indicated that TP8- and TP10-MMT contained significant amounts of absorbed DMMP (m/z = 79), which was desorbed under T_{max} (A) at 148 °C, at a lower temperature than the boiling point of DMMP (which boils at 181 °C), whereas TP12-, TP14- and TP16-MMT exhibited a higher desorption temperature for DMMP under T_{max} (B) at 501 °C. The intensity of the DMMP peak in the TP8- and TP10-MMT samples was reduced due to the vacuuming step employed in the Netzsch TG-MS instrument before the start of each run. Figure 4–55 displays the effect of the vacuuming step more clearly. Without the presence of DMMP the TP_n-MMT series did not exhibit m/z = 79.

Bu16-MMT did not exhibit a low temperature loss of DMMP. A tentative explanation for the ability of TP8- and TP10-MMT to accommodate adsorbed DMMP is that the C8 and C10 alkyl chains are relatively short and therefore there is some space between them in the interlayer for DMMP to occupy. However, when the chain length exceeded 12 carbons there was no longer any space available for DMMP to be adsorbed. Table 4–5 demonstrated that the Cloisite interlayer space was under exchanged with a maximum of 62.8 and 66.1 % exchanged occurring in TP8- and TP10-MMT, therefore there could

possibly be space for DMMP to reside within the interlayer, when the chain length was small (C_n =8 or 10). However, Table 4–11 indicated that sorption of DMMP did not result in an increase in the d-spacing of the organophosphonium clays.
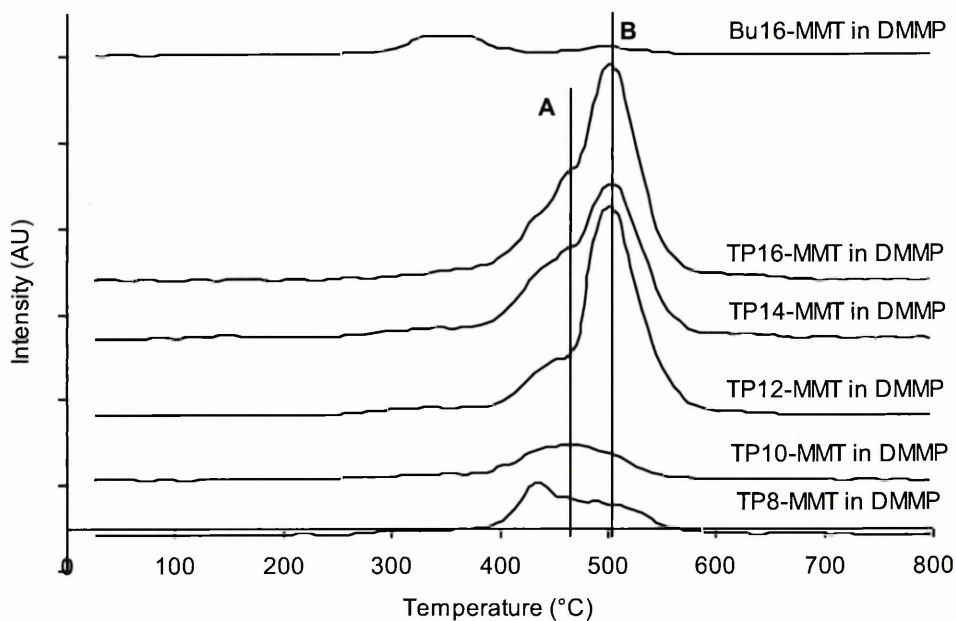
Figure 4–45 m/z = 50 (Air) – TP8- to TP16-MMT and Bu16-MMT dispersed in DMMP – MID – Traces are offset for clarity

Figure 4–45 displays the mass fragment m/z = 50 (present in all organoclays) and demonstrated the thermal desorption from TP8- and TP10-MMT under T_{max} (A) at 472 °C. TP12-, TP14- and TP16-MMT exhibited m/z = 50 thermally desorbing at a higher temperature under T_{max} (B) at 501 °C, TP12-, TP14- and TP16-MMT also displayed a shoulder under T_{max} (B) (T_{max} (A)) at 472 °C. Bu16-MMT dispersed in DMMP demonstrated m/z = 50 desorbing at two temperatures, the main desorption peak occurred at 354 °C and a smaller peak under T_{max} (B) occurred at 501 °C. The relative intensities for desorption of DMMP (m/z = 79) and m/z = 50 were very similar in TP8- and TP10-MMT, and also in TP12- and TP16-MMT.

In comparison Bu16-MMT (Figure 4–25) also exhibited the evolution of ion m/z = 50 at two temperatures, the main desorption peak occurred at 374 °C with a smaller peak at the lower temperature of 283 °C, the intensity of the Bu16-MMT ion was also found to be 40% higher than in the Bu16-MMT/DMMP sample. Neither m/z = 50 or m/z = 79 were desorbed at the same temperature as the main decomposition peak between 330 and 390 °C in the mettler traces, for TP8- to TP16-MMT.

4.16 Nanocomposites Containing Bu16-MMT and DMMP

4.16.1 TGA Analysis of Nanocomposites Containing Bu16-MMT and DMMP

The DTG results presented in Figure 4–46 display Crystic 189LV with increasing concentration of DMMP. It was revealed that as the wt% of DMMP increased from 0 to 10 wt% then the thermal desorption temperature decreased from 283 °C in the 2.5 wt% DMMP sample to 236 °C in the 10 wt% DMMP sample. However in samples containing Crystic 189LV, 5% Bu16-MMT and 0-10D, desorption of DMMP occurred at approximately 200 °C in all samples.
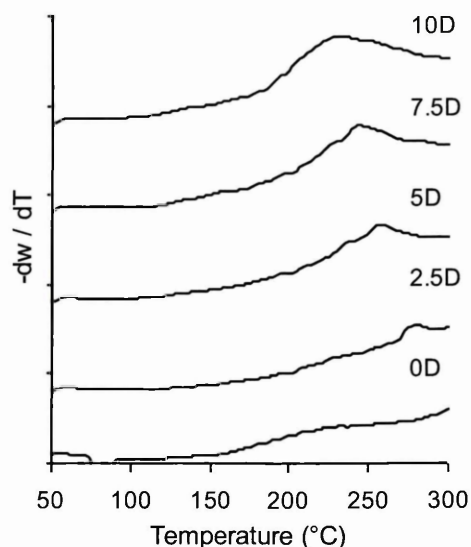
Figure 4–46 DTG (Air) Crystic 189LV containing 0-10 wt% DMMP – Traces are offset for Clarity

4.16.2 TG-MS Analysis of Nanocomposites Containing Bu16-MMT and DMMP

To give an indication of a possible decomposition mechanism with and without the presence of clay, nanocomposites of Crystic 189LV containing 5 wt% Bu16-MMT and 0-10 wt% DMMP (D), along with samples of Crystic 189LV and 0-10 wt% DMMP were analysed using TG-MS. The samples were analysed under an atmosphere of air and nitrogen to compare oxidative (air) and non-oxidative (nitrogen) decomposition. The samples were run in multi ion detection (MID) mode, which made it possible to select particular ions of interest, samples were analysed up to a temperature of 300 °C as this was the region where the main differences occurred.

TG-MS analysis of nanocomposites containing Crystic 189LV, and DMMP revealed that DMMP (m/z = 79) was desorbed at a maximum of 265 °C in samples prepared using 2.5 wt% DMMP under air (Figure 4–47) and nitrogen (Figure 4–48). However as the DMMP loading increased the thermal desorption temperature decreased, when DMMP loading reached 10 wt% the thermal desorption temperature decreased from 265 °C (2.5 wt% sample) to 235 °C. In the nanocomposites containing Bu16-MMT and

DMMP, TG-MS analysis revealed that DMMP was desorbed at 230 °C irrespective of the DMMP loading, under both air (Figure 4–49) and nitrogen (Figure 4–50). It was noted that the intensity of the signal increased as the DMMP loading increased.

A mass fragment of m/z = 50 was identified in the early stage decomposition of nanocomposites containing Crystic 189LV, Bu16-MMT and DMMP, however this fragment ion appeared to be absent in the absence of Bu16-MMT (Figure 4–51 and Figure 4–52). In the nanocomposite samples run under air (Figure 4–53) and nitrogen (Figure 4–54) the intensity of m/z = 50 increased as the DMMP loading increased. DMMP was thermally desorbed at a similar temperature of 225 °C in the 2.5-10 wt% samples, m/z = 50 appears to be thermally desorbed before m/z = 79.
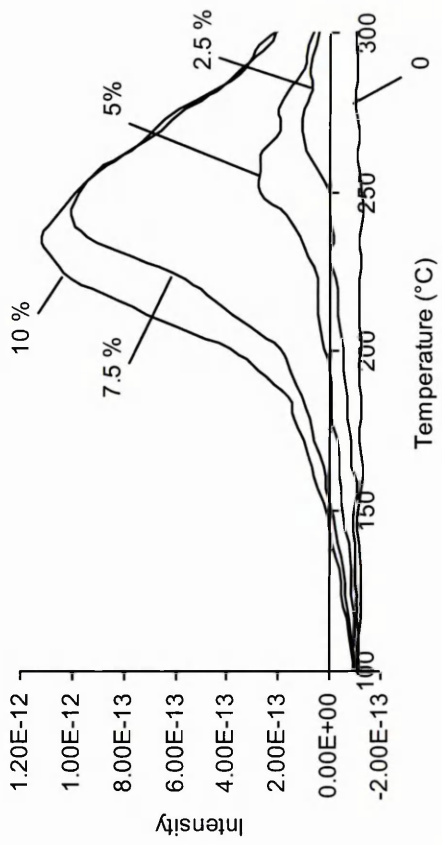
Figure 4–47 m/z = 79 – Crystic 189LV containing 0-10 wt% DMMP - MID - Air
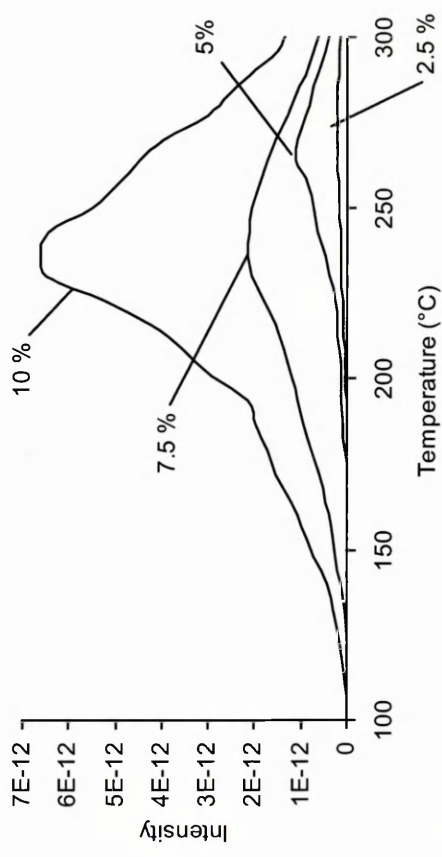
Figure 4–48 m/z = 79 - Crystic 189LV containing 2.5-10 wt% DMMP - MID - N2
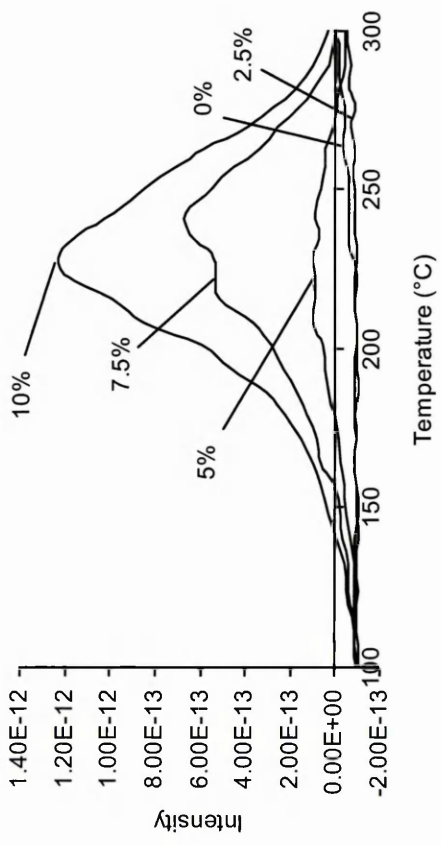
Figure 4–49 m/z = 79 - Crystic 189LV composites containing 5 wt% Bu16-MMT and 0-10 % DMMP - MID - Air
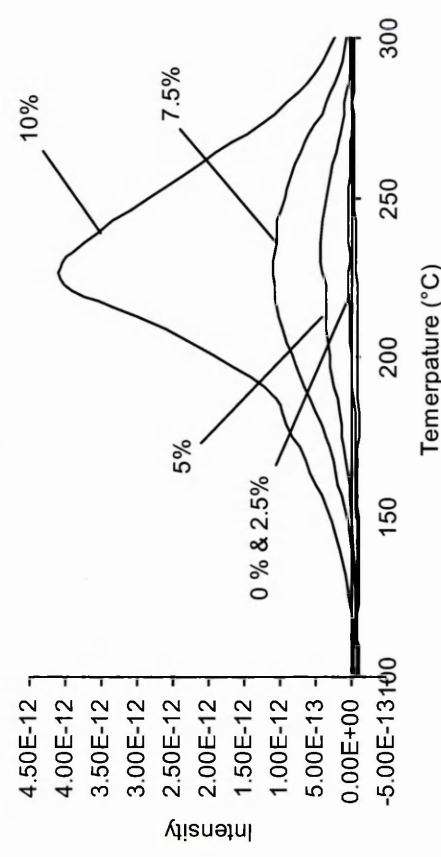
Figure 4–50 m/z = 79 - Crystic 189LV composites containing 5 wt% Bu16-MMT and 0-10 % DMMP - MID - N2
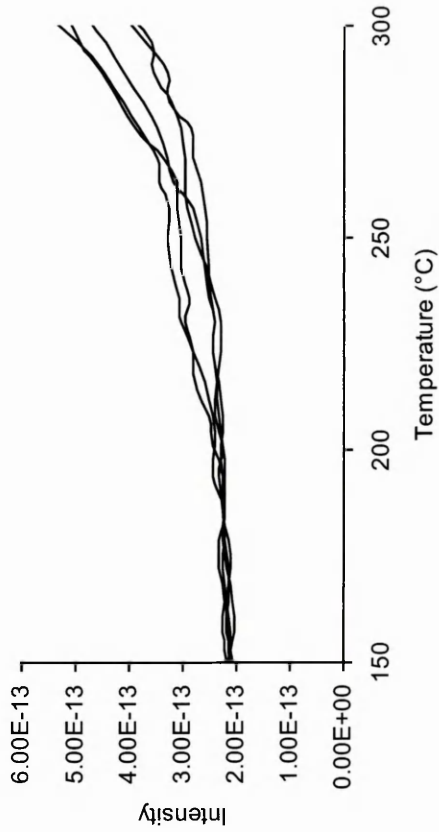
Figure 4–51 m/z = 50 –Crystic 189LV containing 0-10 wt% DMMP - MID - Air
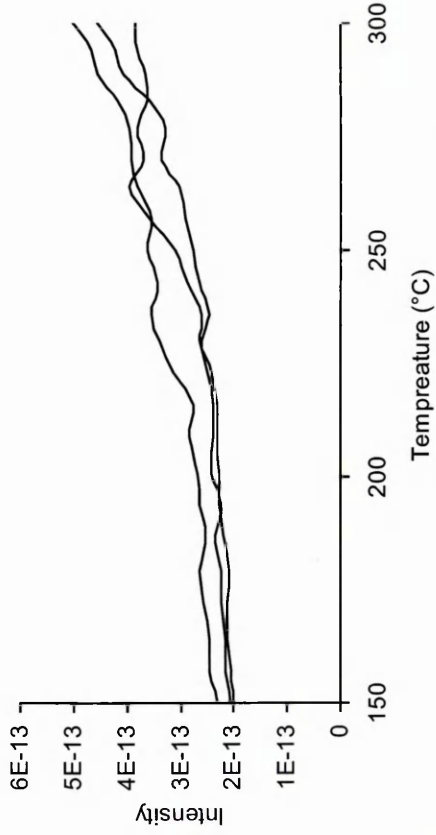
Figure 4–52 m/z = 50 - Crystic 189LV containing 2.5-7.5 wt% DMMP - MID - N2
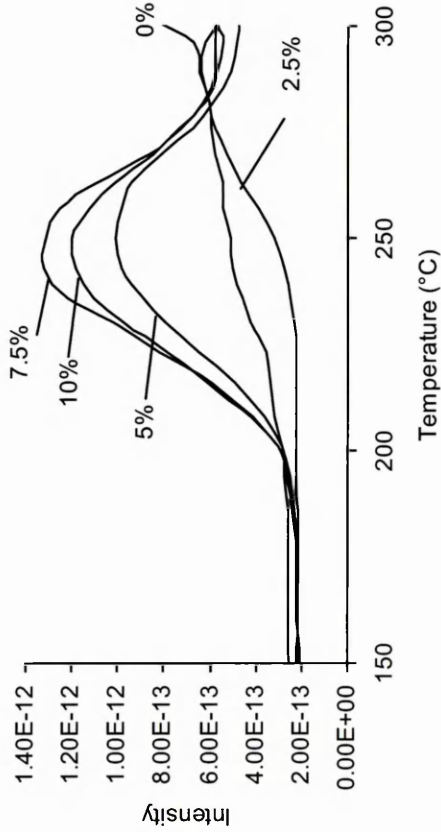
Figure 4–53 m/z = 50 - Crystic 189LV composites containing 5 wt% Bu16-MMT and 0-10 % DMMP - MID - Air
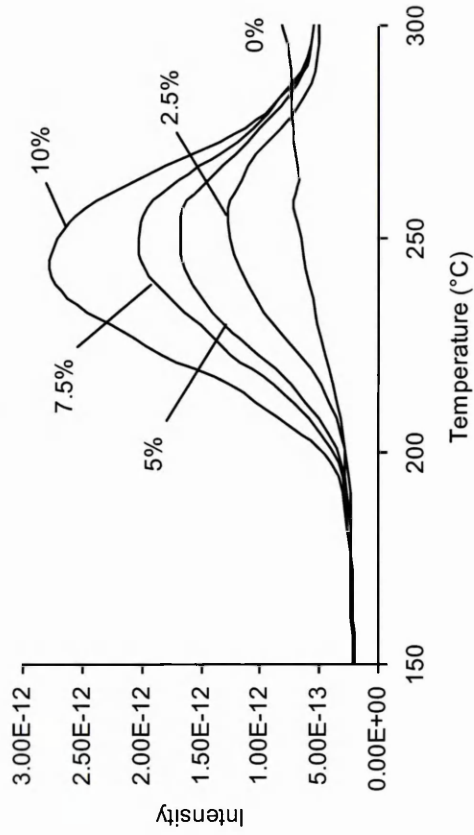
Figure 4–54 m/z = 50 – Crystic 189LV composites containing 5 wt% Bu16-MMT and 0-10 % DMMP - MID - N2

Comparison of the TGA and TG-MS results revealed that the thermal decomposition trend for nanocomposites containing Crystic 189LV and DMMP was observed in both techniques and can be attributed to the thermal desorption of DMMP (m/z = 79). It was also observed that the desorption temperature for m/z = 79 in nanocomposites containing Bu16-MMT remained at a constant temperature of 230 °C regardless of DMMP concentration or decomposition conditions (oxidative or non-oxidative).

Slight temperature differences between samples run using TGA and TG-MS can be attributed to vacuum effects within the TG-MS instrument. Prior to each run the sample chamber was evacuated of atmospheric gases and replaced with the gas of choice (air or N_2), the vacuum was operated at 10^{-2} mbar and so during the evacuation process it was possible that DMMP could have been pulled out of the sample and removed along with the atmospheric gases. Figure 4–55 displays temperature and intensity differences for m/z = 79 in an evacuated and non-evacuated sample of TP10-MMT dispersed in DMMP. A slight temperature decrease was observed in the evacuated sample and the intensity was approximately 6 times less intense compared to the non-evacuated sample.
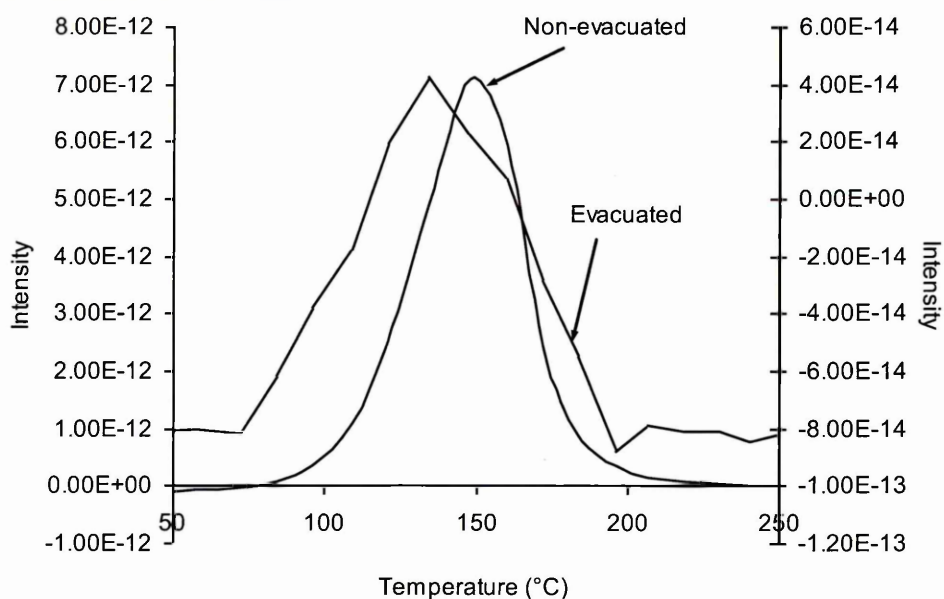
Figure 4–55 Intensity differences in m/z = 79 for TP10-MMT dispersed in DMMP, evacuated vs. non-evacuated sample

The decomposition product represented by m/z = 50 has been tentatively attributed to the evolution of methyl chloride, however this could not be proven using existing equipment. It was clear that m/z = 50 only appeared in the presence of clay and was desorbed after the thermal desorption of m/z = 79. The intensity of the m/z = 50 mass fragment increased as the DMMP loading increased even though this fragment did not appear in the mass spectrum of DMMP. The mass ion m/z = 50 was present in both Bu16-MMT and Bu16-MMT dispersed in DMMP, however m/z = 50 desorbed at the higher temperature of 400 °C in the Bu16-MMT sample compared to 350 °C in the Bu16-MMT dispersed in DMMP sample. The intensity of the Bu16-MMT sample dispersed in DMMP was approximately 40% higher than the intensity of the Bu16-MMT sample.

4.17 Surface Differences in Nanocomposites Containing of Bu16-MMT

The fire retardant properties of samples prepared using Crystic 189LV, Bu16-MMT and DMMP varied greatly, it was suggested that the area sampled could greatly affect the fire retardancy of the composites. The sample preparation procedure may influence platelet exfoliation and orientation [4-30], in such a way that the sample may be composed of several different regions (bulk, front and back) which may behave differently when under thermal degradation. Studies on the thermal stability of Bu16-MMT containing nanocomposites indicated differences between the surfaces of the test piece and the bulk sample, which may contribute to the fire retardant properties of the UP nanocomposites. These surface trends were clearly observed when analysed using TGA under air (oxidative decomposition) but not so apparent under N_2 (non-oxidative decomposition). Analysis using ATR FTIR also revealed surface differences. The 'front' surface denotes the surface that was open to air during the curing process and the 'back' surface denotes the surface which was in contact with the mould during the curing process.

4.17.1 TGA Analysis of Front and Back Surfaces of Nanocomposites Containing Bu16-MMT and DMMP

TG analysis was carried out on samples containing Crystic 189LV, 5 wt% Bu16-MMT and 10D, run under an atmosphere of Air (Figure 4–56) and N_2 (Figure 4–57). Preparation of the front and back samples involved removing the surface of the nanocomposite with a scalpel and running the shavings on the instrument, the bulk sample was prepared in the usual way, using a sample size as stated in section 2.6.2.3 of chapter 2. The derivative thermograms (DTG) were obtained and any differences noted.
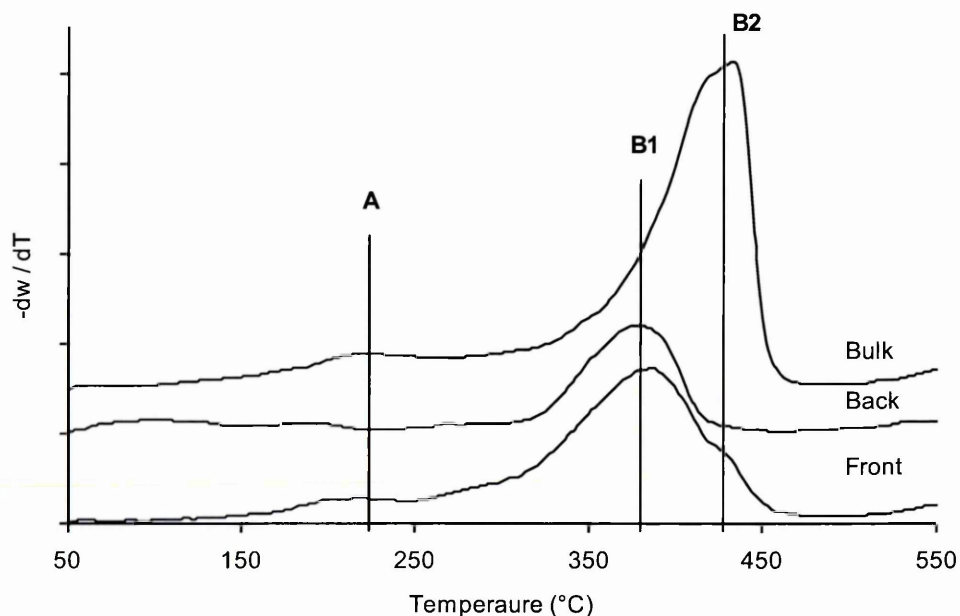
Figure 4–56 DTG traces (Air) Crystic 189LV composites containing, 5 wt% Bu16-MMT and 10D, front, back and bulk differences – Traces are offset for clarity

The DTG traces presented in Figure 4–56, which were run in air displayed two maxima in the decomposition process (A and B (1 or 2)), decomposing over two stages. Significant differences in the position of peak B between the front, back and bulk samples were revealed. The thermal decomposition temperature of peak B, increased from 383 °C under T_{max} (B1) for the front and back samples to 432 °C under T_{max} (B2) for the bulk sample. T_{max} (A) represents the thermal desorption of DMMP and occurred at 225 °C in both the bulk and front samples.

In Figure 4–5 Crystic 189LV composites containing 5 wt% TP8- to TP16-MMT and Bu16-MMT were analysed using DTG under an atmosphere of air. The main decomposition peak A displayed a T_{max} (A) evolving at a higher temperature in the TP8- and TP14-MMT samples. After analysis of the front, back and bulk in Figure 4–56, these temperature differences could possibly be attributed to sampling variations, with more of the bulk material being sampled in the TP8- and TP14-MMT composites, leading to an increased thermal decomposition temperature maximum. Figure 4–15 and Figure 4–31 are good examples of composites where the TG samples have been taken from the same area of the composite (in these cases the bulk). Both figures display a high temperature peak, which is at the same temperature in all composites of that particular series.
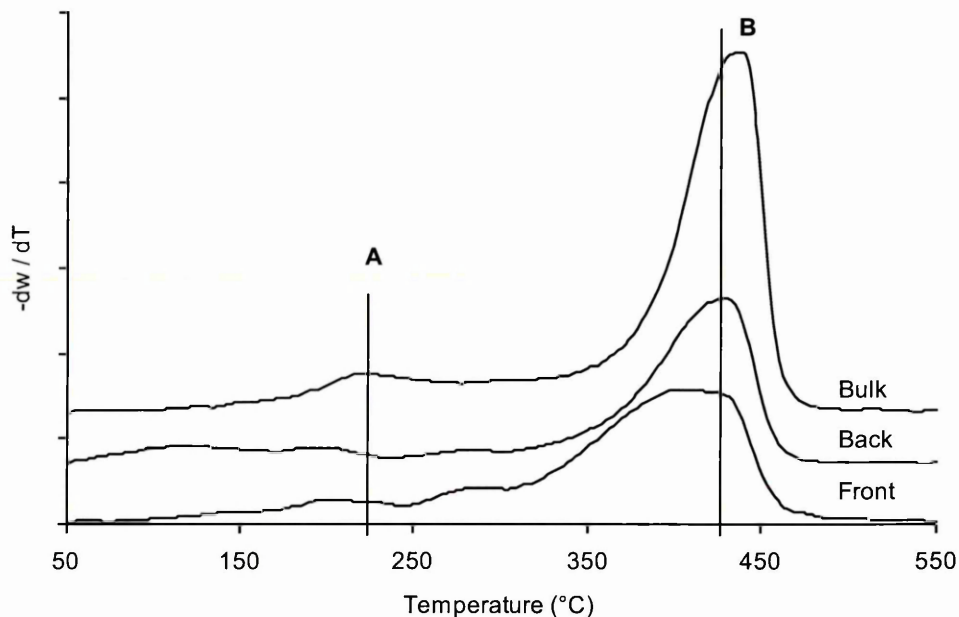
Figure 4–57 DTG traces (N_2) for Crystic 189LV composites containing, 5 wt% Bu16-MMT and 10D, front, back and bulk differences – Traces are offset for clarity

The DTG traces presented in Figure 4–57, run under nitrogen did not reveal any significant differences between the thermal decomposition of the peak under T_{max} (B) which occurred at 430 °C in all samples. The thermal desorption of DMMP occurred under T_{max} (A) at 225 °C in both the bulk and front samples. Therefore, to investigate whether these effects were caused by the clay in the system, Crystic 189LV samples containing 10D were made and the front, back and bulk analysed using TG. Also to investigate whether these differences were only seen at the surface of the samples, a

190

layer approximately 100 μm thick was removed and the new exposed front (Front-1) and back (Back-1) surfaces were analysed, the results are displayed in Figure 4–58.
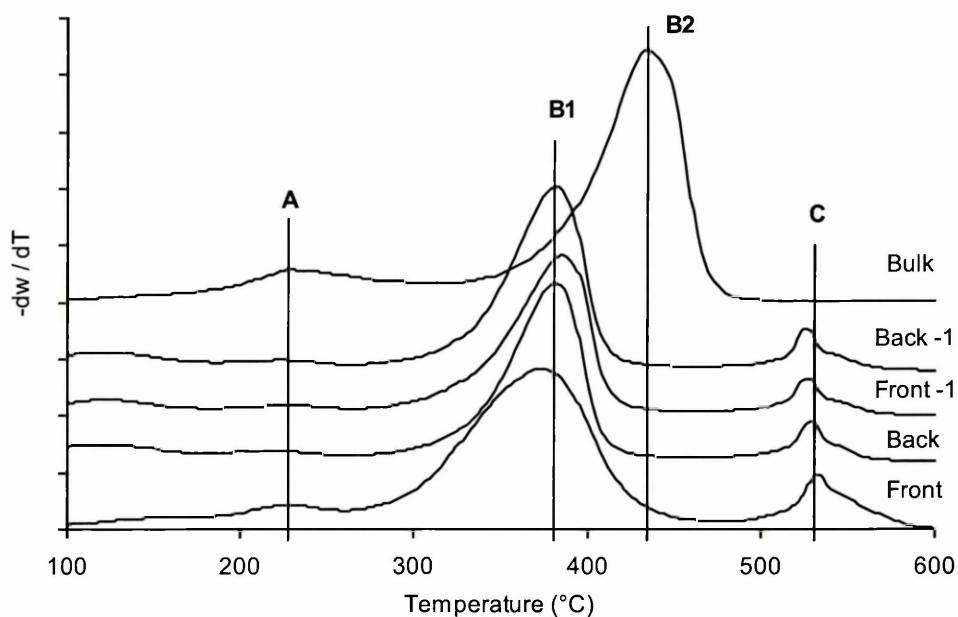
Figure 4–58 DTG traces (Air) for Crystic 189LV composites containing 10D. Front, back and bulk differences – Traces are offset for clarity

The DTG traces presented in Figure 4–58 indicated surface and bulk differences within the samples and this effect was observed with and without the presence of clay. T_{max} (A) occurred at 232 °C and is representative of the thermal desorption of DMMP, this peak also occurred in the bulk sample and to a lesser extent in the front sample. T_{max} (B1) occurred between 376 and 390 °C in the front and back samples, whereas a shift to a higher temperature (439 °C) was displayed in the bulk sample (T_{max} B2). A new peak denoted as T_{max} (C) occurred at 530 °C in the front and back samples, however this peak was not present in the bulk sample and the samples containing Bu16-MMT.

4.17.2 ATR FTIR Analysis of Front and Back Surfaces of Nanocomposites Containing Bu16-MMT and DMMP

ATR FTIR was carried out using the settings outlined in section 2.12.3 of Chapter 2. The front and back surfaces of nanocomposites containing Crystic 189LV, 5% Bu16-MMT and 10D (Figure 4–59) and Crystic 189LV and 10D (Figure 4–60) were analysed in triplicate for reproducibility, the peak positions are displayed in Table 4–30.
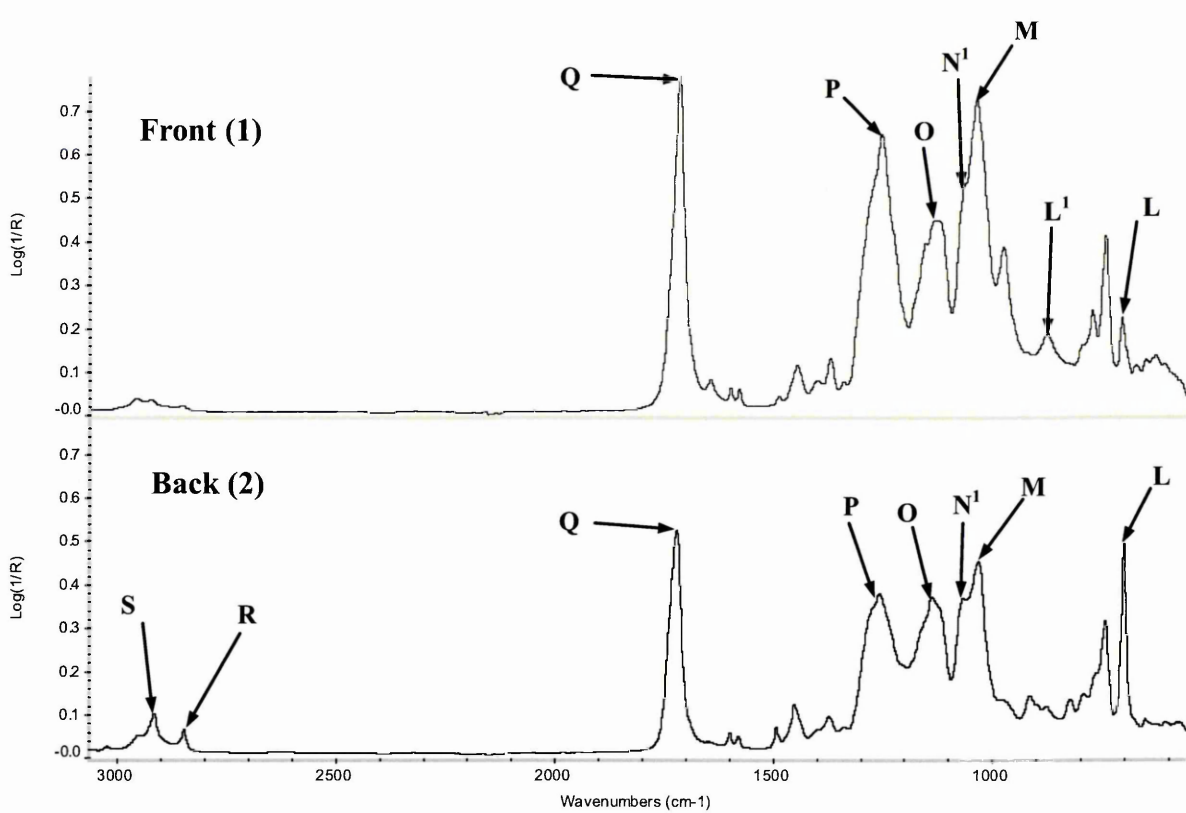
Figure 4–59 ATR FTIR of Crystic 189LV composites containing, 5 wt% Bu16-MMT and 10D - Front and back differences
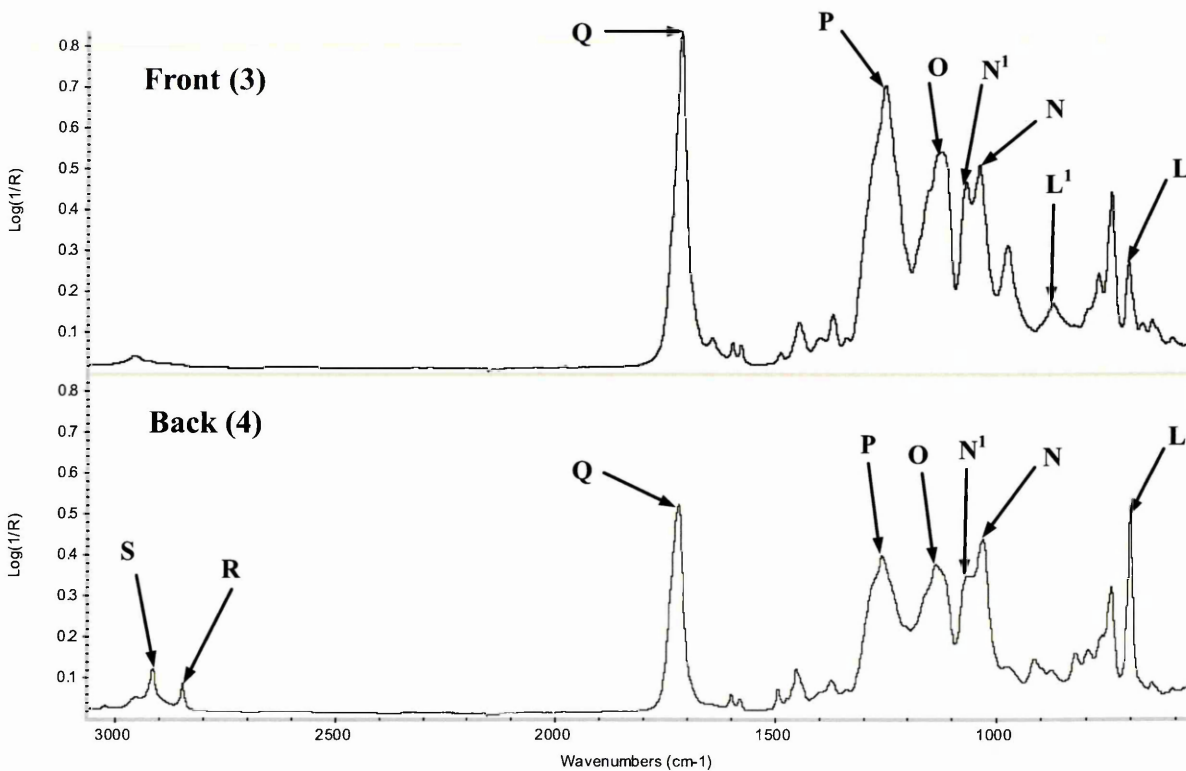
Figure 4–60 ATR FTIR of Crystic 189LV composites containing 10D - Front and back differences

Table 4–30 Peak positions for front and back surfaces of composites prepared using Crystic 189LV, 5 wt% Bu16 and 10D, and Crystic 189LV and 10D, plus DMMP.

	Peak Positions (cm^{-1})									
	L	**L^1**	**M**	**N**	**N^1**	**O**	**P**	**Q**	**R**	**S**
Front 1	703	875	1033	-	1074	1127	1249	1717	-	-
Back 2	700	-	1030	-	1071	1138	1255	1720	2843	2917
Front 3	700	875	-	1036	1068	1124	1252	1714	-	-
Back 4	700	-	-	1030	1065	1135	1258	1717	2848	2917
DMMP	720	-	-	-	-	-	1250	-	2860	2930

In both systems analysed (with and without clay) peak L^1 was present on the front surface, which was not present on the back surface. Peaks L, R and S were thought to originate from DMMP (spectra not included), these peaks were more intense on the back surface than the front. The presence of DMMP on the back surface was contradictory to what was found in the TGA data, as it was originally thought that DMMP was not present on the back surface as no peak was found for DMMP in the DTG traces under air or nitrogen. However, upon examination of the spectra for pure Crystic 189LV peaks R and S were clearly visible on the back surface and so it was more likely that peaks R and S were representative of polystyrene that had shifted to the back surface of the sample during the curing process.

In the presence of clay peak M dominated peak N and peak N^1. On the front surface peak P was more intense than peak O, however on the back surface peaks P and O were equal in intensity and these intensity differences occurred in the presence and absence of clay. On the back surface there was less clay (peaks M, N, N^1, O and P) visible, this was due to the migration of polystyrene towards the back surface, leading to an increased polystyrene content near the ATR window. On the front surface peak Q was more intense than on the back surface, occurring again in the presence and absence of clay. In the absence of clay peaks N and N^1 were clearly defined.

After removing the top layer of the nanocomposites both surfaces appeared the same, peaks R and S were not as intense. The differences between the bulk and surface of the nanocomposites observed using TGA and ATR FTIR could possibly stem from differences in the degree of exfoliation of the clay from the bulk to the surface and/or

differences in the orientation of clay particles in these regions during the mixing and casting processes. However, Lee *et al.* [4-31] has found little mechanistic reason to believe that exfoliation varies across from surface to bulk regions of their polypropylene nanocomposites.

4.18 Conclusions for Commercially Available Organophosphorus Cations

The gallery cations of Na^+ Cloisite were exchanged with triphenyl phosphonium (TP) cations with chain lengths ranging from $C_n = 8$ to $C_n = 16$ ($TP8^+$ to $TP16^+$) and a tributyl phosphonium ($Bu16^+$) cation. XRD and TGA were carried out on all exchanged clays, and nanocomposites incorporating these exchanged clays. XRD results indicated that the phosphonium clays produced intercalated nanocomposites in Crystic 189LV. The d-spacing increased from 12.1 Å for Na^+ Cloisite to 17.4 Å in TP8- to TP12-MMT and 18.7, 17.7 and 20.9 Å in TP14-, TP16- and Bu16-MMT, respectively. A small peak at lower angle occurred, which has been tentatively attributed to the formation of a mixed ion heterostructure, where $TP8^+$ - $TP16^+$ and $Bu16^+$ cations and $Na(H_2O)$ cations are segregated into two interlayers in a regular alternating fashion.

DTG data revealed a two stage decomposition pattern for all phosphonium clays. The decomposition temperature maximum (T_{max} A) decreased as the chain length increased from $C_n = 8$ to $C_n = 12$ (351 to 327 °C) and then increased when $C_n = 14$ and 16 (341 and 360 °C). Shoulders occurred on the main decomposition peak T_{max} A occurring after the main decomposition peak (T_{max} A+1) in the TP8- to TP12-MMT samples and before the main decomposition peak (T_{max} A-1) in the TP14- and TP16-MMT samples. Bu16-MMT displayed a clear sharp decomposition peak under T_{max} A-1, at a much lower temperature of 292 °C.

When the actual amount of organic exchange was calculated all organoclays were slightly under exchanged with TP8-, TP10-, TP14- and Bu16-MMT at 68% ± 5% of the possible organic exchange, however the actual amount exchanged for TP16-MMT was slightly lower at 56% of the possible organic exchange amount.

The incorporation of TP14-, TP16- and Bu16-MMT into Crystic 189LV produced intercalated/exfoliated nanocomposites for the TP14- and TP16-MMT samples and intercalated/aggregated nanocomposites for the Bu16-MMT sample. The d_{001} spacing also increased from 18.7, 17.7 and 20.9 Å, to 33.1, 33.7 and 27.8 Å, respectively. The layer spacing of TP8-, TP10- and TP12-MMT did not expand upon dispersion into Crystic 189LV. The DTG traces indicated a thermal decomposition maxima of 422 °C for pure Crystic 189LV and samples made using Crystic 189LV and 5 wt% TP10-, TP12-, TP16-, and Bu16-MMT.

Composites containing TP8- and TP14-MMT displayed a slightly higher temperature thermal decomposition maxima (+22 °C), demonstrating a stabilising effect on the entire system until the upper thermal limit of the material was reached. It was believed that this shift was due to the formation of a protective barrier layer, due to the surface accumulation of clay platelets held together with a carbonaceous char. This barrier would have thermally insulated the UP matrix.

To investigate the effect of individual components in the nanocomposite systems (DMMP and styrene), on the d-spacing of organophosphonium clays, XRD analysis was carried out on organophosphonium clays dispersed in DMMP, and dispersed in styrene. Dispersion of TP8- to TP16-MMT in DMMP or styrene did not significantly expand the d-spacings of the organoclays. The d-spacing of Bu16-MMT decreased when dispersed into DMMP and increased when dispersed into styrene. It was observed that the small peak at lower angle (found in all organophosphonium clays), was not present when dispersed in DMMP and was only present in TP10- and TP16-MMT samples when dispersed in styrene. These experiments confirmed that the expansion in the d_{001} spacing observed when composites were prepared using these organophosphonium clays and Crystic 189LV, was due to polymerisation of Crystic 189LV in the gallery space, therefore expanding the clay layers further. The increase in the d_{001} spacing cannot be attributed to DMMP or styrene further expanding the clay layers.

The organoclays proved difficult to disperse into the UP resin, however this was overcome by pre-mixing with dimethyl methyl phosphonate (DMMP), which has been identified as an effective gas phase fire retardant. Very interesting results on fire performance were produced that could remove the need for halogenated products to achieve increased fire retardancy. Using DMMP as a pre-swelling agent not only improved the dispersion but also caused the fire retardant properties to reach a much higher classification.

XRD analysis of Bu16-MMT dispersed in DMMP and then incorporated into Crystic 189LV revealed intercalated and aggregated nanocomposites for the 5 wt% Bu16-MMT plus 10D samples, which were similar to Bu16-MMT at 5 wt% without DMMP. The XRD traces for composites prepared using 2.5 wt% Bu16-MMT plus 5D were less intense, possibly due to the decreased amount of clay in the sample. The d_{001} spacing increased from 20.9 Å in Bu16-MMT to 29.1 Å when mixed with Crystic 189LV/5 wt% Bu16 and 28.1 Å when mixed with Crystic 189LV/2.5 or 5 wt% Bu16 plus DMMP. Upon increasing the amount of DMMP in the Bu16-MMT samples from 5 to 10 wt%, the samples remained intercalated, therefore DMMP did not clearly influence the dispersion and size of the stacks within the Bu16-MMT samples.

When mixed with Crystic 189LV and DMMP, an increase in the d-spacing of TP12-, and TP16-MMT occurred from 17.4 and 17.7 Å, to 30.1 and 31.7 Å, respectively. Crystic 189LV did not intercalate into TP12-MMT, however the addition of 5D into the TP12-MMT/Crystic 189LV system produced some intercalated nanocomposite, but lots of undispersed TP12-MMT remained. A more exfoliated/intercalated nanocomposite was formed upon addition of 10D, which was observed through increased low angle scattering and intensity of the d_{001} peak. Intercalated and aggregated nanocomposites were formed when TP16-MMT was mixed with Crystic 189LV, occurring in the presence and absence of DMMP. The 2.5 wt% TP16-MMT/5D samples displayed a more intercalated/aggregated nanocomposite nature, observed through increased intensity of the d_{001} and d_{002} peaks.

DTG traces indicated the same thermal decomposition pathway for all the nanocomposites incorporating DMMP and therefore, DMMP does not appear to affect the decomposition pathway of these systems, at this level of investigation.

Nanocomposites incorporating Bu16$^+$, DMMP and Crystic 189LV were prepared from an original 'one-pot' process, starting with Na$^+$ Cloisite. An efficient one-pot synthesis method involves incorporating all components of an UP-clay nanocomposite simultaneously in a mixture, permitting the in-situ preparation of organophosphonium clays. XRD data revealed an intercalated/exfoliated nanocomposite with increased d_{001} spacing of 34.4 Å in the 'one-pot' method, compared to 28.6 Å in the standard method. However, the thermal decomposition maximum in the DTG traces remained the same at ~ 427 °C for the standard and 'one-pot' methods. The char decomposition temperature in the DTG curves displayed an increase of 9 °C in the 'one-pot' method.

Samples prepared using Crystic 189LV, TP8- to TP16-MMT, Bu16-MMT and either 0 or 10 wt% DMMP were subjected to the in-house version of the UL94 vertical burning test. In order of effectiveness, Bu16-, TP10- and TP8-MMT improved fire resistance (reaching classification V-0, V-0 and V-1, respectively) but TP12-, TP14- and TP16-MMT were less successful. Further analysis using TGA indicated that, for TP8- and TP10-MMT, DMMP was available at relatively low temperatures to extinguish the gas phase flame but, for TP12- and TP16-MMT, it was not. This suggests that the phosphonium salt may interact/react with (some of) the DMMP reducing its active concentration below the required value for effective operation as a gas phase fire retardant.

XRD and TGA data revealed batch-to-batch variation in the Bu16-MMT organoclays, which may influence dispersion, indicating that the loading of the tributylhexadecylphosphonium clay needed to be carefully monitored. XRD data revealed an increase in the intensity of several batches, however the d_{001} spacing remained the same at 21 Å (± 1 Å). The DTG results revealed a shift in the minor pre peak A-1, revealing that as the peak A-1 moved to a lower temperature then the intensity of the d_{001} peak using XRD also increased, which resulted in an increase in the fire retardant properties of the samples. TG-MS measurements performed on Bu16-MMT batches displaying 'good' and 'bad' fire retardant properties displayed peak A-1 at a lower temperature in the 'good' batch and also the intensity of the decomposition ions was almost twice as intense in the 'good' batch.

Variations in the loading of Bu16$^+$ onto Na$^+$ Cloisite affected the level of dispersion and thermal degradation pattern of the resultant nanocomposite. XRD results displayed an increase in the d-spacing from 20.8 Å at 1.0 x CEC to 24.3 Å at 1.5 and 2.0 x CEC, however as the loading of Bu16$^+$ reached 1.0, 1.5 and 2.0 x CEC, the difference between the d_{001} spacing and the spacing for the small peak at higher angle remained the same at approximately 15 Å. DTG results displayed a loss of intensity for the peak under T_{max} (A-1) and a shift to a lower temperature (292 °C at 1.0 x CEC decreasing to 273 °C at 1.5 and 2.0 x CEC) as the loading of Bu16$^+$ increased. However, it was still unclear which factors could potentially link to the fire retardant properties of the sample. It appeared that as the distance between T_{max} (A) and T_{max} (A-1) increased then the fire retardant properties of the resulting composite also increased.

In experiments similar to those performed by Xie et. al. [4-29] washing of Bu16-MMT prepared at 1.5 and 2.0 x CEC of Na$^+$ Cloisite in a mixture of 80:20 EtOH:H$_2$O, indicated that the organic content of the samples corresponded closely to the organic content in the 1.0 x CEC samples. XRD and TG results indicated that when Bu16-MMT prepared at 1.5 and 2.0 x CEC of Na$^+$ Cloisite, was washed in a mixture of 80:20 EtOH:H$_2$O, then excess surfactant was removed. The d_{001} spacing decreased from 24.3 Å at 1.5 and 2.0 x CEC, to 20.8 Å as in the 1.0 x CEC sample. The DTG results also indicated that after washing the peak under T_{max} A-1 increased from 273 °C to ~290 °C which was at the same temperature as the 1.0 x CEC samples. Therefore incorporation of this washing step into the cation exchange process would ensure that excess surfactant was removed from the organoclays, which could reduce plasticization of the polymer or prevent early ignition of the nanocomposite.

When Bu16-MMT washed in a mixture of 80:20 EtOH:H$_2$O was incorporated into the unsaturated polyester Crystic 189LV (plus 10D) and subjected to the 'in-house' version of the UL94 vertical burning test. An increased incidence of cracking after the first flaming occurred as the loading of Bu16$^+$ increased from 1.0 to 1.5 and 2.0 x CEC of Na$^+$ Cloisite, and consequently the samples had to be extinguished manually.

The role of DMMP was investigated in combination with organoclays both as intercalated powders and as components of nanocomposites prepared using Crystic 189LV. TP8- to TP16-MMT and Bu16-MMT were dispersed in DMMP, dried and then any differences in the thermal decomposition of the organoclays after dispersion in DMMP analysed using TGA and TG-MS. The DTG results for the thermal decomposition of TP8- to TP16-MMT and Bu16-MMT dispersed in DMMP, demonstrated three thermal decomposition maxima (A, B and C), however multiple shoulders occurred under T_{max} (C).

TG-MS data indicated that TP8- and TP10-MMT contained significant amounts of absorbed DMMP (m/z = 79), which was desorbed under T_{max} (A) at 148 °C, at a lower temperature than the boiling point of DMMP (which boils at 189 °C), whereas TP12-, TP14- and TP16-MMT exhibited a higher desorption temperature for DMMP under T_{max} (B) at 501 °C. Bu16-MMT did not exhibit a low temperature loss of DMMP. A tentative explanation for the ability of TP8- and TP10-MMT to accommodate adsorbed DMMP is that the C8 and C10 alkyl chains are relatively short and therefore there is some space between them in the gallery for DMMP to occupy. However, when the chain length exceeded 12 carbons there was no longer any space available for DMMP to be adsorbed.

Composites containing Crystic 189LV and DMMP, and Crystic 189LV, Bu16-MMT and DMMP were made. Analysis of the gases released suggested that DMMP (m/z = 79) evolved at lower temperatures when present in greater quantities, possibly leading to improved fire performance. In addition, an unidentified fragment ion m/z = 50, which has been tentatively attributed to the thermal desorption of methyl chloride, (however, this could not be proven using existing equipment) was evolved from specimens containing Bu16-MMT. It was clear that m/z = 50 only appeared in the presence of clay and was desorbed after the thermal desorption of m/z = 79. The intensity of the m/z = 50 mass fragment increased as the DMMP loading increased even though this fragment did not appear in the mass spectrum of DMMP.

Differences between the surface and bulk composition of nanocomposites containing Bu16-MMT were revealed using TGA and infrared (ATR-FTIR) spectral characterisation. DTG data revealed that the surface 'layer' was less thermally stable than the bulk when heated in air, and decomposed at 383 °C at the surface compared to 432 °C in the bulk. Using ATR-FTIR it appeared that polystyrene (characteristic peaks at 2848 and 2917 cm^{-1}) had migrated to the back surface of the sample and that the characteristic organoclay peaks were more intense at the front surface of the sample compared to the back. Fornes and Paul [4-32] have suggested that when a polymer is cast into a mould the surface and bulk regions undergo different cooling rates, which can lead to differences in chain/clay orientation. Therefore, the surface and bulk differences found using DTG and IR could possibly stem from differences in the orientation of the polymer/clay particles, which occurred during the mixing and casting processes.

The most promising nanocomposite system from Chapter 4 comprised Crystic 189LV, 5 wt% Bu16-MMT and 10 wt% DMMP, which achieved UL94 classification V0 and therefore compared favourably with halogenated resins. However, the clay modification process is prohibitively expensive for commercial application, therefore the 'one pot' preparation method should be further developed as an alternative to the standard, intensive process, as preliminary studies displayed comparable results in the UL94 vertical burning test for the standard and 'one-pot' methods.

4.18.1 Literature reports on the distribution of clay from skin to core in PLSNs

Fornes and Paul [4-32] examined the effects of organoclay concentration and degree of exfoliation on a nylon-6 matrix crystal structure in nanocomposites formed by melt processing. Aliphatic polyamides, such as nylon-6, are well known for their strong hydrogen bonding (H-bonding) ability and seek to maximize the number of H-bonds within and between polymer chains. Maximization of H-bonds in the crystalline state of nylon-6 requires the polyamide chains to adopt either a fully extended or twisted configuration.

(Side View)   (Front View)
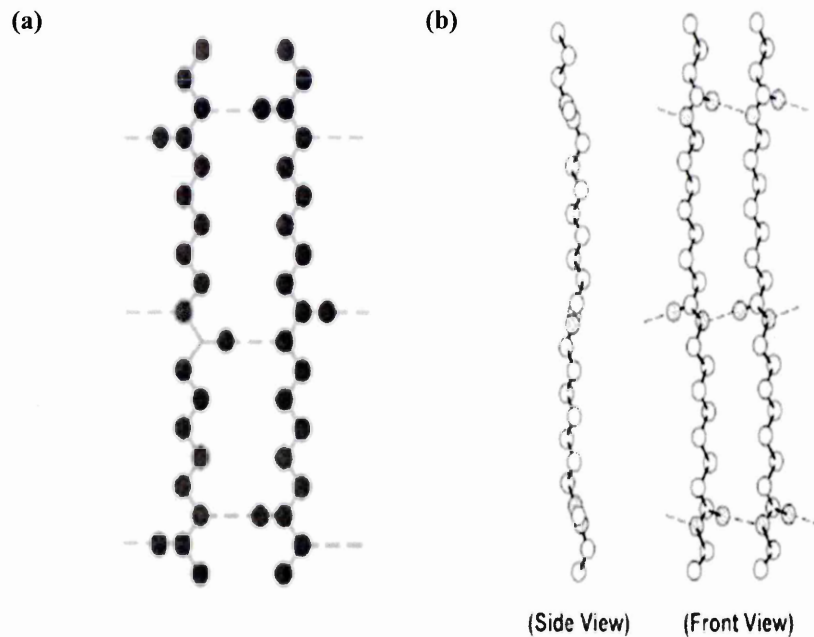
Figure 4–61 Chains in the (a) fully extended configuration of the α-crystalline form and (b) twisted configuration of the γ-crystalline form [4-33].

In the fully extended configuration, termed the α-form polymer chains are oriented in an anti-parallel fashion as displayed in Figure 4–61 (a). Anti-parallel chains are situated such that the amide linkage and methylene units lie within the same plane, and the H-bonds occur between adjacent anti-parallel chains to form sheets of H-bonded chains. The γ-crystalline (Figure 4–61 (b)) form of nylon 6 occurs, when H-bonds form between parallel polyamide chains. To maximise the number of H-bonds, formation requires the amide linkages to twist approximately 60° out of the plane of the molecular sheets.

Early studies [4-34, 4-35] revealed that crystallization for extended periods of time below ~ 130 °C leads solely to the γ-crystallites while above ~ 190 °C only the α-form is produced. Temperatures in between these two limits result in a mixture of the two forms, with higher fractions of α produced at higher temperatures. Rapid cooling or quenching in general produces the γ-form [4-36], however annealing can also affect the structure, annealing for extended times leads to the conversion of the γ phase into α phase [4-34]. Therefore, rapid cooling and low temperature crystallization promotes the γ-form, while higher crystallization temperatures or slow cooling leads to the α-form.

When a polymer is cast into a mould the outer-most layer undergoes rapid cooling, while the central portion experiences slower cooling rates and less stress, this produces a surface-bulk structure due to the differences in cooling and chain orientation [4-37]. Differences in the physical and mechanical properties between the surface and bulk can be significant. Fornes and Paul [4-32] found the surface region to contain only the γ-crystalline form, largely due to rapid cooling of the surface at low temperatures and possibly limited polymer chain mobility. Increasing the concentration of clay within the surface enhanced the formation of the γ-form, which may relate to further restrictions in polymer chain mobility. The bulk region however, contained both α and γ-forms of nylon-6.

Lee *et al.* [4-31] examined the morphology and mechanical properties of polypropylene (PP) reinforced with organoclay (dimethyl, dehydrogenated tallow-MMT) and toughened with an ethylene-octene based elastomer. Four different organoclay concentrations were investigated ranging from 0 to 6.8 wt%, XRD data from the core region (Figure 4–62 (a)) of the injection moulded sample, did not display a characteristic basal reflection for all MMT concentrations, suggesting an exfoliated structure. However, this was opposite to what was observed during TEM particle analysis, which displayed a decrease in the level of dispersion with increasing MMT concentration. The XRD traces from the skin region (Figure 4–62 (b)) of the samples revealed that a strong peak from the organoclay persisted without any significant shift in location; however the intensity of this peak increased with increasing MMT content, indicating that large stacks of platelets existed in the skin portion of the injection moulded samples. These findings suggest distinct structural differences between the skin and core regions of PP nanocomposites.
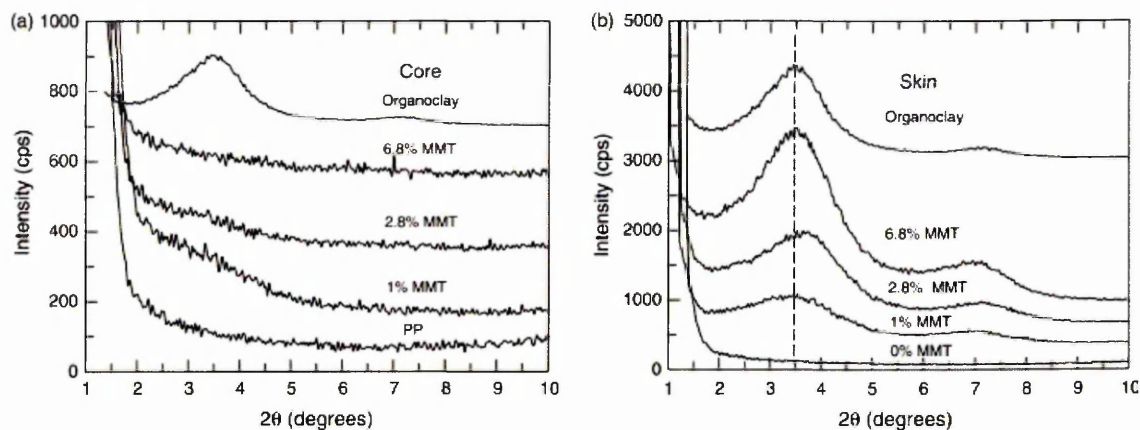
Figure 4–62 XRD traces (Cu-tube) for PP/organoclay nanocomposites containing 1, 2.8 and 6.8 wt% MMT. (a) is taken from the core region, while (b) is taken from the skin region. The curves are shifted vertically for clarity [4-31].

The intensity differences of the characteristic peaks of the clay could possibly stem from differences in the degree of exfoliation of clay from the core to skin and/or difference in the orientation of clay particles in these regions during the injection moulding process. However, there is little mechanistic reason to believe that exfoliation varies across from the skin to core regions, and so, it is believed that there is a significant difference in the orientation of clay particles in the skin and core regions in the injection-moulded specimen. This skin–core effect is particularly of interest from an industrial point of view, since the injection moulding process is largely involved in the production of commercial products, however as yet it has not been considered how the orientation of clay at the surface of an injection moulded part would promote fire retardancy and this is defiantly something to consider in the future. These papers illustrate that differences can occur between the skin and the core regions of injection moulded thermoplastics, however, due to the lack of shear when casting the UP nanocomposites at room temperature, it is difficult to draw realistic parallels.

Gilman et al. [4-38] in an effort to study the changes in the structure and dispersion of the polymer nanocomposite during burning, subjected a polystyrene (PS)-clay nanocomposite to various amounts of thermal degradation under realistic fire conditions. The combination of XRD, TGA, and TEM analysis of the PS nanocomposite samples after various pyrolysis times provided a more detailed picture into the mechanism of flammability reduction. The data collected reinforced, and provided additional understanding of the proposed condensed phase flame retardant mechanism for PLSN materials. As the nanocomposite heats up the polymer

decomposes and volatilizes. This causes the structure to collapse and results in a smaller interlayer spacing between the layered silicate or clay layers. The clay appeared to catalyze formation of carbonaceous char which yielded a clay reinforced carbon char layer with a d-spacing of 13.0 Å; this unique structure formed quickly under pyrolysis conditions, and was stable even after extended pyrolysis times. TGA data suggested that there were two types of carbonaceous materials formed in the carbon phase of the clay-carbon char; a carbon that can be decomposed and volatilized by heating in nitrogen, and a second fraction of material which required more aggressive conditions, (i.e. heating >700 °C) in the presence of air. The data indicated that not until substantial clay-carbon char formed did the pyrolysis rate (MLR) slow.

The clay carbon char provided thermal protection to the underlying material, as evidenced by the XRD, optical, and TGA data from the middle and bottom layers of the PLSN in the early part of the heat exposure. It was suggested that a minimum thickness of clay-carbon char must build up before the effect is produced. The data also indicated that the barrier is not impervious, and that gases and heat do penetrate through the barrier over time, eventually yielding a porous clay-carbon network structure that maintained the shape of the original material. However, even with this porosity, the d-spacing of the PLSN remained intact in the middle layers of the sample up to 200 s after a heat exposure of 50kW/m². However, it was not clear how much protection would be gained if the sample was thinner. It may be that the impressive thermal protection was in part due to the thickness (8mm) of the sample. Since the PLSN protective layer delays combustion of underlying material, in a thinner sample the reduction of heat release rate should still be observed, but the length of prolonged burning and low MLR maybe shortened. The varying thickness of the samples in this chapter may in some part explain the variable fire retardant results for the Bu16-MMT composites, but the industry standard for UL94 is 3mm and this was used in this thesis on a number of occasions, including in the cone calorimetry results.

The PLSN only delays the inevitable combustion of the polymer, rather than preventing combustion once the carbon-clay barrier is set up. Gilman believes that with this new knowledge on how PLSN materials provide flammability reduction, it should be possible to develop additional flame retardant technology that will take greater advantage of the PLSN flammability reduction. Development of clays that promote or

catalyze additional carbonaceous char formation would most likely enhance the flame retardant effectiveness of clay-nanocomposite based flame retardants.

The clay/carbon char model is still widely accepted but the influence of nanofillers on the degradation mechanism is also under investigation. Costache *et al.* [4-39] investigated the effect of different inorganic fillers (cationic and anionic clays and multi-wall carbon nanotubes (CNTs)) and the respective nanocomposite morphologies on the degradation pathway of poly(methyl methacrylate) (PMMA). They found that in the presence of clay (cationic or anionic) or CNTs no qualitative effect on the degradation mechanism of PMMA was observed. PMMA undergoes thermal degradation by a single process and the presence of filler cannot change its degradation pathway, in contrast with other systems such as polyamide-6 (PA-6), polystyrene (PS) and ethylene vinyl acetate copolymer (EVA), where fillers can promote one thermal degradation pathway at the expense of another. The barrier mechanism, which is the most widely proposed mechanism by which nanocomposite formation imparts fire retardancy to polymers, is actually important not only at the surface, but also within the polymer matrix. Therefore, they state that in many cases the reduction to mass transport was much more important than the insulating effect which can arise only at the surface.

Jang *et al.* [4-40] suggested that the number of degradation pathways of a polymer is one of the factors that can affect the fire retardancy of polymer/clay nanocomposites. If degradation occurs by only a single pathway, then more thermally stable products are not produced and the fire retardancy is not significantly improved in the presence of clay. The changes in the degradation pathway of polystyrene (PS) in the presence of clay were discussed and the factors affecting the fire retardancy of polymer/clay nanocomposites such as the relative stability of the radicals produced upon degradation were considered.

Virgin PS evolved a styrene monomer (m/z = 104), dimer (m/z = 208) and trimer (m/z = 312) as the main degradation products during thermal degradation, the formation of these products is depicted in Figure 4–63. Styrene monomer is produced via β-scission of a chain end formed by the initial chain scission, while dimer and trimer are evolved via radical transfer followed by β-scission [4-41, 4-42, 4-43]. In the presence of clay, many different evolved products were detected, produced via radical recombination (Figure

4–64) and extensive random scission (Figure 4–65). The degraded molecules have an opportunity to undergo radical recombination, because the degraded molecules are confined between well-dispersed clay layers. Extensive random chain scission occurred at the same time, since the degrading polymers experienced superheated conditions during the thermal event. The identification of head-to-head structures and many isomers in the evolved products suggested that a recombination reaction between tertiary and/or secondary radicals occurred in the presence of clay [4-44].
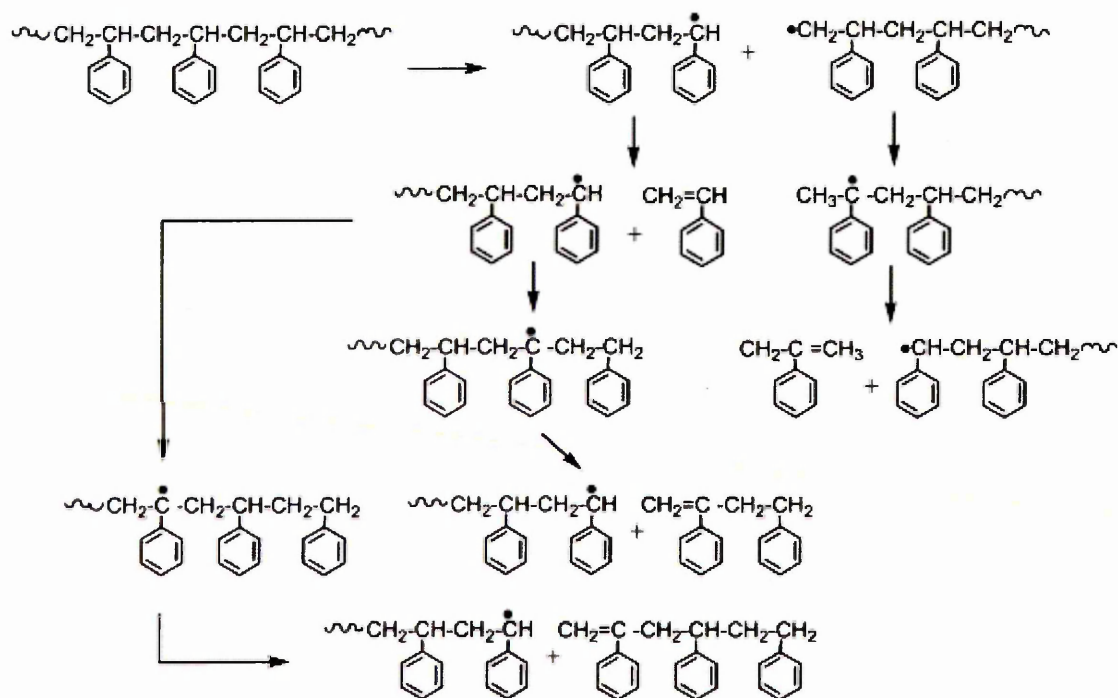
Figure 4–63 The formation of evolved products, styrene monomer, dimer, and trimer [4-44].

PS displayed a large reduction (typically around 60%) in the peak heat release rate (PHRR). Considering the changes of degradation pathway of the polymer in the presence of clay, polystyrene exhibits a significant increase in the intermolecular reaction; radical recombination. The radicals produced when PS degrades may undergo several secondary reactions, disproportionation, β-scission, hydrogen abstraction, radical transfer and radical recombination. The styryl radical in styrene-containing polymers is the most stable. A relatively stable radical has more opportunity to undergo various secondary reactions. In the presence of clay, the clay acts as a barrier to keep the degrading compounds from evolving, hence the radicals have more opportunity to undergo additional reactions. These reactions become significant at higher clay concentrations because the degrading polymer is retained by the clay layers, permitting

206

further reaction [4-44]. Thus, more stable radicals may undergo intermolecular reactions, such as hydrogen abstraction and radical combination, which lead to the reduction in the heat release rate in cone calorimetry.
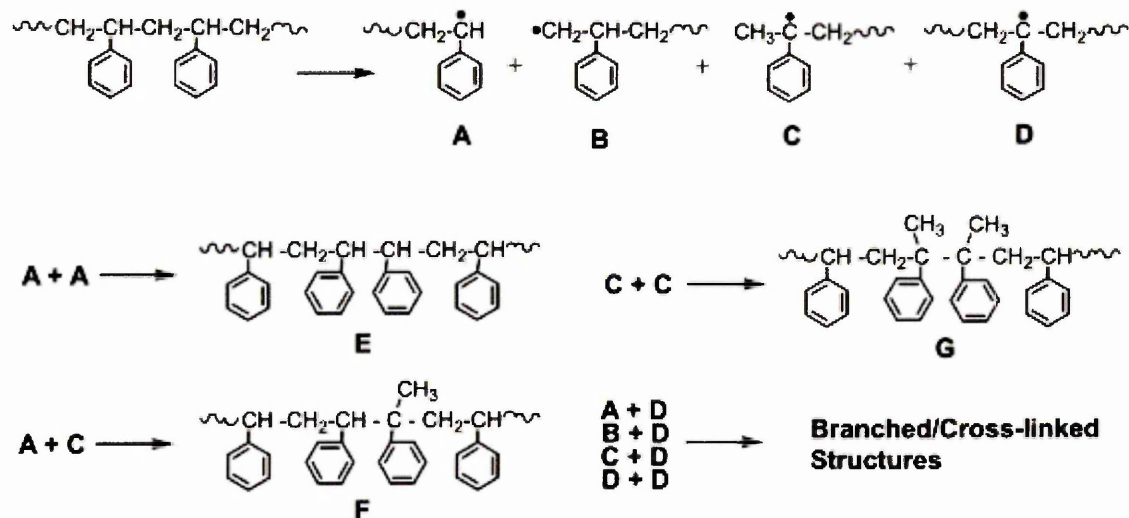
Figure 4–64 Radical Recombination [4-44].

For PS/clay nanocomposites, the secondary styryl radical is as stable as the allylic radical and there are many potential tertiary styryl radical sites available. The hydrogen in the β-position to the benzene ring may be the source of hydrogen abstraction, therefore, in the presence of clay, radical transfer (intra- and inter-) to this position is very probable and the possibility to undergo radical recombination becomes high, along with hydrogen abstraction because of the high stability of the styryl radicals. Thus many head-to-head structures are detected in GC/MS analysis and these significant changes may be the reason for the large reduction in PHRR.
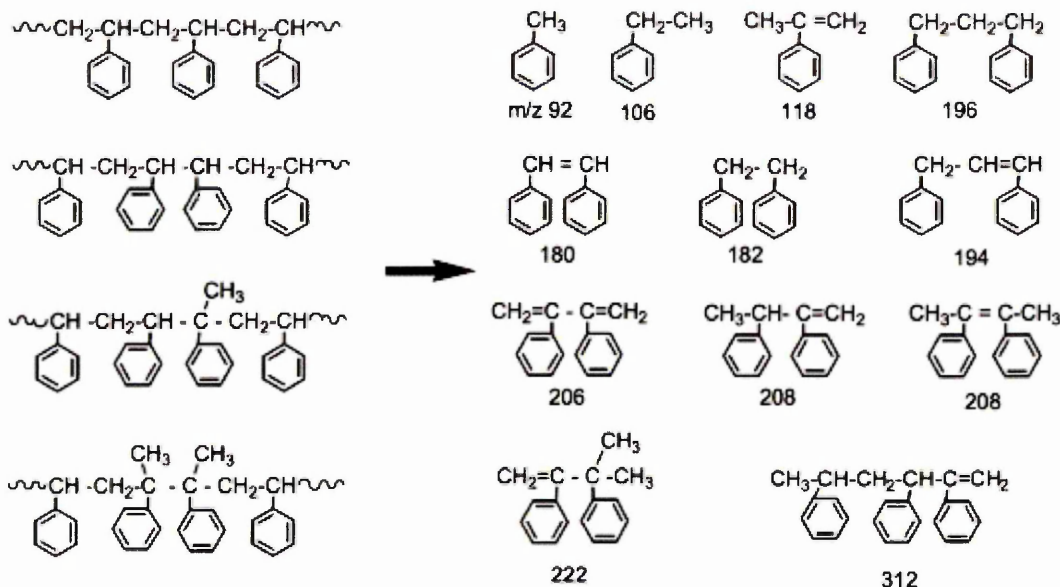
Figure 4–65 Extensive Random Chain Scission [4-44].

Therefore, it can be stated that the stability of the radical produced upon degradation of a polymer is proportional to fire retardancy in terms of the reduction in PHRR. The more stable the radical a polymer produces, the better is the reduction in peak heat release rate upon nanocomposite formation.

Jang et al. [4-45] further utilised GC/MS as well as TGA/FTIR to study the degradation pathway of polyamide-6 clay (PA-6 clay) nanocomposites, using the same techniques as in the previous work [4-40, 4-44]. Since acetonitrile was used as the solvent for the collection of the evolved products, the mass spectra for each GC trace exhibited only molecular mass higher than m/z = 50. The structures were identified through the analysis of mass fragmentation pattern and/or by co-injection with authentic compounds; some structures were speculatively assigned according to the degradation patterns that were proposed by the previous workers [4-46, 4-47, 4-48]. The most dominant species in the evolved products was ε-caprolactam (m/z = 113), which is the monomer of polyamide-6, which can be produced through intra- and/or inter-molecular aminolysis/acidolysis reactions. The dimer (m/z = 226,) was produced in a similar fashion. It was generally accepted that monomer formation was primarily generated by intra-molecular reactions rather than inter-molecular reactions. In the presence of clay, the soluble fractions of PA-6 clay nanocomposite displayed increased viscosity and this increase could be explained by inter-molecular reactions since one chain attacks another, leading to larger molecules. The clay provided more opportunity for degrading

208

polyamide-6 to undergo intermolecular aminolysis/acidolysis by containment of the degrading polymer.

The GC/MS results indicated that the relative intensity of ε-caprolactam decreased with increasing clay content. Apart from the monomer and the dimer, many evolved structures were produced via chain scission. These results implied that evolved products via chain scission also increased during the thermal degradation of polyamide-6 in the presence of clay. Therefore, it is anticipated that through the analysis of the radicals evolved from the polymer clay nanocomposites, structurally identified through the analysis of mass fragmentation pattern and/or by co-injection with authentic compounds, then an indication of the degree of fire retardancy would be determined.

Bourbigot et al. [4-49] combined nanoparticles with traditional flame retardants (intumescents) to achieve low flammability with nanocomposites. Nanocomposites based on three different types of nanoparticles, clay, polyhedral silsesquioxanes (POSS) and carbon nanotubes (CNT) were discussed. Their flammability properties were measured by using cone calorimetry. They observed a significant reduction in the heat release rate (HRR) compared to the virgin polymer, however it was apparent that nano-dispersion of the filler was absolutely necessary to achieve the highest performance. The formation of a coherent char layer (i.e. no cracking) was also found to be imperative to obtain low heat release rates. However, it was found that low flammability of the nanocomposites was only achieved in terms of HRR, and the samples failed in terms of the UL94 and limiting oxygen index (LOI). The combination of traditional intumescents overcame the UL94 and LOI problems. In comparison the UL94 results in this chapter for the composites containing alkyltriphenylphosphonium and alkyltributylphosphonium exchanged Na$^+$ Cloisite, also failed when the samples exhibited non-uniformity of the char layer (i.e. cracking) and the introduction of the fire retardant DMMP increased the amount of samples reaching a UL94 classification of V-0 and V-1.

4-1 Lagaly, G., Clay-organic reactions, interactions, *Phil. Trans. R. Soc.,* London, A-311 (1984)

4-2 Theng, B.K.G., Greenland, D.J. and Quirk, J.P., *Clay Miner.,* **7**, 1 (1967)

4-3 Jones, T.R., *Clay Miner.,* **18**, 399 (1983)

4-4 Chigwada, G. and Wilkie, C.A. *Polym. Degrad. and Stab.,* **80**, 551 (2003)

4-5 Zhu, S. and Shi. W., *Polym. Degrad. and Stab.,* **80**, 217 (2003)

4-6 Street, G.B. and White, D., *J. Appl. Chem.,* 288 (1963)

4-7 Slabough, W.H. and Hanson, D.B., *J. Coll. and Int. Sci.,* **29**: 3, 460 (1969)

4-8 Boyd, S.A., Jaynes, W.F. and Ross, B.S., Organic substances and sediments in waters, 1. Chelsea, MI: Lewis, 181-200, 2619 (1991)

4-9 Brixie, J.M. and Boyd, S.A., J. Environ. Qual., 23, 1283 (1994)

4-10 Qutubuddin, S., Fu, X. and Tajuddin, Y., *Polymer Bulletin*, **48** (2), 143 (2002)

4-11 Weichert, M.W., Chen, H., Giannelis, E.P. and Sogah, D.Y., *J. Am. Chem. Soc.,* **121**, 1615 (1999)

4-12 Xie, W., Xie, R., Pan, W.P., Hunter, D., Koene, B., Tan, L.S. and Vaia, R., *Chem. Mater.,* **14**, 4837 (2002)

4-13 Gilman, J.W., Morgan, A.B., Harris, R.H., Trulove, P.C., DeLong, H.C. and Sutto, T.E. *Polym. Mater. Sci. Eng.,* **83**, 59 (2000)

4-14 Zhu, J.; Morgan, A. B.; Lamelas, F. J.; Wilkie, C. A. *Chem. Mater.,* **13**, 3774 (2001)

4-15 Yeh, J. M.; Liou, S. J.; Lin, C. Y.; Cheng, C. Y.; Chang, Y. W.; Lee, K. R. *Chem. Mater.,* **14**, 154 (2002)

4-16 Kosolapoff, G. M.; Maier, L. *Organic Phosphorus Compounds*, Vol 2; John Wiley & Sons: New York, (1972)

4-17 Ijdo, W.L. and Pinnavaia, T.J., *J. Solid State Chem.,* **139**, 281 (1998)

4-18 Solin, S.A., *Adv. Chem. Phys,* **49**, 455 (1982)

4-19 Yang, Y.S. and Lee, L.J., *Polymer,* **29**, 1793 (1998)

4-20 Gilman, J.W., *Appl. Clay Sci.,* **15**, 31 (1999)

4-21 Weil, E.D. and Levchik, S.V., *Journal of Fire Sciences,* **22**, 293 (2004)

4-22 Banks, M, Ebdon, J.R. and Johnson, M., *Polymer,* **35**, 3470 (1994)

4-23 Alexandre, M., Beyer, G., Henrist, C., Cloots, R., Rulmont, A., Jerome, R. and Dubois, P., *Chem. Mater.,* **13**, 3830 (2001)

4-24 Alexandre, M. and Dubois, P., *Mater. Sci. Eng.,* **28**, 1 (2000)

4-25 Zanetti, M., Camino, G., Thomann, R. and Mülhaupt, R., *Polymer,* **42**, 4501 (2001)

4-26 LeBaron, P.C. and Pinnavaia, T.J., *Chem. Mater.,* **13**, 3760 (2001)

4-27 Morgan, A.B. and Harris, J.D., *Polymer,* **44**, 2313 (2003)

4-28 He, H., Duchet, J., Galy, J. and Gerard, J.F., *J. Colloid Interface Sci.,* **295**, 202 (2006)

4-29 Xie, W., Gao, Z., Pan, W.P., Hunter, D., Singh, A. and Vaia, R., *Chem. Mater.,* **13 (9)**, 2979 (2001)

4-30 Yoon, P.J., Fornes, T.D. and Paul, D.R., *Polymer,* **43 (25)**, 6727 (2001)

4-31 Lee, H., Fasulo, P.D., Rodgers, W.R. and Paul, D.R., *Polymer,* **46 (25)**, 11673 (2005)

4-32 Fornes, T.D. and Paul, D.R., *Polymer,* **44**, 3945 (2003)

4-33 Fornes, T.D. and Paul, D.R., *Macromolecules,* **37**, 7698 (2004)

4-34 Kyotani, M. and Mitsuhashi, S., *J. Polym. Sci., Part A2,* **10 (8)**, 1497 (1972)

4-35 Gurato, G., Fichera, A., Grandi, F.Z., Zannetti, R. and Canal, P., *Makromol Chem,* **175 (3)**, 953 (1974)

4-36 Campoy, I., Gomez, M.A. and Marco, C., *Polymer,* **39 (25)**, 6279 (1998)

4-37 Tadmor, Z. and Gogos C.G., Principles of Polymer Processing. SPE Monorgaphs. New York: Wiley; (1979)

4-38 Gilman, J.W., Harris Jr, R.H., Shields, J.R., Kashiwagi, T. and Morgan, A.B., *Polym. Adv. Technol.,* **17**, 263 (2006)

4-39 Costache, M.C., Wang, D., Heidecker, M.J., Manais, E. and Wilkie, C.A., *Polym. Adv. Technol.,* **17**, 272 (2006)

4-40 Jang, B.N., Costache, M. and Wilkie, C.A., *Polymer,* **46**, 10678 (2005)

4-41 Guyot, A., *Polym Degrad Stab* **15**, 219 (1986)

4-42 McNeill, I.C. and Stevenson, W.T.K., *Polym Degrad Stab* **10**, 247 (1985)

4-43 Guaita, M., Chiantore, O. and Costa, L., *Polym Degrad Stab* **12**, 315 (1985)

4-44 Jang, B.N. and Wilkie, C.A., *Polymer,* **46 (9)**, 2933 (2005)

4-45 Jang, B.N. and Wilkie, C.A., *Polymer,* **46**, 3264 (2005)

4-46 Dussel, H.J., Rosen, H. and Hummel, O., *Makromol. Chem.,* **177**, 2343 (1976)

4-47 Levchik, S.V., Weil, E.D. and Lewin, M., *Polym. Int.,* **48**, 532 (1999)

4-48 Davis, R.D., Gilman, J.W. and VanderHart, D.L., *Polym. Degrad. Stab.,* **79** 111 (2003)

4-49 Bourbigot, S., Duquesne, S. and Jama, C., *Macromol. Symp.,* **233**, 180 (2006)

5. Covalent Binding of Modified Organoclay

The objective of this chapter was to consider covalent binding of modified nanoclays within an UP matrix. This has been studied through the synthesis of a series of vinyl-functionalised alkylammonium and phosphonium cations and methacrylate-functionalised phosphonium-organomodifiers, which have been chosen to include a vinyl (C=C) functionality on the salt. It was expected that the double bond on the salt would be involved in polymerisation along with simple radical polymerisation involving styrene in the unsaturated polyester resin. Therefore, polymerisation could occur in the clay gallery, "tethering" or linking the polymer to the clay surface by a covalent bond to the ammonium or phosphonium cation. The improvement in thermal stability and clay dispersion in the resulting composites have been evaluated using X-ray diffraction (XRD), thermogravimetric analysis (TGA) and in some cases thermogravimetry coupled with mass spectrometry (TG-MS).

Firstly Na^+ Cloisite was modified using the alkylammonium cations decyltrimethylammonium (DTA^+) and ω-decyltrimethylammonium (ω-DTA^+) at different percentages of the CEC. XRD, TGA and TG-MS were utilised to study what effect organocation deficiencies and excesses would have on the physical properties and thermal decomposition of the products.

Secondly the thermal stability of phosphonium-MMT compared to ammonium-MMT was investigated through the synthesis of a triphenylphosphonium and a trimethylammonium cation with a chain length of $C_n = 10$ (ω-$TP10^+$ and ω-DTA^+, respectively). It was anticipated that the vinyl group (CH_2=CH-) on the surfactant tail would be available for polymerisation in the unsaturated polyester.

Thirdly the covalent binding of modified organoclay into the UP matrix was investigated through the synthesis of a series of methacrylate functionalised phosphonium-organomodifiers with increasing chain length ($C_n = 3$ to $C_n = 10$), to maintain/improve the mechanical strength of the nanocomposite, if the addition of clay impaired the normal cross link density of the UP.

Thermosetting polymers, such as polyesters and epoxies exhibit several useful characteristics due to the high degree of cross-linking between individual polymer chains. Superior properties, coupled with ease of processing have led to numerous applications of these polymers [5-1]. Unfortunately cross-linking makes these materials inherently brittle with poor resistance to crack initiation and propagation. Recently it has been demonstrated that the addition of nanometer sized fillers such as Al_2O_3 can be used to significantly enhance the mechanical properties of thermosetting unsaturated polyesters [5-2].

Montmorillonite (MMT) is commonly used as a nanometer sized filler. The efficiency of MMT in improving the properties of a polymeric material is primarily determined by its degree of dispersion in the polymer matrix. However, the hydrophilic nature of the MMT surface impedes homogenous dispersion in many organic polymer phases. To overcome this problem, it is often necessary to make the clay surface organophilic prior to use, through ion-exchange reactions involving the exchange of cationic surfactants for the interlayer cations. The role of the organic cation is to reduce the surface energy of the MMT, to reduce the platelet-platelet attraction and improve the wetting characteristics for an organic polymer [5-3].

5.1   Uptake Isotherms of DTA^+ and ω-DTA^+ on Na^+ Cloisite

For the purposes of initial experiments Na^+ Cloisite was modified using the alkylammonium cations DTA^+ and ω-DTA^+. The organoclay samples prepared for the uptake isotherm experiments will be referred to with respect to their organocation species (Table 5–1).

Table 5–1 Sample Identification for alkylammonioum exchanged Na^+ Cloisite

Organic Component	Abbreviation for Salt	Abbreviation for Cation	Abbreviation when exchanged onto Na^+ Cloisite
decyltrimethylammonium Bromide, $C_n = 10$	DTAB	DTA^+	DTA-MMT
ω-decyltrimethylammonium Bromide, $C_n = 10$	ω-DTAB	ω-DTA^+	ω-DTA-MMT

Na^+ Cloisite was modified at different percentages of the CEC (Table 5–2), to study what effect organocation deficiencies and excesses would have on the physical properties and thermal decomposition of the products. DTA^+ and ω-DTA^+ were compared to evaluate any differences in thermal decomposition upon addition of a terminal double bond on the salt, into the system. The exchanged amounts for ω-DTA^+ were virtually identical to the exchanged amounts for DTA^+.

Table 5–2 CEC Exchange Mass, Example: Organocation = DTA^+ ($C_n = 10$)

Mass of Clay (g)	CEC of Clay	Multiples of CEC	RMM DTAB (g)	Mass Required of DTAB (g)
1	0.925	0.25	280.30	0.065
1	0.925	0.5	280.30	0.13
1	0.925	1	280.30	0.26
1	0.925	1.5	280.30	0.39
1	0.925	2	280.30	0.52

5.1.1 DTA-MMT and ω-DTA-MMT Preparation

Na^+ Cloisite was suspended in deionised water (10g clay in 100 ml of H_2O), in a 250 ml beaker. The clay slurry was mixed for 1 hour to swell the clay galleries with water. The calculated mass of decyltrimethylammonium salt was then pre-dispersed in 50 ml deionised water, added to the beaker, covered and stirred for 24 hr. These samples were repeatedly washed with deionised water until the conductivity fell below 50 μS and then centrifuged at 17,000 rpm for 1 hr. After the washing process the clays were air dried for 48 hours, the thermal decomposition of the organic species, resulting from a Hoffman degradation process was monitored using TGA, TG-MS, and the expansion of the clay was studied using XRD.

5.1.2 XRD Analysis of DTA-MMT and ω-DTA-MMT

DTA-MMT

ω-DTA-MMT
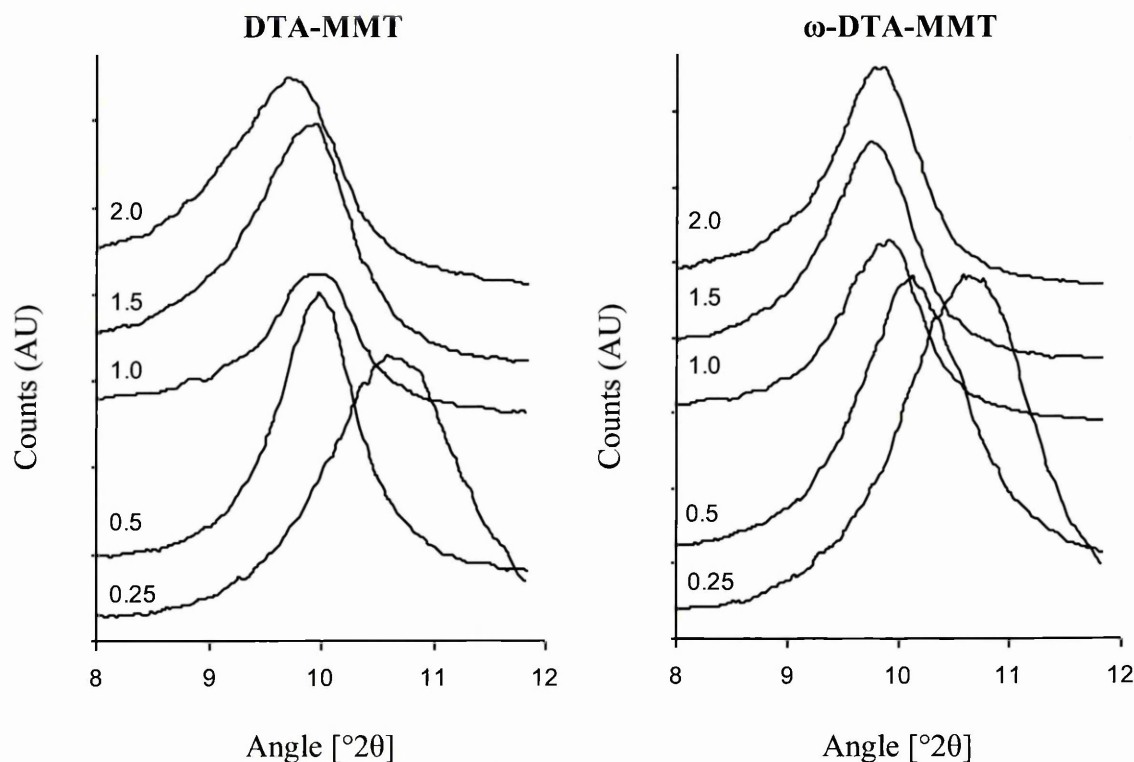
Figure 5–1 XRD traces (Cr-tube) for DTA$^+$ and ω-DTA$^+$ exchanged Na$^+$ Cloisite– Traces are offset for clarity

The XRD traces presented in Figure 5–1 were obtained from DTA$^+$ and ω-DTA$^+$ exchanged Na$^+$ Cloisite. The maximum d_{001} spacing was reached at 1.0 times the CEC. After this loading the d_{001} spacing did not fluctuate significantly. Table 5–3 presents the d_{001} spacings for DTA-MMT and ω-DTA-MMT at each concentration ($\pm$ 0.2 Å).

Table 5–3 d_{001} spacings for DTA-MMT and ω-DTA-MMT

	d_{001}-Spacing (Å)	
% CEC	DTA-MMT	ω-DTA-MMT
0	12.1	12.1
0.25	12.2	12.2
0.5	13.0	12.9
1.0	13.1	13.1
1.5	13.1	13.3
2.0	13.4	13.2

Figure 5–2 depicts the increase in d-spacing as DTA^+ enters the gallery. The distance between one dehydrated clay layer and another is 9.6 Å, and as the clay becomes hydrated the d-spacing expands to 12.5 Å (as in Na^+ Cloisite). After exchange with DTA^+, Na^+ and H_2O were replaced as illustrated in Figure 5–2, and the d-spacing increased to 13.4 Å, therefore confirming that the alkyl chain lies parallel to the basal surface. If the alkyl chain was not parallel to the basal surface and was radiating away from the silicate layers, then the d-spacing would be larger. The hydrated clay gallery was expanded by approximately 1 Å after exchange with DTA^+ and ω-DTA^+ cations. However, the expansion due to the DTA^+ cation is $13.4 - 9.6$ Å = 3.8 Å.
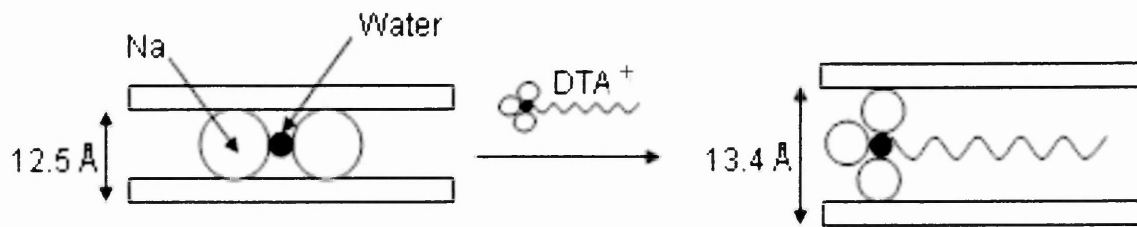
Figure 5–2 Diagram representing the increase in d-spacing when DTA^+ enters the gallery.

Uptake curves (Figure 5–3), which were determined using weight loss data from TG traces (using a temperature ramp of 20 °C min^{-1}), confirmed that both surfactants readily replaced the Na^+ cations in the gallery. When 1 CEC of modifier was introduced approximately 90-96% of the Na^+ ions were displaced, there was good agreement between the data obtained under both air and nitrogen.
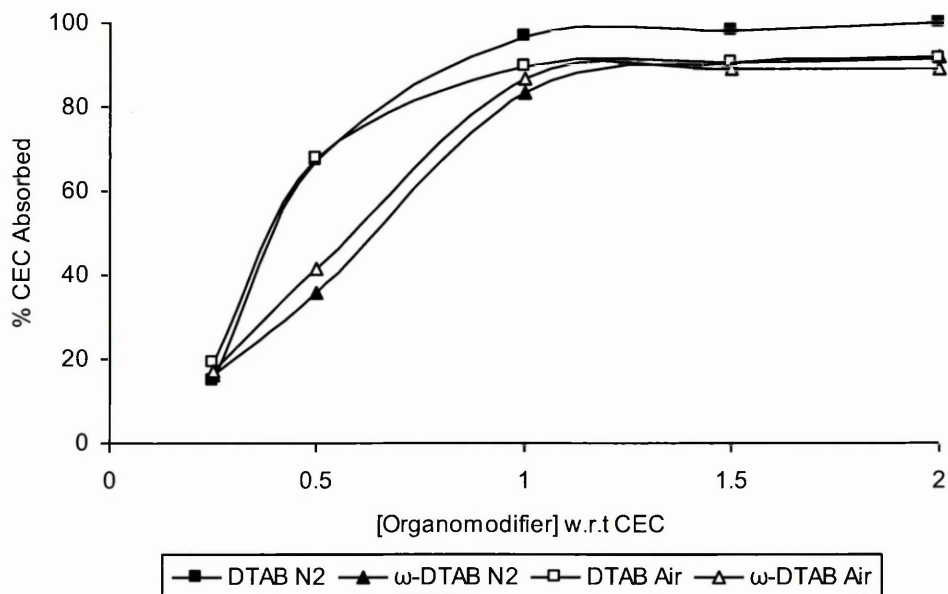
Figure 5–3 Uptake curve showing percentage CEC adsorbed against the concentration of organomodifier (w.r.t CEC) available in original solution.

5.1.3   TGA Analysis of DTA-MMT and ω-DTA-MMT in Air
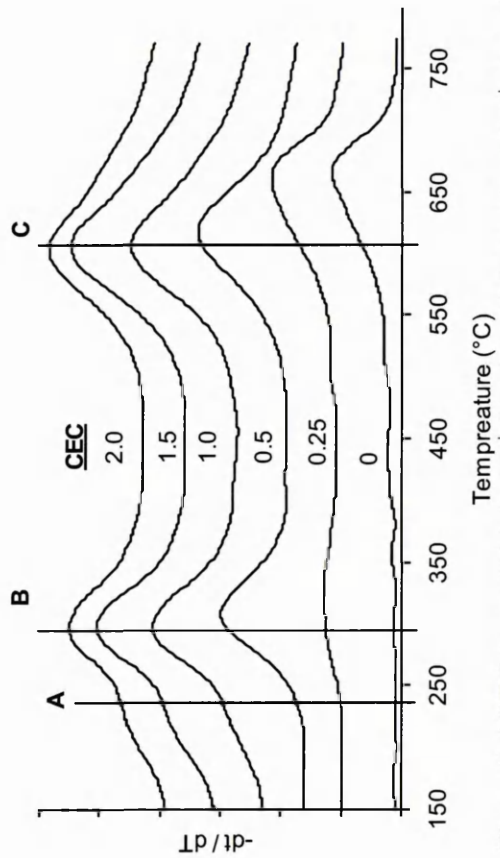
Figure 5–4 DTG traces (Air) for Na$^+$ Cloisite with increasing DTA$^+$ content
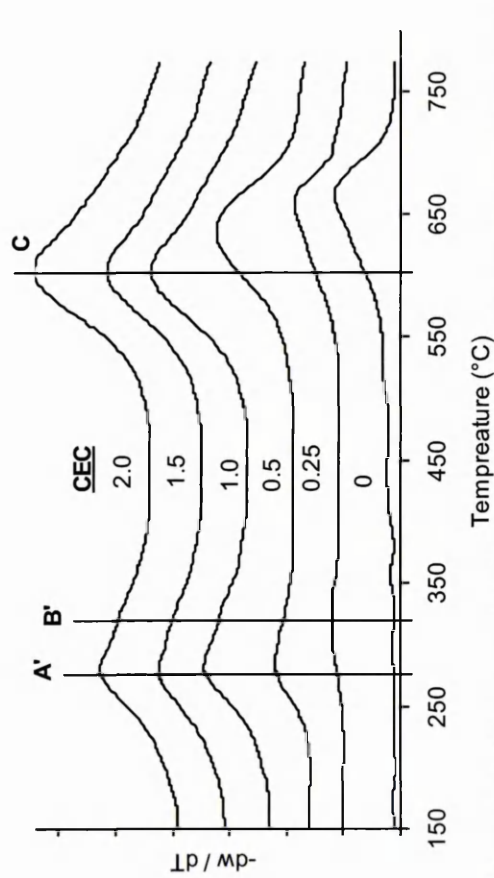
Figure 5–5 DTG traces (Air) for Na$^+$ Cloisite with increasing ω-DTA$^+$ content
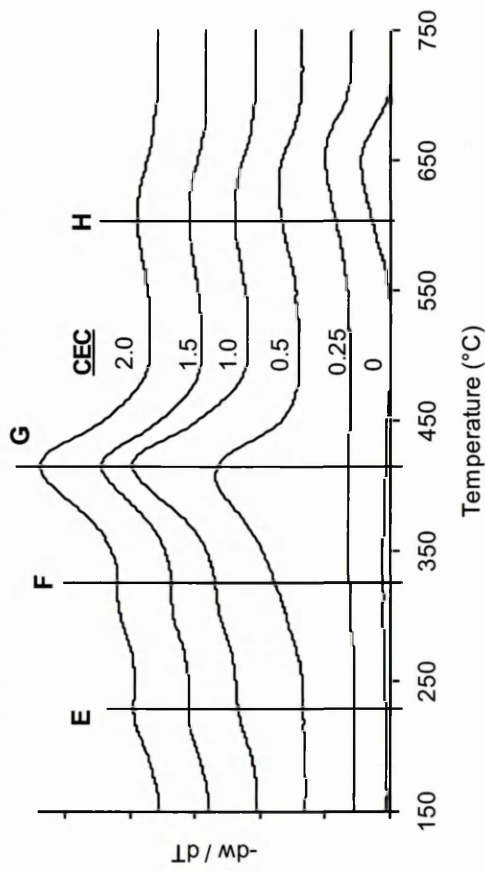
Figure 5–6 DTG traces (N$_2$) for Na$^+$ Cloisite with increasing DTA$^+$ content
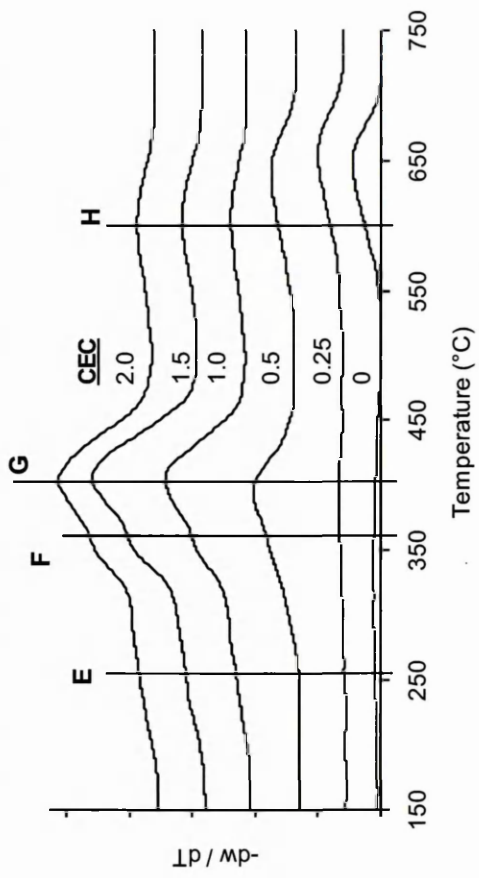
Figure 5–7 DTG races (N$_2$) for Na$^+$ Cloisite with increasing ω-DTA$^+$ content

216

The derivative thermograms (DTG) presented in Figure 5–4 to Figure 5–7 demonstrated several thermal desorption events, which could be grouped into temperature ranges within which the thermal desorption maxima varied, 35-150 °C, 151-430 °C and above 431 °C. An assignment of the events occurring within these temperature ranges, verified later using TG-MS are displayed in Table 5–4.

Table 5–4 Assignment for desorption maxima in DTG traces occurring within specific temperature ranges

Desorption Temperature (°C)	Assignment
35 - 150	evolution of physisorbed water
151 - 430	decomposition of organocations producing aliphatic species, ring compounds, ammonia, water and CO_2
> 431	clay dehydroxylation and CO_2 evolution

The DTG traces presented in Figure 5–4 are for DTA-MMT, prepared at 0 to 2 x the CEC, collected in air. Three temperature maxima (T_{max}) in the decomposition process (A, B and C) were displayed, decomposing over three stages. During stage 1 (35-150 °C) the alkylammonium chains were relatively stable and so small weight losses were attributed to thermal desorption of trapped water molecules. Stage 2 occurred over the range 150-430 °C and represents the decomposition of alkylammonium chains. T_{max} (A) occurred at 241 °C and T_{max} (B) occurred at 302 °C. Stage 3 occurred over the range of 431–800 °C and displayed T_{max} (C), at 610 °C and represents the decomposition of the carbonaceous char layer formed upon oxidation and some clay dehydroxylation. The DTA^+ sample prepared at 0.25 x CEC displayed a similar decomposition profile to Na^+ Cloisite (trace with % CEC = 0), in which clay dehydroxylation occurred with a T_{max} at 670 °C.

The DTG traces presented in Figure 5–5 are for ω-DTA-MMT, prepared at 0 to 2 x the CEC, collected in air. The DTG curves also displayed three maxima in the decomposition process (A', B' and C), decomposing over three stages ((1) 35-150 °C (2) 151-430 °C and (3) 431-800 °C). T_{max} (A') occurred at 285°C and T_{max} (B') occurred at 323 °C. T_{max} (B') however, occurred after the main decomposition event, T_{max} (A'), whereas the peak under T_{max} (A) in DTA^+ exchanged Na^+ Cloisite (Figure 5–4), was

217

before the main decomposition peak, T_{max} (B). T_{max} (C) occurred at 670 °C in the samples prepared using ω-DTA$^+$ at 0.25 and 0.5 x CEC, and represents clay dehydroxylation at a similar temperature to Na$^+$ Cloisite and could indicate a lower loading of ω-DTA$^+$ associated with the clay.

Table 5–5 Comparison of the weight losses for DTA-MMT and ω-DTA-MMT calculated under air

Desorption Temperature Ranges - Air				
DTA-MMT	35-150 °C (peak A) (%)	151-430 °C (peak B) (%)	431-800 °C (peak C) (%)	Total (%)
0	5.2	1.1	4.9	11.2
0.25	7.4	2.0	5.8	15.2
0.5	1.8	5.8	11.4	18.9
1.0	0.8	7.9	13.5	22.1
1.5	1.0	8.1	13.5	22.5
2.0	0.8	8.3	13.5	22.6
ω-DTA-MMT	35-150 °C (peak A') (%)	151-430 °C (peak B') (%)	431-800 °C (peak C) (%)	Total (%)
0	5.2	1.1	4.9	11.2
0.25	6.2	1.9	5.3	13.4
0.5	4.9	3.3	8.9	17.2
1.0	0.7	6.2	14.3	21.2
1.5	0.8	6.6	14.5	21.9
2.0	1.0	6.5	14.7	22.2

Weight losses across the whole temperature range appeared relatively constant when DTA$^+$ and ω-DTA$^+$ were exchanged at 1.0 to 2.0 x CEC, however differences were observed in the samples prepared at 0.25 and 0.5 x CEC (Table 5–5). The weight loss between 35 and 150 °C was higher in the 0.25 CEC sample compared to the 0.5 CEC sample and was due to water associated with the un-exchanged Na$^+$ ions. Over the temperature range 181-450 °C the samples prepared at 1.0-2.0 x CEC appeared fully loaded as the weight loss remained constant in this region. Over the temperature range 451-800 °C, decomposition of the carbonaceous char occurred and was highest in samples prepared at 1.0, 1.5 or 2.0 x CEC. The total weight loss displayed a steady increase following the pattern 0 < 0.25 CEC < 0.5 CEC < 1.0 CEC ≤ 1.5 CEC ≤ 2.0 CEC.

5.1.4 TGA Analysis of DTA-MMT and ω-DTA-MMT in Nitrogen

The DTG traces presented in Figure 5–6 are for samples prepared using DTA$^+$ and collected in nitrogen. Four maxima in the decomposition process (E, F, G and H) occurred, decomposing over three stages. During stage 1 (35-150 °C) the alkylammonium chains were relatively stable and so small weight losses were attributed to adsorbed water being thermally desorbed. Stage two occurred over the temperature range 151-515 °C, and incorporated peaks E, F and G. Peaks E and F were present as shoulders of the main decomposition peak G and exhibited T_{max} (E) and T_{max} (F) at 234 °C and 327 °C, respectively. Peaks E and F evolved before the main decomposition peak G. Decomposition of the alkylammonium chains occurred between 151 °C and 515 °C and displayed a T_{max} (G) at 418 °C. Stage three occurred over the range 516-800 °C and incorporated Peak H, which displayed T_{max} (H) at 612 °C. Peak H represents the decomposition of the char formed upon organocation decomposition and some clay dehydroxylation. Weight loss in this region was much smaller under nitrogen, compared to air, because the non-oxidative decomposition (pyrolysis) occurring under nitrogen, leads to higher proportions of gaseous products and smaller quantities of char. No weight loss associated with the decomposition of the alkylammonium chains was apparent in the 0.25 CEC DTA-MMT sample, however the T_{max} at 655 °C is characteristic of clay dehydroxylation.

The DTG curves for ω-DTA$^+$ under nitrogen presented in Figure 5–7 also displayed four maxima in the decomposition process (E, F, G and H), decomposing over three stages. Stage one (35-150 °C) represents the thermal desorption of adsorbed water molecules. Stage two (decomposition of the alkylammonium chains) occurred over the temperature range 151-515 °C and incorporated peaks E, F and G. Peaks E and F were present as shoulders on the main decomposition peak G and exhibited T_{max} (E) and T_{max} (F) at 255 °C and 367 °C, respectively. Peaks E and F evolved before the main decomposition peak G (T_{max} (G) = 409°C). Stage three occurred over the range 516-800 °C and incorporated Peak H, which displayed a T_{max} at 605 °C.

Table 5–6 Comparison of the weight losses for DTA-MMT and ω-DTA-MMT calculated under N₂

Desorption Temperature Ranges – N₂							
Stage 1					Stage 2	Stage 3	
DTA-MMT	35-150 °C (%)	151-260 °C (peak E) (%)	261-350 °C (peak F) (%)	351-515 °C (peak G) (%)	150-515 °C (%)	516-800 °C (peak H) (%)	Total (%)
0	5.4	0.4	0.7	0.6	1.7	2.6	9.7
0.25	6.5	0.4	0.6	1.6	2.6	4.8	13.9
0.5	2.2	0.5	2.0	8.6	11.1	5.2	18.5
1.0	0.9	1.2	3.1	11.1	15.4	4.4	20.7
1.5	0.9	1.6	3.3	1.8	16.6	4.5	21.1
2.0	1.1	1.7	3.3	11.0	16.0	4.5	21.6

Stage 1			Stage 2	Stage 3	
ω-DTA-MMT	35-150 °C (%)	151-300 °C (peak E) (%)	301-515 °C (peak F and G) (%)	150-515 °C (%)	516-800 °C (peak H) (%)	Total (%)
0	5.4	0.7	1.0	1.7	2.6	9.7
0.25	7.3	0.8	2.1	2.9	5.2	15.4
0.5	4.8	0.6	5.6	6.1	4.9	15.8
1.0	0.7	1.8	11.7	13.4	4.6	18.8
1.5	0.9	1.9	12.5	14.4	4.3	19.7
2.0	0.8	2.1	12.3	14.4	4.4	19.5

When analysed under nitrogen the sample weight loss across the whole temperature range appeared relatively constant when DTA^+ and $\omega\text{-}DTA^+$ were exchanged onto Na^+ Cloisite at 1.0 to 2.0 x CEC with a minor increase as the % CEC offered increased. However differences were observed in the 0.25 and 0.5 x CEC samples (Table 5–6). Weight losses between 35 and 150 °C were higher in the 0.25 and 0.5 x CEC sample compared to the 1.0, 1.5 and 2.0 x CEC samples, and was attributed to the loss of water associated with the remaining Na^+ cations. The total weight loss displayed a steady increase following the pattern $0 < 0.25$ CEC < 0.5 CEC < 1.0 CEC ≤ 1.5 CEC ≤ 2.0 CEC.

5.1.5 TG-MS Analysis of DTA-MMT and ω-DTA-MMT

The decomposition temperature of organoclays controls the upper processing temperature and subsequent thermal stability of polymer-clay nanocomposite materials. A more complete knowledge of the decomposition pathway was important because desorption products evolving at lower temperatures in an organoclay's thermal desorption profile may have a role in the thermal decomposition of the hybrid material. The thermal decomposition of the different organoclay series may be briefly summarised in three distinct regions: (region I) < 150 °C, evolution of adsorbed water, (region II) 150-500 °C, desorption of organic species, (region III) 500-800 °C, dehydroxylation of the aluminosilicate layer and the evolution of products associated with residual organic carbonaceous residue. After a survey of the possible species arising from the alkylammonium cations in contact with the clay surface, the decomposition products were identified and separated into 3 categories (Table 5–7):

Table 5–7 Assignment of TG-MS decomposition products

Category	Assignment Group
1	Water [m/z = 18], and CO_2 [m/z = 44]
2	Linear aliphatic species: Alkyls [m/z = 43, 57, 71, 85] Alkenyls [m/z = 41, 55, 69, 83]
3	Ring Compounds (See Table 5–8)

DTA^+ and ω-DTA^+ modified Na^+ Cloisite were analysed using thermogravimetry coupled with mass spectrometry (TG-MS), at 0.5 and 1.5 times the CEC, in order to compare partially loaded clay with fully loaded clay. An ATI Unicam Automass System 2 quadrupole mass spectrometer was used, and the mass spectra of the gases evolved during the heating process, using a Cahn TG131 thermobalance were collected. The MS was operated in the electron impact (EI), positive ionisation mode. The samples were introduced into the TG-MS instrument at 30 °C and the temperature then ramped at 20 °C/min until 800 °C. The samples were run under nitrogen and the evolved gases transported along a transfer line at 200 °C to the mass spectrometer and analysed.

Several ions, which are representative of the major decomposition products arising from DTA$^+$ and ω-DTA$^+$ were investigated. The major ions in decane and decene were compared for both DTA-MMT and ω-DTA-MMT prepared at 0.5 and 1.5 times the CEC as well as other ions that are common to dienes and cyclic species such as 77, 78 and 79 (Table 5–8).

Table 5–8 Fragment ions for the major decomposition/rearrangement products arising from DTA- and ω-DTA-MMT

m/z ratio	Assignment	Structure
77	1,3-cyclohexadiene and 1-methylcyclohexene	
78	benzene	
79	1,3-cyclohexadiene and 1-methylcyclohexene	
81	1-methylcyclohexene	
82	1-cyclohexene	
91 + 92	Toluene, ethylbenzene	
95	methylbromide	CH_3Br
96	1-methylcyclohexene	
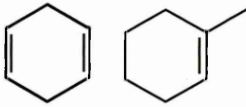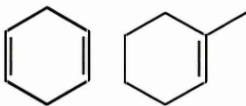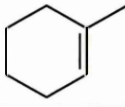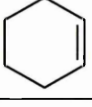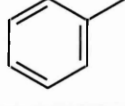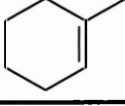
5.1.5.1 Decomposition Ions from DTA-MMT and ω-DTA-MMT

The ions presented in Figure 5–8 (i and ii) incorporate ion 58 representing the -NMe$_3$ head group and ions 138, 140 and 142, which represent the mass ions for C10 diene, C10 alkene and C10 alkane, respectively. Figure 5–8 (iii) and (vi) presents ion 78, which was characteristic of benzene, ion 91, which represented toluene and xylene and ions 95, 106 and 120 which represented methyl bromide (from CH$_3$ decomposing from the head group and combining with free Br in the sample), dimethylbenzene and trimethylbenzene, respectively. No differences occurred in the decomposition pathways between ion 106 (dimethylbenzene) and ion 120 (trimethylbenzene) in either DTA- or ω –DTA-MMT and so these ions have not been displayed. MS identified a proportion of the species desorbed from the organoclay to be cyclic species, evolving as a result of (1) Hoffman degradation of the organocation forming alkene and trimethyl amine moieties, (2) intramolecular reactions or "back biting" mechanisms which occurred on the alkenyl chain. The alkenes then react on the acid-sites on the clay surface resulting in the formation of many new species, Table 5–9 displays the possible decomposition pathways for ions arising from the DTA$^+$ cation.

Table 5–9 Possible decomposition and rearrangement mechanisms for species derived from DTA$^+$. The balancing H$_2$ molecules have been omitted.

-NCH$_3$

Double bond migration and/or isomerisation/ cyclisation.

-CH$_2$NCH$_3$

-(CH$_2$)$_2$NCH$_3$
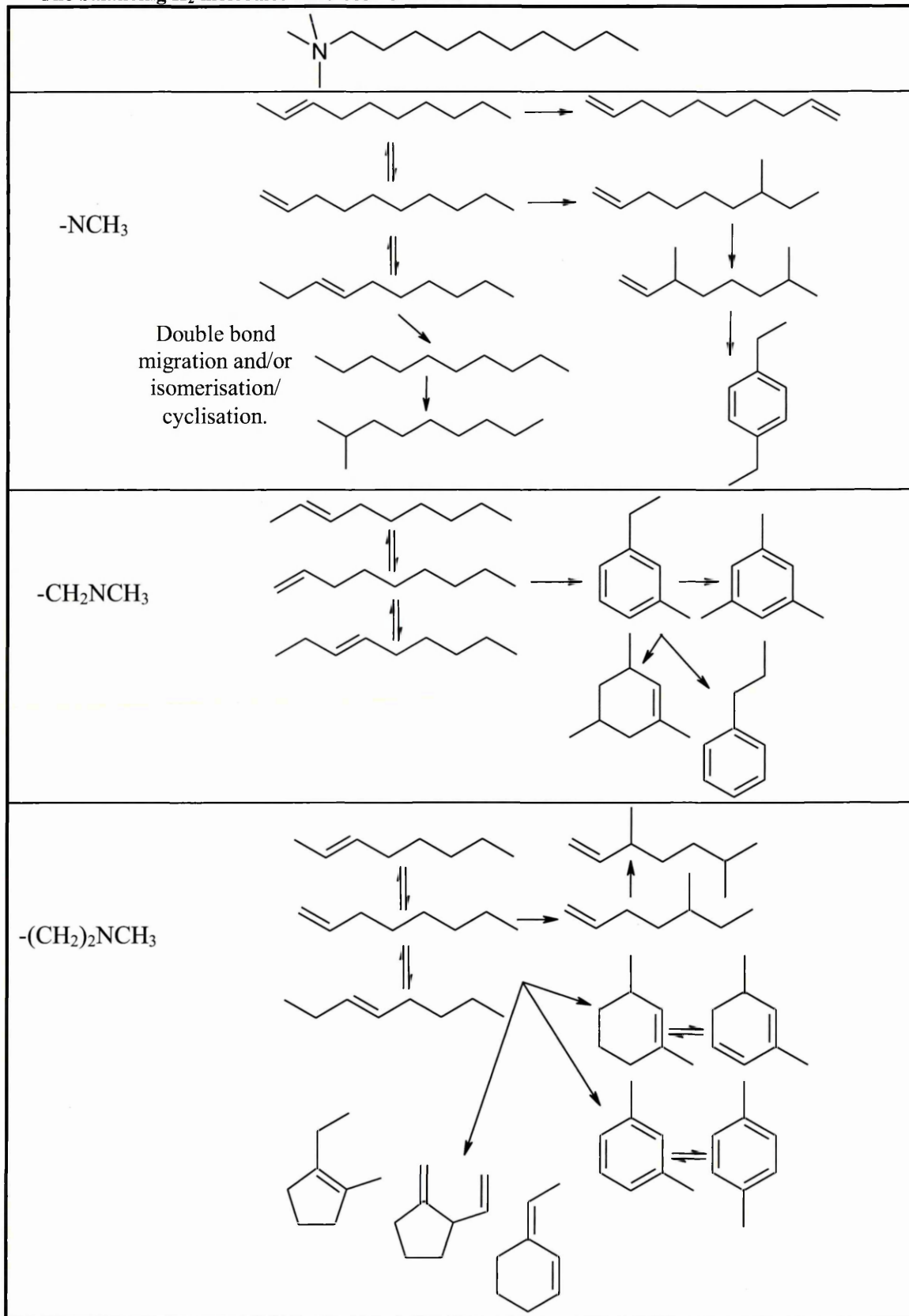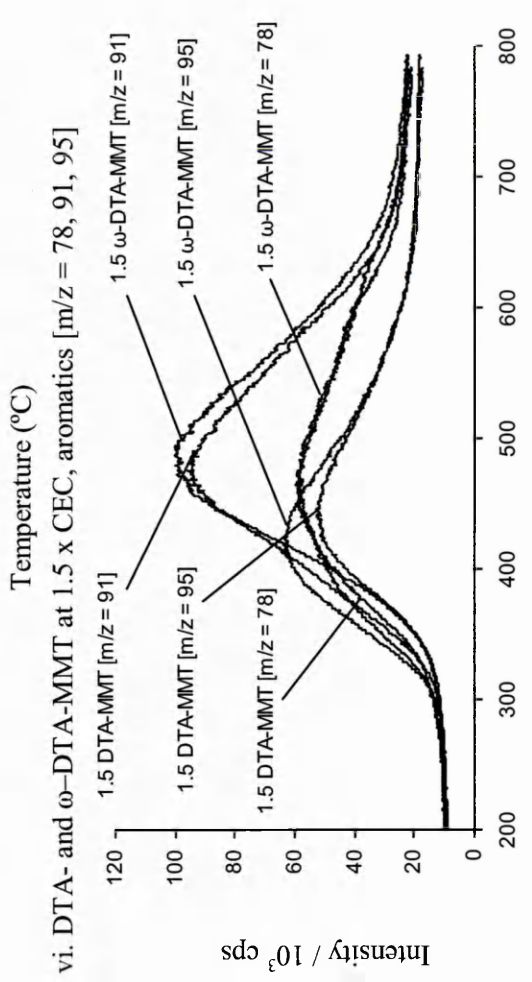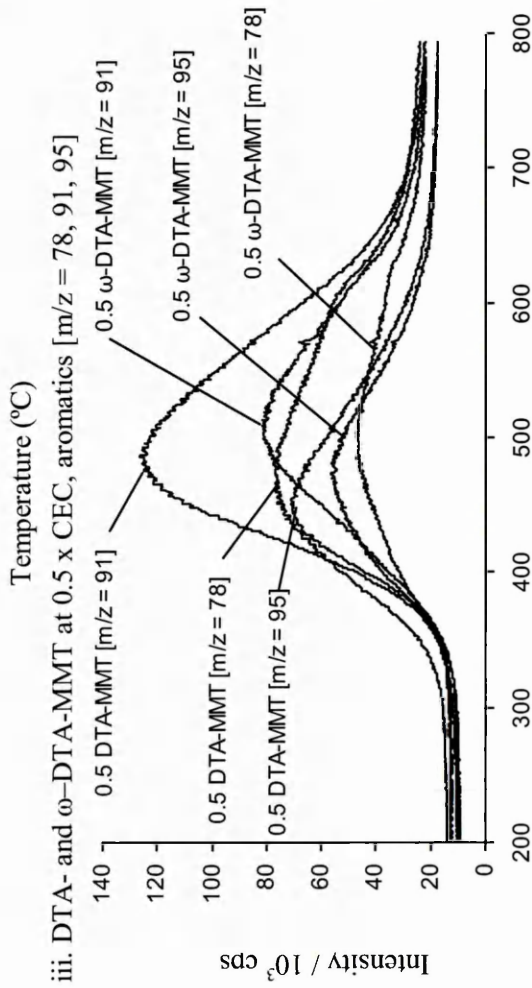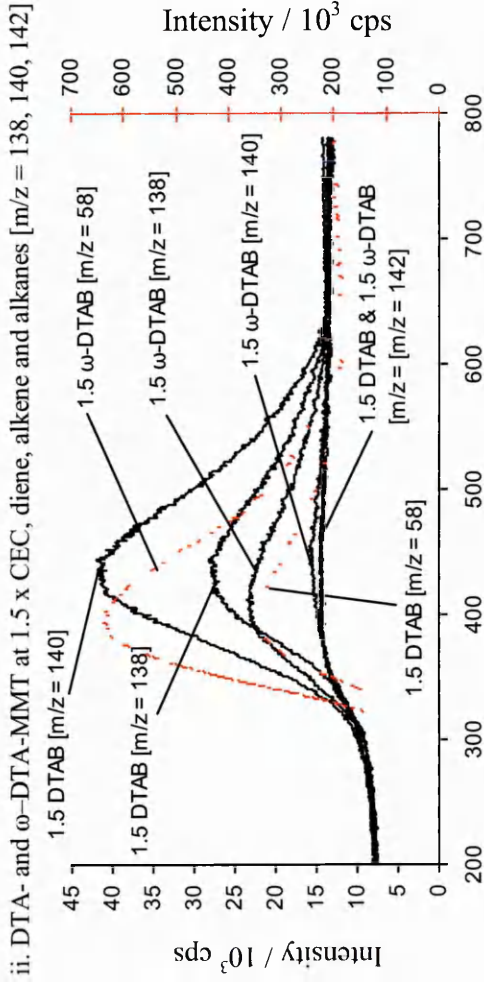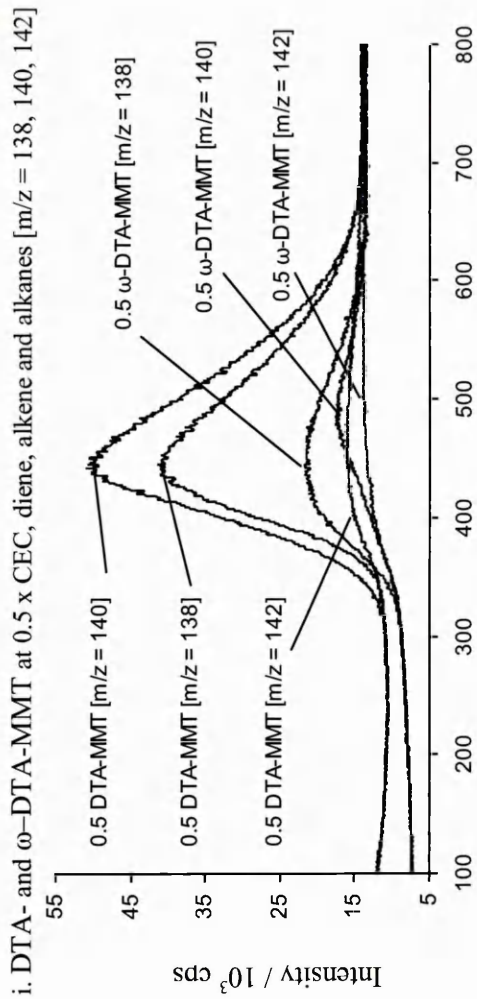
Figure 5–8 Comparison of the temperature dependence of the evolution of selected aliphatic and aromatic species from DTA^+ and $\omega-DTA^+$ at 0.5 and 1.5 x CEC on Na^+ Cloisite.

5.1.6 Aliphatic Hydrocarbons Evolved from DTA-MMT and ω-DTA-MMT

5.1.6.1 Diene [m/z = 138], Alkene [m/z = 140] and Alkane [m/z = 142]

When the intensity ratio of diene/alkene (i.e m/z = 138 : m/z = 140) was studied it was found that a greater proportion of diene evolved from ω-DTA-MMT than DTA-MMT. The ratio of diene/alkene in ω-DTA-MMT was approximately 1.5 compared to 0.7 in DTA-MMT, based on the relative intensities of m/z 138 to m/z 140. In DTA-MMT, ions 138 and 140 had the same T_{max}, however in ω-DTA-MMT the diene preceded the alkene. In DTA- and ω-DTA-MMT the ion count indicated that there was more alkene than alkane in both samples. In samples prepared at 1.5 x CEC, the Me_3N head group (m/z = 58) was detected before ions 138 and 140 (Figure 5–8 ii (lines in red)), and the intensity of ion 58 in ω-DTA-MMT was almost double that of ion 58 in DTA-MMT.

5.1.6.2 Ring Compounds

The majority of secondary species (identified from a comprehensive database search) desorbed from DTA- and ω-DTA-MMT were identified by MS as ring compounds (Table 5–8). Desorption of ring compounds in the 0.5 x CEC samples (Figure 5–8 iii) occurred at a lower temperature and were more intense in DTA-MMT compared to ω-DTA-MMT. The onset temperature at which degradation began (T_{onset}) occurred at the same temperature (300 °C) in all samples. Benzene [m/z = 78] displayed larger concentrations than other ring compounds across the temperature range 300-400 °C in the 0.5 DTA-MMT sample. Above 400 °C the intensity/concentration of toluene [m/z = 91] dominated the evolved spectra. The plot for benzene [m/z = 78] contained two events characterised by a lower T_{max} at 465 °C and a higher T_{max} at 600 °C. This two step evolution occurred in all samples, however, this behaviour was not fully understood but could be due to the occurrence of competing decomposition processes. The intensity of the toluene peak [m/z = 91] was revealed to be at least double that of any other species evolved.

The spectra representing samples prepared using 0.5 x CEC, displayed two temperature maxima for the evolution of the ring compounds [m/z = 91 and 78]. Toluene [m/z = 91] and benzene [m/z = 78] occurred under a T_{max} of 490 °C for the 0.5 DTA-MMT samples and 510 °C for the ω-DTA-MMT samples. Methyl bromide [m/z = 95] occurred under a T_{max} of 450 °C in the 0.5 DTA-MMT samples and 490 °C in the 0.5 ω-DTA-MMT samples.

In comparison, the ring compounds in the spectra collected from samples prepared using 1.5 x CEC, were represented by one temperature maxima, which occurred at 490 °C for toluene [m/z = 91] and benzene [m/z = 78] in both the 1.5 DTA- and ω-DTA-MMT samples. Methyl bromide [m/z = 95] demonstrated a T_{max} at 425 °C for DTA-MMT and 450 °C for ω-DTA-MMT.

5.1.7   Comparison Summary for the Analysis of DTA$^+$ and ω-DTA$^+$ Exchanged Na$^+$ Cloisite

5.1.7.1 Comparison Summary of XRD and TGA Data for DTA$^+$ and ω-DTA$^+$ Exchanged Na$^+$ Cloisite

The basal spacings for Na$^+$ Cloisite exchanged with DTA$^+$ and ω-DTA$^+$ at 0.25-2.0 x CEC displayed in Table 5–3, indicated that expansion of the gallery occurred when exchanged at 0.5-2.0 x CEC. The total weight loss from standard 10 mg samples increased as the loading of DTA$^+$ or ω-DTA$^+$ on the clay increased with respect to the CEC (i.e. 1.0 x, etc.), and the maximum total weight loss for DTA- and ω-DTA-MMT occurred at 2.0 x CEC (Table 5–10), although they were almost identical to those for samples prepared at 1.5 x CEC.

Table 5–10 Comparison of total %wt loss for DTA-MMT and ω-DTA-MMT at 0.25 – 2.0 x CEC

N$_2$		Air	
DTA$^+$	Total wt loss (%)	DTA$^+$	Total wt loss (%)
0	9.7	0	11.2
0.25	13.9	0.25	15.2
0.5	18.5	0.5	18.9
1.0	20.7	1.0	22.1
1.5	21.1	1.5	22.5
2.0	21.6	2.0	22.6
ω-DTA$^+$	Total wt loss (%)	ω-DTA$^+$	Total wt loss (%)
0	9.7	0	11.2
0.25	15.4	0.25	13.4
0.5	15.8	0.5	17.2
1.0	18.8	1.0	21.2
1.5	19.7	1.5	21.9
2.0	19.5	2.0	22.2

The weight loss at <150 °C decreased from 0.25 to 0.5 x CEC but remained constant between 1.0 and 2.0 x CEC (Table 5–5 and Table 5–6), which was believed to be due to the loss of water associated with the surfactant's cationic head groups. The decomposition products from the alkylammonium cations were desorbed within the temperature range of 150-515 °C when run under N$_2$ and 150-450 °C when run under air. Under air and N$_2$ at 0.25 x CEC, the majority of the weight loss occurred under the T$_{max}$ at 60 °C, however at 0.5 to 2.0 x CEC the majority of the thermally desorbed products were evolved under the T$_{max}$ at 430 °C under N$_2$ and 620 °C under air. Under N$_2$, weight loss at temperatures >515 °C was attributed to dehydroxylation of the clay and CO$_2$ evolution and remained relatively constant throughout the series of samples, at ~ 4.5 wt%.

5.1.7.2 Comparison Summary of TG-MS Data for DTA$^+$ and ω-DTA$^+$ Exchanged Na$^+$ Cloisite

Samples prepared using DTA$^+$ at 0.5 x CEC demonstrated the evolution of ions 138 and 140 at the same temperature. The intensity of the peak for toluene [m/z = 91] was greater than that of the peaks for benzene [m/z = 78] and methyl bromide [m/z = 95]. Samples prepared using DTA$^+$ at 1.5 x CEC and ω-DTA$^+$ at 0.5 and 1.5 x CEC, exhibited ion 138 preceding ion 140, and an increased intensity for toluene [m/z = 91] compared to benzene [m/z = 78] and methyl bromide [m/z = 95]. At 1.5 x CEC, the

-NMe$_3$ head group (m/z = 58) was detected before ions 138 and 140, and the intensity of ion 58 in ω-DTA-MMT was almost double that of ion 58 in DTA-MMT. These experiments demonstrated that the intensity of ion 138 > ion 140 for ω-DTA-MMT and was a positive confirmation that the terminal double bond was available for cross linking reactions.

5.2 The Thermal Stability of Phosphonium (TP10$^+$) Compared to Ammonium (DTA$^+$) Exchanged Na$^+$ Cloisite

The use of phosphonium salts as organic modifiers in layered silicates may further enhance the thermal properties of polymer nanocomposites. To provide a better understanding of the thermal behaviour of phosphonium salts and their modified montmorillonites (P-MMT), the thermal stability of a phosphonium modified (n-decyl triphenylphosphonium bromide (TP10B) and ω-decyl triphenylphosphonium bromide (ω-TP10B) MMT was compared with ammonium modified (n-decyl trimethylammonium bromide (DTAB) and ω-decyl trimethylammonium bromide (ω-DTAB)) MMT (Table 5–11). ω-DTAB and ω-TP10B were not commercially available and were therefore synthesised in-house (ω-DTAB was synthesised by a colleague). After exchange the clays were fully characterised using XRD and TGA. It was expected that the vinyl group (CH$_2$=CH-) on the end of the surfactant tail of ω-DTAB and ω-TP10B would be available for polymerisation in the unsaturated polyester.

Table 5–11 Organocation structures
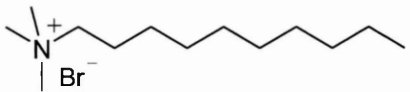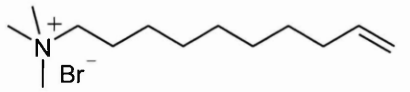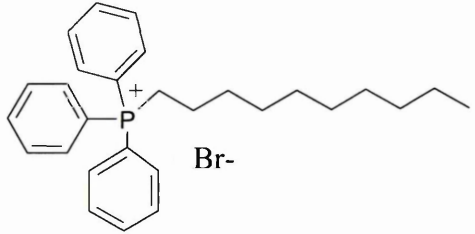
DTAB – RMM - 200.3	ω-DTAB – RMM – 198.3
TP10B – RMM - 483	ω-TP10B – RMM - 481
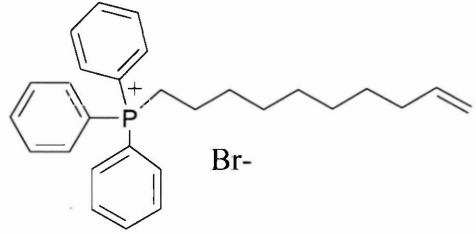
5.2.1 Synthesis of ω-decyl triphenylphosphonium bromide (ω-TP10B)

ω-decyl triphenylphosphonium bromide was not available commercially and so was synthesised in the laboratory. This was achieved using 10-bromo-1-decene and triphenylphosphine:
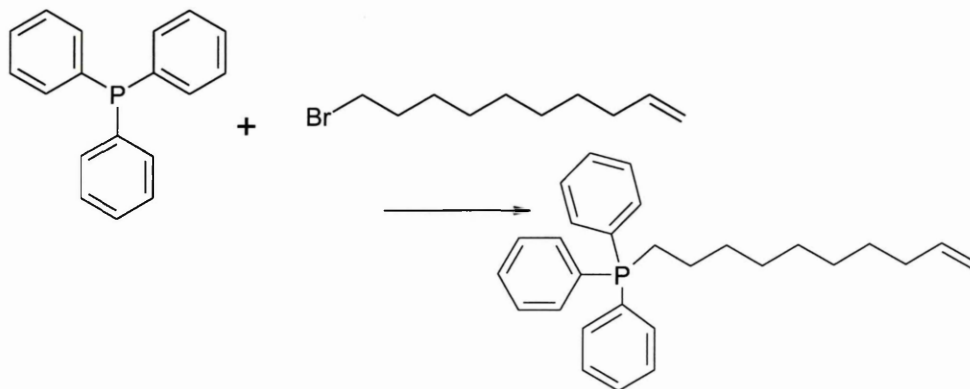
2.62 g of triphenylphosphine and 2.4 g 10-bromo-1-decene were combined in a round bottomed flask and refluxed under an atmosphere of nitrogen for 8 hours, in a heated water bath. An oily residue was produced, which was dissolved in dichloromethane (DCM) (25 ml) and then triturated three times in ether (25 ml), the ether was removed on a rotary evaporator leaving a glassy compound with a weight of ~ 2g. ω-TP10B was then dissolved in 80:20 H_2O:MeOH and exchanged onto Na^+ Cloisite at 1 x CEC using the exchange procedure outlined in section 5.1.1.

5.2.2 XRD Analysis of DTA$^+$, ω-DTA$^+$, TP10$^+$ and ω-TP10$^+$ Exchanged Na$^+$ Cloisite
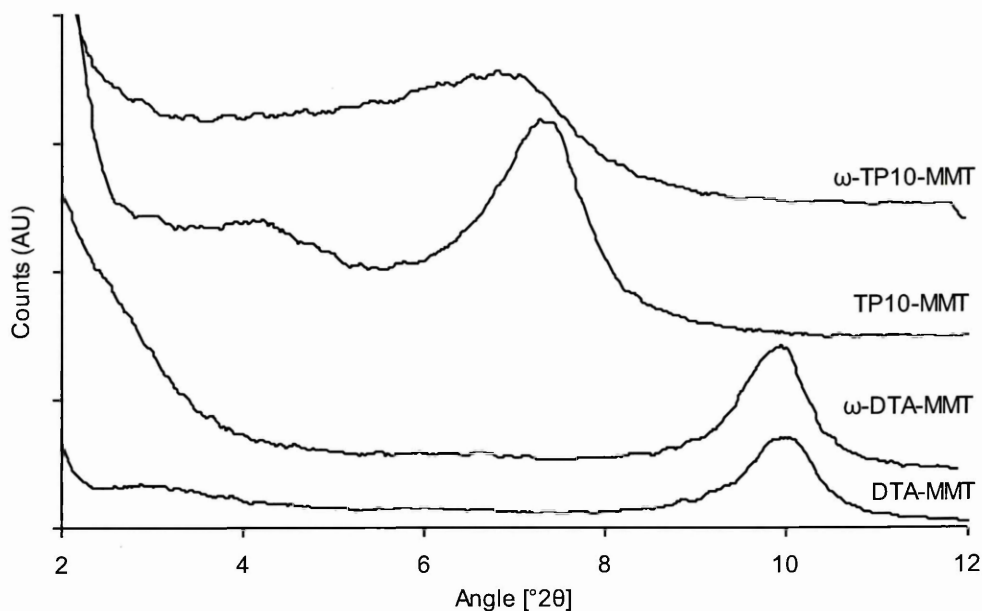
Figure 5–9 XRD traces (Cr tube) for DTA$^+$, ω-DTA$^+$, TP10$^+$ and ω-TP10$^+$ exchanged Na$^+$ Cloisite – Traces are offset for clarity.

The XRD traces presented Figure 5–9 display DTA$^+$, ω-DTA$^+$, TP10$^+$ and ω-TP10$^+$ exchanged Na$^+$ Cloisite at 1 x CEC. An increase in the d$_{001}$ spacing occurred from 12.5 Å in Na$^+$ Cloisite to 13.1 Å in DTA-, 13.1 Å in ω-DTA-, 17.7 Å in TP10- and 18.9 Å in ω-TP10-MMT. The larger d-spacing for TP10-MMT can be attributed to the bulkier PPh$_3$ head group expanding the clay layers further than the Me$_3$N head group.

5.2.3 TGA Analysis of DTA$^+$, ω-DTA$^+$, TP10$^+$ and ω-TP10$^+$ Exchanged Na$^+$ Cloisite
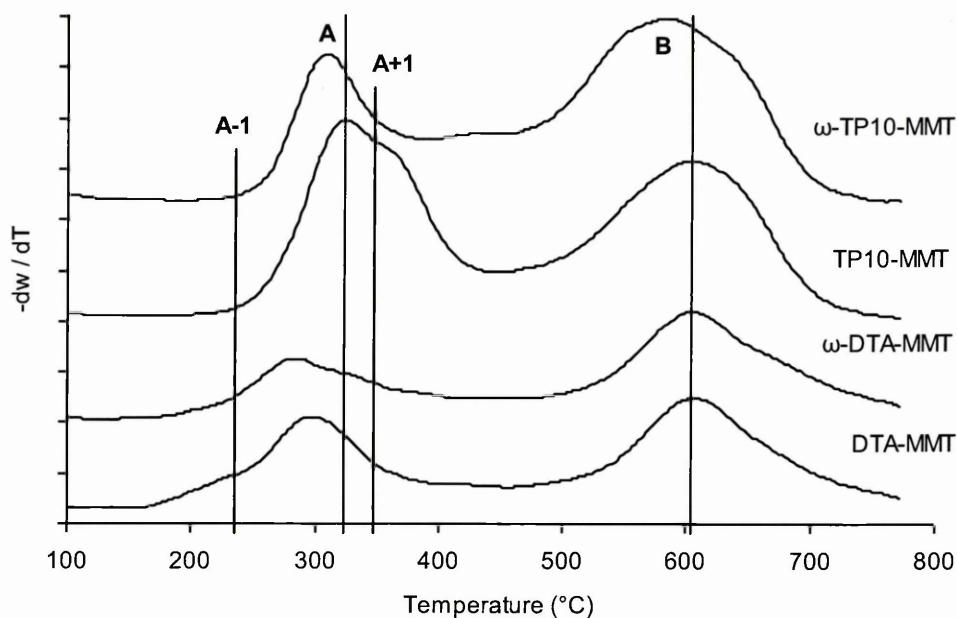
Figure 5–10 DTG traces (Air) for DTA$^+$, ω-DTA$^+$, TP10$^+$ and ω- TP10$^+$ exchanged Na$^+$ Cloisite – Traces are offset for clarity.

The DTG traces presented in Figure 5–10 display the results for DTA-, ω-DTA-, TP10- and ω- TP10-MMT. Two maxima in the decomposition process (A and B) occurred, decomposing over two stages. Below 200 °C, the alkylammonium and phosphonium species were thermally stable, and so, weight loss could be attributed to physically adsorbed water being thermally desorbed. Stage 1 occurred between 200 and 450 °C and was representative of the decomposition of the alkylammonium and phosphonium cations from the Cloisite galleries, T_{max} (A) occurred during stage 1 at 302, 288, 330 and 313 °C for DTA-, ω-DTA-, TP10- and ω-TP10-MMT, respectively. A shoulder occurred for TP10-MMT (T_{max} A+1), after the main decomposition peak (A) at 351 °C and a shoulder occurred for DTA-MMT (T_{max} A-1) before the main decomposition peak (A) at 240 °C. Stage 2 occurred between 480 and 745 °C and was representative of clay dehydroxylation and the further decomposition of carbonaceous char formed upon oxidation, T_{max} (B) occurred during stage 2 at 612, 612, 607 and 586 °C for DTA-, ω-DTA-, TP10- and ω-TP10-MMT, respectively. TG analysis of the organoclays revealed that the onset of degradation for DTA-, ω-DTA-, TP10- and ω- TP10-MMT, were 169, 180, 222 and 229 °C, respectively.

5.2.4 Composites Prepared Using Crystic 189LV, DTA-, ω-DTA-, TP10- and ω-TP10-MMT

The samples displayed in Table 5–12 were mixed with Crystic 189LV at 1, 3 and 5 wt% at 1000 rpm for 15 minutes, accelerator E and catalyst M were used at 2 wt% each. Once cast the samples were postcured at room temperature for 24 hours, and then at 80 °C for 3 hours. All composites were characterised using XRD and TGA. Silent XRD traces were recorded, however this did not mean that an exfoliated composite had been produced, since organoclay particles were clearly visible in the films, therefore these XRD results have not been presented.

Table 5–12 Type of organoclay used and mixing regime adopted

Organomodifier	Organoclay Used (wt%)	Mixing Speed (rpm)	Mixing Time (min)
ω-TP10$^+$	1	1000	15
ω-TP10$^+$	5	1000	15
TP10$^+$	1	1000	15
TP10$^+$	3	1000	15
TP10$^+$	5	1000	15
DTA$^+$	1	1000	15
DTA$^+$	3	1000	15
DTA$^+$	5	1000	15
ω-DTA$^+$	1	1000	15
ω-DTA$^+$	5	1000	15

5.2.5 TGA Analysis of Composites Prepared Using Crystic 189LV, DTA-, ω-DTA-, TP10- and ω-TP10-MMT
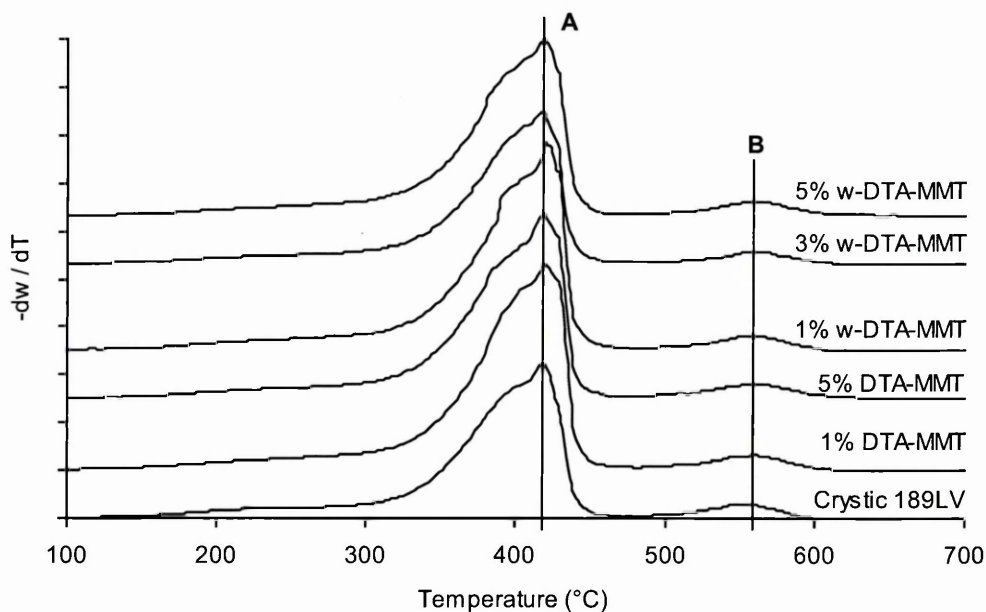
Figure 5–11 DTG traces (Air) for composites prepared using Crystic 189LV, DTA-MMT and ω-DTA-MMT – Traces are offset for clarity

The DTG traces presented in Figure 5–11 displayed two main thermal decomposition events, occurring over two stages. For all composites, T_{max} (A) occurred during stage 1 at 420 °C and T_{max} (B) occurred during stage 2 at 563 °C. Crystic 189LV also displayed two thermal decomposition events occurring over two stages, T_{max} (A) occurred during stage 1 at 420 °C and T_{max} (B) occurred during stage 2 at 556 °C. The increased decomposition temperature of peak B in the nanocomposite samples could be a degradation product that decomposes at a (marginally) higher temperature (e.g. the char that forms when organoclay and resin burns). The T_{onset} (calculated from TG data) for polymers containing 5 wt% organoclay occurred at 280°C decomposing over the range of 280-460°C, compared to the pristine polymer which displayed a T_{onset} of 300 °C, decomposing over the range of 300 – 460 °C.

The TG results for DTA-MMT and ω-DTA-MMT are in contrast with the results obtained by Zhang [5-4] *et al.*, who observed an improvement of 19 °C in the thermal stability of their unsaturated polyester clay nanocomposites, incorporating cetyl trimethylammonium bromide (CTAB) modified montmorillonite as compared to the unsaturated polyester resin.
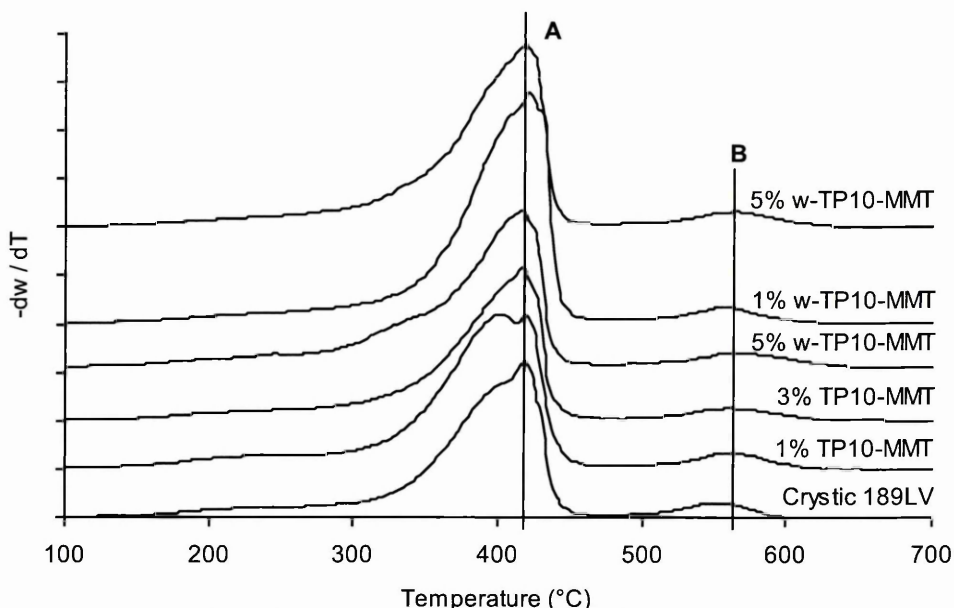
Figure 5–12 DTG traces (Air) for composites prepared using Crystic 189LV, TP10-MMT and ω-TP10-MMT – Traces are offset for clarity

The DTG traces for TP10- and ω-TP10-MMT presented in Figure 5–12 displayed the same decomposition maxima as the composites containing DTA-MMT and ω-DTA-MMT (Figure 5–11), with T_{max} (A) occurring at 420 °C and T_{max} (B) occurring at 563 °C. However, the T_{onset} at 5 wt% appeared to be 20 °C lower in the composite prepared using Crystic 189LV and TP10-MMT than in the sample made using ω-TP10-MMT.

The thermal stability of alkylammonium exchanged organoclay (DTA-MMT and ω-DTA-MMT) was investigated in comparison with alkylphosphonium exchanged organoclay (TP10-MMT and ω-TP10-MMT). Hussain and Simon [5-5] attempted to improve the flame retardancy of tetraglycidyl diaminodiphenylmethane (TGDDM) epoxy resin by the addition of ammonium (octadecyl ammonium exchanged) and phosphonium exchanged nano clays. TGA experiments were performed and the onset of degradation of pure TGDDM commenced at 380 °C with the rate of degradation significantly increasing at 450 °C and a char yield (charred material formed upon decomposition of the samples) of 22 % at 600 °C. With the addition of 5% ammonium exchanged organoclay the char yield increased to 44-48% at 600 °C suggesting that the clay acts as a fire retardant by forming a barrier to degradation and stabilising the layer of char formed when the sample is burned. The addition of phosphonium exchanged organoclay resulted in an earlier onset of degradation at 350 °C with a char yield in the region of 42 – 44 %. Table 5–13 presents the thermal properties of Hussain and Simon's

epoxy resin and modified epoxy resin composites plus the thermal properties of DTA$^+$, ω-DTA$^+$, TP10$^+$ and ω-TP10$^+$ composites:

Table 5–13 Thermal properties of resins and modified organoclays

	Temp. at 10% Weight Loss (°C)	Char Yield %		
		400 °C	450 °C	600 °C
Pure TGDDM	400	90		22
5% Ammonium Clay - TGDDM	420	93		44
3% Phosphonium Clay - TGDDM	395	91		42
Pure Crystic 189LV	302		47	0
5% DTA-MMT in 189LV	318		51.5	7.5
5% ω-DTA-MMT in 189LV	310		50.5	9.5
5% TP10-MMT in 189LV	293		47	4
5% ω-TP10-MMT in 189LV	310		48	5

The results of Hussain and Simon correspond to the results obtained for DTA-MMT and TP10-MMT composites in the respect that the temperature at 10% weight loss was lower in the alkylphosphonium exchanged composites (TP10-MMT) as compared to the alkylammonium exchanged composite (DTA-MMT). The temperatures at 10% weight loss were 318 and 293 °C in composites containing DTA-MMT and TP10-MMT, compared to 420 and 395 °C in Hussain and Simons alkylammonium and alkylphosphonium composites. An unexpected decrease in the onset of degradation was also observed in the composites as compared to pure Crystic 189LV. The char yields at 600 °C for the alkylammonium composites (DTA-MMT and ω-DTA-MMT) were slightly higher (7.5–9.5 %) than the char yields for the alkylphosphonium composites (TP10-MMT and ω-TP10-MMT (4-5 %)), therefore the alkylphosphonium composites would display a higher total weight loss compared to the alkylammonium composites (Table 5–14). This would be expected as alkylphosphonium degradation products further react with aromatic carbon in the system to form a complex phosphorus-carbon structure [5-6] during stage 1 (T_{max} (A) of Figure 5–12), which then undergoes further decomposition during stage 2 (T_{max} (B)), resulting in an increased overall weight loss and lower char yields.

Table 5–14 Comparison of weight losses for Crystic 189LV composites containing 5 wt% DTA-MMT or TP10-MMT

		Stage 1	Stage 2	
	35-150 °C (%)	151-450 °C (%)	>450 °C (%)	Total (%)
Crystic 189LV	0.3	91.6	7.8	99.8
5% DTA-MMT	0.3	85.2	8.4	93.9
5% TP10-MMT	0.6	90.6	8.4	98.0

5.3   Covalent Binding of Modified Organoclays

The covalent binding of modified organoclay into the UP matrix was investigated through the synthesis of a series of methacrylate functionalised phosphonium-organomodifiers (section 5.3.1) with increasing chain length (C_n = 3 to C_n = 10), to maintain/improve the mechanical strength of the nanocomposite, if the addition of clay impaired the normal cross link density of the UP. It was anticipated that the reactive vinyl double bond at the end of the C_n chain or on the end of the methacrylate group would cross-link into the UP matrix. The modified organoclay was incorporated into the UP resin Crystic 189LV and the resulting nanocomposites evaluated for improvements in clay dispersion (XRD), thermal stability (TGA), and flame retardancy using an in-house version of the UL94 vertical burning test.

5.3.1   Synthesis of TP3MM, TP6MM, TP8MM and TP10MM

The methacrylate functionalised phosphonium-organomodifiers were synthesised, using the procedure outlined in section 5.3.2. They will be denoted as TP3MM (3 = C_3), TP6MM (6 = C_6), TP8MM (8 = C_8) and TP10MM (10 = C_{10}). The phosphonium-organomodifiers were characterised using ^{1}H and ^{13}P solution NMR spectroscopy (Bruker B-ACS 60, 200 MHz) and Mass Spectrometry (Hewlett Packard (agilent) 5988A GC/ MS System) (MS) operated in electron impact mode. Characterisation data obtained in the synthesis of these compounds are displayed in Table 5–15.
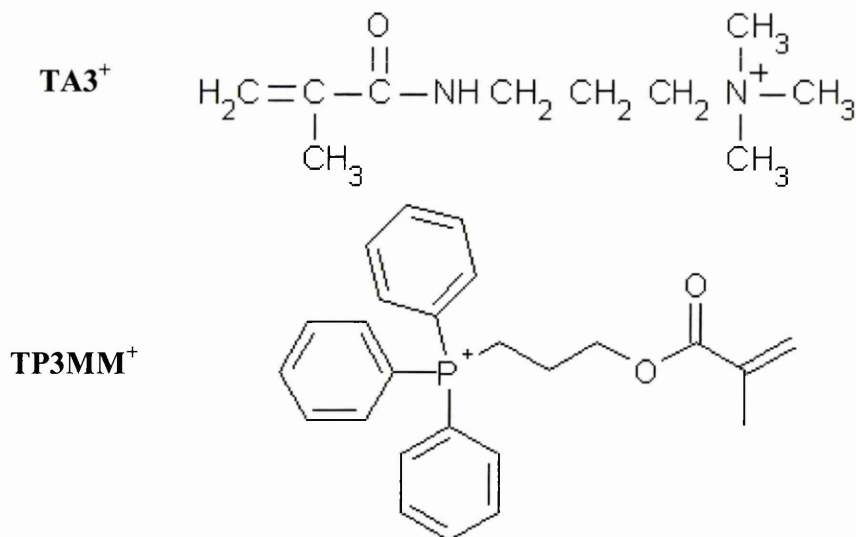
Figure 5–13 Structures of TA3$^+$ and TP3MM$^+$

Na$^+$ Cloisite was also exchanged with commercially available [3(methacryloylamino)propyl] trimethylammonium chloride (TA3) (Sigma Aldrich). Even though TA3 had a trimethylammonium head group as compared to a triphenylphosphonium head group (for TP3MM to TP10MM) it was hoped that the reactive vinyl double bond at the end of the methacrylate group would give an indication of how effective the synthesised compounds would be at cross-linking into the UP. The structures of TA3 and TP3MM are displayed in Figure 5–13.

5.3.2 Synthesis of TP3MM

Stage 1

- Triphenylphosphine (2.62g), 3-bromo-1-propanol (1.50g) and acetonitrile (~ 25 ml) were combined in a round bottomed flask. The mixture was then heated in an oil bath under reflux for 6 hours.

- The reaction progress was evaluated using thin layer chromatography (TLC) (10% MeOH in DCM as the running solvent). Triphenylphosphine and the reaction mixture were spotted parallel to each other and once triphenylphosphine was no longer visible in the reaction mixture, then the reaction was considered to be complete.

- A white crystalline solid was produced in 75% yield, which was washed twice in ether (25ml) and dried on a Buchner funnel.

Stage 2

- Methacrylic anhydride (~ 1.54g) was added to the salt produced in stage 1 and heated under reflux in an oil bath at 90 °C for 12 hours.

- The reaction progress was evaluated using TLC (10% MeOH in DCM as the running solvent). The salt from stage 1 was spotted parallel to the reaction mixture and once the salt was no longer visible in the reaction mixture, then the reaction was considered to be complete.

- A yellow oily product resulted, which was dissolved in DCM (25ml) and washed in a solution of sodium bicarbonate and water (40ml) using a separating funnel.

- The layers were separated. The bottom layer was run off and washed again in water.

- The layers were separated. The bottom layer was run into a beaker and dried with magnesium sulphate powder (1-2 g), filtered and washed again with DCM (25ml).

- The product was then checked using TLC (10% MeOH in DCM as the running solvent).

- Once washing was complete the DCM was removed on a rotary evaporator to leave an oily residue as the final product in 30% yield.

TP6MMBr, TP8MMBr and TP10MMBr were made using the same procedure as above, however the starting material 3-bromo-1-propanol was substituted with 6-bromo-1-hexanol, 8-bromo-1-octanol and 10-bromo-1-decanol, as appropriate.

Table 5–15 NMR and MS data for TP3- to TP10MMBr

	Starting Material	^{1}H NMR (ppm)	^{31}P NMR (ppm)	MS m/z (amu)
TP3MMBr	3-bromo-1-propanol	1.87 (t, 3H, CH_3), 3.99 (m, 2H, CH_2-O), 4.43 (m, 2H, CH_2=), 4.94 (s, 2H, CH_2-P), 5.54 (d, 1H, CH_2), 6.01 (s, 1H, CH_2), 7.81 (m, 15H, Ph_3P^+)	24.4	388.8
TP6MMBr	6-bromo-1-hexanol	1.95 (t, 3H, CH_3), 3.8 (m, 2H, CH_2-O), 4.08 (m, 2H, =CH_2), 5.5 (m, 1H, CH_2-P), 5.6 (m, 1H, CH_2-P), 5.81 (m, 4H, CH_2), 6.25 (m, 4H, CH_2), 7.86 (m, 15H, Ph_3P^+)	24.0	431.0
TP8MMBr	8-bromo-1-octanol	1.29 (m, 5H, CH_2), 1.63 (m, 5H, CH_2), 1.93 (m, 3H, CH_3), 3.75 (m, 2H, CH_2-O), 4.1 (m, 2H, CH_2=), 5.53 (m, 1H, CH_2-P), 5.63 (m, 1H, CH_2-P), 6.06 (m, 1H, CH_2), 6.2 (m, 1H, CH_2), 7.7 (m, 15H, Ph_3P^+)	24.3	438.3
TP10MMBr	10-bromo-1-decanol	1.25 (m, 9H, CH_2, CH_3), 1.65 (m, 6H, CH_2), 1.9 (s, 4H, CH_2), 3.88 (m, 2H, CH_2-O), 4.15 (q, 2H, =CH_2), 5.55 (m, 1H, CH_2-P), 6.05 (s, 1H, CH_2-P), 7.8 (m, 15H, Ph_3P^+)	24.3	487.6

NMR (^{1}H and ^{31}P) and MS were used to confirm the structure of TP3MMBr – TP10MMBr. MS data revealed the molecular ion peak for TP6MMBr, TP8MMBr and TP10MMBr and the (M-1)$^+$ peak for TP3MMBr, which were the expected molecular weights of the products. ^{31}P NMR displayed sharp peaks with chemical shifts of 24 ppm for all compounds, no other peaks were seen in the ^{31}P NMR confirming the formation of one single product. ^{1}H NMR was performed on all compounds, all spectra were clean of impurities and all expected peaks arising from the absorption of all protons were accounted for.

5.4 TA3-MMT and its Composites with Crystic 189LV

TA3$^+$, which was purchased as an aqueous solution was exchanged onto Na$^+$ Cloisite using the procedure outline in section 5.1.1. The modified organoclay was then pre-dispersed in DMMP and mixed with Crystic 189LV using the procedure outlined in section 3.4.2 of Chapter 3, using a mixing speed of 2000 rpm for 30 minutes.

5.4.1 XRD Analysis of TA3-MMT and its Composites with Crystic 189LV
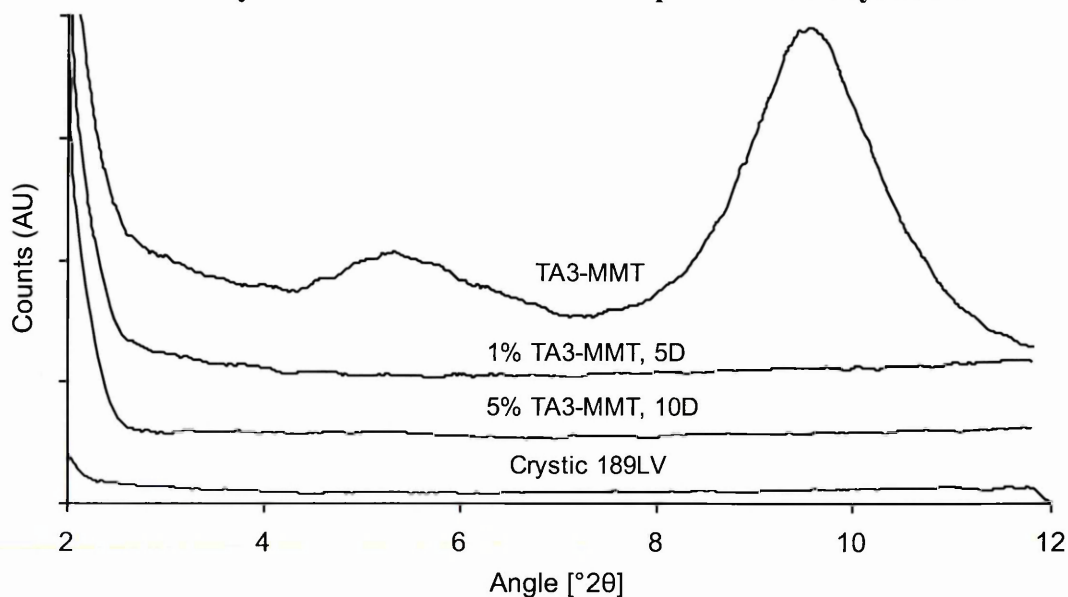
Figure 5–14 XRD traces (Cr tube) for TA3-MMT and Crystic 189LV composites containing 1 or 5 wt% TA3-MMT and 5 or 10 wt% DMMP (D) – Traces are offset for clarity

The XRD traces presented in Figure 5–14 display TA3-MMT and Crystic 189LV composites containing TA3-MMT and DMMP. TA3-MMT displayed promising evidence for an intercalated morphology as it exhibited a d-spacing of 13.5 Å, which is usual for a tetramethylammonium type head group. A smaller peak occurred with a d-spacing of 20.0 Å, which could indicate the formation of a mixed ion heterostructure as explained in detail in section 4.6.1 of Chapter 4. The XRD traces for Crystic 189LV composites containing TA3-MMT at 1 or 5 wt% with 5 or 10 wt% DMMP (D) appeared to be XRD silent, however, clay particles were clearly visible in the resin samples indicating the formation of a microcomposite. An exfoliated nanocomposite would display an increase in scattering at low angle, indicating disruption of the once ordered clay layers. However, a scattering profile, such as the one presented for the composites in Figure 5–14 could indicate that the clay stacks in the microcomposite are not aligned correctly (i.e. Figure 2.5 (e) of Chapter 2) and do not diffract.

5.4.2 TGA Analysis of TA3-MMT and its Composites with Crystic 189LV
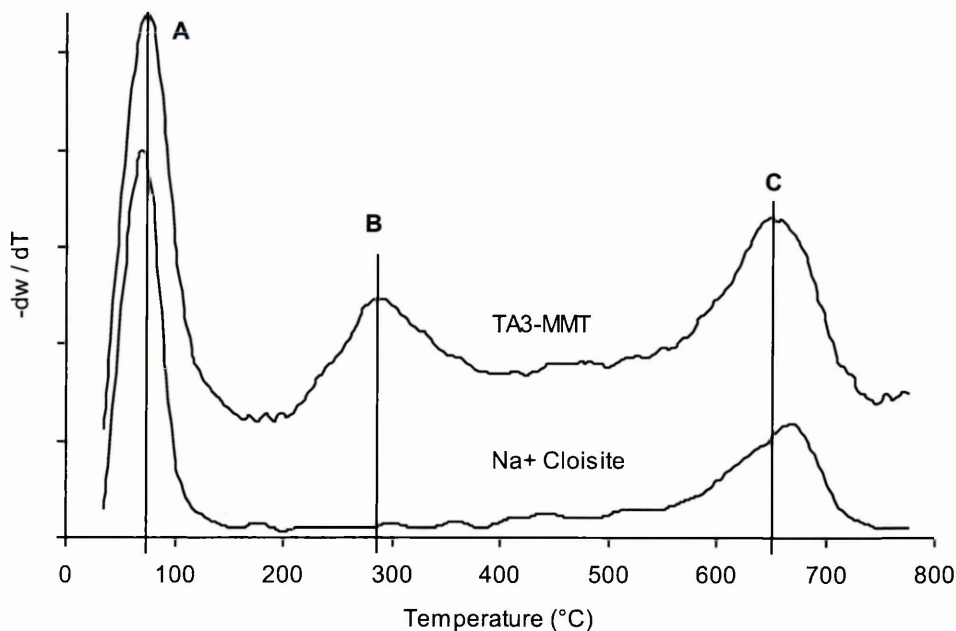
Figure 5–15 DTG traces (Air) for TA3-MMT and Na$^+$ Cloisite – Traces are offset for clarity

The DTG trace for TA3-MMT presented in Figure 5–15 displayed three thermal decomposition events, which were grouped into three temperature ranges 35-200 °C, 201-450 °C and above 451 °C, within which the thermal decomposition temperature maximum varied. An assignment of the events occurring within these temperature ranges were given in Table 5–4. T_{max} (A) occurred during stage 1 at 78 °C, T_{max} (B) occurred during stage 2 at 292 °C and T_{max} (C) occurred during stage 3 at 700 °C. The DTG trace for Na$^+$ Cloisite also presented in Figure 5–15 displayed two thermal desorption events, occurring over two stages, T_{max} (A) occurred during stage 1 at 78 °C and T_{max} (B) occurred during stage 3 at 675 °C.
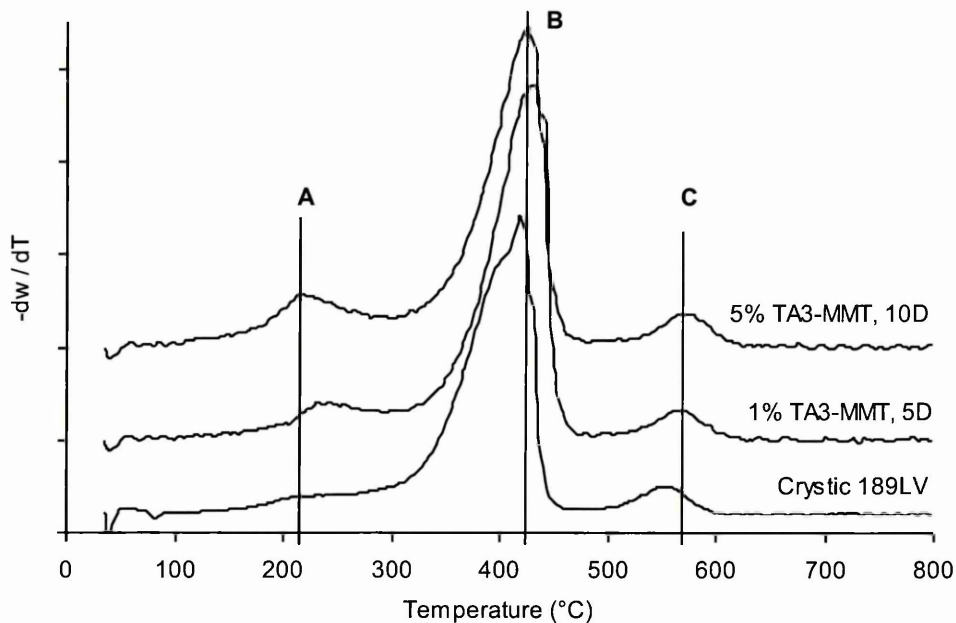
Figure 5–16 DTG traces (Air) Crystic 189LV composites containing 1 or 5 wt% TA3-MMT and 5 or 10 wt% DMMP (D) – Traces are offset for clarity

The DTG traces presented in Figure 5–16 for Crystic 189LV composites containing 1 and 5 wt% TA3-MMT and 5 or 10 wt% DMMP (D), displayed three main thermal decomposition maxima, occurring over three stages. Stage 1 occurred between 35 and 295 °C and represents the evolution of DMMP and absorbed water, stage 2 occurred between 296 and 495 °C and represents the decomposition of the resin and organocations and stage 3 occurred between 496 and 800 °C and represents decomposition of the carbonaceous char. T_{max} (A) occurred during stage 1 at 240 °C, T_{max} (B) occurred during stage 2 at 420 °C and T_{max} (C) occurred during stage 3 at 575 °C. Samples containing 1 wt% TA3-MMT demonstrated loss of DMMP at a higher temperature (T_{max} = 253 °C) compared with samples containing 5 wt% TA3-MMT (T_{max} = 220 °C). However, T_{max} (B) and T_{max} (C) remained the same in both samples at 430 and 575 °C, respectively. Crystic 189LV displayed T_{max} (B) in a similar position to the composites ±5 °C, however peak C was almost 20 °C lower. Table 5–16 compares the weight losses for Crystic 189LV composites containing TA3-MMT.

Table 5–16 Comparison of weight losses for Crystic 189LV composites containing 1 or 5 wt% TA3-MMT and 5 or 10 wt% DMMP

	Stage 1	Stage 2	Stage 3	
	35-295 °C (%)	296-495 °C (%)	>496 °C (%)	Total (%)
Crystic 189LV	9.5	83.3	6.7	99.6
1% TA3-MMT, 5D	12.0	79.1	6.7	97.6
5% TA3-MMT, 10D	16.7	65.7	7.4	89.6

The total weight loss for Crystic 189LV composites containing TA3-MMT was considerably smaller in the sample containing 5 wt% TA3-MMT compared to the sample containing 1 wt% TA3-MMT. The amount of clay added to the system was 5 wt% however, 10 wt% residue remained. This decrease in weight loss can be attributed to the increased amount of DMMP, which increased the amount of carbonaceous char formed during stage 2, which then underwent further decomposition during stage 3, resulting in an increase in the amount of carbonaceous residue remaining in the system.

5.5 Phosphonium-organomodified Clays

The synthesised organomodifiers TP3MM$^+$ - TP10MM$^+$, were all oily residues. These oily residues were dissolved in a mixture of 80:20 H_2O:MeOH and then exchanged onto Na$^+$ Cloisite using the procedure outline in section 5.1.1. The modified organoclays were then pre-dispersed in DMMP and mixed with Crystic 189LV using the procedure outlined in section 3.4.2 of Chapter 3 using a mixing speed of 2000 rpm for 30 minutes.

5.5.1 XRD Analysis of Phosphonium-organomodified Clays
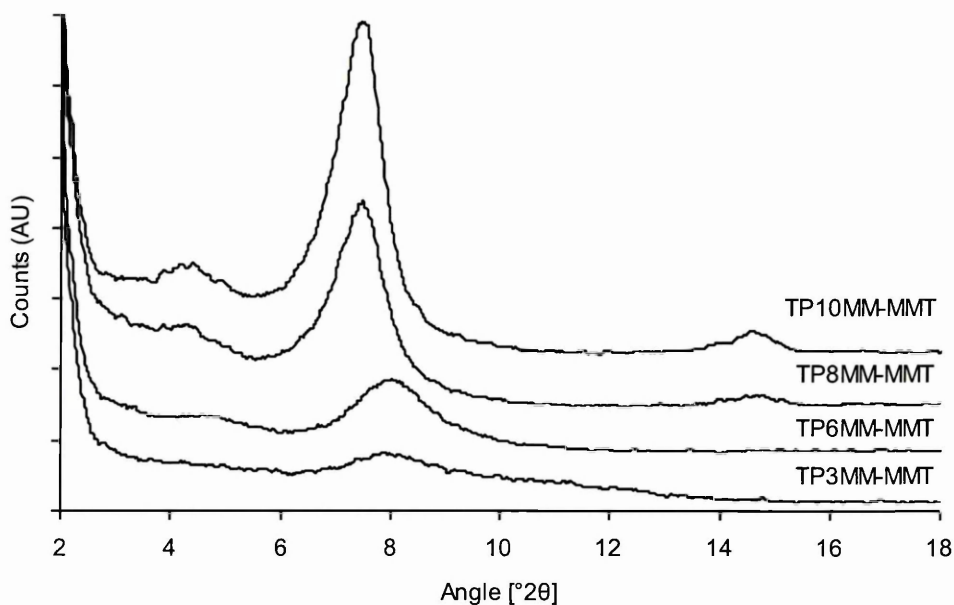
Figure 5–17 XRD traces (Cr tube) for the phosphonium-organomodified clays - TP3MM-, TP6MM-, TP8MM- and TP10MM-MMT – Traces are offset for clarity

The XRD traces presented in Figure 5–17 are for TP3MM-, TP6MM-, TP8MM- and TP10MM-MMT. All phosphonium-organomodified clays displayed an intercalated structure with TP8MM- and TP10MM-MMT displaying intense d_{001} and d_{002} peaks with spacings of 17.2 and 8.8 Å, respectively. TP3MM- and TP6MM-MMT displayed much weaker d_{001} spacings of 16.2 Å, which could possibly be due to poor loading of TP3MM$^+$ and TP6MM$^+$ onto Na$^+$ Cloisite. The smaller peaks at higher d-spacing (24.4 Å in TP3MM- and TP6MM-MMT and 30.1 Å in TP8MM- and TP10MM-MMT) indicated the possible formation of a mixed ion heterostructure as explained in detail in section 4.6.1 of Chapter 4.

5.5.2 TGA Analysis of Phosphonium-organomodified Clays
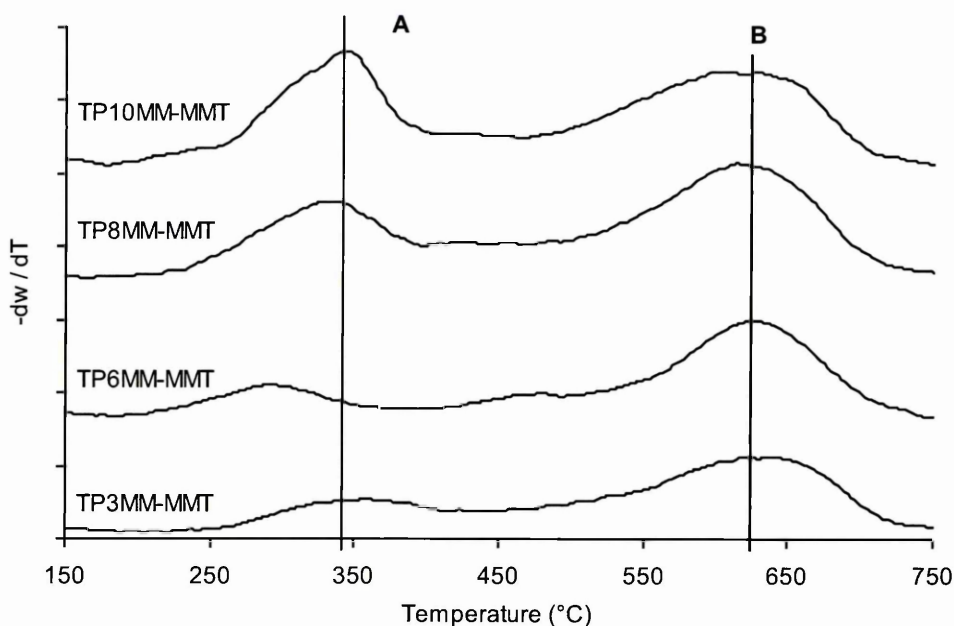
Figure 5–18 DTG traces (Air) for the phosphonium-organomodified clays - TP3MM-, TP6MM-, TP8MM- and TP10MM-MMT – Offset for clarity

The DTG traces presented in Figure 5–18 displayed two main thermal decomposition events, which were grouped into three temperature ranges 35-150 °C, 151-450 °C and 451 to 800 °C °C. An assignment of the events occurring within these temperature ranges are displayed in Table 5–4. T_{max} (A) occurred during stage 2 at 360, 295, 334 and 346 °C for TP3MM-, TP6MM-, TP8MM- and TP10MM-MMT, respectively. T_{max} (B) occurred during stage 3 at 630 °C for TP3MM- and TP6MM-MMT and 624 °C for TP8MM- and TP10MM-MMT. The DTG trace for TP10MM-MMT displayed a similar degradation pattern to that of TP10-MMT in Figure 5–10.

Table 5–17 Comparison of weight losses for TP_nMM-MMT, TP8-MMT, TP10-MMT, TA3-MMT and Na^+ Cloisite

	Stage 1	Stage 2	Stage 3	
	35-150 °C (%)	151-450 °C (%)	> 451 °C (%)	Total (%)
TP3MM-MMT	2.9	3.1	8.3	14.3
TP6MM-MMT	2.9	5.0	13.6	21.5
TP8MM-MMT	1.5	9.2	18.2	28.9
TP10MM-MMT	1.3	13.6	21.3	36.2
TP8-MMT	0.7	12.6	18.1	31.4
TP10-MMT	0.8	14.1	19.1	34.0
TA3-MMT	4.5	4.1	7.8	16.4
Na^+ Cloisite	5.4	1.0	4.8	11.2

246

Table 5–17 displays the weight losses for TP_nMM-MMT, TP8-MMT, TP10-MMT, TA3-MMT and those for Na^+ Cloisite have also been included for comparison. Below 200 °C water evolved from the samples, more water was associated with TP3MM- and TP6MM-MMT, although the loss of water from TA3-MMT and Na^+ Cloisite was 2-3 % greater than that of the TP_nMM-MMT series. Between 200 and 450 °C decomposition of TP_nMM^+ and TP_n^+ occurred. As the carbon chain length increased the weight loss in this region increased. This trend was also observed above 450 °C when clay dehydroxylation was also occurring. The weight losses for TP8- and TP10-MMT were similar to those for TP8MM- and TP10MM-MMT ± 2 wt%.

5.5.3 ATR FT-IR Analysis of Phosphonium-organomodified Clays

ATR FTIR was carried out on TP3MM-MMT, TP6MM-MMT and TP10MM-MMT, using the settings outlined in section 2.6.6.3 of Chapter 2. The spectra for TP6MM-MMT and TP10MM-MMT are displayed in Figure 5–19. The spectra for TP3MM-MMT exhibited the same peak positions and intensities as TP6MM-MMT and so it has not been displayed.
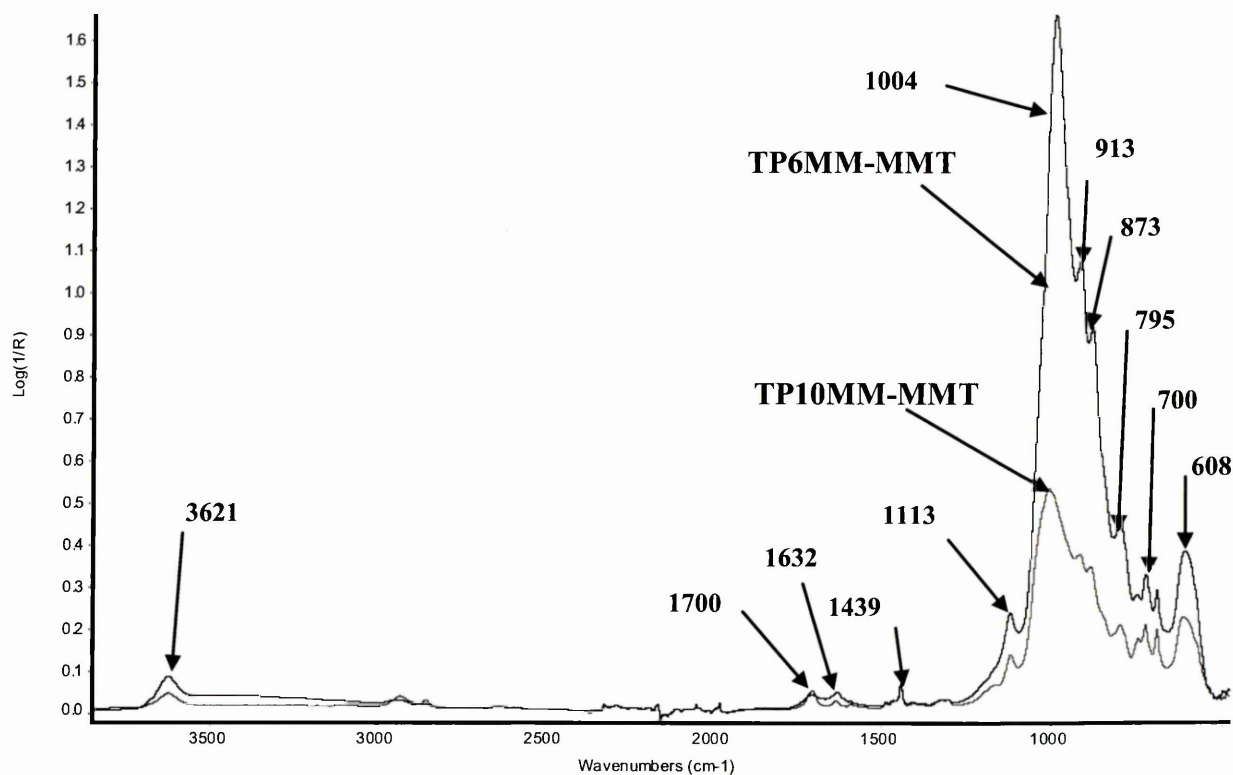
Figure 5–19 ATR FTIR spectra for TP6MM-MMT and TP10MM-MMT

The ATR FTIR data presented in Figure 5–19 displayed very similar peak positions in the spectra of TP6MM- and TP10MM-MMT, however the peak intensity of TP10MM-MMT was approximately one third that of TP6MM-MMT, indicating less clay in the beam in the TP10MM-MMT sample. An assignment of the peaks and possible group frequencies are given in Table 5–18.
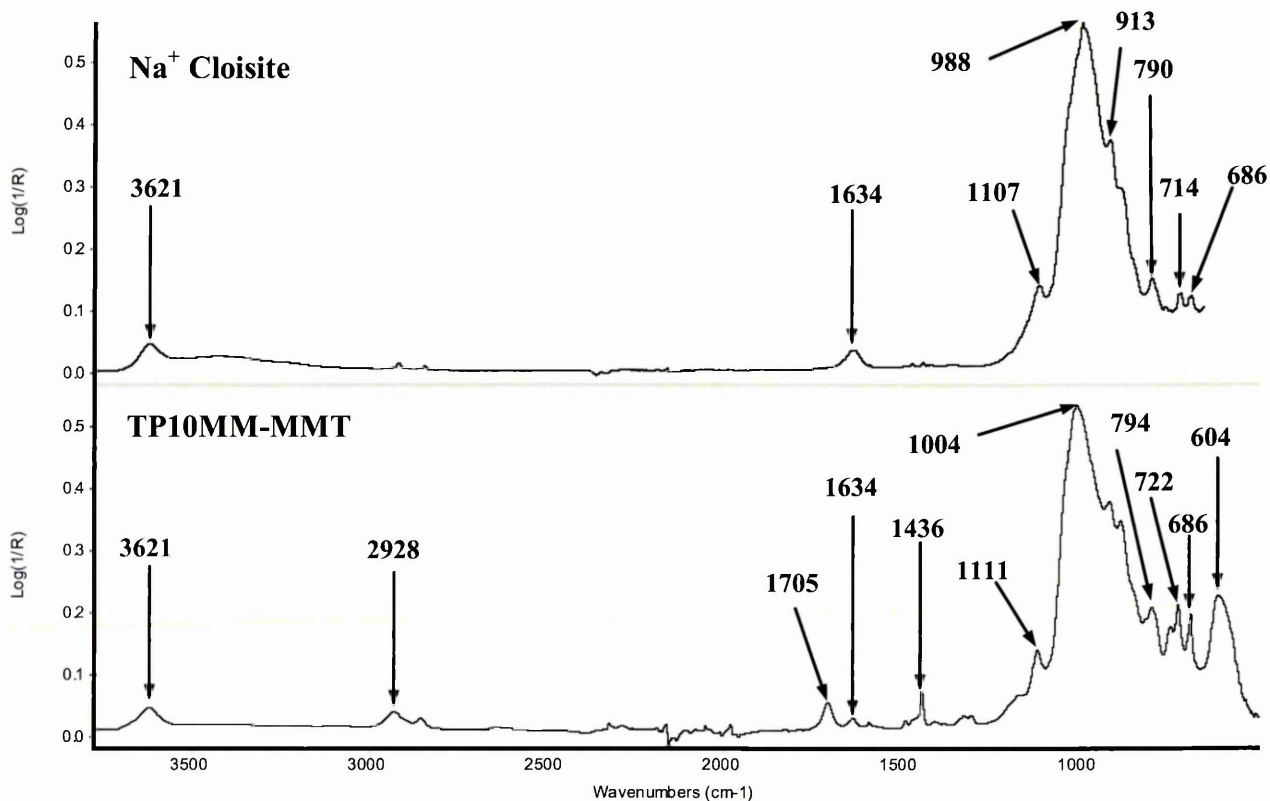
Figure 5–20 ATR FTIR spectra for Na$^+$ Cloisite and TP10MM-MMT

The ATR FTIR data presented in Figure 5–20 exhibited some similarities between Na$^+$ Cloisite and TP10MM-MMT, both traces displayed a strong Si-O band at ~ 1000 cm^{-1}, which is present in all (organo)clays. The main bands of interest were the C=C stretch, which occurs at approximately 1650 cm^{-1} and the C=O stretch, which occurs at 1700 cm^{-1}. The peak at 1700 cm^{-1} confirms the presence of the C=O stretch, however due to the shape and position of the peak at 1634 cm^{-1} it is more likely that this peak corresponds to the OH stretch frequency of water than the C=C stretch of the alkene. The trace for Na$^+$ Cloisite displayed a strong OH stretch of adsorbed H$_2$O at 1634 cm^{-1}, TP10MM-MMT however, displayed a weaker OH bend and therefore incorporated much less adsorbed H$_2$O.

Table 5–18 Peak assignments and possible group frequencies

Peak Position	Possible Bond	Type of Compound	Frequency Range, (cm^{-1})
~ 1000	Si-O	Organoclays	-
1004	Benzene Ring Stretch & Bend	Benzene	1000-1100
1113	C-O	Alcohols, ethers, carboxylic acids, esters	1050-1300
1439	C-H (bend) P-C	Alkane, Water	1340-1470
1632	H$_2$O	-	1590-1670
1700	C=O (stretch)	From methacrylate group	1690-1760
2928	C-H (stretch)	-	2800-3000
3621	O-H (stretch)	Structural OH	3590-3650

5.6 Crystic 189LV Composites Prepared Using TP8MM$^+$ and TP10MM$^+$ Exchanged Na$^+$ Cloisite

TP3MM$^+$, TP6MM$^+$, TP8MM$^+$ and TP10MM$^+$ were exchanged onto Na$^+$ Cloisite, dispersed in DMMP (D) and then mixed with Crystic 189LV. TP8MM- and TP10MM-MMT were selected for further analysis as these clays displayed the largest increase in d-spacing following exchange onto Na$^+$ Cloisite. The resulting composites were characterised using XRD and TGA. All samples were then subjected to the in-house version of the UL94 Vertical Burning test.

5.6.1 XRD Analysis of Crystic 189LV Composites Prepared Using TP8MM$^+$ and TP10MM$^+$ Exchanged Na$^+$ Cloisite
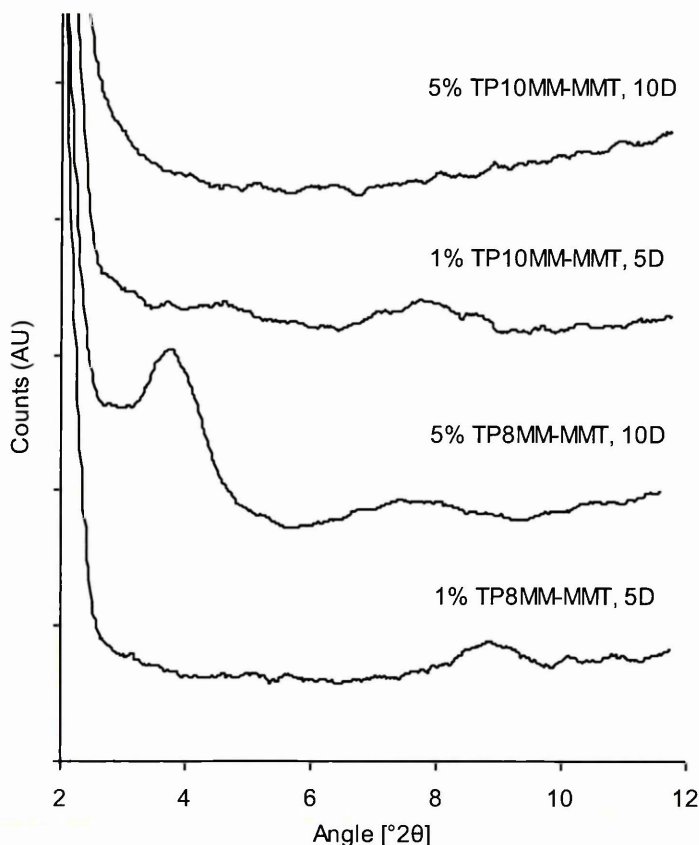
Figure 5–21 XRD traces (Cr tube) for Crystic 189LV composites prepared using 1 or 5 wt% TP8MM$^+$ or TP10MM$^+$ exchanged Na$^+$ Cloisite, with 5 or 10 wt% DMMP (D) – Traces are offset for clarity

The XRD traces presented in Figure 5–21 display Crystic 189LV composites prepared using 1 or 5 wt% TP8MM$^+$ or TP10MM$^+$ exchanged Na$^+$ Cloisite, with 5 or 10 wt% DMMP (D). The composites prepared using 1 wt% TP8MM- and TP10MM-MMT displayed very weak d_{001} spacings of 14.6 and 16.6 Å, respectively, which could be representative of unexpanded TP8MM- and TP10MM-MMT, however at 1 wt% clay it was difficult to detect a real peak in the XRD trace. The composite prepared using 5 wt% TP8MM-MMT and 10D exhibited an intercalated/exfoliated morphology, with d_{001} and d_{002} spacings of 34.0 and 17.1 Å, respectively. The increase in background at low angle and loss of intensity of the d_{001} peak are characteristic of an intercalated composite incorporating some exfoliated clay layers, no peaks were present in the composite prepared using 5 wt% TP10MM-MMT and 10D.

5.6.2 TGA Analysis of Crystic 189LV Composites Prepared Using TP8MM⁺ and TP10MM⁺ Exchanged Na⁺ Cloisite
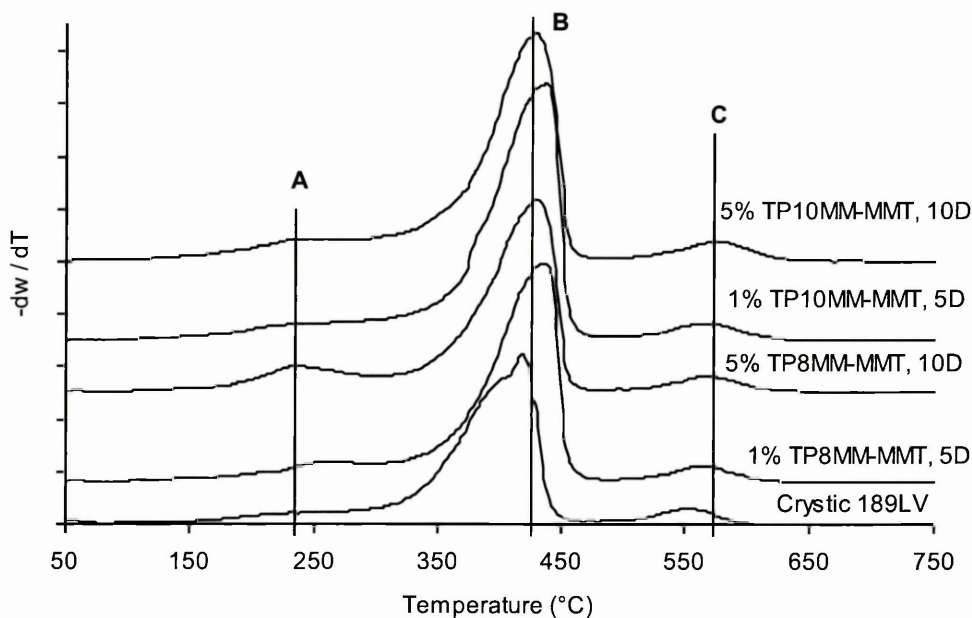
Figure 5–22 DTG traces (Air) for Crystic 189LV composites prepared using 1 or 5 wt% TP8MM- or TP10MM, with 5 or 10 wt% DMMP (D) – Traces are offset for clarity

The DTG traces presented in Figure 5–22 are for Crystic 189LV composites prepared using TP8MM- and TP10MM-MMT. Three main thermal decomposition maxima (A, B and C) were present, taking place over three stages. Stage 1 occurred between 146 and 295 °C and represents the evolution of DMMP (which boils at 181 °C), stage 2 occurred between 296 and 495 °C and represents organocation and resin decomposition and stage 3 occurred between 496 and 800 °C and represents decomposition of the carbonaceous char. The decomposition maxima varied slightly in decomposition temperature, between samples prepared using 1 and 5 wt% TP8MM- and TP10MM-MMT, and 5 or 10 wt% DMMP, the peak position temperatures are displayed in Table 5–19.

Table 5–19 Peak position temperatures for Crystic 189LV composites prepared using TP8MM- and TP10MM-MMT

	T_{max} (A) (°C)	T_{max} (B) (°C)	T_{max} (C) (°C)
1 wt % TP8MM-MMT, 5D	264	435	565
1 wt% TP10MM-MMT, 5D	243	437	568
5 wt% TP8MM- or TP10MM-MMT, 10D	241	432	579
Crystic 189LV	-	421	556
Crystic 189LV, 5D	232	430	577
Crystic 189LV, 10D	232	430	577

Loss of DMMP under T_{max} (A) displayed an increase in the decomposition temperature from 232 °C in the composites prepared using Crystic 189LV and 5 or 10 wt% D, to 264 and 241 °C in the samples prepared using Crystic 189LV and 1 and 5 wt% clay (5 wt% and 10 wt% D), respectively. The sample prepared using 1 wt% clay displayed the largest increase in thermal decomposition temperature compared to pure Crystic 189LV.

Table 5–20 Comparison of weight losses for Crystic 189LV composites prepared using TP8MM- and TP10MM-MMT

		Stage 1	Stage 2	Stage 3	
	35-145 °C (%)	146-295 °C (%)	296-495 °C (%)	>496 °C (%)	Total (%)
1% TP8MM, 5D	0.57	10.21	83.42	5.41	99.62
5% TP8MM, 10D	0.83	13.42	73.95	7.54	95.74
1% TP10MM, 5D	0.41	9.17	83.11	6.27	98.96
5% TP10MM, 10D	0.75	11.26	75.58	7.60	95.18

The total weight loss for the composites prepared using Crystic 189LV and TP8MM- and TP10MM-MMT (Table 5–20) decreased as the amount of inorganic material in the sample increased, the difference reflected the clay content. These results also indicated that the thermal stability decreased slightly as the wt% of organoclay increased. Loss of DMMP over the 146-295 °C temperature range for the composites prepared using 5 wt% organoclay decreased T_{max} (A) by 23 °C compared to the composites prepared using 1 wt% organoclay, also T_{max} (B) under the region 296-495 °C decreased by 5 °C in the composites prepared using 5 wt% of TP8MM- and TP10MM-MMT as compared to the 1 wt% samples.

5.7   UL94 Vertical Burning Test Results

Crystic 189LV composites containing TA3$^+$, TP3MM$^+$, TP6MM$^+$, TP8MM$^+$ and TP10MM$^+$ exchanged Na$^+$ Cloisite, were prepared at 2000 rpm for 30 minutes, postcured and then subjected to the in-house version of the UL94 Vertical Burning test. The results are displayed in Table 5–21 and UL94-V ratings have been applied where possible.

Table 5–21 Vertical Burning Test Results

Composition	Burn 1	Burn 2	Burn 3	Burn 4	Total	UL94- V Rating
1% TA3-MMT, 5D	5, 8	6, 7	6, 9	10, >60	6.8, 20.8	Fail
5% TA3-MMT, 10D	14, >60	2, 13	11, 9	-	9, 27	Fail
1% TP3MM-MMT, 5D	4, 24	2, 9	3, 12	17, 22	6.5, 16.8	V-1
5% TP3MM-MMT, 10D	10, Ex	4, 18	2, Ex	3, Ex	4.8, Ex	Fail
1% TP6MM-MMT, 5D	13, Ex	6, Ex	5, Ex	3, Ex	6.8, Ex	Fail
5% TP6MM-MMT, 10D	3, 20	4, 35	2, 18	3, 17	3, 22.5	V-1
1% TP8MM-MMT, 5D	3, 15	20, 12	4, Ex	18, Ex	11.3, Ex	Fail
5% TP8MM-MMT, 10D	4, 18	2, 16	1, 22	4, 12	2.8, 17	V-1
1% TP10MM-MMT, 5D	4, Ex	11, Ex	6, 16	3, 17	6, Ex	Fail
5% TP10MM-MMT, 10D	5, 16	5, 50	5, 43	4, 15	4.8, 31	Fail

(Ex = Extinguished manually after 60 seconds)

After the first flaming, many of the samples cracked, disrupting the char layer that is responsible for the increased fire retardancy of the composites. Therefore, many individual samples continued to burn after the second flaming due to this non-uniformity of the char layer and had to be extinguished manually. The samples that achieved a UL94-V rating were intercalated composites prepared using Crystic 189LV, containing 1% TP3MM-MMT, 5D, and 5% TP6MM-MMT, 10D, and 5% TP8MM-MMT, 10D.

Composites prepared using TA3-MMT displayed some promising results, however at least 1 out of the 4 samples tested failed to extinguish and therefore, the overall classification for TA3-MMT composites was 'Fail'. Gilman et al. [4-7] suggested that there were two types of carbonaceous materials formed upon thermal degradation of their PLSNs (a lower and a higher temperature char), and that clays that promote or catalyze additional carbonaceous char formation would most likely enhance the flame retardant effectiveness of clay-nanocomposite based flame retardants. Therefore, the

increased amount of char formed in stages 2 (lower temperature) and 3 (higher temperature) of the thermal degradation of the 5 wt% TA3-MMT nanocomposites (Table 5–16) could tentatively explain the increased flame retardancy of this alkylammonium based nanocomposite.

From these results it was apparent that composites prepared using clays with a triphenylphosphonium based organomodifiers were more stable than composites prepared using clays with a tetramethylammonium type modifier, and reached a UL94-V classification of V-1. In comparison the UL94 vertical burning test results for composites prepared using 5% TP8-MMT and 10D (Table 4-15 of Chapter 4) reached a V-0 classification.

5.8   Conclusions for the Covalent Binding of Modified Organoclay

To study what effect organocation deficiencies and excesses would have on the physical properties and thermal decomposition of the products, Na^+ Cloisite was modified with the alkylammonium cations DTA^+ and ω-DTA^+, at different percentages of the CEC of Na^+ Cloisite. XRD results (Figure 5–1) revealed that a maximum d_{001} spacing of 13.4 Å was reached at 1.0 times the CEC, confirming that the alkyl chains were laying parallel to basal surface. Uptake curves (Figure 5–3) revealed that when 1 CEC of modifier was introduced approximately 90-96% of the Na^+ ions were displaced.

The total weight loss calculated from TG data, increased as the clay loading of DTA^+ or ω-DTA^+ increased with respect to the CEC (i.e. 1.0 x, etc..), the maximum total weight loss for DTA- and ω-DTA-MMT occurred at 2.0 x CEC. DTG results displayed the alkylammonium cations being thermally desorbed over a wider temperature range (150-515 °C) when run under N_2 (Figure 5–6 and Figure 5–7), as compared to when run under air (180-450 °C) (Figure 5–4 and Figure 5–5). Under air the DTG traces displayed three temperature maxima (A, B and C) with T_{max} A being thermally desorbed before T_{max} B in the DTA^+ samples and T_{max} B being thermally desorbed after T_{max} A in the ω-DTA^+ samples. Under N_2 the thermal degradation pattern of DTA^+ and ω-DTA^+ followed a similar pattern. Under air and N_2 at 0.25 x CEC, the majority of the weight loss occurred under the T_{max} at 60 °C. However, the majority of weight loss for samples prepared at between 0.5 and 2.0 x CEC occurred at 620 °C under N_2 and 420 °C under

air. TG-MS analysis showed that the diene/alkene ratio (i.e $m/z = 138 : m/z = 140$) in the gases evolved from the DTA^+- and ω-DTA$^+$-clay (under nitrogen) was approximately 1.5 compared to 0.7. This confirmed that the vinyl group on the end of the surfactant tail was still available after exchange onto the clay and therefore potentially able to crosslink with styrene and/or the UP oligomer.

ω-decyltriphenylphosphonium bromide (ω-TP10B) and ω-decyl trimethylammonium bromide (ω-DTAB) were successfully prepared and exchanged onto Na$^+$ Cloisite before being characterised using XRD and TGA. The XRD traces (Figure 5–9) for the ω-TP10-MMT and ω-DTA-MMT exhibited expansion of the clay gallery from 12.5 Å in Na$^+$ Cloisite to 13.1 and 18.9 Å in ω-DTA-MMT and ω-TP10-MMT, respectively. This suggested that a single layer of ω-DTA$^+$-organocations resided in the clay gallery, whilst the spacing for ω-TP10-MMT was attributed to the PPh$_3$ head group. TGA analysis (Figure 5–10) revealed a higher decomposition temperature under T_{max} A in the phosphonium clay (330 °C) as compared to the ammonium clay (302 °C), however T_{max} B occurred at the same temperature of approximately 602 °C ($\pm$ 10 °C) in both samples.

Composites prepared using Crystic 189LV and ω-DTA-MMT/ω-TP10-MMT displayed the same thermal degradation pattern when analysed using TGA (Figure 5–11 and Figure 5–12, respectively), with T_{max} A occurring at 420 °C and T_{max} B occurring at 560 °C ($\pm$ 3 °C) in both the ω-TP10-MMT/ω-DTA-MMT composites and pure Crystic 189LV.

The second type of functionalised surfactant was based on a triphenylphosphonium head group separated from a methacrylate end group by a hydrocarbon chain of differing length i.e. 3, 6, 8 and 10 methylene groups, which are subsequently referred to as TP3MM (3 = C$_3$), TP6MM (6 = C$_6$), TP8MM (8 = C$_8$) and TP10MM (10 = C$_{10}$, respectively.

The exchange of Na$^+$ Cloisite with commercially available [3(methacryloylamino)propyl] trimethylammonium chloride (TA3) was investigated, the XRD traces exhibited a d-spacing of 13.4 Å, corresponding to a single layer of the modifier in the gallery. The triphenylphosphonium based modifiers all resulted in a d-spacing of 17.5 Å, regardless of the alkylchain length, and therefore supports the view

that the triphenyl head group controlled the gallery expansion, this was also observed in section 4.4 of Chapter 4 with organoclays prepared using $TP8^+$ and $TP10^+$. A small peak at higher d-spacing occurred for TP8MM- and TP10MM-MMT, corresponding to a d-spacing of 30.1 Å. The separation distance between the d_{001} peak and the small peak at lower angle was 13.4 Å, and this separation distance was also observed in the organoclays prepared using $TP8^+$ and $TP10^+$ in Chapter 4 (Table 4-8). The separation distance was approximately the same as that found in the hydrated form of Na^+ Cloisite and therefore supports the formation of a mixed ion heterostructure, as displayed in Figure 5–23. The $TP8MM^+$ and $TP10MM^+$ cations and $Na(H_2O)$ cations were segregated into two interlayers (Figure 5–23) in a regular alternating fashion.

Na (H₂O) layer in between the clay layers

TP$_n$MM layer
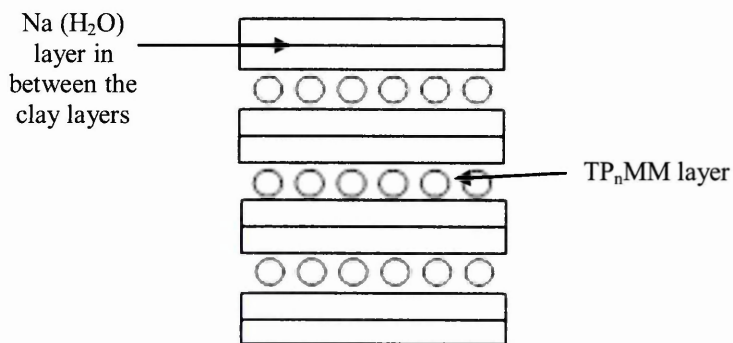
Figure 5–23 Schematic Illustration of the possible structure for TP$_n$MM exchanged Na$^+$ Cloisite

TP3MM- and TP6MM-MMT did not display an intense d_{001} peak or peaks at higher d-spacing. Ijdo and Pinnavaia [5-8] investigated the intercalation process that leads to the formation of heterostructures, elucidating the role of onium ion geometry in the synthesis of regularly ordered heterostructures. They found that C_4 to C_6 onium ions were too hydrophilic to quantitatively displace Na^+ from the exchange sites. No heterostructured intercalate was formed under these equilibrium conditions because there was little or no onium ion binding. The onium ion did not compete effectively with Na^+ in the exchange process. Therefore, most of the aqueous onium salts were lost upon washing and drying of the products. Using TG data, this theory can be confirmed, when the amount of organic exchange for TP3MM- to TP10MM-MMT and TA3 was compared to the actual amount of organic exchange possible, the results are displayed in Table 5–22.

Table 5–22 Possible organic exchange against actual organic exchange for TP3MM- to TP10MM-MMT and TA3 at 1 x CEC

	TP3MM-MMT	TP6MM-MMT	TP8MM-MMT	TP10MM-MMT	TA3-MMT
Possible Organic Exchange (mg/ g)	360.2	399.2	405.4	451.1	171.1
Actual Organic Exchanged (mg/ g)	86	162.1	229.2	285.3	113.8
Percentage Occupied by Onium Ion (%)	24	41	57	63	67

* All exchange amounts are ± 5%

As the alkyl chain length increased, the actual amount of organic exchange also increased, however when C_n = 10 only 63% exchange occurred. Therefore, the affinity between these bespoke modifiers and the clay surface appeared rather low. Consequently the dispersion issue, which caused the samples to crack when subjected to the in-house version of the UL94 vertical burning test, has been attributed to low percentage coverage of the clay surface by the bespoke modifier. This trend was also observed in the triphenylphosphonium exchanged organoclays prepared in Chapter 4, however, when C_n = 8 and C_n = 10 only 63 and 66% exchanged occurred (Table 4-5). To overcome this problem, the concentration of all triphenylphosphonium organomodifiers, methacrylate functionalised phosphonium-organomodifiers and TA3$^+$ could be increased beyond the CEC of Na$^+$ Cloisite. In section 4.11 of Chapter 4 the loading of Bu16$^+$ was increased from 1.0 x CEC to 1.5 and 2.0 x CEC of Na$^+$ Cloisite. This resulted in an increase in the percentage occupied by the onium ion of 90 and 84% at 1.5 and 2.0 x CEC, respectively, when calculated against the possible organic exchange for 1.0 x CEC of Na$^+$ Cloisite. The extent of exchange may also be increased if the equilibration time for the surfactant when added to the aqueous clay suspension could also be increased.

From TG data, an increase in the T_{onset} of 25 °C was observed when alkylammonium exchanged TA3$^+$ (Figure 5–15) was compared with the alkylphosphonium exchanged TP$_n$MM$^+$ series (Figure 5–18). This trend was also observed upon comparison of the T_{onset} of the alkylammonium exchanged ω-DTA-MMT as compared to alkylphosphonium exchanged ω-TP10-MMT (Figure 5–10). The T_{onset} increased from 180 °C in ω-DTA-MMT to 229 °C in ω-TP10-MMT.

These results are similar to those presented by Xie et al. [5-9] who compared the thermal stability and degradation mechanism of quaternary phosphonium modified montmorillonites to ammonium modified montmorillonites. They also observed an increase in the thermal stability, under N_2, of alkyl and aryl quaternary phosphonium-modified montmorillonite (P-MMT) compared to ammonium-modified montmorillonite (N-MMT). The thermal stability of exchanged MMT was related to the thermal stability of the parent salts, the phosphonium salts have a much higher initial decomposition temperature compared to the ammonium salts.

Zhang et al. [5-4] focused on the influences of the polymerisable quaternary ammonium (methacryloxylethyl benzyl dimethyl ammonium chloride (MBDAC)) on the structure and properties of the resulting nanocomposites of unsaturated polyester. The effects of organophilic MMTs obtained from different quaternary ammonium ions on the mechanical properties and the structure of unsaturated polyester-based nanocomposites were compared. TGA results indicated that the starting weight loss (T_{onset}) of the hybrids was between 11 and 19 °C higher and the temperature at maximum weight loss was between 24 and 30 °C higher than that of UP. The DTG results (Figure 5–22) for nanocomposites prepared using Crystic 189LV, TP8MM- and TP10MM-MMT indicated that the T_{onset} was 32 °C higher in the composites and the temperature at maximum weight loss (T_{max} (B)) was between 14 and 21 °C higher in the composites, as compared to pure Crystic 189LV. This could be attributed to a strong interaction or chemical bonding between the inorganic layers and the UP. However, in comparison the T_{onset} for the composites prepared using Crystic 189LV, TP8- to TP16-MMT and 10D from Chapter 4 was very similar to that of Crystic 189LV at ~ 124 °C. The temperature at maximum weight loss (T_{max} (B)) increased by a maximum of 10 °C in the TP8-MMT composite but did not increase in the composite prepared using TP10-MMT, therefore the incorporation of the methacrylate group did significantly increase the T_{onset} of the resulting composites and also slightly the temperature at maximum weight loss (T_{max} (B)).

Evaluation of the exchanged organoclays using ATR-FTIR confirmed the presence of the C=O stretching vibration at 1700 cm^{-1}. Wang et al. [5-10] hypothesised that exfoliated nanocomposites were more likely to be formed when a double bond, that may be involved in the polymerisation reaction is present in the organocation on the clay.

However, composites prepared using Crystic 189LV, TA3-MMT, TP8MM- and TP10MM-MMT plus DMMP, which contained a double bond, displayed largely XRD silent traces for most of the composites with the exception of the sample prepared using 5 wt% TP8MM-MMT and 10D, which displayed an intercalated/exfoliated morphology (d_{001} 34 Å). The XRD silent traces contained clumps of clay, which were visible by eye and therefore poor dispersion of the organoclay into Crystic 189LV occurred. A scattering profile, such as the one presented for the TA3-MMT and TP10MM-MMT nanocomposites, which were very similar to the XRD trace for pure Crystic 189LV, could indicate that there was very little clay in that part of the sample.

The dispersion of all clays exchanged with a functionalised modifier in Crystic 189LV was generally poor despite presenting nominally 'x-ray silent' diffraction traces. Large particles of poorly dispersed clay were clearly present. This poor dispersion of the functionalised nanoclay prevented the formation of a coherent char which in turn led to an increased incidence of cracking within the surface of the specimen after the first flaming. Consequently the sample continued to burn after the second flaming due to the resulting non-uniformity of the char layer and because the gases were able to leave the polymer and fuel the flame.

When the UL94 vertical burning test was carried out on all the composite samples, the most promising fire retardant results (Table 5–21) were observed with intercalated/exfoliated composites containing 5 wt% TP8MM-MMT and 10D in Crystic 189LV, the samples reached a V-1 classification. However, higher UL94-V classifications were reached with the composites prepared in Chapters 3 and 4. Samples prepared in Chapter 4 using 5 wt% TP8-MMT and 10D in Crystic 189LV (Table 4-15 of Chapter 4) achieved a V-0 classification with all samples self extinguishing in 2.5 seconds after the first flaming. The UL94-V test results from Chapter 4 were comparable to those from Chapter 3 for halogenated resins, which also reached a V-0 classification and self extinguished in 3 seconds after the first flaming. Due to these dispersion issues work was not continued on the methacrylate functionalised phosphonium-organomodifiers.

5.9   Literature Reports on the Preparation of Polystyrene-Clay Composites

In the literature, there is little evidence for the preparation of unsaturated polyester-clay composites and therefore the following reviews report on the preparation of polystyrene-clay (PS/MMT) composites, as the systems within this thesis incorporated the unsaturated polyester as a polymeric oligomer dispersed in styrene. A common technique involves dispersing clay into the styrene monomer followed by polymerisation. Also anchoring organic surfactants into the interlayer region containing polymerisable ammonium or phosphonium groups may provide an additional driving force for layer separation.

Doh and Cho [5-11] investigated the effect of the chemical structure of organophilic MMTs on the process of PS/MMT composite preparation. The composites were prepared by direct polymerisation of styrene in the presence of organophilic MMTs (ammonium and benzylammonium exchanged MMT (Ta-MMT and Bz-MMT, respectively) where $C_n = 18$). XRD measurements of the PS/Bz-MMT hybrid indicated an increased basal spacing from 19.1 to 34.0 Å due to the swelling of the interlayer by the styrene monomer and successive polymerization. As the structural affinity between the styrene monomer and the organic group of org-MMT increased, the dispersibility of org-MMT in the styrene monomer also increased. The penetration of monomers into the lamellae of organophilic MMT can be facilitated by the attractive forces between the org-MMT interlayers and the free monomer molecules. The interlayer distance of Ta-MMT barely changed because, according to the authors, there was already enough space to accommodate the intercalating PS polymer chains without expanding the interlayer.

As the alkyl chain length of the alkylammonium cations in org-MMT increased, the basal spacing (d_{001}) of org-MMT also increased, however, when monomer was introduced into the org-MMT interlayer space followed by polymerization, the increase in interlayer distance depended on the structure of the organic group rather than the chain length of the alkylammonium cation. In support of Doh and Cho's findings, data in section 4.7 of Chapter 4 displayed an increase in the basal spacing of tributylphosphonium ($Bu16^+$) exchanged Na^+ Cloisite by 4 Å when the organoclay was dispersed in styrene. No increase was observed with the triphenylphosphonium

exchanged organoclays (TP8$^+$-TP16$^+$) however, this can be attributed to the polymerisation of styrene in the TP-clays when dried at elevated temperature.

TGA thermograms displayed a delayed decomposition of the PS/Bz-MMT hybrid as compared to a PS/Na-MMT microcomposite, which was attributed to confinement of PS polymer chains between MMT layers as well as the MMT surface-polymer interactions in the nanostructured hybrid. Therefore, the structural affinity between the styrene monomer and the organic group is an important factor in preparing hybrid composites. The structural affinity in PS/Bz-MMT was attributed to the presence of the benzyl-unit, which improved thermodynamic compatibility by being similar to the structure of the styrene monomer.

Fu and Qutubuddin [5-12] reported on the synthesis of exfoliated polystyrene-clay nanocomposites using the reactive cationic surfactant vinylbenzyldimethyldodecylammonium chloride (VDAC), which was exchanged onto MMT. Exfoliated polystyrene-clay nanocomposites were prepared by direct dispersion of organophilic MMT in the styrene monomer followed by free radical polymerisation. The exfoliation of MMT in the polystyrene matrix was attributed to a strong interaction between styrene and VDAC-MMT.

The cationic surfactant VDAC contained a polymerisable aromatic group, which exhibited good affinity with styrene and encompassed the ability to homopolymerize as well as copolymerize with monomers in an organic medium such as acetonitrile [5-13]. VDAC functionalised MMT was found to have strong swelling ability and formed a viscous gel in styrene. Exfoliated nanocomposites were successfully synthesised using this functionalised form of Na-MMT. PS-VDAC-MMT nanocomposites displayed a higher thermal degradation temperature than pure polystyrene and the nanocomposites exhibited higher dynamic modulus with increased loading of VDAC-MMT in polystyrene.

Akelah and Moet [5-14] investigated the ability of styrene intercalated between swelled MMT interlayers to polymerise, to produce organophilic polystyrene-MMT through chemical bonds. They suggested that interlayer accessibility to styrene molecules is

related to the solvation energy of the solvent mixture used. It was presumed that polymerisation was initiated in the interlayer region and once the polymerisation started, the MMT-PS propagating chains were swollen by the styrene molecules because of sufficiently attractive forces between styrene and the interlayer polystyrene propagating chains. Therefore, the effect of the initial amount of styrene monomer inserted between the interlayers before the onset of polymerisation is the main factor causing the increase in the intercalation of PS molecules between the interlayers.

The synthesis of exfoliated poly (methyl methacrylate) (PMMA) and PS/ clay nanocomposites via bulk polymerisation has been reported on by Zeng and Lee [5-15]. They found that the polarity and hydrophilicity of the initiators and monomers greatly affected clay dispersion. The combined use of a more polar, less hydrophobic monomer and initiator lead to better clay layer separation and a more disordered intercalated nanocomposite, which results from favourable interactions of the clay surface with both the monomer and the initiator. Introducing a vinyl functionalised group onto the clay surface improved clay dispersion significantly, and exfoliated PMMA and PS/clay nanocomposites were successfully synthesised with a clay concentration of 5 wt%.

By applying the knowledge that has been gained through the preparation of polystyrene-clay nanocomposites, exfoliated unsaturated polyester-clay nanocomposites could possibly be made. For example to improve the dispersion of the methacrylate functionalised phosphonium organomodified MMT, direct dispersion into styrene prior to incorporation into the unsaturated polyester resin could be employed, as in experiments by Fu and Qutubuddin [5-12]. Doh and Cho [5-11] also employed direct dispersion into styrene, they stated that the interlayer distance of their ammonium exchanged MMT did not expand as there was already enough space to accommodate the intercalating PS polymer chains. Therefore, direct dispersion into styrene may only be beneficial to the methacrylate functionalised phosphonium organomodified MMT and not TA3-MMT.

To improve the thermal stability of the methacrylate functionalised phosphonium-organomodified MMT, exchange salts with an increased thermal stability could be investigated. For instance Xie et al. [5-9] found that the thermal stability of exchanged MMT was related to the thermal stability of the parent salts, with phosphonium salts

having a much higher initial decomposition temperature as compared to ammonium salts.

Zeng and Lee [5-15] hypothesised that the use of a more polar, less hydrophobic monomer and initiator can lead to better clay layer separation and a more disordered intercalated nanocomposite. Therefore, a larger study could be conducted incorporating a wider range of resins and initiators, to possibly find a more polar and less hydrophobic combination, to produce more disordered intercalated nanocomposites.

5-1 Zhang, M. and Singh, R., *Materials Letters*, **58**, 408 (2004)

5-2 Ng, B.B., Ash, B.J., Schadler, L.S. and Siegel, R.W., *Adv. Compos. Lett.*, **10**, 101 (2001)

5-3 Awad, W.H., Gilman, J.W., Nyden, M., Harris, R.H., Sutto, T.E., Callahan, J., Trulove, P.C., DeLong, H.C. and Fox, D.M., *Thermochimica Acta*, **409**, 3 (2004)

5-4 Zhang, Y., Cai, Q., Jiang, Z. and Gong, K., *J. Applied Polym. Sci.*, **92**, 2038 (2004)

5-5 Hussain, M. and Simon, G.P., *Journal of Materials Science Letters*, **22**, 1471 (2003)

5-6 Zhu, S. and Shi. W., *Polymer Degradation and Stability* **80**, 217 (2003)

4-7 Gilman, J.W., Harris Jr, R.H., Shields, J.R., Kashiwagi, T. and Morgan, A.B., *Polym. Adv. Technol.*, **17**, 263 (2006)

5-8 Ijdo, W.L. and Pinnavaia, T.J., *J. Solid State Chemistry*, **139**, 281 (1998)

5-9 Xie, W., Xie, R., Pan, W.P., Hunter, D., Koene, B., Tan, L.S. and Vaia, R., *Chem. Mater.*, **14**, 4837 (2002)

5-10 Wang, D., Zhu, J., Yao, Q. and Wilkie, C.A., *Chem. Mater.*, **14 (9)**, 3837 (2002)

5-11 Doh, J.G. and Cho, I., *Polymer Bulletin*, **41**, 511 (1998)

5-12 Fu, X. and Qutubuddin, S., *Matterials Letters*, **42**, 12 (2000)

5-13 Fu, X. and Qutubuddin, S., *Polymer*, **42**, 807 (2001)

5-14 Akelah, A. and Moet, A., *J. of Materials Science*, **31**, 3589 (1996)

5-15 Zeng, C. and James Lee, L., *Macromolecules*, **34**, 4098 (2001)

6. Conclusions

6.1   Preparation and Characterisation of Polymer Clay Nanocomposites

Nanocomposites were prepared by in-situ polymerisation of commercially available organically modified montmorillonites. Three types of unsaturated polyester, an orthophthalic (Crystic 189LV) and two isophthalic resins (Crystic 272 and Crystic R935, all received as polymeric oligomers dispersed in styrene) were intercalated into three clays (Cloisite 30B, Cloisite 15A and Cloisite 10A) with different organic modifications.

Differences in organic modification of commercially available organoclays resulted in changes in the interlayer spacing of the organoclay when dispersed in Crystic 272. The XRD traces demonstrated intercalated/exfoliated composites for Cloisite 30B, Cloisite 10A and Cloisite 15A when blended with Crystic 272, however Cloisite 15A displayed the most order within the nanocomposites, displaying clear, sharp, d_{001} and d_{002} peaks. For the nanocomposites an increase in the d-spacing was observed from 17.2 Å to 34.4 Å (+ 100 %) for Cloisite 30B, from 19.2 to 34.0 Å (+ 76 %) for Cloisite 10A and from 31.5 to 34 Å (+ 8 %) for Cloisite 15A. Cloisite 30B displayed the largest percentage increase in the d_{001} spacing upon intercalation, however all of the clays reached a similar 'final spacing' near 34 Å. The thermal decomposition temperature maxima (T_{max} A and T_{max} B) increased by 16 °C upon addition of all four commercially available organoclays into Crystic 272.

The thermal decomposition temperature maximum (T_{max}) increased as the clay loading in Crystic 272 increased and intercalated nanocomposites were produced. The absence of the d_{001} reflection did not indicate an exfoliated nanocomposite but rather a composite which was intercalated (confirmed through the absence of low angle scattering), but had little/no clay in the beam. Increasing the clay loading of Cloisite 30B from 0 to 5 wt%, increased T_{max} (A) by 19 °C, and produced intercalated nanocomposites for samples containing 1 and 3 wt% clay. Samples containing 5 and 10 wt% Cloisite 30B yielded an intercalated/exfoliated structure, confirmed through an increase in low angle scattering coupled with a broad and less intense d_{001} reflection. The peak width increased with increasing clay content, increasing by a maximum of 14

°C at 10 wt% Cloisite 30B. Based on these XRD and TGA results it was decided to carry out further experiments using 5 wt% organoclay as this produced a more exfoliated/intercalated composite with an increased T_{max}.

Increasing the stirring time and mixing speed did not result in an increase in the d-spacing of Cloisite 30B when mixed in Crystic R935, all peaks were of similar intensity suggesting that all samples had a similar degree of intercalation/exfoliation, with the exception of the composite prepared at 8000 rpm for 30 minutes, which showed evidence of low angle scattering and therefore more exfoliated clay layers within the sample, leading to a more exfoliated/intercalated composite. Increasing the mixing time from 15 to 30 minutes in the 1000, 8000 and 14,000 rpm samples increased the thermal decomposition temperature maximum (T_{max} A) by 7 °C in all samples. Based on XRD results it was decided to use 1000 rpm for 15 minutes as the standard conditions because they produced what was thought to be an exfoliated nanocomposite, however further understanding of the interpretation of the XRD spectra revealed that the composites (including composites prepared using Cloisite 10A and Cloisite 15A) were actually intercalated.

The d-spacing of Cloisite 15A when dispersed in Crystic 189LV, Crystic 272 and Crystic R935 increased from 31.5 Å to 34.9, 33.7 and 31.7 Å, respectively. Therefore, Crystic R935 did not intercalate into the gallery of Cloisite 15A, however Crystic 272 and Crystic 189LV did increase the d-spacing of Cloisite 15A slightly. The thermal decomposition temperature maximum did not increase upon addition of Cloisite 15A into Crystic 189LV and Crystic R935, however, an increase of 14 °C was observed when Cloisite 15A was dispersed in Crystic 272. The biggest difference between the nanocomposites and resins was the increased peak width upon addition of organoclay, with the largest increase observed in the Crystic 189LV/Cloisite 15A sample.

It was found that the use of ultrasound and mixing did not significantly change the extent of dispersion or thermal properties of Cloisite 30B when mixed with Crystic 189LV.

The synergistic effect between halogenated resins and clays has been investigated. Halogenated resins were provided by Scott Bader, namely Crystic D3644LV (chlorine-containing) and Crystic PD7343 (bromine-containing), denoted as Cl-resin and Br-resin, respectively. Oven tests illustrated that the addition of clay promoted the formation of more integral char and the halogen-containing samples all extinguished in 3s, although halogenated compounds are undesirable from a health and safety viewpoint. Halogens act mainly in the vapour phase, the mixture of Cl-resin and Crystic 189LV formed more char with increasing Cl-resin content and the incorporation of clay reinforced this behaviour.

Crystic 189LV was blended with Cl-resin concentrations of 0, 10, 20, and 40 wt% and 0, 1, 3 and 5 wt% Cloisite 10A nanoclay. Cloisite 10A was chosen before Cloisite 15A was selected as the optimum clay. XRD analysis indicated that at each clay content, the d-value increased and the peak intensity decreased with increasing Cl-resin content. At each halogen content the d-value decreased with increasing clay content. The degree of dispersion decreased with increasing clay content.

It was found that the char decomposition onset temperature and maximum char decomposition temperature remained unchanged by the addition of clay or halogenated resin alone, however a synergistic effect between clay and halogenated resin existed, more clay and more halogenated resin created more char and an increased decomposition range. The addition of 10 wt% Cl-resin almost doubled the amount of char formed (4.9 to 9.7 wt%), increased the maximum char decomposition temperature (552 to 560 °C) and char decomposition range (from 136 to 168 °C), a reduction in the 5%, 30% and maximum weight loss temperatures were also observed (9 and 18 °C reduction, respectively). The 100 wt% Cl-resin samples produced the most char (23.7 wt%) and widest char decomposition range (268 °C) as well as the lowest maximum weight loss temperature (325 °C compared to 418 °C for pure Crystic 189LV) and temperature at 30% weight loss (331 °C compared to 375 °C for pure Crystic 189LV). The addition of clay into the Cl-resin formulations increased the 5 and 30% weight loss temperatures and slightly decreased the maximum weight loss temperature. The addition of clay into UP increased the amounts of char formed and char decomposition range and this increase was greater than the amount of clay added into the system, for example the addition if 3 wt% clay formed 4.1 wt% char in the 0% Cl-resin sample. A

synergistic effect occurred upon addition of Cloisite 10A in Crystic 189LV plus Cl-resin, in the 3 wt% Cloisite 10A samples the amount of char formed increased from 9 to 11% when 10 wt% Cl-resin was incorporated into the system and the amount of char increased from 9 to 18 % when 40 wt% Cl-resin was incorporated into the system.

Crystic 189LV was identified as the polymer system of choice at this stage as it contained no additional additives such as pigments, thixotropes and stabilisers. Crystic 189LV displayed the broadest peak width and increased temperature maximum (T_{max} (A)) compared to the other UP resins, also rudimentary horizontal burning tests identified Crystic 189LV as displaying the most promising fire retardant properties when clay was added. The mixing speed of 1000 rpm and time of 15 minutes were chosen as the standard mixing conditions because they produced what was thought at this stage to be an exfoliated nanocomposite. Based on XRD and TGA results it was decided to carry out further experiments using 5 wt% organoclay as this produced a more exfoliated/intercalated composite with an increased thermal decomposition temperature maximum.

These experiments were carried out in the early stages of the project and the original criterion for identifying the most appropriate organoclay was based on the extent to which the organoclay dispersed in different resins, however oven tests (performed by a colleague) and rudimentary flame tests clearly identified an intercalated structure as offering the most effective fire retardant properties. Therefore the intercalated composites formed using Cloisite 15A and Crystic 189LV offered the most effective fire retardant properties and were chosen over the exfoliated/intercalated composites incorporating Crystic 189LV and Cloisite 30B. The highly intercalated structure arising from Cloisite 15A dispersed in Crystic 189LV, produced the most integral and dense char which is the best type of insulation layer for enhanced fire retardant properties. Cone calorimetry data collected for the halogenated resin systems resulted in a predicted Euroclass rating of D. The promising fire retardant system incorporating Crystic 189LV/Cloisite 15A (Surefire hand lay-up resin (Cloisite 15A at 1 wt%)) also reached a Euroclass rating of D, in the cone calorimetry test results and therefore reinforce comparability to the halogenated resin systems and could possibly eliminate the need for halogenated resins in the future.

Unfortunately, the aim of the project was to formulate halogen free resin systems, however the performance of the halogenated resins in the horizontal burning test proved to be a benchmark value against which the other flame retardant systems within this thesis were compared. Therefore, unsaturated polyester/clay nanocomposites containing small amounts of non-halogenated flame retarding agents, which offer superior flame retardant properties became the ultimate target for this project.

6.2 Commercially Available Organophosphorus Cations

Clays modified using phosphonium-based surfactants exhibit greater thermal stability than ammonium-based surfactants and have been found to increase the fire resistance of polystyrene. Phosphonium clays were prepared, characterised, combined with resin and tested using an in-house version of the UL94 Vertical Burning test. Special emphasis was placed on the determination of whether the different organocations and clay compositions that were produced lead to improved thermal stability of the organocation, and therefore the nanocomposite in which it was used.

The gallery cations of Na^+ Cloisite were exchanged with triphenyl phosphonium (TP) cations with chain lengths ranging from $C_n = 8$ to $C_n = 16$ ($TP8^+$ to $TP16^+$) and a tributyl phosphonium ($Bu16^+$) cation. XRD and TGA were carried out on all exchanged clays, and nanocomposites incorporating these exchanged clays. XRD results indicated that the phosphonium clays produced intercalated nanocomposites in Crystic 189LV. The d-spacing increased from 12.1 Å for Na^+ Cloisite to 17.4 Å in TP8- to TP12-MMT and 18.7, 17.7 and 20.9 Å in TP14-, TP16- and Bu16-MMT, respectively. A small peak at lower angle occurred, which has been tentatively attributed to the formation of a mixed ion heterostructure, where $TP8^+$ - $TP16^+$ and $Bu16^+$ cations and $Na(H_2O)$ cations are segregated into two interlayers in a regular alternating fashion.

DTG data revealed a two stage decomposition pattern for all phosphonium clays. The decomposition temperature maximum (T_{max} A) decreased as the chain length increased from $C_n = 8$ to $C_n = 12$ (351 to 327 °C) and then increased when $C_n = 14$ and 16 (341 and 360 °C). Shoulders occurred on the main decomposition peak T_{max} A occurring after the main decomposition peak (T_{max} A+1) in the TP8- to TP12-MMT samples and before the main decomposition peak (T_{max} A-1) in the TP14- and TP16-MMT samples. Bu16-

MMT displayed a clear sharp decomposition peak under T_{max} A-1, at a much lower temperature of 292 °C.

When the actual amount of organic exchange was calculated all organoclays were slightly under exchanged with TP8-, TP10-, TP14- and Bu16-MMT at 68% ± 5% of the possible organic exchange, however the actual amount exchanged for TP16-MMT was slightly lower at 56% of the possible organic exchange amount.

The incorporation of TP14-, TP16- and Bu16-MMT into Crystic 189LV produced intercalated/exfoliated nanocomposites for the TP14- and TP16-MMT samples and intercalated/aggregated nanocomposites for the Bu16-MMT sample. The d_{001} spacing also increased from 18.7, 17.7 and 20.9 Å, to 33.1, 33.7 and 27.8 Å, respectively. The layer spacing of TP8-, TP10- and TP12-MMT did not expand upon dispersion into Crystic 189LV. The DTG traces indicated a thermal decomposition maxima of 422 °C for pure Crystic 189LV and samples made using Crystic 189LV and 5 wt% TP10-, TP12-, TP16-, and Bu16-MMT.

Composites containing TP8- and TP14-MMT displayed a slightly higher T_{max} (+22 °C), compared to pure Crystic 189LV. TP10-, TP12- and TP16-MMT, demonstrated a stabilising effect on the entire system until the upper thermal limit of the material was reached. It was believed that this shift was due to the formation of a protective barrier layer, due to the surface accumulation of clay platelets held together with a carbonaceous char. This barrier would have thermally insulated the UP matrix.

To investigate the effect of individual components in the nanocomposite systems (DMMP and styrene), on the d-spacing of organophosphonium clays, XRD analysis was carried out on organophosphonium clays dispersed in DMMP, and dispersed in styrene. Dispersion of TP8- to TP16-MMT in DMMP or styrene did not significantly expand the d-spacings of the organoclays. The d-spacing of Bu16-MMT decreased when dispersed into DMMP and increased when dispersed into styrene. It was observed that the small peak at lower angle (found in all organophosphonium clays), was not present when dispersed in DMMP and was only present in TP10- and TP16-MMT samples when dispersed in styrene. These experiments confirmed that the expansion in the d_{001} spacing observed when composites were prepared using these organophosphonium clays and

Crystic 189LV, was due to polymerisation of Crystic 189LV in the gallery space, therefore expanding the clay layers further. The increase in the d_{001} spacing cannot be attributed to DMMP or styrene further expanding the clay layers.

The organoclays proved difficult to disperse into the UP resin, however this was overcome by pre-mixing with dimethyl methyl phosphonate (DMMP), which had been identified as an effective gas phase fire retardant. Using DMMP as a pre-swelling agent not only improved the dispersion of the organoclay but also caused the fire retardant properties to reach a much higher classification in the UL94 vertical burning test.

Composites prepared using Crystic 189LV, 5 wt% Bu16-MMT and 10 wt% DMMP constituted the first real breakthrough with respect to fire properties. The results showed very impressive flame retardant improvement achieving UL-94 V0 which can be directly compared with pure halogenated resin. In order of effectiveness, Bu16-, TP10- and TP8-MMT improved fire resistance but TP12-, TP14- and TP16-MMT were less successful. Further analysis using TGA indicated that, for TP8- and TP10-MMT, DMMP was available at relatively low temperatures to extinguish the gas phase flame but, for TP12- and TP16-MMT, it was not. This suggested that the phosphonium salt reduced the active concentration of DMMP, although the exact mechanism has not been established.

Analysis using TGA revealed significant differences in the thermal behaviour of the different groups of DMMP treated clays. The clays containing $TP8^{+}$ and $TP10^{+}$ exhibited a large weight loss (T_{max} = 140 °C), whereas those containing $TP12^{+}$, $TP14^{+}$ and $TP16^{+}$ did not display this weight loss but did exhibit another which maximised at 500 to 520 °C. Using TG-MS, analysis of the evolved gases indicated that the early weight loss was due to the evolution of DMMP and water. Suggesting that DMMP was available at relatively low temperatures to extinguish the gas phase flame. For TP12- and TP16-MMT however, the only evidence for fragments of the sorbed DMMP occurred during the mass loss which maximised near 510 °C. Suggesting that the phosphonium salt may interact/react with (some of) the DMMP reducing its active concentration below the required value for effective operation as a gas phase fire retardant.

TG-MS data indicated that TP8- and TP10-MMT contained significant amounts of adsorbed DMMP ($m/z = 79$), which was desorbed at a lower temperature than the boiling point of DMMP (which boils at 189 °C), under a T_{max} (A) at 148 °C. Whereas TP12-, TP14- and TP16-MMT exhibited a higher desorption temperature for DMMP under T_{max} (B) at 501 °C. Bu16-MMT did not exhibit a low temperature loss of DMMP. A tentative explanation for the ability of TP8- and TP10-MMT to accommodate adsorbed DMMP is that the C8 and C10 alkyl chains are relatively short and therefore there is some space between them in the gallery for DMMP to occupy. However, when the chain length exceeded 12 carbons there was no longer any space available for DMMP to be adsorbed.

The clay modification process can be a major investment in developing a commercial application, therefore a 'one pot' preparation method was investigated as an alternative to the standard, resource intensive process. XRD data revealed an intercalated/exfoliated nanocomposite with increased d_{001} spacing of 34.4 Å in the 'one-pot' method, compared to 28.6 Å in the standard method. However, the thermal decomposition maximum in the DTG traces remained the same at ~ 427 °C for the standard and 'one-pot' methods. The char decomposition temperature in the DTG curves displayed an increase of 9 °C in the 'one-pot' method. The fire properties of specimens produced using the 'one pot' method showed some promise but have not been fully optimised. This route is attractive because the phosphonium clay does not have to be prepared and extensively washed prior to inclusion in the formulation.

Important variations occurred in the fire test results from nanocomposites containing Bu16-MMT. Dispersion seemed to be more of an issue with this clay and retrospective examination of the XRD and TGA traces, revealed subtle differences between different batches which probably influenced the ability of Bu16-MMT to disperse into Crystic 189LV. XRD data revealed an increase in the intensity of several batches, however the d_{001} spacing remained the same at 21 Å ($\pm$ 1 Å). The DTG results revealed a shift in the minor pre peak A-1, revealing that as the peak A-1 moved to a lower temperature then the intensity of the d_{001} peak using XRD also increased, which resulted in an increase in the fire retardant properties of the samples. TG-MS measurements performed on Bu16-MMT batches displaying 'good' and 'bad' fire retardant properties displayed peak A-1

at a lower temperature in the 'good' batch and also the intensity of the decomposition ions was almost twice as intense in the 'good' batch.

TG-MS was utilised to explore the gases released from nanocomposites prepared using Crystic 189LV and Bu16-MMT, plus DMMP, prior to the onset of unsaturated polyester decomposition. The temperature at which DMMP was released was of particular interest as loss during post-curing was always a possibility. Composites containing Crystic 189LV and 10 wt% DMMP were made. Analysis of the gases released suggested that DMMP (m/z = 79) evolved at lower temperatures when present in greater quantities, possibly leading to improved fire performance. In composites containing 5 wt% Bu16-MMT, DMMP evolved at 230 °C irrespective of the amount of DMMP. In addition an unidentified fragment ion m/z = 50 evolved, which has been tentatively attributed to the thermal desorption of methyl chloride, (however, this could not be proven using existing equipment). It was clear that m/z = 50 only appeared in the presence of clay and was evolved after the thermal desorption of m/z = 79. The intensity of the m/z = 50 mass fragment increased as the DMMP loading increased even though this fragment did not appear in the mass spectrum of DMMP.

Differences between the surface and bulk composition of nanocomposites containing Crystic 189LV, 5wt% Bu16-MMT and 10D (plus Crystic 189LV and 10D) were revealed using TGA and infrared (ATR-FTIR) spectral characterisation. DTG data revealed that the surface 'layer' was less thermally stable than the bulk when heated in air, and decomposed at 383 °C at the surface compared to 432 °C in the bulk. Using ATR-FTIR, in both systems analysed (with and without clay) it appeared that polystyrene (characteristic peaks at 2848 (R) and 2917 cm^{-1} (S)) had migrated to the back surface of the sample, leading to an increased polystyrene content near the ATR window. The characteristic organoclay peaks were more intense at the front surface of the sample compared to the back. After removing the top layer of the nanocomposites both surfaces appeared the same, peaks R and S were not as intense. The differences between the bulk and surface of the nanocomposites observed using TGA and ATR FTIR could possibly stem from differences in the degree of exfoliation of the clay from the bulk to the surface and/or differences in the orientation of clay particles in these regions during the mixing and casting processes.

Variations in the loading of Bu16$^+$ onto Na$^+$ Cloisite affected the level of dispersion and thermal degradation pattern of the resultant nanocomposite. XRD results displayed an increase in the d-spacing as the loading of Bu16$^+$ increased (14.8 to 24.3 Å at 0.25 to 2.0 x CEC), however as the loading of Bu16$^+$ reached 1.0, 1.5 and 2.0 x CEC, the difference between the d_{001} spacing and the spacing for the small peak at higher d-spacing remained the same at approximately 15 Å. These diffraction patterns could be further evidence for a staged intercalate, and variation in the basal spacing of the galleries containing the inorganic cations in the heterostructure, have been tentatively attributed to variable hydration of the inorganic cations. The main peaks of interest in the DTG traces were the main decomposition peak T_{max} (A) and a much smaller peak T_{max} (A-1), which occurred before the main decomposition peak T_{max} (A). The DTG results displayed a loss of intensity for the peak under T_{max} (A-1) and a shift to a lower temperature as the loading of Bu16$^+$ increased (from 292 °C at 1.0 x CEC to 273 °C at 2.0 x CEC). However, it was still unclear which factors could potentially link to the fire retardant properties of the sample. It appeared that as the distance between T_{max} (A) and T_{max} (A-1) increased then the fire retardant properties of the resulting composite also increased.

Organoclays that contain excess surfactant have been reported to be detrimental to the level of dispersion and flammability properties of the composites prepared using them. Therefore incorporation of a washing step into the cation exchange process would ensure that excess surfactant was removed from the organoclays, which could reduce plasticization of the polymer or prevent early ignition of the nanocomposite. XRD and TG results indicated that when Bu16-MMT prepared at 1.5 and 2.0 x CEC of Na$^+$ Cloisite, was washed in a mixture of 80:20 EtOH:H$_2$O, the excess surfactant was removed. The d_{001} spacing decreased from 24.3 Å at 1.5 and 2.0 x CEC back to 20.8 Å as in the 1.0 x CEC sample. The DTG results also indicated that after washing the peak under T_{max} A-1 increased from 273 °C to ~290 °C which was at the same temperature as the 1.0 x CEC samples.

When Bu16-MMT washed in a mixture of 80:20 EtOH:H$_2$O was incorporated into the unsaturated polyester Crystic 189LV (plus 10D) and subjected to the 'in-house' version of the UL94 vertical burning test. An increased incidence of cracking after the first

flaming occurred as the loading of Bu16$^+$ increased from 1.0 to 1.5 and 2.0 x CEC of Na$^+$ Cloisite, and consequently the samples had to be extinguished manually.

The most promising nanocomposite system from Chapter 4 comprised Crystic 189LV, 5 wt% Bu16-MMT and 10 wt% DMMP, which achieved UL94 classification V0 and therefore compared favourably with halogenated resins. However, the clay modification process is prohibitively expensive for commercial application, therefore the 'one pot' preparation method should be further developed as an alternative to the standard, intensive process, as preliminary studies displayed comparable results in the UL94 vertical burning test for the standard and 'one-pot' methods.

6.3   Covalent Binding of Modified Organoclay

The covalent binding of modified nanoclays within an UP matrix, was studied since evidence in the literature suggested that the addition of 5-10 wt% clay can interfere with the crosslink density of the resulting composite. This issue was addressed by producing alkylammonium and phosphonium surfactants which offered a cross-linking group on the end of the alkyl tail, vinyl and methacrylate groups particularly.

To study what effect organocation deficiencies and excesses would have on the physical properties and thermal decomposition of the products, Na$^+$ Cloisite was modified with the alkylammonium cations DTA$^+$ and ω-DTA$^+$, at different percentages of the CEC of Na$^+$ Cloisite. XRD results revealed that a maximum d_{001} spacing of 13.4 Å was reached at 1.0 x the CEC, confirming that the alkyl chains were laying parallel to the basal surface. Uptake curves and XRF analysis revealed that when 1 x CEC of modifier was introduced approximately 90-96% of the Na$^+$ ions were displaced.

The total weight loss calculated from TG data, increased as the clay loading of DTA$^+$ or ω-DTA$^+$ increased with respect to the CEC (i.e. 1.0 x, etc.), the maximum total weight loss for DTA- and ω-DTA-MMT occurred at 2.0 x CEC. DTG results displayed the alkylammonium cations being thermally desorbed over a wider temperature range (150-515 °C) when run under N$_2$, as compared to when run under air (180-450 °C). Under air and N$_2$ at 0.25 x CEC, the majority of the weight loss occurred under the T_{max} at 60 °C.

However, the majority of weight loss for samples prepared at 0.5 and 2.0 x CEC occurred at 420 °C under N_2 and 300 °C under air.

TG-MS analysis showed that the diene/alkene ratio in the gases evolved from DTA- and ω-DTA-MMT (under nitrogen) was 1.5 to 0.7. Therefore confirming that the vinyl group on the end of the surfactant tail was still available after exchange onto the clay and potentially able to crosslink with styrene and/or the UP oligomer.

To provide a better understanding of the thermal behaviour of phosphonium salts and their modified MMT, the thermal stability of a phosphonium modified ω-decyl triphenylphosphonium bromide (ω-TP10B) MMT was compared with ammonium modified ω-decyl trimethylammonium bromide (ω-DTAB), exchanged onto Na^+ Cloisite and characterised using XRD and TGA. The XRD traces suggested that a single layer of ω-DTA$^+$-organocations resided in the clay gallery, whilst the spacing for ω-TP10-MMT was attributed to the PPh$_3$ head group, confirmed as a result of expansion of the clay gallery from 12.5 Å in Na^+ Cloisite to 18.9 and 13.1 Å in ω-TP10- and ω-DTA-MMT, respectively. Phosphonium based clays exhibited much greater thermal stability than alkylammonium based clays in air. TG analysis of the organoclays revealed that the onset of degradation for ω-TP10-MMT and ω-DTA-MMT were 229 and 180 °C, respectively.

The second type of functionalised surfactant was based on a triphenylphosphonium head group separated from a methacrylate end group by a hydrocarbon chain of differing length i.e. 3, 6, 8 and 10 methylene groups, which are subsequently referred to as TP3MM (3 = C_3), TP6MM (6 = C_6), TP8MM (8 = C_8) and TP10MM (10 = C_{10}), respectively. Na^+ Cloisite was also exchanged with commercially available [3(methacryloylamino)propyl] trimethylammonium chloride (TA3). TA3 had a trimethylammonium head group as compared to a triphenylphosphonium head group (for TP3MM to TP10MM) and it was hoped that the reactive vinyl double bond at the end of the methacrylate group would give an indication of how effective the synthesised compounds would be at cross-linking into the UP.

The exchange of Na^+ Cloisite with TA3$^+$, revealed a d-spacing of 13.4 Å, which corresponded to a single layer of modifier in the gallery. The triphenylphosphonium

based modifiers resulted in a d-spacing of 17.5 Å for TP8MM- and TP10MM-MMT, and supported the view that the triphenyl head group controlled the gallery expansion. A small peak at higher d-spacing occurred for TP8MM- and TP10MM-MMT, corresponding to a d-spacing of 30.1 Å. The separation distance between the d_{001} peak and the small peak at higher d-spacing was 13.4 Å. The separation distance was approximately the same as that found in the hydrated form of Na^+ Cloisite (12.4 Å) and therefore supports the formation of a mixed ion heterostructure, incorporating $TP8MM^+$ and $TP10MM^+$ cations and $Na(H_2O)$ cations, which were segregated into two interlayers in a regular alternating fashion.

As the alkyl chain length increased, the actual amount of organic exchange also increased, however when $C_n = 10$ only 63.2 % exchange occurred. Therefore, the affinity between these bespoke modifiers and the clay surface appeared rather low. Consequently the clay dispersion issue, which caused the samples to crack when subjected to the in-house version of the UL94 vertical burning test, has been attributed to low percentage coverage of the clay surface by the bespoke modifier. This trend was also observed in the triphenylphosphonium exchanged organoclays (TP8- to TP16-MMT), however, when $C_n = 8$ and $C_n = 10$ only 62.8 and 66.1 % exchanged occurred, this decreased percentage coverage could possible indicate that there is space within the interlayer of the clay for DMMP to reside, and could explain the higher UL94-V ratings for TP8-MMT composites.

From TG data, an increase in the T_{onset} of 25 °C was observed when the alkylammonium exchanged $TA3^+$ was compared to the alkylphosphonium exchanged TP_nMM^+ series. This trend was also observed upon comparison of the T_{onset} of the alkylammonium exchanged ω-DTA-MMT as compared to alkylphosphonium exchanged ω-TP10-MMT. The T_{onset} increased from 180 °C in ω-DTA-MMT to 229 °C in ω-TP10-MMT.

For the nanocomposites prepared using Crystic 189LV, TP8MM- and TP10MM-MMT, the T_{onset} was 32 °C higher in the nanocomposites, and the temperature at maximum weight loss was between 14 and 21 °C higher in the nanocomposites compared to pure Crystic 189LV. In comparison however, the T_{onset} did not increase significantly for composites prepared using Crystic 189LV, TP8- and TP10-MMT, and the temperature at maximum weight loss increased by only 10 °C for TP8-MMT composites and did not

increase for TP10-MMT composites, therefore the incorporation of the methacrylate group did significantly increase the T_{onset} of the resulting composites and also increased the temperature at maximum weight loss.

Evaluation of the methacrylate functionalised organophosphonium clays using ATR-FTIR confirmed a strong Si-O band at $\sim$ 1000 cm^{-1}, which is present in all (organo)clays. The main bands of interest were the C=C (1632 cm^{-1}) and C=O (1700 cm^{-1}), which were both present in the exchanged organoclays and confirmed the presence of a double bond for possible cross-linking into the UP. The trace for Na^+ Cloisite displayed a broad OH stretching band for adsorbed H_2O at between 3000 and 3600 cm^{-1}, TP10MM-MMT however, did not display a broad OH stretch and therefore incorporated much less adsorbed H_2O.

The most promising fire retardant results were observed with intercalated/exfoliated composites containing 5 wt% TP8MM-MMT and 10D in Crystic 189LV, the samples reached a V-1 classification. However, higher UL94-V classifications were reached with the composites prepared using triphenylphosphonium modified clay TP8-MMT, the incorporation of 5 wt% TP8-MMT and 10D in Crystic 189LV achieved a V-0 classification with all samples self extinguishing in 2.5 seconds after the first flaming. The UL94-V test results for halogenated resins (Cl-resin) however, also reached a V-0 classification and self extinguished in 3 seconds after the first flaming.

The dispersion of all clays exchanged with a functionalised modifier in Crystic 189LV were generally poor despite presenting nominally 'x-ray silent' diffraction traces. Large particles of poorly dispersed clay were clearly present. This poor dispersion of the functionalised nanoclay prevented the formation of a coherent char which in turn led to an increased incidence of cracking within the surface of the specimen after the first flaming. Consequently the sample continued to burn after the second flaming due to the resulting non-uniformity of the char layer and because the gases were able to leave the polymer and fuel the flame. Due to these dispersion issues work was not continued on the methacrylate functionalised phosphonium-organomodifiers.

6.4 Considerations for Future Work

The work in this thesis could be expanded upon in a number of ways:

- The percentage exchange of all triphenyl phosphonium (TP) clays was found to be rather low, however increasing the loading of $Bu16^+$ to 1.5 x CEC, increased the percentage exchange to 89.6%. Therefore, by increasing the loading of $TP8^+$ to $TP16^+$ to 1.5 x CEC, the percentage exchange of the resulting organoclay could also be increased.

- It became evident in Chapter 4 that when $Bu16^+$ was exchanged onto Na^+ exchanged Na^+ Cloisite, then the percentage exchange increased from 67.1% in the as received form to 83.8% in the fully exchanged form. In the fully exchanged form, Calcium (Ca^{2+}) had been removed from the exchange sites, therefore more exchange sites were available for organic exchange with $Bu16^+$ cations. So by exchanging $TP8^+$ to $TP16^+$ onto Na^+ exchanged Na^+ Cloisite, the percentage exchange may also be increased.

- The products evolved during TG-MS experiments could be identified using gas chromatography coupled with mass spectrometry (GC-MS). In experiments similar to those carried out by Jang et al. [6-1], the identity of evolved products would be established by collecting them (the evolved products) using a cold trap and the structures identified through the analysis of the mass fragmentation pattern and/or by co-injection with authentic compounds. GC-MS could be utilised to identify what is being released under the small pre-peak T_{max} (A-1) in the DTG traces of Bu16-MMT, and also to identify whether $m/z = 50$ is from a single compound or a mixture of compounds.

- The fire properties of specimens produced using the 'one pot' method showed some promise but were not fully optimised. This route was considered attractive because the phosphonium clay did not have to be prepared and extensively washed prior to inclusion in the formulation. $Bu16^+$ was studied first simply because it presented the best fire retardant results. The XRD patterns indicated that the 'one-pot' method produced nanocomposites with similar clay dispersion to the standard

method. More importantly, the nanocomposites produced by the standard and 'one-pot' methods had comparable fire retardant properties. A more extensive investigation into the 'one-pot' method is required as a maximum number of three samples for each alkylphosphonium salt were previously surveyed.

- Differences in the ATR FT-IR spectra were observed between the front and back surfaces of samples prepared using Crystic 189LV, 5 wt% Bu16-MMT and 10D. To determine whether these differences were a result of the casting surface in which the samples were exposed, the samples could be cast between two glass sheets and any differences between the samples investigated using ATR FT-IR.

- The percentage exchange of all methacrylate functionalised phosphonium-organomodifiers was also quite low, to overcome this problem the synthesis of the modifiers could be scaled up to provide a larger amount of product. Therefore, increasing the exchange of the modifiers to 1.5 x CEC would hopefully increase the percentage exchange of the modified clays. Again Na^+ exchanged Na^+ Cloisite could be used instead of as received Na^+ Cloisite.

- In Chapter 4, successful fire retardant results were achieved with samples incorporating Bu16-MMT. Therefore, the synthesis of Bu16MM-MMT could be employed to try and increase the fire retardant properties of the methacrylate functionalised organomodifiers.

- Other flame retardants such as ammonium polyphosphate [6-2] could be utilised as improvements in fire performance have been observed in the work of a colleague using DMMP and other commercially available phosphates with commercially available clays.

6.5 Conferences Attended

- IRDG University Research Meeting
  Location: UMIST, Manchester. **Date:** 15th October 2003.

- IRDG Christmas Meeting
  Location: Kings College, London. **Date:** 15th December 2003.

- Materials Research Day
  Location: Sheffield Hallam University. **Date:** 10th September 2004.

- Current Knowledge on the Layer Charge of Clay Minerals
  Location: Smolenice castle, Slovakia. **Date:** 18th-19th September 2004.
  Poster: *TG-MS Analysis of the Desorption of Organocations from Smectities*

- 2nd Mid-European Clay Conference
  Location: Miskolc, Hungary. **Date:** 20th-24th September 2004.
  Poster: *TG-MS Analysis of the Desorption of Organocations from Smectities*

- IRDG Christmas Meeting
  Location: Kings College, London. **Date:** 16th December 2004.

- IRDG Christmas Meeting
  Location: The Royal Institute, London. **Date:** 15th December 2005.

- Materials and Engineering Research Innovation Day
  Location: Sheffield Hallam University. **Date:** 19th January 2006.
  Poster: *Fire Retardant Nanocomposites.*

- UK GRAD Programme
  Location: Windermere. **Date:** 20th – 24th February 2006.

6-1 Jang, B.N., Costache, M. and Wilkie, C.A., *Polymer*, **46**, 10678 (2005)
6-2 Nazare, S., Kandola, B.K. and Horrocks, A.R., *Polym. Adv. Technol.*, **17**, 294 (2006)